COMPARATIVE STUDY OF ANAMMOX-MEDIATED NITROGEN REMOVAL IN THREE REACTOR CONFIGURATIONS

By

Kiprotich Eric Kosgey

Thesis submitted in fulfilment of the requirements for the Degree

Of

DOCTOR OF ENGINEERING: CHEMICAL ENGINEERING

Department of Chemical Engineering

Faculty of Engineering and the Built Environment

Durban University of Technology

Supervisor

Prof Sheena Kumari Kuttan Pillai

Co-supervisors

Prof Sammy Lewis Kiambi

Prof Faizal Bux

Prof Kartik Chandran

10TH FEBRUARY 2021

Declaration

I, Kiprotich Eric Kosgey, declare that:

(i) The research reported in this thesis, except where otherwise indicated, is my original work.

(ii) This thesis has not been submitted for any degree or examination at any other university.

(iii) This thesis does not contain other persons' data, pictures, graphs or other information, unless specifically acknowledged as being sourced from other persons.

(iv) This thesis does not contain other persons' writing, unless specifically acknowledged as being sourced from other researchers. Where other written sources have been quoted, then:

a) their words have been re-written but the general information attributed to them has been referenced;

b) Where their exact words have been used, their writing has been placed inside quotation marks, and referenced.

(v) Where I have reproduced a publication of which I am an author, co-author or editor, I have indicated in detail which part of the publication was actually written by myself alone and have fully referenced such publications.

(vi) This thesis does not contain text, graphics or tables copied and pasted from the Internet, unless specifically acknowledged, and the source being detailed in the thesis and in the references sections.

Signature: …… …. Date…… 25/02/2021

Kiprotich Eric Kosgey **(Candidate)**

As the candidate's supervisor, I approve this Thesis for submission:

Signature: …… ……. Date…… 25/02/2021

Dr. Sheena Kumari Pillai **(Supervisor)**

As the candidate's co-supervisor, I approve this Thesis for submission:

Signature: … ……. Date…… 26/02/2021

Prof. Sammy Kiambi **(Co-supervisor)**

As the candidate's co-supervisor, I approve this Thesis for submission:

Signature: … ……. Date…… 25/02/2021

Prof. Faizal Bux **(Co-supervisor)**

As the candidate's co-supervisor, I approve this Thesis for submission:

Signature: June 23rd, 2020 . Date……

Prof. Kartik Chandran **(Co-supervisor)**

PREFACE

Journal Papers - published/accepted/under review

1. Kosgey K., Kiambi S. L., Mushal A., Arshad I., Bux F., Chandran K., and Sheena K. 2020. Impact of mixing conditions on process performance and microbial community structures in ANAMMOX-mediated systems: experimental and modelling studies. *Chemical Engineering Journal* - Under review.
2. Kosgey K., Kiambi S. L., Mushal A., Arshad I., Bux F., Chandran K., and Sheena K. 2020. Process performance and microbial community structures in three anammox-mediated systems with different mixing conditions. *Chemosphere* – Under review.
3. Kosgey, K., Chandran, K., Gokal, J., Kiambi, S. L., Bux, F. and Kumari, S. 2021. Critical Analysis of Biomass Retention Strategies in Mainstream and Sidestream ANAMMOX-Mediated Nitrogen Removal Systems. *Environmental Science & Technology*, 55 (1): 9-24.
4. Gasa, N. P., Nnadozie, C. F., Kosgey, K., Bux, F. and Kumari, S. 2019. Effect of ammonium to nitrite ratio on reactor performance and microbial population structure in anammox reactors. *Environmental Technology*: 1-16.

Conference papers and technical reports

5. Kosgey K., Oluyemi O. A., Sammy L. K., Allam M., Ismail A., Bux F., Chandran K., Kumari S. 2020. Autotrophic Bacterial Growth and Process Performance in Three Systems Mediated by Anaerobic Ammonium Oxidation. *Water Institute of Southern Africa conference*, Johannesburg, South Africa (*Virtual conference*).
6. AWOLUSI, O. O., KOSGEY, E. K., GOKAL, J., KUMARI, S. & BUX, F. 2020. Development of a Two-Stage Nitritation-Anammox Process for Improved Ammonia Removal from Wastewater. *Water research commission*.
7. Kosgey, K. E., Kiambi1, S. L., Bux, F., Chandran, K. and Kumari, S. 2019. Process performance and autotrophic bacterial diversity in three systems mediated by anaerobic ammonium oxidation. *Sixth South African Young water professionals Biennial Conference*, Durban, South Africa.
8. Kosgey, K. E., Kiambi1, S. L., Bux, F., Chandran, K. and Kumari, S. 2019. Impact of reactor configuration on process performance and microbial population dynamics

in three systems mediated by anaerobic ammonium oxidation. *Tenth Forum of Ecological Engineering*, Kazimierz Dolny, Poland.

9. Kosgey, K. E., Kiambi1, S. L., Bux, F., Chandran, K. and Kumari, S. 2018. Effect of fluctuating operating conditions on the physical characteristics of ANAMMOX biomass. *Water Institute of Southern Africa conference,* Cape Town, South Africa.
10. Kosgey, K. E., Kiambi1, S. L., Bux, F., Chandran, K. and Kumari, S. 2018. Potential application of magnetic fields for the retention of ANAMMOX biomass in reactors. *International water Association conference,* Tokyo, Japan.

Abstract

Anaerobic ammonium oxidation (ANAMMOX) is an efficient and cost-effective process developed for biological nitrogen removal from wastewater. However, widespread application of the ANAMMOX process for wastewater treatment remains constrained due to the slow growth of ANAMMOX bacteria, propensity for out-competition by fast growing microbes, and its sensitivity to environmental and operational conditions. Consequently, understanding the influence of mixing conditions in different reactor configurations on this process is paramount in its improvement.

This study focused on the comparative analysis of ANAMMOX-mediated nitrogen removal in a hybrid up-flow anaerobic sludge blanket reactor (H-UASB), moving bed biofilm reactor (MBBR) and a gas-lift reactor (GLR). The study involved experimental study of nitrogen removal, bacterial population dynamics and physical properties of the bacterial biomass within the reactors, as well as the description of process performance and the growth of nitrifying and ANAMMOX bacteria in the reactors using a calibrated mechanistic model. All the reactors were operated for 535 days using the same synthetic feed under anaerobic conditions. K1-type carrier materials were added to each reactor for biofilm development.

The concentrations of ammonium (NH_4^+), nitrite (NO_2^-) and nitrate (NO_3^-) in the effluent from the reactors were determined colorimetrically. Among the three reactors, MBBR displayed the highest nitrogen removal efficiency (NRE) during the study (66±36%), and contained the lowest concentration of free ammonia (FA) (19±22 mg-N/L) and free nitrous acid (FNA) (0.001±0.001 mg-N/L). In comparison, the NRE and the concentrations of FA and FNA in H-UASB during the study were 63±28%, 91±41 mg-N/L and 0.006±0.004 mg-N/L, respectively, while in the GLR, they were 54±39%, 28±29 mg-N/L and 0.002±0.002 mg-N/L, respectively. Based on the ratios of NO_2^- consumed to NH_4^+ consumed, and the ratios of NO_3^- produced to NH_4^+ consumed, the start-up of ANAMMOX process was faster in the MBBR (144 days) compared to H-UASB (193 days) and GLR (272 days). MBBR also displayed less fluctuations in the NREs and nitrogen removal rates (NRRs) during the study compared to H-UASB and GLR.

The microbial communities in the suspended biomass in the reactors were characterised using high-throughput sequencing on an Illumina MiSeq platform on days 125, 192, 260, 309 and 535, while the microbial communities in the biofilms were only characterised on day 535 (last day) due to slow biofilm development. Gradual increases in the relative

abundance of ANAMMOX bacteria were observed in the suspended biomass in all the reactors between days 125 and 309, which corroborated the observed increases in the NREs. The relative abundance of ANAMMOX bacteria remained consistently higher in H-UASB during the study than in MBBR and GLR. On the contrary, the highest relative abundance of ammonia oxidising bacteria (AOB) was observed in the suspended biomass in the MBBR on day 125 at approximately 38%, while the highest relative abundance of nitrite oxidising bacteria (NOB) and complete ammonia oxidising (COMAMMOX) bacteria was recorded in the suspended biomass in the MBBR at approximately 30% and 5%, respectively. In all the reactors, the relative abundance of AOB in the biofilms and the suspended biomass was comparable on day 535. In addition, on day 535, higher relative abundance of NOB was observed in the biofilms in both GLR and H-UASB at approximately 7% compared to the suspended biomass, while their abundance in the suspended biomass in the MBBR was comparable to that recorded in the biofilms. Furthermore, in both H-UASB and MBBR, higher relative abundance of ANAMMOX bacteria was observed in the suspended biomass compared to the biofilms on day 535, while comparable abundance was observed in the GLR. The highest total microbial diversity (Shannon and Simpson indices) and evenness (Pielou's Evenness) was observed in the suspended biomass in the MBBR.

Granulation of the suspended biomass was observed in both GLR and H-UASB, while the suspended biomass in the MBBR was flocculent. In the MBBR, the colour of the biomass had turned brown on day 125, while the biomass in H-UASB and GLR on this day was tawny and dark-tawny, respectively. However, on day 309, the biomass in all the reactors had turned red, corroborating the highest relative abundance of ANAMMOX bacteria observed during the study. Faster attachment of biomass on the carrier materials in MBBR was observed in the course of study compared to H-UASB and GLR. On the last day, the concentrations of the biomass on the carrier materials in the MBBR was also higher (12 mg/carrier) in the MBBR than in the H-UASB (8 mg/carrier) and GLR (10 mg/carrier).

Activated sludge model 1 (ASM 1), which was modified by separating the activities of *Nitrospira* spp. from those of *Nitrobacter* spp. as well as by adding both ANAMMOX and COMAMMOX bacterial activities, was used to describe process performance in the reactors. The modified ASM 1 was able to predict the trends in the effluent concentrations of NH_4^+, NO_2^- and NO_3^- in all the reactors. In addition, the correlation of the actual relative abundance of nitrifying and ANAMMOX bacteria, with the model-predicted relative abundance, was positive. The model also indicated higher heterotrophic activities in both GLR and MBBR

compared to H-UASB, an indication that continuous mixing in MBBR and alternation of plug-flow conditions with internal gas circulation in GLR favoured heterotrophic bacterial growth. However, the model was limited in predicting the fluctuations in bacterial abundance and the fluctuations in the effluent concentrations of NH_4^+, NO_2^- and NO_3^- in the reactors.

The obtained results indicate that better-mixed conditions in the MBBR led to comparable relative abundance of nitrifying bacteria between the biofilms and the suspended biomass, while plug-flow conditions in the H-UASB favoured ANAMMOX bacterial growth in the suspended biomass and the nitrifying bacterial growth in the biofilms. The alternation of internal gas circulation with plug-flow conditions in the GLR also favoured the growth of nitrifying bacteria in the biofilms. Overall, nitrogen removal in H-UASB was likely dominated by ANAMMOX process, while nitrogen removal in MBBR and GLR was as a result of combined ANAMMOX and sequential nitrification-denitrification processes. The novelty of this study stem from the impact of mixing conditions on process performance and microbial ecology of ANAMMOX-mediated systems.

Keywords: plug-flow, mixing, ANAMMOX, reactor configuration, biofilms, suspended biomass.

Dedication

This work is dedicated to my late mother Emily Cheptanui Cheres who toiled hard to provide for us but could not live to witness this achievement. Love you mum.

Acknowledgements

I would like to first thank my supervisors, Dr Sheena Kumari Pillai, Prof Sammy Lewis Kiambi, Prof Faizal Bux and Prof Kartik Chandran, for their support and guidance during my journey as a PhD student. I lack words to express my appreciation for the sacrifice you made for me. Your words of encouragement during my study kept me going.

To my Chemical Engineering colleagues, thank you! I will never forget your constant positive criticism of my work. It is impossible to mention all of you here but remember that I will always cherish the beautiful memories you gave me. Special thanks to Martha Chollom, Peter C Tumwet, Sheriff Mustapha, Emmanuel Tettah, Usman Aliyu, Boldwin Mutsvene, Ronald Musamali and Endifenge Haikela.

I thank Saieshna Rajcoomar, Keith Allan Chetty, Nomalihle Malambule and Nomalanga Gasa of Institute for Water and Wastewater Technology (IWWT) for their assistance in running the reactors. I also thank Kriveshin Pillay for his assistance during sample analyses. I appreciate Jashan Gokal, Thobela Conco, Precious Nonsikelelo Mthethwa and Oluyemi A. Awolusi for allowing me to use their kits for PCR and qPCR. I also thank you for the mini-lectures and tutorials on molecular technologies that I previously knew little about. Special thanks to Ismail Rawat, Nashia Deepnarain and Trisha Mogany for their assistance during the procurement of equipment and chemicals used in this study.

The assistance I received during fabrication and repair of reactors from Lincoln Govender, Prof Mark Walker, Ebrahim Cassim, Shikaar Gudar, Tharish Chaithram, Zwethanda Khuzwayo, Njabulo Kunene and Mzokhulayo Mbuli of composite technology workshop is greatly appreciated. I also appreciate the assistance by Sithembiso V Nyawo and Jayendran Veerasamy of Mechanical Engineering workshop during fabrication of some of the parts for my reactors.

I acknowledge Water Research Commission and the National Research Foundation of South Africa for their financial support. Merlien Reddy and Prof. Chris Buckley (University of KwaZulu Natal) are greatly appreciated for their kind assistance with particle size analysis. Dr Mushal Allam and Dr Arshad Ismail of National Institute for Communicable Diseases are also appreciated for their assistance with molecular analyses of biomass samples.

Last but not least, I would like to thank my family for the many sacrifices they made for me in the course of this journey. To my soulmate Joan Chepkoech, thank you for standing with me even when the road was bumpy and steep. To my son Shujaa Kiptoo and daughter Zahara Chelimo Chepng'etich, thank you for letting me use my laptop when you most needed to watch your favourite cartoons. The laptop is all yours now!

Table of Contents

List of figures

List of tables

LIST OF ABBREVIATIONS AND ACRONYMS

Abbreviation	Description
ANAMMOX	anaerobic ammonium oxidation
AOB	ammonia oxidising bacteria
NOB	nitrite oxidising bacteria
DAMO	denitrifying anaerobic methane oxidising
COMAMMOX	complete ammonia oxidation
BNR	biological nitrogen removal
MBBR	moving bed biofilm reactor
H-UASB	hybrid up-flow anaerobic sludge blanket reactor
GLR	Gas-lift reactor
MBfR	Membrane biofilm reactor
RPM	revolutions per minute
NRR	nitrogen removal rate
NLR	nitrogen loading rate
HRT	hydraulic retention time
SRT	solids retention time
DO	dissolved oxygen
CANON	completely autotrophic nitrogen removal over nitrite
SHARON	Single reactor system for High activity Ammonia Removal Over Nitrite
FNA	free nitrous acid
FA	free ammonia
SAA	specific ANAMMOX activity
PCR	polymerase chain reaction

qPCR	quantitative polymerase chain reaction
FISH	fluorescence in situ hybridization
EPS	extra-polymeric substance
WWTP	wastewater treatment plant
RTD	residence time distribution
ASM	activated sludge model
CMC	carboxymethylcellulose
PVA	Polyvinyl alcohol
PEG	polyethylene glycol
SA	sodium alginate

Chemical formulas and symbols

CO_2	carbon dioxide
NH_4^+	aqueous ammonia
NO_2^-	aqueous nitrite
NO_3^-	aqueous nitrate
NO	nitric oxide
N_2O	nitrous oxide
N_2	nitrogen gas
Fe	iron
Zn	zinc
Co	cobalt
Cu	copper
Mn	manganese
Mo	molybdenum

Ni	nickel
Mg	magnesium
P	phosphorus

LIST OF SYMBOLS

b	decay coefficient
μ_{max}	maximum specific growth rate
E_{act}	activation energy
R	universal gas constant
Θ	Arrhenius constant
$(K_L a)$	oxygen transfer coefficient
φ	temperature correction factor
η	anoxic reduction factor
X_I	inerts (non-biodegradable organics)
X_S	slowly biodegradable substrate
f_I	fraction of X_I in decaying biomass
i_{NBM}	concentration of nitrogen in biomass
i_{NXI}	nitrogen content of non-biodegradable organics
Y	biomass yield

ANALYTICAL TECHNIQUES

SEM	scanning electron microscopy
EDX	energy dispersive x-ray
MP - AES	microwave plasma - atomic emission microscopy

Thesis structure

This thesis is structured with chapters 1, 2, 3, 4, 5 and 6 covering introduction, literature review, objective 1, objective 2, objective 3, and objective 4, respectively. The methodologies, results, discussion and conclusions for each objective are given in the respective chapters. General conclusions were made after the sixth chapter and the list of references has been placed after the general conclusions. Supplementary information has been provided in appendices A, B, C and D.

CHAPTER ONE

1 Introduction

1.1 Background of study and research motivation

Excess nitrogenous compounds in wastewaters can cause serious ecological problems when released into the environment without adequate treatment (Foglar and Briški 2003). In receiving streams, they can cause eutrophication, induce water stagnation, odour problems, ammonia (NH_3) and nitrite (NO_2^-) toxicity as well as decrease dissolved oxygen concentration (Arbib *et al.* 2014; Cho *et al.* 2016). Within wastewater treatment systems, the biologically mediated processes such as Nitrification followed by Denitrification, and ANAMMOX, are employed for nitrogen removal (Wiesmann 1994; Val del Río, Campos Gómez and Mosquera Corral 2016). Nitrification is a chemolithoautotrophic process by which ammonium (NH_4^+) is oxidised to nitrate (NO_3^-) either in two-step reactions through the synergistic activities of ammonia oxidising bacteria (AOB) and nitrite oxidising bacteria (NOB), or in a single step by complete ammonia oxidising (COMAMMOX) bacteria. In a two-step nitrification process, NH_4^+ is first oxidized to NO_2^- by AOB and then the NO_2^- is oxidised to NO_3^- by NOB under strict aerobic conditions (Hira *et al.* 2018), while in a single-step nitrification, COMAMMOX bacteria oxidise NH_4^+ to NO_3^- using oxygen as an electron acceptor (Daims *et al.* 2015). In this process, inorganic carbon is used as a carbon (C) source (Awolusi, Kumari and Bux 2015). Denitrification is a subsequent process where heterotrophic bacteria reduce oxidized nitrogen species to gaseous nitrogen under anaerobic conditions, using NO_2^- or NO_3^- as electron acceptors and organic matter for C and energy source (Breisha and Winter 2010). The ANAMMOX process is a relatively newer addition to the Nitrogen cycle, and represents a direct conversion of NH_4^+ to dinitrogen (N_2) gas by anaerobic ammonium oxidising (ANAMMOX) bacteria in a single step using CO_2 as C source (*equation 1.1*) (Kartal *et al.* 2013). However, in its inception, Mulder *et al.* (1995) had proposed *equation 1.2* to represent ANAMMOX process, which was later disapproved by Strous *et al.* (1998) through rigorous experimentation.

$$NH_4^+ + 1.32NO_2^- + 0.066HCO_3^- + 0.13H^+ \rightarrow 1.02N_2 + 0.256NO_3^- + 0.066CH_2O_{0.5}N_{0.15} + 2.03H_2O \quad (1.1)$$

$$3NO_3^- + 9NH_4^+ \rightarrow +N_2 + 9H_2O + 2H^+ \quad (1.2)$$

The ANAMMOX process exhibits many advantages over the conventional nitrification and denitrification processes, viz., the need for less aeration, lower sludge generation and utilisation of inorganic carbon as the sole carbon source (Abbas *et al.* 2015; Ali and Okabe 2015). These advantages have made it an attractive option, and currently, over 100 full-scale ANAMMOX-mediated treatment plants are in operation worldwide (Lackner *et al.* 2014; Bowden, Stensel and Tsuchihashi 2015). Despite this success, widespread application of the ANAMMOX process is still hampered by the lack of access to sufficient quantities of active ANAMMOX biomass, particularly in developing countries (Ni *et al.* 2011b). Due to the slow growth rate of ANAMMOX bacteria, its sensitivity to inhibition, and proclivity to out-competition, generating suitable amounts of active ANAMMOX biomass is still a challenge (Tsushima *et al.* 2007; Zhang *et al.* 2017c). Minimising the excess washout of the slow-growing ANAMMOX biomass fraction and improving its retention during operation are key strategies in ANAMMOX reactor start-up and stable operation (Fernández *et al.* 2008; Chen *et al.* 2012). Further, complex substrates such as municipal, digester effluents and industrial wastewaters could present unprecedented influence on process performance and microbial community structures (Laureni *et al.* 2015; Li *et al.* 2017b).

In full-scale systems, the co-culturing of ammonia oxidising bacteria (AOB) and ANAMMOX bacteria ensures that the process is self-sustaining as AOB generate NO_2^- for ANAMMOX bacteria, which, in turn, is used by ANAMMOX bacteria as an electron acceptor in the oxidation of residual NH_4^+ to nitrogen gas. However, dissolved oxygen (DO) concentrations above 0.5 mg/L could inhibit ANAMMOX bacteria (Strous *et al.* 1997a). Excess supply of oxygen could also promote the growth of undesired microorganisms such as NOB in ANAMMOX-mediated systems, which compete with ANAMMOX bacteria for NO_2^-. As a consequence, several process control strategies have been engineered for both mainstream and sidestream ANAMMOX-mediated systems to stabilise the ANAMMOX-mediated processes.

In the current full-scale ANAMMOX-mediated installations, moving bed biofilm reactors (MBBRs), integrated fixed-film activated sludge (IFAS) systems, rotating biological contactors (RBCs), granular up-flow reactors and SBRs are common (Lackner *et al.* 2014; Bowden, Stensel and Tsuchihashi 2015). However, previous reports have highlighted disparities in process performance with reactor configuration in full-scale systems, possibly due to variation in biomass concentration in the reactors (Lackner and Horn 2013; Lackner *et al.* 2014). Variation in full-scale reactor start-up periods with reactor configuration has

also been reported, possibly due to the variation in biomass retention capacities and mass transfer within the different reactor configurations (van der Star *et al.* 2007; Isaka *et al.* 2017; Xu *et al.* 2018). Similarly, niche segregation of bacteria in different ANAMMOX-mediated systems has also been reported in many previous studies (Park *et al.* 2010a; Vlaeminck *et al.* 2010; Veuillet *et al.* 2014; Park *et al.* 2015). While ANAMMOX bacteria are reportedly growing mainly within the granular and the biofilm structures where anoxic conditions prevail, AOB, NOB and other aerobic bacteria have been observed to grow mainly in floccular biomass or on the peripheries of biofilms and granules where they can easily access oxygen (Winkler *et al.* 2013; Lotti *et al.* 2015; Park *et al.* 2015). Therefore, comparative study of ANAMMOX-mediated nitrogen removal in different reactors under baseline conditions could be necessary to understand the impact of reactor configuration on reactor start-up, nitrogen removal kinetics, microbial ecology and properties of biomass aggregates. Furthermore, describing process performance using a calibrated mechanistic model could be necessary to understand the extent of nitrogen transformation by the newly discovered bacteria such as COMAMMOX bacteria.

The novelty of this work stem from the evaluation of the impact of mixing conditions within the reactors on microbial ecology and process performance, and the description of process performance using modified activated sludge model 1 (ASM 1). The addition of COMAMMOX bacteria to ASM 1, and the inclusion of *Nitrospira* spp. and *Nitrobacter* spp. as separate bacterial groups in the model are novel approaches in the modelling of ANAMMOX-mediated systems. None of the currently existing models describing process performance of ANAMMOX-mediated systems has included the activities of COMAMMOX bacteria, even though Annavajhala *et al.* (2018) reported that these bacteria are co-existing with ANAMMOX bacteria in nitrogen removal systems.

1.2 Aim

Study the impact of reactor configuration on the performance and properties of ANAMMOX-mediated systems

1.3 Objectives

The objectives of the study are:

- Evaluate process performance and kinetics of nitrogen removal in three reactor configurations (*Chapter 3*)
- Evaluate the impact of reactor configuration on microbial ecology (*Chapter 4*)
- Evaluate the impact of reactor configuration on physical properties of reactor biomass (*Chapter 5*)
- Describe process performance in the three selected reactor configurations using calibrated mechanistic model (*Chapter 6*)

CHAPTER TWO

2 Literature review

2.1 Engineering the biological nitrogen removal processes

2.1.1 Nitrification/denitrification

Nitrification followed by denitrification is a conventional process that has been in employed for nitrogen removal for decades in wastewater treatment plants (Grady Jr *et al.* 2011). Until the discovery of COMAMMOX bacteria that can oxidise NH_4^+ to NO_3^- in a single step, nitrification was thought to be a two-step process involving two groups of microorganisms working synergistically to oxidise NH_4^+ to NO_3^- (first to NO_2^- then to NO_3^-). AOB oxidise NH_4^+ to NO_2^- in the first step, and nitrite oxidising bacteria (NOB) oxidise NO_2^- to NO_3^- in the second step (Awolusi *et al.* 2015). The AOB and NOB are mutually beneficial to each other as NOB depend on AOB for nitrite while the NOB relieve AOB of nitrite toxicity (Peng and Zhu 2006). NO_2^- consumption by NOB not only prevents NO_2^- accumulation but also the formation of by-products such as nitric oxide (NO) which can affect the normal functioning of bacterial enzymes (Peng and Zhu 2006).

Full nitrification by both AOB and NOB yields 3.373 moles of nitrate per ammonium consumed (Grady Jr *et al.* 2011) (*equation 2.3*). A large amount of alkalinity is consumed in the process (6.708mg HCO_3^-/mg NH_4^+), mainly for neutralization of the hydrogen ions produced in the first step by AOB (*equation 2.2*). In addition, a substantial amount of oxygen is also consumed (3.3 mg-O_2/mgNH_4^+). However, the biomass yield is quite low (0.129 mg biomass/ mg NH_4^+) as is known of autotrophic growth, with the growth of AOB generating most of the biomass (*equations 2.1-2.3*) (Grady Jr *et al.* 2011).

$$NH_4^+ + 2.457O_2 + 6.716HCO_3^- \rightarrow 2.509NO_2^- + 6.513H_2CO_3 + 0.114C_5H_7NO_2 + 1.036H_2O \quad (2.1)$$

$$0.001NH_4^+ + NO_2^- + 0.339O_2 + 0.014H_2CO_3 + 0.003HCO_3^- \rightarrow 1.348NO_3^- + 0.006C_5H_7NO_2 + 0.003H_2O \quad (2.2)$$

$$NH_4^+ + 3.3O_2 + 6.708H_2CO_3 \rightarrow 3.373NO_3^- + 0.129C_5H_7NO_2 + 1.041H_2O + 6.463HCO_3^- \quad (2.3)$$

Recent studies have revealed the existence of a distinct group of bacteria (COMAMMOX-complete ammonia oxidising bacteria) belonging to *Nitrospira* genus that can directly

oxidise NH_4^+ to NO_3^- in a single step (Daims *et al.* 2015; Annavajhala *et al.* 2018). To date, only three species of COMAMMOX bacteria have been identified (*Candidatus* Nitrospira nitrosa, *Candidatus* Nitrospira inopinata and *Candidatus* Nitrospira nitrificans) (Annavajhala *et al.* 2018). Although studies of physiological, molecular and kinetic properties of COMAMMOX bacteria are ongoing, it has been reported in some studies that they have a higher affinity for NH_4^+ than most ammonia oxidisers (Kits *et al.* 2017). In addition, Kits *et al.* (2017) also reported that the biomass yield of COMAMMOX bacteria (*Candidatus* Nitrospira inopinata) is higher than that of incomplete ammonia oxidisers. Indeed, Costa, Pérez and Kreft (2006) postulated that COMAMMOX organisms are slow growing *K*-strategists (bacteria with high substrate affinity, slow growth and able to grow under limited substrate). To date, COMAMMOX bacteria have been detected in different BNR (biological nitrogen removal) systems, suggesting a significant impact of COMAMMOX bacteria in nitrogen transformation (Annavajhala *et al.* 2018; Cotto *et al.* 2020).

Denitrification is a subsequent step after nitrification that is carried out by heterotrophic, mixotrophic or autotrophic bacteria (Di Capua *et al.* 2019). In this stage, nitrate is reduced via NO_2^-, nitric oxide (NO) and nitrous oxide (N_2O) to dinitrogen gas (N_2) (*equations 2.4 and 2.5*) (Loick *et al.* 2016). The reported electron donors during denitrification are hydrogen gas, inorganic sulphur compounds, organic carbon, metallic ions, etc. (Wang *et al.* 2016; Su, Liang and Lian 2018). However, nitrous oxide (N_2O) and nitric oxide (NO) emissions at low oxygen concentrations have been the major concern of nitrification/denitrification since both gases have greenhouse effect and can deplete the earth's ozone (Kester, De Boer and Laanbroek 1997). For instance, (N_2O) is approximately 300 times more radiatively active than carbon dioxide (CO_2) (Smith 2010; Lackner *et al.* 2014). According to Trimmer *et al.* (2016) and (Ma *et al.* 2016) N_2O production by AOB is stimulated under limited oxygen concentrations.

$$NO_3^- \rightarrow NO_2^- \rightarrow NO \rightarrow N_2O \rightarrow N_2 \quad (2.4)$$

$$electron\ donor + NO_3^- \rightarrow N_2 + biomass \quad (2.5)$$

In the treatment of domestic wastewater streams rich in NH_4^+ and organic carbon, it is thus inevitable to provide conditions conducive for both autotrophic and heterotrophic bacteria through time/space-variant dissolved oxygen concentration (Grady Jr *et al.* 2011). For instance, in a Modified Ludzack-Ettinger (MLE) process (*Figure 2.1*), the heterotrophic bacteria using organic carbon in the influent remove NO_3^- in the recycled streams. This way,

the removal of both carbon and nitrogen from domestic wastewater can be effected without the addition of an external carbon source. Excess oxygen supply could also be avoided if carbon is first utilised in the anoxic tank (through denitrification) before the water is fed to an aerated tank. However, in the treatment of wastewater streams with low organic carbon concentrations, the addition of external organic carbon, such as methanol, is necessary for efficient nitrogen removal (Grady Jr *et al.* 2011).

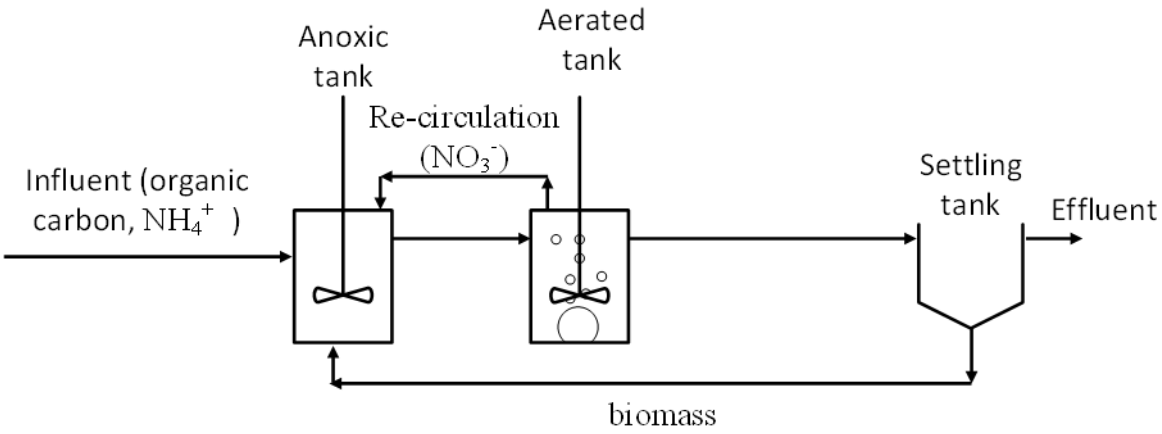

Figure 2. 1. Schematic representation of the MLE process.

2.1.2 Partial nitrification/denitrification

Partial nitrification followed by denitrification was developed as a short-cut BNR process to full nitrification/denitrification. In this process, NH_4^+ oxidation is limited to nitritation (at NO_2^-), which is then reduced to nitrogen gas using organic carbon as electron donor and energy source (*figure 2.2*) (Hellinga, van Loosdrecht and Heijnen 1999). To achieve this, the temperature and pH of the reactors for partial nitrification are maintained between 30-40ºC and 8-8.5, respectively, which enable faster growth of AOB than NOB, leading to nitrite accumulation (Hellinga, van Loosdrecht and Heijnen 1999; van Kempen *et al.* 2001b). The DO concentration, substrate loading rate and aeration pattern are also regulated for efficient nitrogen removal (Hellinga *et al.* 1998). This process has been termed SHARON (Single reactor system for High activity Ammonia Removal Over Nitrite) (Hellinga, van Loosdrecht and Heijnen 1999).

The maintenance of the solids retention time (SRT) similar to the hydraulic retention time (HRT) in the SHARON process leads to washout NOB since the operating conditions do not favour their growth (SRT<doubling time), unlike the AOB which regenerate fast enough within the system (Hellinga *et al.* 1998; van Kempen *et al.* 2001b). This is advantageous as

oxygen consumption and sludge production is reduced (Hellinga *et al.* 1998; van Kempen *et al.* 2001b).

van Kempen *et al.* (2001a) reported on the full-scale application of partial nitrification/denitrification process for nitrogen removal from digester filtrate. In this two-stage process, NO_2^--rich streams generated in partial nitrification (SHARON) reactor are recycled and mixed with the influent of the wastewater treatment plant that is rich in COD (chemical oxygen demand), allowing heterotrophic bacteria to denitrify. In some systems, methanol is added to the first stage to enhance heterotrophic bacterial activities, leading to the consumption of acidity according to *equations 2.6 and 2.7*.

Partial nitrification/denitrification is favoured to full nitrification/denitrification because of the following (Hellinga, van Loosdrecht and Heijnen 1999; van Kempen *et al.* 2001a):

(i) 60% reduction in energy consumption as oxygen requirement is 25% lower

(ii) consumption of electron donor is about 40% lower

(iii) nitrite denitrification is 1.5-2 times faster than nitrate reduction

(iv) CO_2 production is 20% lower

(v) sludge production is 33-35% lower in nitrification and 55% lower in denitrification

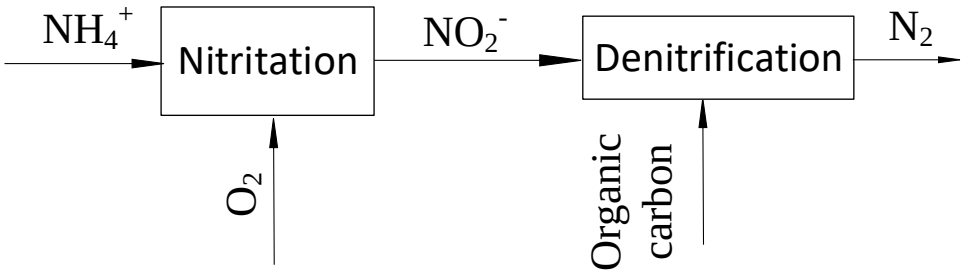

Figure 2. 2. Schematic representation of partial nitrification/denitrification process

$$H_2O + CO_2 \rightarrow HCO_3^- + H^+ \quad (2.6)$$

$$NO_2^- + 0.5CH_3OH \rightarrow 0.5CO_2 + OH^- + 0.5N_2 + 0.5H_2O \quad (2.7)$$

2.1.3 Partial nitrification/ANAMMOX

ANAMMOX process is the denitrification of NO_2^- with NH_4^+ as the electron donor, and carbon dioxide as the source of carbon. ANAMMOX process takes place in two stages: (1) the energy generation from the oxidation of NH_4^+ to dinitrogen gas (*equation 2.8*) and (2) the fixation of bicarbonate into cell biomass (*equation 2.9*). Broda (1977) postulated the existence of these bacteria in 1977 based on the metabolic versatility of prokaryotes and the

low Gibbs energy of the process. Costa, Pérez and Kreft (2006) argued that because of the economical usage of the substrate by ANAMMOX bacteria, their growth rate is very low compared to other bacteria such as AOB and NOB.

$$1NH_4^+ + 1NO_2^- \rightarrow 1N_2 + 2H_2O \qquad \Delta G^\circ = -357\ kJmol^{-1}N_2 \tag{2.8}$$

$$0.27\ NO_2^- + 0.066HCO_3^- \rightarrow 0.26NO_3^- + 0.066CH_2O_{0.5}N_{0.15} \tag{2.9}$$

$$NH_4^+ + 1.32NO_2^- + 0.066HCO_3^- + 0.13H^+ \rightarrow 1.02N_2 + 0.26NO_3^- + 0.066CH_2O_{0.5}N_{0.15} + 2.03H_2O \tag{2.10}$$

In full-scale applications, partial nitrification and ANAMMOX are either coupled in a single reactor (CANON-completely autotrophic nitrogen removal over nitrite) or two reactors connected in series (SHARON/ANAMMOX) for synergistic cooperation in nitrogen removal (Sliekers *et al.* 2002). In both systems, NH_4^+ is partially oxidised to NO_2^- by the AOB and the residual NH_4^+ is then oxidised to nitrogen gas by the ANAMMOX bacteria using the NO_2^- produced by AOB as the electron acceptor.

In a single reactor configuration (CANON systems) (*figure 2.3*), oxygen supply is regulated to suppress NOB growth and to avoid oxygen-inhibition of ANAMMOX bacteria (Joss *et al.* 2011). The control of NOB growth, in particular, is of paramount importance in ANAMMOX-mediated systems as they compete for NO_2^- with ANAMMOX bacteria, and oxygen with AOB (Joss *et al.* 2011; Li *et al.* 2018). Because both the AOB and ANAMMOX bacterial activities take place in CANON systems simultaneously, the bacterial aggregates are structured such that the AOB and other aerobes are found on the outer lying layers while the ANAMMOX bacteria occupy the inner lying anoxic layers (Winkler *et al.* 2013). However, in small aggregates (flocs), ANAMMOX bacterial growth is inhibited by oxygen while the AOB growth is favoured (Vlaeminck *et al.* 2010; Yang *et al.* 2016). Therefore, to promote the activities of both AOB and ANAMMOX bacteria, either intermittent or continuous aeration of the reactors is implemented (Klaus *et al.* 2017).

Intermittent aeration allows the creation of aerobic and anoxic phases in the reactors within which AOB and ANAMMOX activities take place, respectively (Bowden, Stensel and Tsuchihashi 2015). This alternation of aerobic and anoxic phases limit NOB activities as they have longer enzymatic lags than AOB when conditions change from anoxic to oxic (Wett *et al.* 2013). Under such conditions, ANAMMOX bacteria can compete with the NOB for NO_2^-, further limiting their growth (Lotti *et al.* 2014a). Many full-scale suspended-growth ANAMMOX-mediated systems implemented intermittent aeration for better

nitrogen removal (Lackner *et al.* 2014; Val del Río, Campos Gómez and Mosquera Corral 2016).

In continuous aeration modes, DO control between 0.3–1.5 mg-O_2/L has been reported in full-scale systems (Christensson *et al.* 2013; Val del Río, Campos Gómez and Mosquera Corral 2016). Conversely, in intermittent aeration modes, the duration of aeration of the reactors is regulated (Val del Río, Campos Gómez and Mosquera Corral 2016). However, according to Klaus *et al.* (2017), intermittent aeration is vulnerable to high shear rates that can affect biofilm developments and granulation, while shear rates in continuous aeration mode can be easily managed by maintaining low aeration rates.

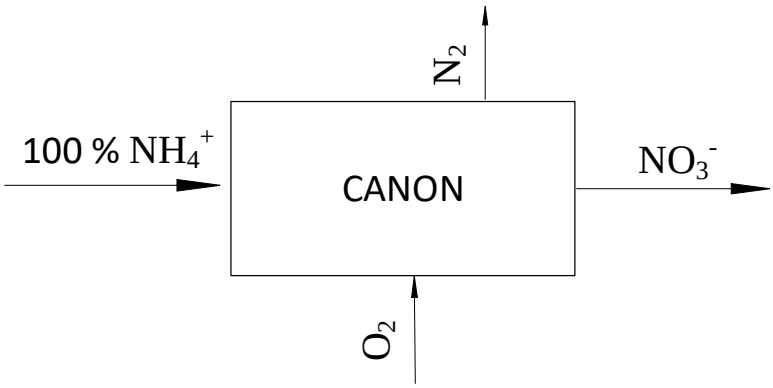

Figure 2. 3. Schematic diagram of the CANON concept

The two-stage SHARON/ANAMMOX concept is designed much like the partial nitrification-denitrification, in which ammonia is partially oxidised in the first reactor (SHARON) and the residual ammonium is oxidised by ANAMMOX bacteria in the second reactor (van der Star *et al.* 2007) (*figure 2.4*). In the SHARON reactor, the HRT is kept high enough for AOB to grow but low for NOB growth, similar to partial nitrification/denitrification concept. As a result, the NOB are washed out of the reactors, as the SRT in the SHARON system is kept equal to its HRT (van der Star *et al.* 2007). As demonstrated by van Dongen, Jetten and van Loosdrecht (2001), the effluent concentration of the SHARON reactor is only dependent on the growth rate of bacteria and not the concentration of the influent.

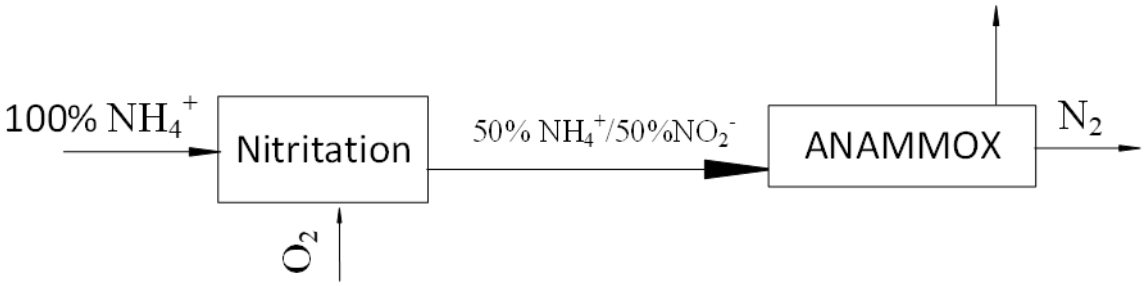

Figure 2. 4. Schematic diagram of a two-stage partial nitrification/ANAMMOX concept

2.1.4 Partial denitratation/ANAMMOX

Recent lab-scale studies have demonstrated that coupling denitratation with ANAMMOX bacterial activities is feasible (Ma *et al.* 2017; Xie *et al.* 2017). In this process, NH_4^+ is first oxidised to NO_3^- (*equation 2.3*), and then the NO_3^- is partially reduced to NO_2^- either by denitrifying bacteria under organic carbon-limited conditions (*equation 2.11 and figure 2.5*) or by denitrifying anaerobic methane oxidising (DAMO) archaea using methane (CH_4) (*equation 2.12 and figure 2.56*) (Ma *et al.* 2017; Xie *et al.* 2017). ANAMMOX bacteria then use the NO_2^- produced by DAMO archaea or denitrifying bacteria to oxidise the residual NH_4^+ to nitrogen gas. Coupling denitratation with ANAMMOX could be attractive for mainstream wastewater systems with high COD to nitrogen (C/N) ratios where limitation of NH_4^+ oxidation to NO_2^- might be challenging (Ma *et al.* 2017). However, denitratation/ANAMMOX process consumes approximately 21% more oxygen than partial nitrification/ANAMMOX, which translates into increased operational costs for this treatment process. This notwithstanding, the NO_2^- production through denitratation is more stable (Ma *et al.* 2017).

Xie *et al.* (2017) demonstrated that coupling denitratation by DAMO archaea with ANAMMOX process can achieve high NRRs (>1 kg-N/m^3). However, the supply of methane to DAMO archaea could require the use of membranes, which could increases the capital and operational costs of the treatment system. However, despite these challenges, coupling denitratation with ANAMMOX could play a key role in mainstream ANAMMOX-mediated processes where otherwise the conventional partial nitritation/ANAMMOX could be challenging (Ma *et al.* 2017; Li *et al.* 2018). This is because mainstream wastewaters contain high C/N ratios that, in turn, can lead to increased DO consumption as heterotrophic bacteria would use part of the oxygen meant for AOB (Li *et al.* 2018). The control of NOB in mainstream wastewaters is also a challenge as conventional sidestream process control technologies face limitations (Li *et al.* 2018).

$$organic\ carbon + 4NO_3^- \rightarrow NO_2^- \quad (2.11)$$

$$CH_4 + 4NO_3^- \rightarrow CO_2 + 4NO_2^- + 2H_2O \quad (2.12)$$

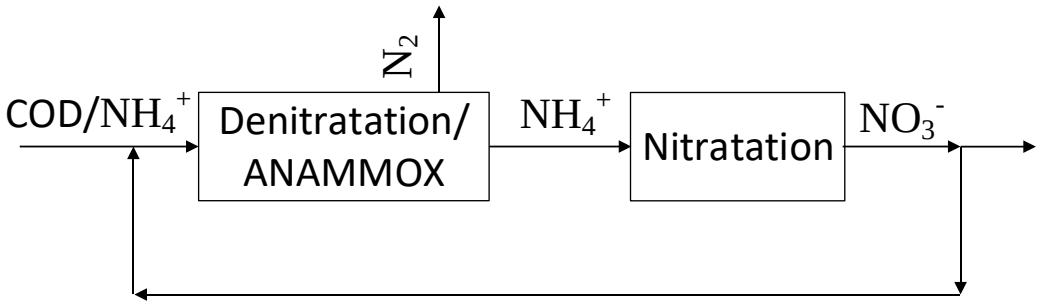

Figure 2. 5. Conceptualised coupling of ANAMMOX with denitratation using denitrifying bacteria

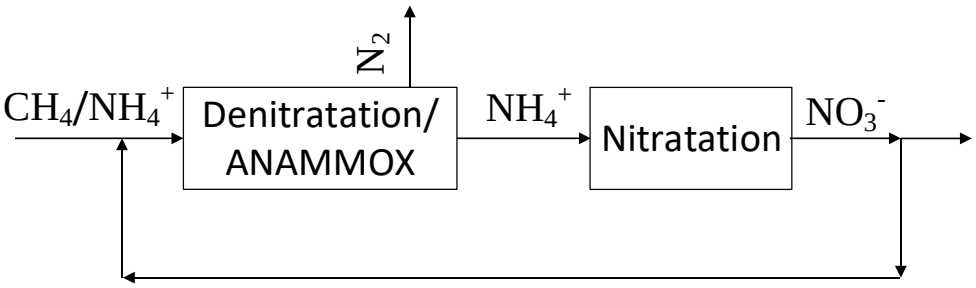

Figure 2. 6. Conceptualised coupling of ANAMMOX with denitratation using DAMO archaea

2.2 Factors affecting ANAMMOX-mediated processes

2.2.1 Dissolved oxygen

ANAMMOX bacteria are reversibly inhibited by oxygen (Strous *et al.* 1997a). Different inhibitory concentrations of oxygen have been reported in different studies: Carvajal-Arroyo *et al.* (2013) reported 20% inhibition of ANAMMOX activities at 1 mg/L DO and complete inhibition at 8 mg/L, while Strous *et al.* (1997a) reported inhibition at air saturations above 0.5% (ca. 0.04 mg/L). However, Carvajal-Arroyo *et al.* (2013) reported that the inhibitory oxygen concentration could vary with the growth morphology of the biomass.

In full-scale applications, process control technologies regulate the DO by controlling the rate of aeration and/or the duration of aeration. This is largely because of the three reasons (Rosenwinkel and Cornelius 2005; Val del Río, Campos Gómez and Mosquera Corral 2016):

(I) AOB consume oxygen fed into the system hence assist in regulating the DO concentration within the non-inhibitory concentration,

(II) The process control strategy could allow intermittent aeration leading to the creation of both oxic and anoxic phases within which AOB and ANAMMOX bacterial activities could take place, respectively,

(III) The process control strategy could maintain the DO at non-inhibitory concentration.

2.2.2 Temperature and pH

Temperature and pH are critical parameters in wastewater treatment whose influence in nutrient removal has been extensively studied and recorded (Awata *et al.* 2012; Puyol *et al.* 2014; Lackner *et al.* 2015; Tomaszewski, Cema and Ziembińska-Buczyńska 2017; He *et al.* 2018). Both temperature and pH could affect the normal function of ANAMMOX bacteria, in turn influencing the reaction rate kinetics (Tomaszewski, Cema and Ziembińska-Buczyńska 2017). Additionally, both the temperature and pH could also influence FA and FNA concentrations within ANAMMOX-mediated systems (*equations 2.13-2.16*) (Anthonisen *et al.* 1976), both of which are inhibitory to ANAMMOX bacteria and AOB (Giustinianovich *et al.* 2018).

According to Anthonisen *et al.* (1976) and (Soliman and Eldyasti 2016), an increase in temperature and pH triggers a rise in FA concentration as a result of ammonium dissociation (*equations 2.13 and 2.15*), while the reverse is true for FNA produced when aqueous NO_2^- dissociate (*equation 2.15*). This was demonstrated by applying *equations 2.15* and *2.16* at pH between 7 and 8 as well as the temperature between 20ºC and 30ºC (*figures 2.7* and *2.8*).

$$NH_4^+ + OH^- \leftrightarrow NH_3 + H_2O \quad (2.13)$$

$$HNO_2 \leftrightarrow H^+ + NO_2^- \quad (2.14)$$

$$FA, mgNL^{-1} = \frac{17}{14}\frac{NH_4^+ - N, mgNL^{-1} * 10^{pH}}{e^{\left(\frac{6344}{T(K)} + 10^{pH}\right)}} \quad (2.15)$$

$$FNA, mgNL^{-1} = \frac{46}{14}\frac{NO_2^- - N, mgNL^{-1}}{e^{\left(\frac{-2300}{T(K)} + 10^{pH}\right)}} \quad (2.16)$$

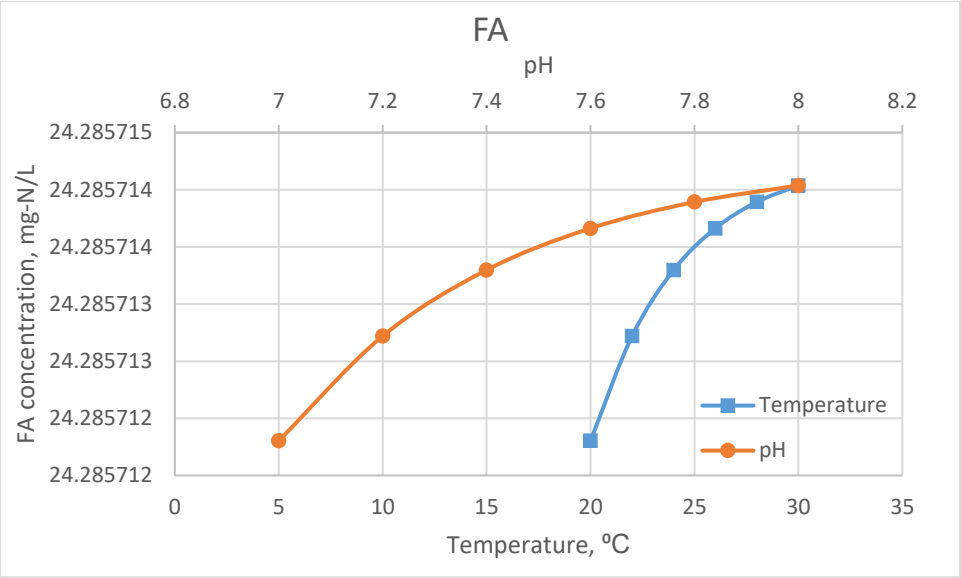

Figure 2. 7. Simulation of FA at increasing pH and temperature (NH_4^+=NO_2^-= 20 mg-N/L) based on Anthonisen et al. (1976).

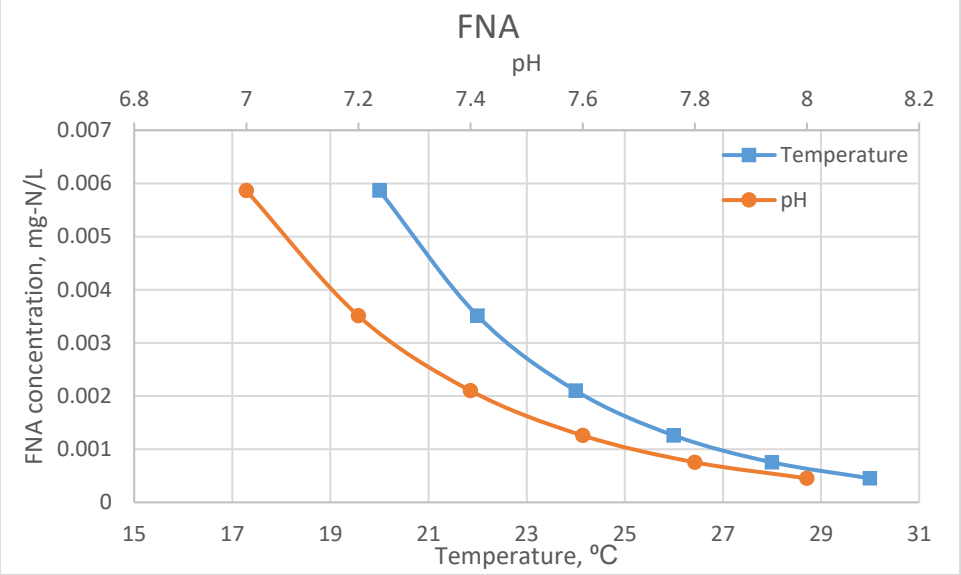

Figure 2. 8. Simulation of FNA at increasing pH and temperature (NH_4^+=NO_2^-= 20 mg-N/L) based on Anthonisen et al. (1976).

Inhibition of ANAMMOX bacterial activities has been reported at FA concentrations as low as 2 mg/L (Jaroszynski *et al.* 2012). According to Jaroszynski *et al.* (2012), FA diffuses through the cell membranes of bacterial cells, consequently changing the cytoplasmic pH and subsequently neutralising the membrane potentials, leading to cell death. At approximately 40 mg/L FA concentrations, about 50% reduction in specific ANAMMOX activity (SAA) was reported (Dapena-Mora *et al.* 2007; Fernández *et al.* 2012; Jaroszynski

et al. 2012). On the other hand, FNA affects SAA at much lower concentrations than FA (0.5 μg HNO_2-N/L) (Fernández *et al.* 2012). However, FNA inhibition of ANAMMOX activities has been demonstrated to be reversible, an indication that NO_2^- is only inhibitory and not toxic to ANAMMOX bacteria (Lotti *et al.* 2012b). The inhibitory effect of NO_2^- on ANAMMOX bacteria is also less in the presence of NH_4^+ than in its absence (Lotti *et al.* 2012b). Indeed, 50% and 30% loss in ANAMMOX activities were reported in the absence and presence of NH_4^+ (85 mg NH_4^+-N) (Lotti *et al.* 2012b), respectively.

In few studies, however, it has been suggested that aqueous NO_2^- is the inhibitor of ANAMMOX bacterial activities and not the FNA (Lotti *et al.* 2012b; Puyol *et al.* 2014). However, according to Puyol *et al.* (2014), at pH below 7.1, FNA is the main inhibitor while aqueous NO_2^- is the main inhibitor at pH above 7.1.

Besides the effect of temperature and pH on the FA and FNA concentrations, they could also seriously affect the metabolic activities of ANAMMOX bacteria, particularly at temperatures and pH below 20ºC and 6.5, and above 40 ºC and 9, respectively, (Egli *et al.* 2001; Oshiki *et al.* 2011; Hendrickx *et al.* 2014) (*table 2.1*). For instance, (Lotti *et al.* 2014b) reported a 20% decline in specific activity on the reduction of temperature from 20 ºC to 10 ºC. Yang *et al.* (2018) also reported a decline in NRRs on switching from side-stream (30-35 ºC) to mainstream conditions (20-26 ºC) while Laureni *et al.* (2015) reported a 90% decrease in NRRs when the temperature was gradually decreased from 29 ºC to 12.5 ºC. Since the growth rates of bacteria are functions of temperature (Isaka *et al.* 2008), low temperatures could considerably reduce the doubling times of ANAMMOX bacteria. According to Isaka *et al.* (2008), increasing or decreasing the temperature could result in a lapse in one or some of the enzymes involved in ammonium oxidation due to different optimum temperatures for the different enzymes.

The optimum growth temperatures and pH for different species of ANAMMOX bacteria reported in different studies are summarised in *table 2.1*. Within the ANAMMOX bacterial communities, marine species have been reported to have low optimal temperatures (≤25ºC) (Rysgaard *et al.* 2004; Kawagoshi *et al.* 2012). In literature, the reported activation energy of ANAMMOX bacteria ranges between 33 and 94 kJ/mol at the temperature range of 20 to 40ºC (*table 2.1*). In comparison, the average activation energies for NH_4^+ and NO_2^- oxidisers reported in the literature at 20ºC are approximately 68 and 44 kJ/mol, respectively (Wyffels *et al.* 2004).

Table 2. 1. A summary of the reported growth temperatures, pH and activation energies of ANAMMOX bacteria.

ANAMMOX bacteria	Growth temperature (ºC)	Optimum temperature (ºC)	Adaptation period (days)	Growth morphology	Activation energy (kJ/mol)	pH	Reference
Candidatus Brocadia fulgida	10	20-30	722	Suspended (MBR)	66	7.5	(Hendrickx *et al.* 2014)
Candidatus Brocadia fulgida	12	25	~200	Suspended (SBR)	-	7.3	(Hu *et al.* 2013)
Candidatus Kuenenia stuttgartiensis	~6-15	37	>200	encapsulated	28-37ºC (33) 22-28ºC (93) 6-22ºC (94)	7.2	(Isaka *et al.* 2008)
Candidatus Brocadia sinica	25-45	35–40	146	flocs	56±3	6.5 - 8.8	(Oshiki *et al.* 2011)
Candidatus Jettenia caeni	20–42.5	37	-	-	55.4 ± 6.8	6.5 – 8.5	(Ali *et al.* 2015a)
Candidatus Brocadia Anammoxidans	11-22	-	528	Suspended (UASB)	71 ± 3	8.1 ± 0.3	(Reino *et al.* 2018)

2.2.3 Salinity

The influence of salinity on ANAMMOX bacterial activities has also been studied and recorded previously (Dapena-Mora *et al.* 2007; Awata *et al.* 2015; Lin *et al.* 2020). The inhibitory salinity concentrations of ANAMMOX bacteria could be expected to vary with the species and the duration of acclimatisation (Kartal *et al.* 2006; Wei *et al.* 2016). Lin *et al.* (2020) recently indicated that the inhibitory salinity concentration for ANAMMOX bacteria could be lower in the presence of NO_2^- than in its absence. It is possible that with increasing salinity, ANAMMOX bacterial cells utilise more energy for maintenance and/or adjustments of osmotic cell pressures, consequently affecting the normal cell functioning (Dapena-Mora *et al.* 2007; Awata *et al.* 2015).

For marine species (*Candidatus* Scalindua spp.), enhanced nitrogen removal was reported at 0.5% - 3.5% salinity, while inhibition was reported at 4% salinity (Awata *et al.* 2015). In mixed cultures containing fresh-water and marine ANAMMOX bacteria, an increase in salinity could lead to population shifts towards the dominance of marine ANAMMOX

bacteria (Kartal *et al.* 2006). According to Kartal *et al.* (2006), fresh water ANAMMOX bacteria could adapt to high salinity better when gradual increment of salinity of the wastewater is made. However, Kartal *et al.* (2006) also reported that ANAMMOX bacterial community dominated by fresh water ANAMMOX bacteria could not adapt to NaCl concentrations above 30 g/l. Furthermore, at NaCl concentrations higher than 20 g/l, lower ANAMMOX activity was observed, and a complete loss of ANAMMOX activity at 60 g/L NaCl, even though 30% of ANAMMOX bacterial population was the marine species *Candidatus* Scalindua wagneri. Wei *et al.* (2016) also reported 85% nitrogen removal at 50 g/L NaCl concentration using marine ANAMMOX culture.

Dapena-Mora *et al.* (2007) reported a 50% reduction in ANAMMOX activities at 80 mM, 200 mM and 230 mM concentrations of Na_2SO_4, KCl, and NaCl, respectively, using fresh-water ANAMMOX culture *Candidatus* Kuenenia stuttgartiensis. According to Dapena-Mora *et al.* (2007), the lower inhibitory threshold of Na_2SO_4 than NaCl could be due to the presence of 2 sodium ions (Na^+) in Na_2SO_4 compared to NaCl. Carvajal-Arroyo *et al.* (2013) reported 50% inhibition of ANAMMOX activities at 93 ± 4 mM NaCl and complete inhibition at 200 mM for fresh-water ANAMMOX species *Candidatus* Brocadia spp.

2.2.4 Chemical oxygen demand to nitrogen (C/N) ratio

The presence of COD in wastewater could affect the normal functioning of ANAMMOX-mediated processes mainly due to the growth of heterotrophic bacteria in the reactors, which compete for oxygen with AOB, and NO_2^- with ANAMMOX bacteria (O'Shaughnessy 2015; Li *et al.* 2018). However, in sidestream wastewaters, C/N ratios are <1, while in mainstream wastewaters, it is >1 (Bowden, Stensel and Tsuchihashi 2015; O'Shaughnessy 2015; Li *et al.* 2018).

Besides supporting heterotrophic bacterial growth, some compounds contributing in the overall COD of the wastewater could be inhibitory to ANAMMOX bacteria. For instance, alcohols have been reported to irreversibly inhibit ANAMMOX bacterial activities, while some organic carbon compounds such as propionate have been reported to enhance ANAMMOX bacterial activities (Güven *et al.* 2005; Kartal *et al.* 2007). It has been suggested that methanol can be converted to formaldehyde by hydroxylamine oxidoreductase enzyme, which destroys enzymatic activities through irreversible cross-linking of peptide chains (Güven *et al.* 2005). Güven *et al.* (2005) reported immediate and irreversible inhibition of ANAMMOX activities at 0.5 mM methanol concentration, while

ethanol at 2 mM only resulted in a 30% loss of ANAMMOX activity. On the contrary, Güven *et al.* (2005) reported that ANAMMOX bacteria could oxidise propionate at approximately 0.8 nmol/g-protein-min to CO_2 using either NO_2^- or NO_3^- as the electron acceptor. It could be possible that ANAMMOX bacteria first reduce NO_2^- to NH_4^+ and then subsequently oxidise NH_4^+ to nitrogen gas through the normal pathway, or use the denitrification pathway (*figure 2.9*). Güven *et al.* (2005) reported that approximately 50% of the organic carbon is oxidised to CO_2 while less than 10% is incorporated into the cell biomass, contrary to Kartal *et al.* (2007) who argued that propionate oxidation only generates energy. In a different study, Dapena-Mora *et al.* (2007) reported enhancement in nitrogen gas production in an ANAMMOX-mediated reactor at 10 mM acetate concentration while at 25 mM and 50 mM acetate concentrations, there was 22% and 70% inhibition of ANAMMOX activities, respectively.

Niche segregation of ANAMMOX bacterial species in the presence of organic compounds has also been observed previously (Kartal *et al.* 2007; Kartal *et al.* 2008; Winkler, Kleerebezem and van Loosdrecht 2012) (*table 2.2*). In the presence of propionate, *Candidatus* Anammoxoglobus propionicus was reported to out-compete other ANAMMOX bacterial species (Kartal *et al.* 2007), while in the presence of acetate, *Candidatus* Brocadia fulgida dominated (Kartal *et al.* 2008; Winkler, Kleerebezem and van Loosdrecht 2012). This is probably due to the different rates of organic carbon utilisation by the different ANAMMOX bacterial species, leading to differential growth rates.

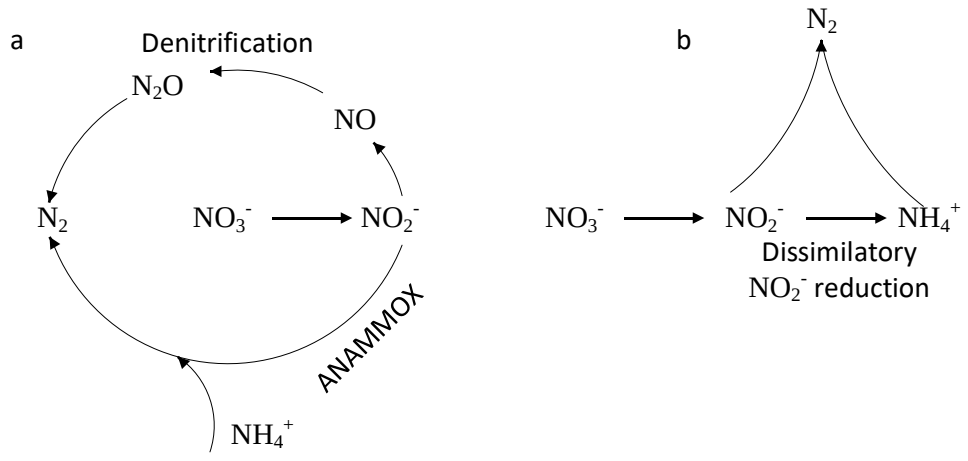

Figure 2. 9. Schematic model of nitrate reduction by ANAMMOX bacteria: a-denitrification pathway and pathway for nitrate reduction to nitrite then to nitrogen gas by ANAMMOX bacteria, b-dissimilatory nitrate reduction to NH_4^+ pathway based on a report by Güven et al. (2005).

Table 2. 2. A summary of the reported oxidation rates of propionate, formate and acetate by different ANAMMOX bacterial species.

ANAMMOX bacterial species	Organic carbon oxidation rate (μmol/g-protein-min)			References
	Propionate	Formate	Acetate	
Ca. Brocadia fulgida	0.88±0.02	3±0.22	1.5±0.06	(Kartal *et al.* 2008)
Ca. Brocadia anammoxidans	0.12±0.01	6.5±0.6	0.57±0.05	(Kartal *et al.* 2007)
Ca. Anammoxoglobus propionicus	0.64±0.05	6.7±0.6	0.79±0.07	
Ca. Kuenenia stuttgartiensis	0.12±0.01	5.8±0.6	0.31±0.03	
Ca. Scalindua sp.	0.36±0.05	5.2±0.1	0.78±0.19	(Awata *et al.* 2015)
-	0.0008	-	-	(Güven *et al.* 2005)

2.2.5 Sulphides and phosphates

Chemical and petrochemical wastewater may contain high levels of sulphide, while phosphates are readily available in wastewater because they are used in fertilizers and detergents (Carvajal-Arroyo *et al.* 2013). Both compounds could inhibit ANAMMOX bacterial activities (Dapena-Mora *et al.* 2007; Carvajal-Arroyo *et al.* 2013).

The sulphides in wastewater could be derived from sulphate reduction or mineralization of organic matter (Carvajal-Arroyo *et al.* 2013). Sulphide toxicity to ANAMMOX bacteria has previously been associated with undissociated H_2S. According to Dapena-Mora *et al.* (2007), sulphide concentration between 1 and 2 mM causes a decrease in ANAMMOX activities by 60%, and at ca. 5 mM, ANAMMOX activities are completely inhibited. Carvajal-Arroyo *et al.* (2013) reported 50% inhibition of ANAMMOX activities at 0.03 and 0.11 mM H_2S concentrations for suspended and granular biomass, respectively. It has been suggested that haem centers of cytochrome oxidase within the ANAMMOX bacterial cells interact with sulphide, causing the reduction of haem iron in cytochrome c, which in turn disrupts the ANAMMOX metabolic activities (Pietri, Román-Morales and López-Garriga 2011; Carvajal-Arroyo *et al.* 2013).

Phosphates, on the other hand, could enhance ANAMMOX bacterial activities at ≤155 mg-P/L, while at concentrations above 310 mg-P/L, there could be ca. 10% reduction in SAA (Zhang *et al.* 2016c). Phosphate inhibition could be due to dihydrogen phosphate ion ($H_2PO_4^-$), which bonds with complexes of substrate and enzymes, leading to the formation of triple-complexes, inhibiting ANAMMOX metabolic processes (Zhang *et al.* 2016c). According to Carvajal-Arroyo *et al.* (2013) and Dapena-Mora *et al.* (2007), ca. 25 mM and ca. 20 mM concentrations of phosphate, respectively, lead to 50% reduction in SAA.

2.2.6 Heavy metals

Heavy metals such as copper (Cu), zinc (Zn), cadmium (Cd), lead (Pb) and nickel (Ni) are found in municipal landfill leachates, effluents from fertiliser factories, effluents from digesters of dairy and piggery slurries, and the effluents from semiconductor manufacturing plants (Ochoa-Herrera *et al.* 2011; Kimura and Isaka 2014; Zhang *et al.* 2016d; Zhang *et al.* 2019). Most heavy metals accumulate in ANAMMOX granules through adsorption because extracellular polymeric substances (EPS) and surfaces of ANAMMOX bacterial cells contain amino, carboxylic, hydroxyl and phosphate functional groups (that are negatively charged) (Zhang *et al.* 2016d).

The SAA could decrease with heavy metal concentrations in wastewater and with the period of exposure time (Kimura and Isaka 2014; Zhang *et al.* 2019). Zhang *et al.* (2016d) reported 50%-loss in ANAMMOX activity on exposure to media containing 30 mg/L Cu and 25 mg/L Zn for 24 hours, while Kimura and Isaka (2014) reported 10% inhibition at 5 and 10 mg/L by copper and zinc. Lotti *et al.* (2012a) reported 50% loss in ANAMMOX activity on addition of 1.9 and 3.9 mg/l Cu and Zn, respectively. In addition, Zhang *et al.* (2016d) reported more acute inhibition on pre-exposure to Cu and Zn in the absence of substrate (NH_4^+ and NO_2^-) than in their presence.

Zhang *et al.* (2016d) suggested that Cu ions within ANAMMOX bacterial cells could chelate sulfhydryl groups, affecting the metabolic activities of ANAMMOX bacteria. In addition, Cu-induced rupture of cytoplasmic membranes may accelerate the accumulation of other heavy metals such as Zn, seriously affecting the normal functioning of ANAMMOX bacterial cells. Furthermore, Ni, Co and Mo were reported by Kimura and Isaka (2014) to inhibit 10% of ANAMMOX activity at 5,5 and 0.2 mg/L.

According to Kimura and Isaka (2014), the inhibition of Ni, Cu, Zn and Co is reversible. However, Mo-inhibition was reported by Kimura and Isaka (2014) to be irreversible,

probably because Mo replaces some metal in the proteins, inactivating the enzyme(s) and proteins.

2.3 Physiological and phylogenetic characteristics of ANAMMOX bacteria

Phylogenetic, cellular and molecular analyses place ANAMMOX bacteria under the phylum *Planctomycetes* and the order *Brocadiales*. All the known ANAMMOX bacterial species bear taxonomical status '*Candidatus'* because none of them was obtained as pure culture (Kartal *et al.* 2013).

The known species are grouped under five genera (Kartal *et al.* 2013; Park *et al.* 2017b):

1. *Candidatus* Kuenenia under which 'Kuenenia stuttgartiensis' falls
2. *Candidatus* Brocadia under which 'Brocadia anammoxidans', 'Brocadia fulgida', 'Brocadia caroliniensis' and 'Brocadia sinica' are grouped
3. *Candidatus* Anammoxoglobus with one known species ('Anammoxoglobus propionicus')
4. *Candidatus* Jettenia in which 'Jettenia asiatica' and 'Jettenia caeni' fall
5. *Candidatus* Scalindua with four species ('Scalindua brodae', 'Scalindua sorokinii', 'Scalindua wagneri' and 'Scalindua profunda')

Within the genus *Candidatus* Brocadia, *Candidatus* Brocadia sp. 40, *Candidatus* Brocadia sp. 1 and *Candidatus* Brocadia sp. 2 have also been discovered (Park *et al.* 2010a; Bhattacharjee *et al.* 2017).

ANAMMOX bacterial cells are coccoid in shape with diameters ranging between 0.8 and 1.1 µm (Kartal *et al.* 2013; Erdim *et al.* 2018). The internal structure of ANAMMOX bacteria combines the features of archaea, bacteria and eucarya (Erdim *et al.* 2018). In addition, ANAMMOX bacterial cells consist of three compartments each surrounded by two layers of membrane typical of *Planctomycetes (Kartal et al. 2013) (figure 2.10)*. The outermost membrane, enclosing both the cell and the outer compartment, the paryphoplasm, constitute the cell wall together with a thin peptidoglycan (Kartal and Keltjens 2016). The second membrane, surrounds riboplasm harbouring both nucleoid and ribosomes. Anammoxosome, the central cell structure is bounded in the third highly curved innermost membrane. Several *heme c* proteins including hydroxylamine oxidoreductase (HAO)-like proteins, hydrazine synthase (HZS) and nitrite-nitrate oxidoreductase complexes which are involved in catabolism are harboured in the anammoxosome (Kartal *et al.* 2013; Kartal and Keltjens

2016). The energy released in the ANAMMOX process is conserved by adenosine triphosphate synthase (ATPase) which is bounded by a membrane (Kartal *et al.* 2013). ANAMMOX membranes are composed of glycerolipids just like all other living organisms (Kartal *et al.* 2013). The glycerolipids contain ester-linked fatty acids, which is common with bacteria and Eukarya, or ether-linked long-chain alcohols which is common with Archaea (Kartal *et al.* 2013). The presence of saturated C17-C20 fatty acids and alcohols fused with *cis*-ring junctions to make ladder-like cyclobutane rings, with or without cyclohexane rings, making ANAMMOX bacteria special. The fatty acids are esterified with glycerol or methanol backbone and the alcohols are ether-linked in different directions to glycerol (Kartal *et al.* 2013; Kartal and Keltjens 2016).

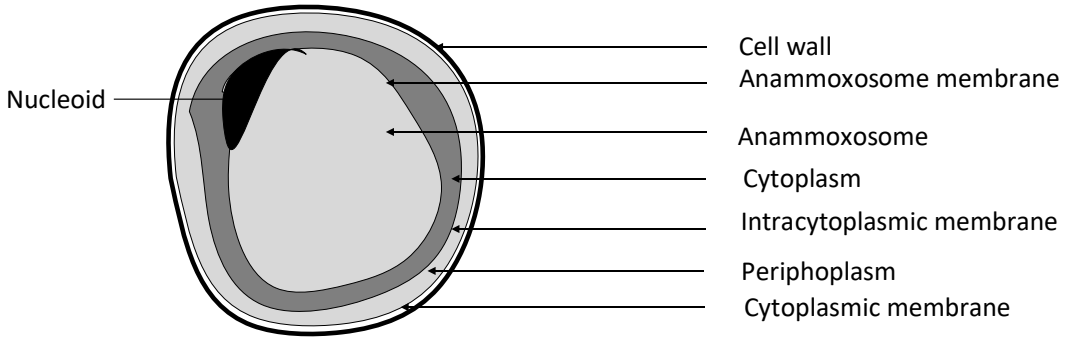

Figure 2. 10. The cell plan of ANAMMOX bacterium based on Kartal and Keltjens (2016)

2.4 Enrichment of ANAMMOX bacteria

Following the discovery of ANAMMOX bacteria in a BNR system in the mid-1990s (Mulder *et al.* 1995), several ensuing studies reported their presence in the WWTPs, oceans, soil sediments and fresh-water bodies (Rysgaard *et al.* 2004; Wang *et al.* 2012a; van de Vossenberg *et al.* 2013; Nejidat *et al.* 2018). After the discovery, the first enrichment of ANAMMOX bacteria in a laboratory reactor was reported by van de Graaf *et al.* (1996) in a 2.5L fluidised bed reactor (FBR). The composition of the synthetic media used in their study has since been adopted in several other lab-scale studies (*table 2.3*). The enrichment of ANAMMOX bacteria has since been undertaken in reactors of different configurations (*table 2.3*). The ratios of NO_2^--N consumed to NH_4^+-N consumed ($\Delta NO_2^-/\Delta NH_4^+$) as well as the NO_3^--N produced to the NH_4^+-N consumed ($\Delta NO_3^-/\Delta NH_4^+$) are used to determine when the ANAMMOX process is the dominant nitrogen removal pathway in nitrogen removal systems (Strous *et al.* 1998).

Wang *et al.* (2012b) demonstrated that reactor configuration has an impact on the duration of the start-up period of ANAMMOX process. In their study, they reported that a membrane

reactor was started up in 59 days, while SBR could only be started up in 101 days. Chen *et al.* (2012) also reported faster start-up of ANAMMOX process in an up-flow reactor with bamboo charcoal compared with a reactor without any carrier materials, an indication that biomass retention plays an important role during reactor start-up.

From the studies summarised on *table 2.3*, only the study by Hendrickx *et al.* (2014) enriched ANAMMOX bacteria at low temperatures which are not ideal for the growth of ANAMMOX bacteria (Wu *et al.* 2020), and hence the observed long start-up period of 412 days. This is because ANAMMOX activities are slower at low temperatures compared to high temperatures (Lotti, Kleerebezem and van Loosdrecht 2015). However, previous findings have indicated that the optimal growth temperatures vary with the ANAMMOX bacterial species *(table 2.1*).

Table 2. 3. A summary of enrichment studies of ANAMMOX bacteria in different reactor configurations

	Source of inoculum	Reactor configuration	Duration of start-up period (days)	Operating conditions	Remarks	Reference
1	WWTPs	Gas-lift reactor (GLR)	412	Anoxic, 20 ºC	Membrane modules used to retain biomass; van de Graaf *et al.* (1996) media	(Hendrickx *et al.* 2014)
2	WWTP	Membrane aerated biofilm reactor (MABR)	80	CANON, 31.3 ± 0.7 ºC	van de Graaf *et al.* (1996) media	(Augusto, Camiloti and Souza 2018)
3	WWTP	Sequencing batch reactor (SBR)	-	Anoxic, 35 ºC	van de Graaf *et al.* (1996) media	(Dapena-Mora *et al.* 2004d)
4	WWTP	Moving bed biofilm reactor (MBBR)	100	Anoxic, 20 ºC	Ring-shaped carriers	(Zekker *et al.* 2012)
5	WWTP	Up-flow Anaerobic Sludge Blanket reactor (UASB)	117	Anoxic, 30 ± 1 °C	van de Graaf *et al.* (1996) media	(Chen *et al.* 2012)
6	Marine sediment	SBR	90 days	Anoxic, 15–23°C	Feed media containing Red Sea salt	(Van De Vossenberg *et al.* 2008)
7	WWTP	Continuously stirred tank reactor (CSTR)	80 days	Anoxic, 20 ºC	van de Graaf *et al.* (1996) media; gel encapsulated biomass	(Bae *et al.* 2015)

2.5 Microbial ecology of ANAMMOX-mediated nitrogen removal systems

Since the discovery of ANAMMOX bacteria in mid-1990s (Mulder *et al.* 1995), a lot of research efforts have been made leading to a better understanding of their physiology and ecology. All the ANAMMOX bacteria that have so far been discovered belong to the phylum Planctomycetes, order *Candidatus* Brocadiales and family *Candidatus* Brocadiaceae *(Kartal et al. 2013)*. All the discovered ANAMMOX-bacterial species fall into either of the following genera: *Candidatus* Brocadia, *Candidatus* Jettenia, *Candidatus* Kuenenia, *Candidatus* Anammoxoglobus or *Candidatus* Scalindua (Kartal *et al.* 2013).

However, the bacterial communities in ANAMMOX-mediated systems are diverse, and bacteria, protozoans, viruses and archaea are known to co-exist together (Bae, Chung and Jung 2010; Suarez, Persson and Hermansson 2015). Within the bacterial community, the co-existence of ANAMMOX bacteria with nitrifying bacteria (AOB, NOB and COMAMMOX bacteria, and heterotrophic bacteria have been reported in several studies (Bhattacharjee *et al.* 2017; Li *et al.* 2017b; Gu *et al.* 2018; Yang *et al.* 2018). AOB (*Ca. Nitrosoglobus* spp., *Nitrosovibrio* spp., *Nitrosospira* spp., *Nitrosomonas* spp., *Nitrosococcus* spp.) fall within the phylum Proteobacteria, whilst the NOB are spread among the phyla Nitrospirae, chloroflexi (*Nitrolancea hollandica*), Nitrospina and Proteobacteria (*Nitrobacter* spp. and *Nitrococcus* spp.) (Prosser 2005). Aerobic heterotrophs, fermentative organisms and denitrifiers are distributed across Bacteroidetes, Ignavibacteriae, Armatimonadetes, Chlorobi, Acidobacteria and Chloroflexi phyla, amongst many other phyla (Speth *et al.* 2016).

The abundance of heterotrophic bacteria could vary with the C/N ratios of the influent wastewaters. The C/N ratios, in turn, could vary with the type of sludge treated, pre-treatment method, digestion and de-watering processes (Gu *et al.* 2018; Zhang *et al.* 2018). However, typical sidestream wastewater has a C/N ratio well below 1 (*tables 2.4 and 2.5*). On the contrary, mainstream wastewaters have higher C/N ratios (>1) than the sidestream wastewaters (Constantine *et al.* 2016; Li *et al.* 2018). Therefore, in order to stabilise mainstream ANAMMOX-mediated systems, carbon removal and/or diversion normally precede nitrogen removal (Lotti *et al.* 2015; Li *et al.* 2018); carbon removal/diversion in the first stage (A-process) and nitrogen in the second stage (B-process).

2.5.1 Growth of nitrifying and ANAMMOX bacteria in suspended-growth ANAMMOX-mediated systems

Affinity for substrate could drive niche segregation between different bacterial groups, with *K*-strategists (bacteria with high affinity for substrate) outcompeting *r*-strategists (bacteria with high maximum specific growth rates) at low-substrate concentration systems, while the *r*-strategists outcompete the *K*-strategists in high-substrate concentration systems (van der Star *et al.* 2008; Park *et al.* 2015). In some instances, heterotrophic bacterial groups including *Prosthecobacter* that consume oxygen, N-acetylglucosamine and ammonium, could induce substrate limitation leading to the selection of autotrophic *K*-strategists over *r*-strategists (Gonzalez-Martinez *et al.* 2016). *Nitrosomonas* spp., *Nitrobacter* spp. and *Candidatus* Brocadia spp. are regarded as *r*-strategists while *Nitrosospira* spp., *Nitrospira* spp. and *Candidatus* Kuenenia spp. are regarded as *K*-strategists (Park *et al.* 2015; Gonzalez-Martinez *et al.* 2016).

Park *et al.* (2010a) demonstrated that the key factors influencing the diversity of microbial communities in ANAMMOX-mediated systems are the operating conditions. In contrast, Date *et al.* (2009) had earlier reported that the diversity of microbial communities in ANAMMOX-mediated systems depend on the inoculum. Park *et al.* (2010a) reported that in both an anaerobic granular reactor and PN/A MBBR, *Candidatus* Brocadia sp. 40 dominated although the two systems were inoculated with biomass from different sources, but fed with centrate from the same WWTP. Similarly, NOB and AOB communities were comparable in both systems: *Nitrobacter* and *Nitrosomonas eutropha,* respectively. The dominance of *Nitrobacter* spp. and *Nitrosomonas* spp. in both systems might have been expected as the substrate concentrations were quite favourable to both groups of bacteria (granular reactor: 490±194 mgNH_4^+-N/L and 518±222 mgNO_2^-N/L, MBBR: 616±165 mgNH_4^+-N/L and 2.5-3 mg-O_2/L during aeration period) (Park *et al.* 2015). It appears that *Candidatus* Brocadia spp. proliferate easily in ANAMMOX-mediated systems treating COD-containing wastewaters (*table 2.4*), as they have been previously linked with COD consumption, giving them an added advantage over other species (Winkler, Kleerebezem and van Loosdrecht 2012). The dominance of *Nitrosomonas* spp. could also be expected in sidestream ANAMMOX-mediated systems because of the high ammonia concentrations (Park *et al.* 2010a) (*table 2.4*). Although none of the previous studies reported on the dominance of *Nitrosococcus*-like bacteria in ANAMMOX-mediated systems, Fumasoli *et al.* (2017) recently reported their growth at pH below 6. Between *Nitrospira* and *Nitrobacter*-

related species, the prevailing DO concentrations could drive niche segregation between the two groups, with *Nitrospira* expected to dominate at DO concentrations below 0.5 mg/L whilst *Nitrobacter* could dominate at DO concentrations above 1 mg/L as *Nitrobacter* have lower affinity for oxygen than *Nitrospira* (Park, Park and Chandran 2017).

In SBRs, regulating the duration of the settling phases maintains an optimal fraction of flocculent biomass in the reactors is widely believed to regulate the growth of NOB in the reactors through washout (Bowden, Stensel and Tsuchihashi 2015; Val del Río, Campos Gómez and Mosquera Corral 2016). Recent reports, however, have indicated that shortening the settling periods could not only destabilise the process performance but also increase the abundance of NOB in the granular biomass, particularly the *Nitrospira* spp. (Li *et al.* 2019).

Table 2. 4. AOB, NOB and ANAMMOX bacterial species in suspended-growth ANAMMOX-mediated systems.

	Influent concentrations				DO (mg-O_2/L)	T(ºC)	HRT (hrs)	NRR (gN/m^3/d)	Dominant bacteria species			Other detected bacterial species			Remarks	References
	NH_4^+-N (mg/L)	NO_2^-N (mg/L)	NO_3^- N (mg/L)	COD (mg/L)					AOB	NOB	AMX	AOB	NOB	AMX		
1	1615±68.5	0.0±0.1	0.2±0.3	204±43	<0.4	30-35	15.3 - 717.6	830	-	-	*Ca. Brocadia* spp. ~ 51%	-	-	*Ca.* Kuenenia spp. ~ 49%	Full scale SBR	(Yang *et al.* 2016)
2	1,230±61	-	-	400±57	-	32ºC	24	297±27	*Nitrosomonas europaea*	-	*Candidatus* Kuenenia stuttgartiensis	-	-	-	Two-stage PN/A; filtrate as feed	(Kotay *et al.* 2013)
4	490±194	518±222	-	-	-	35	-	-	-	*Nitrobacter* spp.	*Candidatus* Brocadia sp. 40	-	*Nitrospira* spp.	*Candidatus* Brocadia fulgida	Partially nitrified centrate feed	(Park *et al.* 2010b)
5	1420 ± 130	0.9 ± 0.1	0.3 ± 0.1	841 ± 186	-	-	-	0.0033	-	-	*Ca.* Brocadia spp.	-	-	-	Regular sidestream WW*	(Gu *et al.* 2018)
6	2190 ± 280	0.1 ± 0.1	0.4 ± 0.2	3290 ± 640	-	-	-	-	-	-	*Ca.* Brocadia spp.	-	-	-	Thermally hydrolysed WW*	
7	176 - 839	-	-	43.7 - 110.3	≤0.38	32 ± 2	-	0.42 - 0.80	*Nitrosomonas* spp.	-	*Ca.* Brocadia spp.	-	-	-.	PN/A SBR; SWW	(Cheng *et al.* 2017)
					≤1.5			0.18-1.23	*Nitrosomonas* spp.	-	*Ca.* Brocadia spp.				PN/A SBR; SWW	

AMX – ANAMMOX bacteria, WW - wastewater, SWW - synthetic wastewater, *anaerobic system

2.5.2 **Growth of nitrifying and ANAMMOX bacteria in attached-growth ANAMMOX-mediated systems**

Comparative studies of attached-growth and granular systems have reported similarities in bacterial communities even in systems started with different inocula (Park *et al.* 2010a; Guo *et al.* 2016; Bhattacharjee *et al.* 2017). However, Park *et al.* (2015) found that the ratio of *Nitrospira* spp. in biofilms to suspension increased with the reduction in HRT, whilst that of *Nitrobacter* spp. remained largely unchanged. Because of high affinities for oxygen, *Nitrospira* spp., can adapt well to biofilm conditions (Park *et al.* 2015). It is interesting that some *Nitrospira* spp. are evolutionarily connected to ANAMMOX bacteria and share similar forms of the enzyme nitrite oxidoreductase (*nxr*) and other proteins involved in metabolic activities (Lucker *et al.* 2010). *Nitrobacter* spp., on the other hand, not only has lower affinity for both oxygen and nitrite, but also has lower biomass yield than *Nitrospira* spp. (Park, Park and Chandran 2017). Indeed, literature survey revealed the out-competition of *Nitrospira* spp. by *Nitrobacter* spp. at DO concentrations above 1 mg-O_2/L (*table 2.5*). The selection of *Nitrosomonas* spp. and *Candidatus* Brocadia spp. was commonly reported in attached-growth systems (*table 2.5*), similar to that of suspended-growth systems (*table 2.4*), which hints that the selection is mainly based on operating conditions and not the growth morphology, in line with Park *et al.* (2010a), Agrawal *et al.* (2017) and Guo *et al.* (2016).

Table 2. 5. AOB, NOB and ANAMMOX bacterial species in attached-growth ANAMMOX-mediated systems

	Influent concentrations				**DO (mg-O_2/L)**	**T (ºC)**	**HRT (hrs)**	**NRR (gN/m^3/d)**	**Dominant bacteria species**			**Other detected bacterial species**			**Remarks**	**References**
	NH_4^+-N (mg/L)	**NO_2^-N (mg/L)**	**NO_3^-N (mg/L)**	**COD (mg/L)**					**AOB**	**NOB**	**AMX**	**AOB**	**NOB**	**AMX**		
1	761-837	-	-	-	1.1-1.7	10-19	1.7 - 3.7	0.17-1.67[a]	*Nitrosomonas* spp. *Clone14*	*Nitrobacter* spp.	*C.* Brocadia sp.40	-	*Nitrospira* spp.	-	200L pilot scale MBBR	(Persson *et al.* 2014)
2	616 ± 165	-	-	-	2.5-3	-	-	3.1[a]	*Nitrosomonas eutropha*	*Nitrobacter* spp.	*C.* Brocadia sp.40	-	*Nitrospira* spp.	-	4L centrate fed PN/A MBBR	(Park *et al.* 2010a)
3	1460–1750	0.3–2.2	1.1–2.3	500-800	0.3–0.5	27-30	48-72	0.41	*Nitrosomonas* spp.	-	*C.* Brocadia spp.	-	-	-	832 m^3 full scale SNAD reactor	(Xu *et al.* 2018)
4	120-920*	1.07**	-	400±57	-	-	-	86±2 [b]	-	-	*C.* Brocadia spp.[#]	-	-	-	2-stage partially nitrified centrate feed	(Bhattacharjee *et al.* 2017)

[a] gN/m^2.d; AS – activated sludge; AMX – ANAMMOX bacteria; SNAD-simultaneous partial nitrification, ANAMMOX and denitrification, *influent for 1st stage aerated reactor, ** NO_2^-N/ NH_4^+-N ratio, [b]-total inorganic nitrogen removal (%), [#]new species

2.6 Reactor configurations for full-scale applications of ANAMMOX-mediated processes

The development of ANAMMOX-mediated nitrogen removal has increased since the installation of the first full-scale plant in the Rotterdam (van der Star *et al.* 2007; Lackner *et al.* 2014). As of 2014, 88% of the over 100 full-scale plants worldwide were sequencing batch reactors (SBRs) (Lackner *et al.* 2014). According to Bowden, Stensel and Tsuchihashi (2015), granular systems were the second most popular, while moving bed biofilm reactors (MBBRs) were the third most popular for full-scale applications. Few applications of ANAMMOX-mediated processes in rotating biological contactors (RBCs) and new activated sludge (NAS) were also reported by Bowden, Stensel and Tsuchihashi (2015), while only one full-scale system employing gel encapsulation was reported by Isaka *et al.* (2017). However, most of the reported full-scale installations are in Europe and all of them are designed for sidestream wastewater treatment (Bowden, Stensel and Tsuchihashi 2015), except for the recent modifications incorporating mainstream applications of ANAMMOX (Wett *et al.* 2015; Constantine *et al.* 2016).

In SBR configurations, feeding, reaction/aeration, settling and decanting are sequenced (Yang *et al.* 2016). This is largely necessitated by the need to control the concentration of dissolved oxygen (DO) and the retention of biomass rich in the slow growing ANAMMOX bacteria, while wasting the slowly settling-flocculent biomass rich in the NOB (Li *et al.* 2019). However, the nitrogen removal capacity of the SBRs is lower than that of continuous granular systems (Lackner *et al.* 2014).

Continuously operated granular systems include the internal circulation (IC) reactors and Up-flow anaerobic sludge blanket reactors (UASB) and expanded granular sludge bed reactor (EGSB) (Castro-Barros *et al.* 2015; Wang and Zheng 2017). The IC reactor configuration was applied in the first full-scale ANAMMOX-mediated system developed in Rotterdam, Netherlands (van der Star *et al.* 2007), and since then other IC configurations have been developed by Paques, which is behind the SHARON/ANAMMOX process (Bowden, Stensel and Tsuchihashi 2015).

In the MBBR configuration, biofilms develop on carrier materials which have density less than that of water, allowing them to move around during stirring with the motion of water *(section 2.7*). The carrier materials could be open-ended cylinders with protected inner surfaces, hollow spheres or thin discs with honey comb-like compartments on either side

(Almstrand *et al.* 2014; Kanders *et al.* 2014; Bowden, Stensel and Tsuchihashi 2015). On the contrary, in the RBCs, biofilms develop on discs mounted on a rotating shaft which is positioned just above the water while ca. 45% of the disc surfaces are submerged at all times (Clark, Moseng and Asano 1978; Lackner *et al.* 2014). The rotation of the shaft is used to control access to oxygen and the substrate (Lackner *et al.* 2014).

In the NAS process, the treatment is configured with three or four reactors, each containing activated sludge (Desloover *et al.* 2011; Bowden, Stensel and Tsuchihashi 2015). In the first reactor, DO is kept low in order to allow for nitrite to accumulate, while the second reactor is maintained under anaerobic conditions, enabling ANAMMOX bacteria to grow (Desloover *et al.* 2011; Bowden, Stensel and Tsuchihashi 2015). The third and fourth reactors are mainly for effluent polishing through nitrification/denitrification (Desloover *et al.* 2011).

A survey of ANAMMOX-mediated full-scale systems that was conducted by Lackner *et al.* (2014) revealed that SBRs had lower NRRs compared to biofilm-based systems including granular and MBBR systems. Many factors could inform the selection of one reactor configuration over another. These factors could range from the capital costs to the characteristics of the wastewater to be treated (Bowden, Stensel and Tsuchihashi 2015; O'Shaughnessy 2015). However, despite the vast knowledge accumulated over the years on the ANAMMOX process, a lot is still not clearly understood, including the unexplained system failures in full-scale applications (Lackner *et al.* 2014). Although sulphide, substrate and oxygen inhibition of ANAMMOX-mediated processes have been associated with some of these failures (Joss *et al.* 2011; Lackner *et al.* 2014), the performance of different reactor configurations under a wide range of these conditions has not been explored. In addition, the impact of reactor configuration on the growth of different bacterial groups has not been adequately addressed in the currently existing literature despite the findings by Arnaldos *et al.* (2017), Chu, van Veldhuizen and van Loosdrecht (2003) and Wells *et al.* (2017) highlighting its possible impact on the growth of microorganisms with different substrate affinities.

2.7 Biomass retention in ANAMMOX-mediated systems

Sufficient ANAMMOX bacterial consortia must be retained within ANAMMOX-mediated systems as unchecked washout of biomass could affect process performance since ANAMMOX bacteria have long doubling periods (2.1-11 days) (van der Star *et al.* 2007;

Fernández *et al.* 2008; Zhang *et al.* 2017b). For this purpose, different biomass retention strategies have been employed in ANAMMOX-mediated systems, viz. granulation, biofilm development, gel encapsulation, application of membranes and hydrocyclones for biomass separation from the effluent (Lackner *et al.* 2014; Isaka *et al.* 2017; Klaus *et al.* 2017).

2.7.1 Suspended-growth ANAMMOX-mediated systems

Among the full-scale ANAMMOX-mediated systems, SBR configuration is the most popular (Lackner *et al.* 2014), owing to its excellent biomass retention efficiency, homogeneous substrate distribution, simplicity and flexibility of operation (Vázquez-Padín *et al.* 2013). In the SBR configuration, the AOB grow mainly in the flocculent biomass, while the ANAMMOX bacteria grow mainly in the granular biomass (Yang *et al.* 2016). However, the proportion of flocculent and granular biomass in the SBRs could depend on the operational regime such as the duration of settling phases and the intensity of mixing (Cheng *et al.* 2017).

The sequencing of operations in the SBRs allows for the enrichment of AOB in the aerobic phase and ANAMMOX bacteria in the anoxic phase. Moreover, alternation of aerobic and anoxic phases could favour AOB growth over NOB growth since NOB have longer enzymatic lag-phases than the AOB in transitioning from the anoxic to aerobic conditions (Wett 2007). This is particularly important in limiting NOB growth in the reactors, in addition to maintenance of low DO as is the practice with most SBR-based process control strategies (Innerebner *et al.* 2007; Jeanningros *et al.* 2010). However, poor settling of biomass in SBRs due to the attachment of nitrogen bubbles on the biomass could present challenges to biomass retention in SBRs (Dapena-Mora *et al.* 2004a). Once-off addition of flocculants and/or the avoidance of short air pulses at the beginning of settling phases could eliminate this setback (Joss *et al.* 2009). In addition, the inclusion of short stirring periods towards the end of the operational cycle without the addition of substrate could also limit biomass floatation in the settling phase (Dapena-Mora *et al.* 2004a). Furthermore, system modification with the incorporation of a settler, as well as the extension of reaction phase to allow complete utilisation of NO_2^- before the settling phase begins would eliminate gas production in the settling phase, mitigating biomass floatation (Dapena-Mora *et al.* 2004a). The incorporation of hydrocyclones or screens on the effluent lines could also be useful in retaining biomass washed out of the reactors during effluent withdrawal. This could be particularly useful in stabilising process performance as increased washout could have disastrous implications on process stability (Arrojo *et al.* 2006).

Shear stress due to mixing could detach biomass from the granule surfaces, leading to washout of biomass on granule surface, mostly AOB and NOB, as they are located on the outer layers (*figure 2.13*), while ANAMMOX bacteria which grow in the inner layers of granules could be protected from these shear forces (Strous *et al.* 1998). However, if the mixing forces are too strong, they could cause granule disintegration leading to washout, consequently affecting process performance. Indeed, Arrojo *et al.* (2006) reported a decrease in process performance by ca. 40% on increasing stirring speed from 180 revolutions per minute (rpm) to 250 rpm in a lab-scale anaerobic ANAMMOX-mediated SBR, which was accompanied by 400% increase in the biomass washout. Literature survey revealed that mixing speeds between 50 and 120 revolutions per minute (rpm) in lab-scale ANAMMOX-mediated systems are common (Dapena-Mora *et al.* 2004a; Dapena-Mora *et al.* 2004b; Third *et al.* 2005; Fernández *et al.* 2009), which are lower than that reported by Arrojo *et al.* (2006).

In continuous systems such as up-flow reactors such as UASB (up-flow anaerobic sludge blanket), EGSB (expanded granular sludge bed) and IC (internal circulation), granulation is crucial for successful operations (Dolfing 1986; Wang and Zheng 2017). Unlike the SBRs, continuous reactor systems are characterised by higher biomass concentrations and NRRs than the SBRs (Lackner *et al.* 2014). As a consequence, the nitrogen loading rates (NLRs) in sidestream up-flow reactors (0.9-7 kg-N/m^3-day) are higher than for sidestream SBRs (0.04-0.65 kg-N/m^3-day) (Lackner *et al.* 2014).

However, due to the absence of external mixing in the UASB reactor configuration is not included, mass transfer limitations could affect process performance (Reino and Carrera 2017). On the contrary, in both IC and EGSB reactor configurations, due to the higher fluid velocities than in the UASB reactor configurations, and as a result, mass transfer in those configurations could be better enhanced than in the UASB reactor configuration (Reino and Carrera 2017). In addition, due to the lower fluid velocities in UASB reactors than in both EGSB and IC reactors, the accumulation of inert particles in UASB reactors could reduce the capacity of the reactors. Although mixing of reactors through gas circulation and/or increasing liquid flow rates could result in higher mass transfer of substrate to bacteria in both EGSB and IC reactors than in UASB, high velocities of liquids and gases could disrupt granular structures and/or increase washout of biomass. Therefore, the control of reactor hydrodynamics through process design and control is paramount. However, detachment of biomass from granules, and the control of physical properties of granules (such as density,

size, shape, porosity and texture), present challenges as there is no applicable design rule for their mitigation.

In mixed systems such as SBRs and IC reactors, shear stress from the mixing forces could shear off some biomass from the granules leading to reduction in the granule sizes. Although reduction of granule sizes would increase the surface area of biomass aggregates, and consequently improve mass transfer, if too small aggregates were produced as a result of strong mixing forces, it could lead to poor biomass settleability. On the other hand, however, strong shear forces could yield smooth and strong granules, while weak shear forces could result in rough and fluffy granules as was reported by Kwok *et al.* (1998).

According to Wu *et al.* (2009), strong shear conditions of approximately 8 s^{-1} shear rate, promote faster biomass granulation than more violent conditions (shear rate of ca. 12 s^{-1}) and low shear rates (0.05 s^{-1}). Better granulation at strong shear rate than at violent and low shear rates could be due to enhanced EPS (extracellular polymeric substances) secretion by bacteria in response to increase in shear stress, which benefit nucleation of bacterial cells (Wu *et al.* 2009). However, under violent conditions, over production of EPS weakens the biomass aggregates, leading to aggregate disruption and washout, while low EPS secretion at 0.05 s^{-1} shear rate limits nucleation (Wu *et al.* 2009).

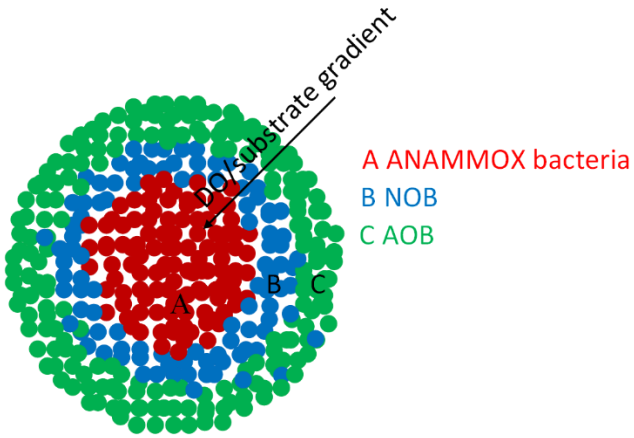

Figure 2. 11. Conceptualised stratification of AOB, NOB and ANAMMOX bacteria in the granules.

The incorporation of hydrocyclones into the ANAMMOX-mediated systems has made the retention of biomass in the effluent feasible (Shi, Wells and Morgenroth 2016). This could be implemented by applying centrifugal force at approximately 2 bars on sludge recycle flows which strip the less dense flocs into the overflow, and the denser granular biomass rich in ANAMMOX bacteria into the underflow, which could then be recycled back into the

reactors (Wett *et al.* 2010; Daigger *et al.* 2011) (*figures 2.12 and 2.13*). The solid retention times (SRTs) of AOB and ANAMMOX bacteria in such systems could thus be adjusted separately from the hydraulic retention times (HRTs) by installing hydrocyclones on the waste activated sludge lines of both mainstream and sidestream ANAMMOX-mediated systems (Wett *et al.* 2010) (*figure 2.13*). In addition, whenever recirculation of biomass into sidestream systems is not necessary, the hydrocyclones could still play a crucial role in the development of mainstream ANAMMOX-mediated systems as the biomass in the effluent from sidestream systems can be retained using hydrocyclones and then bio-augmented into the mainstream systems (*figure 2.15*) (Wett *et al.* 2015). Bio-augmentation of both AOB and ANAMMOX bacteria into mainstream systems from sidestream systems could be useful in suppressing NOB growth within the mainstream systems as AOB and ANAMMOX bacteria present competition to them for oxygen and NO_2^-, respectively (Wett *et al.* 2015).

According to Daigger *et al.* (2011), 90% of the bacterial activity in the underflow of the hydrocyclone, which constitute about 10-20% of the total flow, could be related to ANAMMOX. However, the unintended selection of NOB, particularly *Nitrospira* spp., together with ANAMMOX bacteria in granules, and an increase in the ratios of NOB to AOB populations with the increase in aggregate sizes has been reported in mainstream systems using hydrocyclones for biomass retention (Constantine *et al.* 2016). This is probably because *Nitrospira* have higher affinities for oxygen than AOB, making them more competitive at DO (<1 mg/L) than the AOB, and hence they could adapt to the conditions within the granules (Wett *et al.* 2013; Regmi *et al.* 2014).

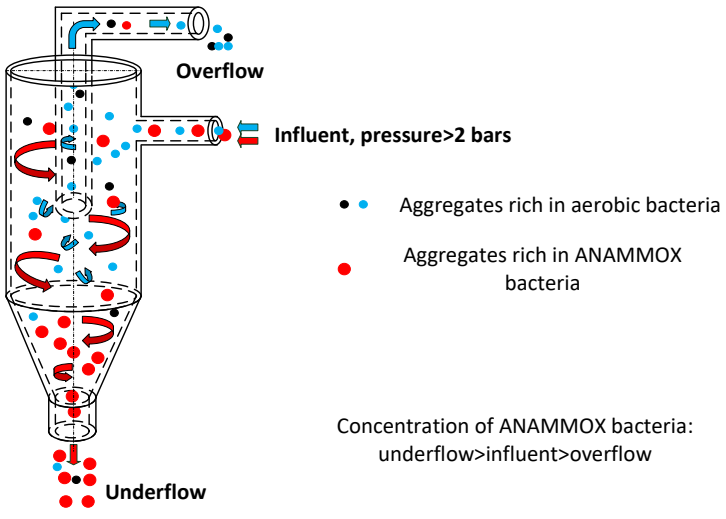

Figure 2. 12. Schematic diagram of biomass separation in a hydrocyclone.

Besides hydrocyclones, screens could also be used in ANAMMOX-mediated systems to retain biomass washed out of the reactors (Han *et al.* 2016). Screen usage involves the application of physical (tangential or normal) forces on the suspended sludge (containing flocs and granules) on a screen mesh. The size of screen mesh could determine the size of particles retained on it, as well as the vacuum applied, the washing volume/velocity, or the applied forces (Murthy *et al.* 2014). The compressible aggregates (mainly flocs) are pushed through the screens during washing, while the non-compressible aggregates (granules) are retained on the screens. The tangential forces, on the other hand, depending on the applied shear frequency, intensity or duration, could shear off the fast-growing (superficial) biomass from the surfaces of the slow-growing biomass (Murthy *et al.* 2014).

Han *et al.* (2016) reported better retention of granular biomass rich in ANAMMOX bacteria on switching from vacuum screens to vibrating screens in a PN/A pilot-scale system. Besides the enrichment of ANAMMOX bacteria, Han *et al.* (2016) reported an improvement in ANAMMOX bacterial activities at the expense of NOB activities on witching from vacuum screens to vibrating screens. Similarly, Zhang *et al.* (2016a) reported an improvement in ANAMMOX bacterial activities on the installation of a vibrating screen on effluent lines of a 20L ANAMMOX-mediated sidestream SBR treating thermally hydrolysed digestate, with the retention efficiency of a vibrating screen decreasing to 14.7±5.2%, compared to 54.2±8% on a gravity screen. This, suggests that, because of the additional forces due to the vibrations on the screens, better separation of sludge is achieved as the flocs trapped in the sludge are forced through the mesh while the granules are retained because of their bigger sizes and incompressibility. As a result of better sludge separation, improved process performance could be expected as NOB and heterotrophic bacteria (which mainly grow in flocs) are washed out, while the ANAMMOX-rich granules are retained in the reactors (Zhang *et al.* 2016a).

Membrane modules could also be installed on the effluent lines to separate biomass from wastewater, allowing 100% biomass separation (Zhang and Okabe 2017, 2020). However, their application for biomass retention in ANAMMOX-mediated systems is currently limited to lab-scale studies as no study in the reviewed articles reported on pilot-scale or full-scale applications. conversely, Cotto *et al.* (2020), Wen *et al.* (2015) and Wang *et al.* (2019) indicated that this technology is already in application in full-scale nitrification-denitrification systems, activated sludge processes, and pilot-scale nitritation-denitritation systems, respectively. In previous lab-scale studies of ANAMMOX-mediated systems,

membrane modules were installed on the effluent lines to separate biomass from wastewater, allowing 100% biomass separation (Zhang and Okabe 2017, 2020). Therefore, membranes enable independent separation of SRT of the systems from the HRTs as biomass wastage can be controlled (van der Star *et al.* 2008).

2.7.2 Attached-growth ANAMMOX-mediated systems

The addition of carrier materials represents an economical reactor modification that can significantly enhance biomass retention, reducing the start-up period of ANAMMOX-mediated systems. Carrier materials generally provide an increased surface area, within or upon which bacteria can become attached, saving on space for wastewater treatment plant (Ødegaard *et al.* 2012). Biofilm-based systems include rotating biological contactors (RBC), moving bed biofilm reactors (MBBRs), packed bed reactors, IFAS (integrated fixed-film activated sludge) and membrane aerated biofilm reactors (MABRs) (Lackner *et al.* 2014; Zhang *et al.* 2015; Bhattacharjee *et al.* 2017; Klaus *et al.* 2017). Attachment of biomass on carrier materials could be achieved through adsorption, electrostatic binding to a surface, flocculation, entrapment, and encapsulation (Dzionek, Wojcieszyńska and Guzik 2016). The major advantage is that the bacteria in the biofilms are often protected from shear forces, starvation, and inhibitory compounds (Veys *et al.* 2010; Jaroszynski *et al.* 2012; Boltz *et al.* 2017). They may be composed of a single monoculture or can be composed of multiple synergistic species that metabolically complement each other (Burmolle *et al.* 2014; Cordero and Datta 2016).

However, where fast-growing microorganisms (>0.1 h^{-1}) are cultured, the use of biofilms might be unnecessary as enough biomass could be generated with relatively short SRTs without the need for biomass retention (Van Loosdrecht and Heijnen 1993). Conversely, the use of biofilms could be ideal for ANAMMOX-mediated systems as ANAMMOX bacteria, have long doubling times (2.1-11 days) (Zhang *et al.* 2017b).

The structural and physical properties of biofilms on support surfaces are similar to that of granules, except the biofilms forming on aerated membrane modules (in MABRs). As a result, therefore, the mass transfer, hydrodynamics and reaction characteristics of both granules and conventional biofilms (on carrier materials) are similar. For instance, both granulation and biofilm formation on carrier materials have been reported to occur when the maximum bacterial growth rates are lower than the dilution rates (van Loosdrecht *et al.* 1995; Beun *et al.* 1999). Although granulation could also sometimes occur in systems operated at

dilution rates lower than the maximum growth rates, the bacterial activity in such systems mainly occurs in suspension (Van Loosdrecht and Heijnen 1993).

Available surface area is a key parameter for the effectiveness of a carrier material. A large surface area allows for the greatest available binding surface for bacterial adhesion and possible biofilm formation. Surface charge plays an essential role in electrostatic attachment of biological molecules and can be a key discriminator in the type of particles that attach to the carrier (Chen *et al.* 2012). The surface charge can vary with the material composition of the particle, the coating or the colonisers of the particle itself.

Development of ANAMMOX bacterial biofilms on zeolite, biochar, sand, bio-carriers, and the non-woven fabric has been well studied and documented (Strous *et al.* 1997b; Tsushima *et al.* 2007; Fernández *et al.* 2008; Wenjie *et al.* 2015). Zeolite and sand have cavities and channels within the internal matrix where cations, water, and/or small molecules may reside (Chang *et al.* 2009; Montalvo *et al.* 2012). These features promote the attachment of bacteria leading to the formation of biofilms. However, the high densities of zeolite and sand (1.42g/cm3 and 2.38 g/cm3, respectively (Chang *et al.* 2009)), could limit their application for biofilm development in mechanically agitated ANAMMOX-mediated reactors as strong mixing forces are essential in bringing the biomass in contact with the particles (Fernández *et al.* 2008). That notwithstanding, Fernández *et al.* (2008) reported a drop in biomass concentration in the effluent on the addition of zeolite particles into a lab-scale ANAMMOX-mediated reactor. In a lab-scale fluidised-bed ANAMMOX-mediated reactor, Strous *et al.* (1997b) demonstrated that biofilms could develop on sand particles. Although the limitation of zeolite application in agitated reactors could be circumvented by using linear channel-type reactors packed with zeolite, pore-clogging, need for zeolite regeneration and 'short-circuiting' still present challenges to these kind of reactors (Grismer and Collison 2017; Collison and Grismer 2018). On the other hand, biochar materials have large surface areas, relatively high specific gravities, high cation exchange capacities and high surface charge densities, which make them attractive carrier materials (Wu *et al.* 2009; Chen *et al.* 2012; Wenjie *et al.* 2015; Jin, Wang and Zhang 2016). Wenjie *et al.* (2015) reported successful formation of biofilms with high settling velocities (200 mh^{-1}) on activated charcoal in ANAMMOX-mediated EGSB reactor, which were higher than that of granular biomass (73-78 mh^{-1}) reported by Tang *et al.* (2011). Additionally, the high porosity and adsorption capacity of biochar have been argued to reduce the reactor start-up period and

seed sludge dosage of ANAMMOX-mediated systems (Wu *et al.* 2009; Chen *et al.* 2012; Jin, Wang and Zhang 2016).

Currently, bio-carriers constructed of materials with densities slightly less than water that allow the media to move around with the motion of the water column and gain suitable mixing have received wide application in full-scale ANAMMOX-mediated systems (Lackner *et al.* 2014). Literature survey indicates that bio-carrier fill capacity of between 32% and 50% is practised in full-scale systems (Rosenwinkel and Cornelius 2005; Lackner *et al.* 2014; Klaus *et al.* 2017). This is particularly important as fill capacities higher than these values could bring about challenges with mixing.

The development of biofilm on bio-carriers could take several months (Almstrand *et al.* 2014; Kanders *et al.* 2014; Kowalski, Devlin and Oleszkiewicz 2018). Almstrand *et al.* (2014) and Rosenwinkel and Cornelius (2005) argued that bacterial growth on carrier materials is sequential, with AOB being the first colonizers and ANAMMOX bacteria only colonizing when conducive conditions created by AOB prevail. As the biofilms develop, the concentration of the slow-growing (ANAMMOX) bacteria increase in the anaerobic sections deeper in the biofilm, while the faster-growing bacteria (AOB) grow mainly on the outer layers closer to the biofilm surface, similar to granules (Almstrand *et al.* 2014). However, the microbial composition and structures in biofilms could change with reactor configuration and the operating conditions. For instance, the existence of micro-channels in the biofilms that could allow oxygen-rich wastewater to flow, enabling AOB and other fast-growing organisms to grow deep in the biofilms, where, normally, anoxic conditions would be expected to prevail (Vlaeminck *et al.* 2010). Reactor start-up strategies in place could also influence the biofilm structures. For instance, Cho *et al.* (2011) reported indistinguishable distribution of AOB and ANAMMOX bacteria in MBBR biofilms started with nitrifying sludge (*figure 2.16b*), while in another MBBR started with enriched ANAMMOX bacterial consortia, the biofilms were stratified (*figures 2.16a*). Furthermore, Cho *et al.* (2011) reported that the biofilms developed from nitrifying biomass were fluffy, while those developed from enriched ANAMMOX bacterial biomass were rigid.

Continuous ANAMMOX-mediated up-flow and MBBR systems can be operated with nitrogen loading rates in the range of 0.9-7 kg-N/m^3-day, which are comparatively higher than SBRs (van der Star *et al.* 2007; Lackner *et al.* 2014). However, mass transfer into the biofilms limits the capacity of MBBRs (Zhao *et al.* 2013). To mitigate this shortcoming,

modification of MBBR systems with the incorporation of settlers that would enable re-circulation of suspended biomass back into the reactors in a system referred to as IFAS (Integrated Fixed-Film Activated Sludge) have been made (Zhao *et al.* 2013; Trojanowicz, Plaza and Trela 2016) (*figure 2.17*). According to Veuillet *et al.* (2014), retention of suspended biomass in the modified MBBR configuration (known as IFAS), lead to niche segregation of AOB and ANAMMOX bacteria between the biofilms and the suspension, enabling better access to oxygen by the AOB in suspension. As a consequence of better accessibility of oxygen by the AOB, more NO_2^- would be generated which increases its concentration in the bulk liquid, creating a concentration gradient with the biofilms, subsequently improving NO_2^- diffusion into the biofilms (Zhao *et al.* 2013). The process performance of the IFAS systems could thus be better than that of conventional MBBR systems because of enhanced diffusion of the substrate (Zhao *et al.* 2013; Veuillet *et al.* 2014). Consequently, because of better mass transfer in IFAS systems than in MBBR, the operational DO in IFAS systems could be kept below that of MBBR systems, as was demonstrated by Veuillet *et al.* (2013) in a full-scale plant. Lower operational DO, in turn, could translate into lower operational costs in IFAS than in MBBR as the aeration costs are lower than in MBBR. In a lab-scale mainstream system, Malovanyy, Trela and Plaza (2015) also reported better process performance in a mainstream IFAS configuration than in a mainstream MBBR system, underpinning the suitability of this configuration not only for sidestream applications but also mainstream applications. Similar findings were reported by Trojanowicz, Plaza and Trela (2016) from a pilot-scale study of IFAS and MBBR PN/A mainstream systems. Also, Trojanowicz, Plaza and Trela (2016) reported lower NOB activities in IFAS configurations than in MBBR configurations, whose suppression was argued to have been easier in IFAS than in MBBR as they grow in suspension as they do not get biofilm protection in IFAS against free ammonia. As a result of better NOB suppression in IFAS configuration than in MBBR configuration, higher nitrogen removal was reported in IFAS than in MBBR by Trojanowicz, Plaza and Trela (2016).

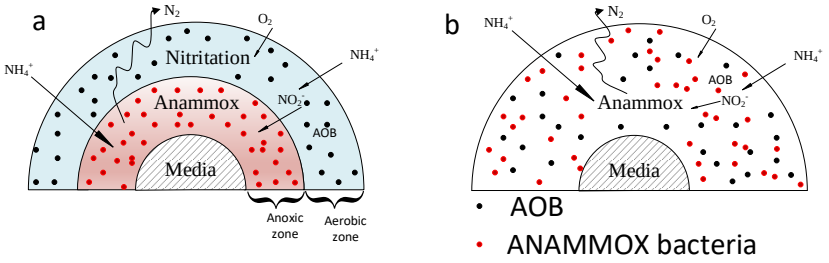

Figure 2. 13. Schematic diagrams of biofilms depicting the distribution of ANAMMOX bacteria and AOB on biofilms developed using two different strategies; a – biofilms developed from biomass dominated by ANAMMOX bacteria, b – biofilms developed from nitrifying sludge.

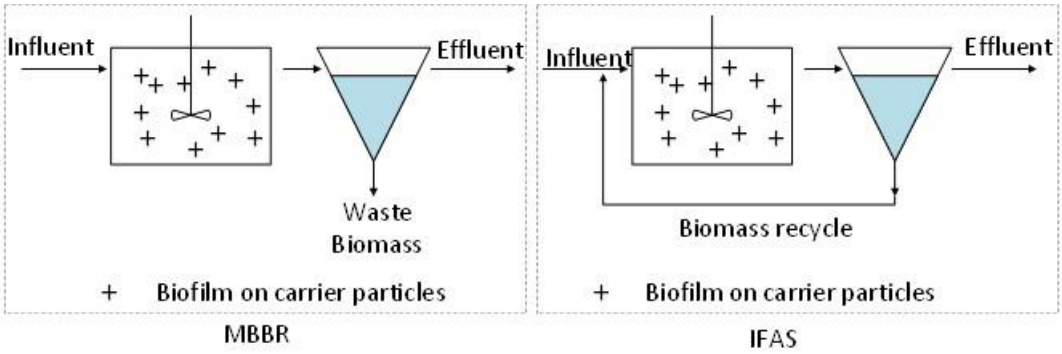

Figure 2. 14. Conceptualised MBBR and IFAS systems

In MABRs, bacterial biofilms develop on membranes modules that are also used to supply air into the wastewater (Pellicer-Nàcher *et al.* 2010). However, the operation of MABRs could vary with configuration: in some, the membrane lumen is pressurised with air, while in others, wastewater flows through the membrane lumens with volatile components diffusing through the membrane to the biofilms (Brookes and Livingston 1994; Reij *et al.* 1995).

The biofilm structures in ANAMMOX-mediated MABRs are thus different from those of conventional systems (*figure 2.18*) as AOB, NOB and other aerobes grow in the inner layers where there is easy access to oxygen, while ANAMMOX bacteria grow in outer (anoxic) layers (Pellicer-Nàcher *et al.* 2010; Li *et al.* 2016). However, the growth of NOB, in the inner layers is a concern, as their repression becomes a challenge. Their repression is limited due to the creation of regions of high DO concentrations within the biofilms which favour their growth, as well as their protection by ANAMMOX bacteria growing on the surface which make the conventional approaches of NOB repression ineffective (Pellicer-Nàcher *et*

al. 2010). In a study by Li *et al.* (2016), a 5.4% relative abundance of *Nitrospira* spp. was reported in the biofilms forming on membrane modules of MABR (*table 2.6*). Earlier, Pellicer-Nàcher *et al.* (2010) had demonstrated that this setback could be managed with sequential aeration as AOB excrete hydroxylamine when oxygen supply is abruptly stopped and/or produce nitric oxide (NO) under anaerobic conditions, both of which are toxic to NOB. Augusto, Camiloti and Souza (2018), however, argued that maintaining low DO in MABR, (<0.5 mg-O_2/L) effectively suppress NOB in MABRs.

Uncontrolled biofilm growth could also cause serious mass-transfer challenges, subsequently affecting the process performance (Pellicer-Nàcher *et al.* 2010). Normally, shear forces are applied to regulate biofilm thickness, and one way of achieving this is by installing rotating modules (Pellicer-Nàcher *et al.* 2010). However, detachment of biofilms due to sloughing or erosion could make it challenging to control biofilm thickness (Syron and Casey 2008).

Despite the above challenges, Xie *et al.* (2017) and Shi *et al.* (2013) demonstrated that MABR-type reactors could still play an important role in mainstream ANAMMOX-mediated systems incorporating DAMO (denitrifying anaerobic methane oxidising) organisms, that could otherwise be challenging to implement in other reactor configurations. This is because DAMO organisms require methane, a highly flammable gas whose supply needs to be strictly regulated. In addition, MABRs could still be ideal for PN/A systems as they not only allow independent regulation of substrate and oxygen supply, but also provide higher efficiencies of gas transfer than conventional diffusers, thus allowing higher substrate utilisation rates (Li *et al.* 2016).

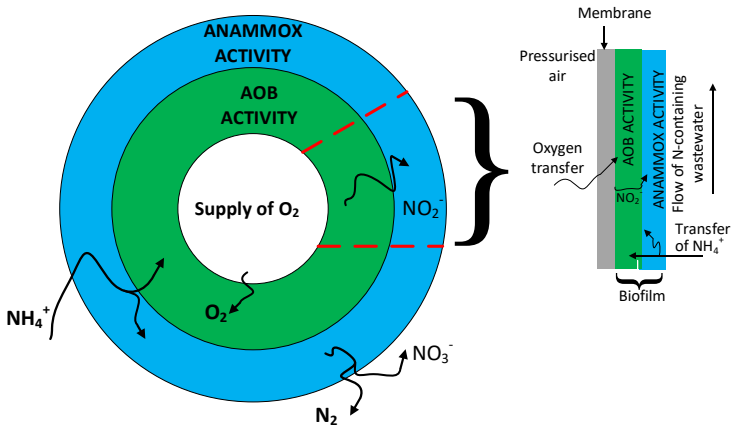

Figure 2. 15. Schematic diagram of biofilm on a membrane surface.

Table 2. 6. Application of MABRs and MBfRs (membrane biofilm reactors) in ANAMMOX-mediated systems.

	Reactor	SRT (days)	Concentration (mg/L)			HRT (h)	T (°C)	pH	NRR kg/m³/day	Air/gas pressure (kPa)	Affiliation of AOB, NOB and ANAMMOX bacteria	References
			DO	Influent NH_4^+-N	Influent NO_2^--N							
1	2.5L MABR		0.1-0.6	70	0-84	16-32	25±1	7-7.5	0.052 – 0.105	2.07-4.82	*Ca. Jettenia* sp. *Nitrosomonas* sp.; *Nitrospira* sp.	(Li *et al.* 2016)
2	2.41L MABR	-	<0.5	530-780	-	-	32	6.71-8.31	0.78	2.5-60	Biofilm: AOB+ANAMMOX~60%, *Nitrobacter* sp.>*Nitrospira* sp.	(Pellicer-Nàcher *et al.* 2010)
3	2.356L MBfR*	-	-	46-500	46-530	24 - 192	-	7-8	1.030	250	*C. Brocadia* sp. *(57%), C. Kuenenia* sp. *(43%): ANAMMOX-DAMO reactor*	(Xie *et al.* 2017)
4	1.15L MBfR	-	-	200	-	Ca. 72	-	-	0.25	121.59 – 151.99	*DAMO bacteria (20–30%), DAMO archaea (20–30%) and anammox bacteria (20–30%)*	(Shi *et al.* 2013)

DAMO – denitrifying anaerobic methane oxidation; [a]$kgNO_2$-N/m^3/day; *membrane biofilm reactor: MBfR - membrane biofilm reactor

2.7.3 Gel encapsulation of bacterial biomass in ANAMMOX-mediated systems

Gel encapsulation is relatively a new strategy employed for retention of biomass in full-scale ANAMMOX-mediated systems (Isaka *et al.* 2017). The gel capsules allow for the diffusion of gas and liquid media but retain biomass within the matrix, effectively creating pseudo-microenvironments with conducive conditions for AOB/ANAMMOX bacterial growth (Bae *et al.* 2017). Each gel-capsule can self-regulate under stress conditions, and the AOB/ANAMMOX bacteria may gain a competitive advantage due to less competition within each self-contained capsule. In addition, gel-encapsulation protects biomass from shear forces, reduces the working volume of the reactor, and improves resilience to substrate inhibition and toxicity (Sumino *et al.* 1992; Vanotti and Hunt 2000; Cho *et al.* 2017). Therefore, gel-encapsulation could allow for independent SRT and HRT regulation in the reactors (Zhu, Hu and Wang 2009). High gel porosity, good compressive strength, low deformation rate, low surface charges and stability in acidic, basic and saline solutions are essential parameters of gel beads (Sumino *et al.* 1992; Zhu, Hu and Wang 2009; Bae *et al.* 2015). Polyvinyl alcohol (PVA), polyethylene glycol (PEG) and a combination of PVA with sodium alginate (SA) are the commonly used hydrogels (*table 2.7*).

Biomass immobilisation starts with mixing polymer and biomass, followed by curing through the addition of a chemical initiator or freezing (Magrí, Vanotti and Szögi 2012). This hardening procedure, however, could affect AOB/ANAMMOX bacterial activity as prolonged freezing could inactivate the ANAMMOX bacteria, whilst the addition of a chemical compound could affect the permeability of the gel beads. A study by Magrí, Vanotti and Szögi (2012) reported a 90% drop in ANAMMOX activity on reactivation after freezing at -8ºC for 17 hours. Choi *et al.* (2018) also reported a long lag phase (54 days) on inoculating with gel-encapsulated biomass, probably because of freezing and thawing. Both boric acid and SA have been reported to reduce porosity, leading to floatation as nitrogen gas produced by ANAMMOX bacteria get trapped within the gel beads (Choi *et al.* 2018).

Zhu, Hu and Wang (2009), in their studies on biomass-encapsulation with sodium carboxymethylcellulose (Na-CMC), SA, PVA and PVA/SA, found that ANAMMOX activity varies with the physical properties of the polymers. While the ANAMMOX activity increased in the following order: Na-CMC>SA>PVA/SA>PVA, the compressive strength increased in the following order: PVA/SA>PVA>SA>Na-CMC. In their study, it was found that although Na-CMC has a loose highly porous structure that enables faster transfer of substrates within the beads, it is unstable in saline solutions. On the other hand, although SA

beads have thin shells and porous internal structures that could enhance faster mass transfer, Ca^{2+}, Mg^{2+} and phosphates, can destroy its porous structure (Zhu, Hu and Wang 2009). Conversely, PVA forms compact spherical shells with a porous interior that could negatively affect the mass transfer, is unstable in salty solutions, has many hydrophilic groups making it susceptible to expansion in water solutions and can easily agglutinate. Therefore, of the four gel beads, PVA/SA presents the best option as gel beads aggregate less, material cost is low and nitrogen removal is high (Zhu, Hu and Wang 2009).

Isaka *et al.* (2017) demonstrated that the start-up of full-scale ANAMMOX-mediated reactors could be faster with biomass-encapsulation. In their studies, they showed that full-scale ANAMMOX-mediated reactor could be started-up in about 69 days, which was faster than over 3 years start-up period reported by (van der Star *et al.* 2007). It was further demonstrated by Isaka *et al.* (2007) that through biomass encapsulating, the seed sludge concentration required for a successful start-up of ANAMMOX reactor could also be minimised to a greater extend. Ali *et al.* (2015b) also reported NRRs of 7 kg-N/m^3-day in 5 up-flow column reactors inoculated with different concentrations of sludge (0.33-1.67 gVss/L) in 7-25 days. However, it was also reported that for systems with fixed amounts of gel-trapped biomass have maximum NRRs beyond which no further increase in NRRs could be expected even if the nitrogen loading rates are increased (NLRs). It would thus be desirable to reduce the sizes of gel beads (to enhance mass transfer) and increase in the bead fill ratio in reactors (Isaka *et al.* 2007).

Unlike up-flow reactors, fixed bed reactors or SBRs that require settlers for influent pre-treatment, a high concentration of suspended solids cannot affect the performance of systems employing gel-entrapment (Isaka *et al.* 2011). However, the performance of systems employing gel-encapsulation could be affected by bead thickness (Choi *et al.* 2018). Indeed, using 1 mm, 2 mm and 3 mm thick-beads, Choi *et al.* (2018) reported successful reactor start-up in 63, 65 and 94 days respectively. Notwithstanding the challenges associated with gel encapsulation of bacterial biomass, the NRR (3.2 kg-N/m^3-day) of full-scale ANAMMOX-mediated system reported by Isaka *et al.* (2017) were within the range of biofilm systems reported by (Lackner *et al.* 2014).

Table 2. 7. Encapsulation of ANAMMOX bacterial consortia

Gel	Inoculum % (w/v)	Reactor	Influent (mg-N/L)		Hardening procedure	Operating conditions	NRR (kg-N/m^3-day)	Feed	Affiliated ANAMMOX bacterial species	Reference
			NH_4^+	NO_2^-						
PVA		CSTR	90 - 196.3	90-700	Freezing-thawing	pH 7.5, HRT 2.6-11.7h, Temp (33ºC)	3.0	Synthetic WW	-	(Magrí, Vanotti and Szögi 2012)
PEG	0.88	100L			chemical	pH 7.5, HRT 7.2h, Temp (30ºC)	3.8	Digester supernatant	-	(Isaka *et al.* 2011)
PVA	-	0.23L	50	66	Freezing - thawing	pH 7.8±0.15, HRT 2.52h, Temp (35ºC)	1.1	Synthetic feed	Shift to *C. Brocadia sinica* from *C. Jettenia asiatca*	(Choi *et al.* 2018)
PVA /SA	-	0.5L	51.7-102	-	Chemical	pH 7.1-7.45, HRT 4.08h, Temp (35ºC)		Synthetic WW, core-shell beads	*C. Jettenia asiatca*	(Bae *et al.* 2017)
PVA /SA	1.67	1.2L CSTR	50-550	50-550	Chemical	pH 6.8-7.3, HRT 2-12h, Temp (23-33ºC)	27.3	Synthetic and reject wastewater	-	(Quan *et al.* 2011)
PEG	0.24	CSTR	63.63 - 154.84	71.01 – 190.72	Chemical	pH 7.2, HRT 2h, Temp (36ºC)	12.3	synthetic	-	(Isaka *et al.* 2007)
PEG	0.24	0.5L CSTR	63.63 - 154.84	71.01 – 190.72	Chemical	pH 7.2, HRT 1-13h, Temp (6.3-32ºC)	0.36-6.2	Synthetic feed	*C. Kuenenia Stuttgartiensis, C. Brocadia anammoxidans*	(Isaka *et al.* 2008)

2.8 Modelling and simulation of ANAMMOX-mediated systems

Since the discovery of ANAMMOX bacteria in the mid-1990s, their contribution in nitrogen removal has always been modelled using modified activated sludge models (ASMs) (Wyffels *et al.* 2004; Cema *et al.* 2012; Ni, Joss and Yuan 2014; Trojanowicz, Plaza and Trela 2017). The original model, ASM 1, which was developed by a task group formed in 1983 by International Association on Water Pollution Research and Control (IAWPRC) (now called International Water Association - IWA) incorporated only the nitrifiers, denitrifiers and heterotrophic bacteria (Henze *et al.* 1987). However, several users have since modified this model in their applications to incorporate the activities of ANAMMOX bacteria. For instance, Dapena-Mora *et al.* (2004c) and Trojanowicz, Plaza and Trela (2017) modified ASM 1 for modelling and simulation of a lab-scale SBR and a pilot-scale MBBR, respectively, while Ni, Joss and Yuan (2014) simulated nitrogen and carbon removal in a full-scale SBR using a modified ASM 1.

The ASMs are based on a matrix format introduced by Petersen (1965). A simplified model based on this format incorporating three components is presented on *table 2.8* (Henze *et al.* 1987). According to this format, the processes (*j*) are listed on the leftmost column, while the process rate expressions (ρ) are listed on the rightmost column, while the components (*i*) are listed on the first row of the columns in between the leftmost and rightmost columns, and the stoichiometric coefficients ν_{ij} are listed in the rows below the components (*table 2.8*).

Process rates (r_i) are obtained by summing the products of process rate expressions and stoichiometric coefficients ν_{ij} (Henze *et al.* 1987);

$$r_i = \sum_j v_{ij}\rho_i \tag{2.17}$$

For instance, the rate of reaction of substrate S_S would be:

$$r_{S_S} = -\frac{1}{Y}\frac{\mu_{max}S_S}{K_S+S_S}X \tag{2.18}$$

To balance the component(s) in a system, the basic mass balance equation would then be used (Henze *et al.* 1987):

$$Input - output + reaction = accumulation \tag{2.19}$$

In the ASM 1, the inhibition of bacterial activities is accounted for using a switching function adopted as:

$$\frac{s_0}{k_0+s_0} \tag{2.20}$$

However, Trojanowicz, Plaza and Trela (2017) were able to demonstrate that inhibition could also be accounted by using *Aiba-Edwards model:*

$$\mu = \frac{\mu_{max} S_S}{K_S+S_S} \exp(-\frac{S_S}{Ki}) \tag{2.21}$$

Where μ and K_i are the specific bacterial growth rate and inhibition constant, respectively.

Similarly, Haldane kinetics can also be used to describe the inhibition instead of the switching function (Choi *et al.* 2008; Trojanowicz, Plaza and Trela 2017):

$$\mu = \frac{\mu_{max} S_S}{K_S+S_S+S_S^2/K_i} \tag{2.22}$$

Table 2. 8. A simplified activated sludge model 1 (ASM 1) matrix.

Process j ↓	*Component* i →			*Process rate* ρ_i
	Biomass	Substrate	Oxygen	
	X	S_S	S_O	
Growth	1	$-\frac{1}{Y}$	$-\frac{1-Y}{Y}$	$\frac{\mu_{max} S_S}{K_S + S_S} X$
Decay	-1		-1	bX
Units	mgCOD L^{-1}	mgCOD L^{-1}	mgCOD L^{-1}	Mass/(volume*time)

Y - *growth yield,* μ_{max} *- maximum specific growth rate,* K_S *- half-velocity constant,* b *- specific decay rate*

CHAPTER 3

3 PROCESS PERFORMANCE AND KINETICS OF NITROGEN REMOVAL IN THE ANAMMOX-MEDIATED SYSTEMS

3.1 Introduction

Process stability, kinetics and efficiencies form critical aspects of BNR processes. In ANAMMOX-mediated systems, resilience and process stability during periods of transient perturbations could vary with the reactor configuration (Lackner and Horn 2013; Wells *et al.* 2017). In addition, the NRRs could also vary with reactor configurations (Lackner and Horn 2013; Ali *et al.* 2015b), leading to significant variations in start-up periods of ANAMMOX-mediated processes in different reactor configurations (Tao *et al.* 2012; Wang *et al.* 2012b).

Start-up of full-scale ANAMMOX-mediated systems, therefore, is a daunting task that could take several months or even years depending on reactor configuration (van der Star *et al.* 2007; Isaka *et al.* 2017; Xu *et al.* 2018). According to Ali *et al.* (2015b), reactor start-up periods and process performance can be attributed to several factors affecting process kinetics, among which is the variation in mass transfer rates with reactor configurations. Similarly, variation in the inhibitory threshold of the substrate with reactor configuration has also been reported (Magrí, Vanotti and Szögi 2012).

Although pioneering comparative studies provide crucial information about the impact of reactor configuration on the performance of ANAMMOX-mediated processes, more studies could still be necessary to understand the impact of reactor configuration on the long-term process performance. The operation of reactors at baseline conditions could also be necessary to understand the impact of reactor configuration on reactor start-up, kinetics and process efficiency.

In this chapter, comparative study of moving bed biofilm reactor (MBBR), hybrid up-flow anaerobic sludge blanket reactor (H-UASB) and gas-lift reactor (GLR) based on reactor start-up periods, NRRs and NREs over 535 days is presented. For each reactor, NRRs and NREs were determined, and the activities of AOB, NOB, ANAMMOX and heterotrophic bacteria were monitored based on the ratios of NO_2^- consumed per NH_4^+ consumed and NO_3^- produced per NH_4^+ consumed. The concentrations of FA and FNA in each reactor during the

study period were also estimated. All the reactors were inoculated with biomass from a mainstream MBBR that was fed with effluent from a sidestream aerated MBBR.

3.2 Methodology

3.2.1 Fabrication of reactors and experimental set-up

The reactors used in this study viz., moving bed biofilm reactor (MBBR), gas-lift reactor (GLR) and a hybrid up-flow anaerobic sludge blanket reactor (H-UASB) were fabricated using Perspex cylinders and Perspex sheets (*figure 3.1*). All the three reactors had a total volume of 5.64 L (110 mm deep conical bases and 330 mm by 140 mm by 2 mm cylinders) (*figures A.3.1-A.3.3, appendix A*). External 440 mm x 180 mm x 4 mm Perspex cylinders were used as water jackets in each reactor (*Figures A.3.1-A.3.3, appendix A*). Each reactor contained three sampling points along the reactor height, which were closed with PVC (polyvinyl chloride) ball valves. Additionally, in GLR, an internal 300 mm by 70 mm by 2 mm draft tube and 55 mm – diameter air-stone which acted as a gas diffuser, were included (*figures 3.1 and A.3.3, appendix A*). Furthermore, in MBBR, a 180 W motor was connected to a 19 mm-diameter-mixing shaft with 3, 100 mm by 20 mm by 2 mm blades. The shaft was fixed to the top of the reactor using a set of ball bearings (*figure A.3.1, appendix*). To each reactor, a 2.5L settler was attached for biomass separation from the effluent (*figures 3.1, 3.2 and A.3.1-A.3.3, appendix A*).

PVC pipes, adapters and connectors were used to join different pieces of the reactors together. PVC ball valves were used in all the effluent lines and influent lines. Silicone tubes (4 mm internal diameter) were used in the effluent lines to interconnect the settlers to the reactors as well as in the feed lines to interconnect the feed tank and the reactors.

The water jackets in each reactor were connected to a water-circulating pump in a water bath with silicone tubes. A loop for circulation of argon/carbon dioxide (CO_2) gas mixture was created in GLR by connecting the ends of a bicycle tubing (cut at the middle to form an open-ended tubing) to the gas exit and gas entry points of the reactor (*figure 3.2*). Argon/CO_2 gas mixture was circulated in GLR within the loop using an air compressor (*figure 3.2*). Polyethylene K1 type carrier materials (Azacore, South Africa) were added to each reactor during inoculation for biofilm development (*figures 3.3 and A.3.9*). Each of the carrier materials contained 25 equally spaced fins that were 1.5 mm long and 0.1 mm thick (*figure A.3.9*). The carrier materials were 14 mm long and 20 mm in diameter. The inner sections of the carrier materials were subdivided into 8 chambers by 0.2 mm thick crosses (*figure A.3.9*).

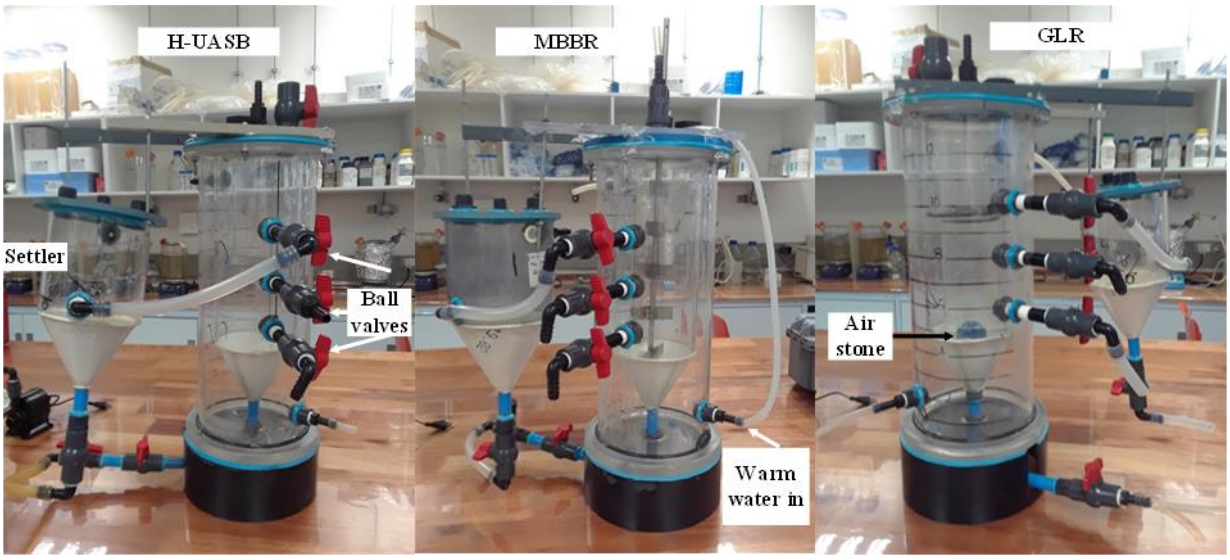

Figure 3. 1. Photographic images of the reactors before inoculation.

3.2.2 Synthetic feed

All the three reactors were fed with the same feed using a four channel peristaltic pump (Gilson, UK). The concentration of Mg^{2+}, Ca^{2+} and trace elements I and II in the feed were as previously described by van de Graaf *et al.* (1996) (*table 3.1*). $NaNO_2$ and $(NH_4)_2SO_4$ were used to make the required concentrations of NO_2^- and NH_4^+, respectively (*table 3.1*). The feed also contained NaCl (15 mg/L - between the first day and the day 327), $NaHCO_3$ (1g/L), K_2HPO_4 (13.6 mg/L) and KH_2PO_4 (13.6 mg/L).

The pH in the influent was maintained at 6.2±0.2 using CO_2. The concentration of dissolved oxygen (DO) in the feed was maintained below 0.5 mg-O_2/L by sparging with argon-carbon dioxide (CO_2) mixture (95% argon, 5% CO_2) at 5 L/min throughout the study except between days 46-86 of reactor operation when the DO was not controlled in the feed. During this period (i.e. days 46-86), the DO varied from approximately 8.0 mg-O_2/L to approximately 8.8 mg-O_2/L (*table 3.2*).

Table 3. 1. Composition of the synthetic feed.

Compound	Concentration (mg/L)	Compound	Concentration (mg/L)
$MgSO_4.7H_2O$	300	EDTA	0.015
$CaCl_2.2H_2O$	180	$ZnSO_4.7H_2O$	0.00043
$NaHCO_3$	1000	$CoCl_2.H_2O$	0.00024
K_2HPO_4	13.6	$MnCl_2.4H_2O$	0.00099
KH_2PO_4	13.6	H_3BO_4	0.000014
NaCl*	15	$CuSO_4.5H_2O$	0.00025
$FeSO_4$	0.005	$NaMoO_4.2H_2O$	0.00022
EDTA**	0.005	$NiCl_2.6H_2O$	0.00019
$NaNO_2$	variable	$NaSeO_4.10H_2O$	0.00021
$(NH_4)_2SO_4$	variable		

*provided for the first 327 days only, *Ethylenediaminetetraacetic acid

3.2.3 Initialisation and operation of reactors

All the reactors were inoculated with approximately 30 ml of seed biomass collected from the effluent of an anaerobic mainstream (operated at 15ºC) MBBR, which was in turn fed with effluent from an aerated sidestream MBBR (operated at 30ºC) at the Earth and Environmental Engineering department, Columbia University, USA. The biomass samples were then shipped to our labs in a cooler box.

The period of reactor operation was divided into 9 phases over a 535-day study period based on the influent DO, NO_2^- and NH_4^+ concentrations as described on *table 3.2*. The concentrations of NO_2^- and NH_4^+ were gradually increased based on NRR of the reactors.

The biomass retained in the settlers were recycled back into the respective reactors once a week using peristaltic pumps (Masterflex, USA). Throughout the entire period of study, anaerobic conditions in the settlers were maintained as the reactors were sealed.

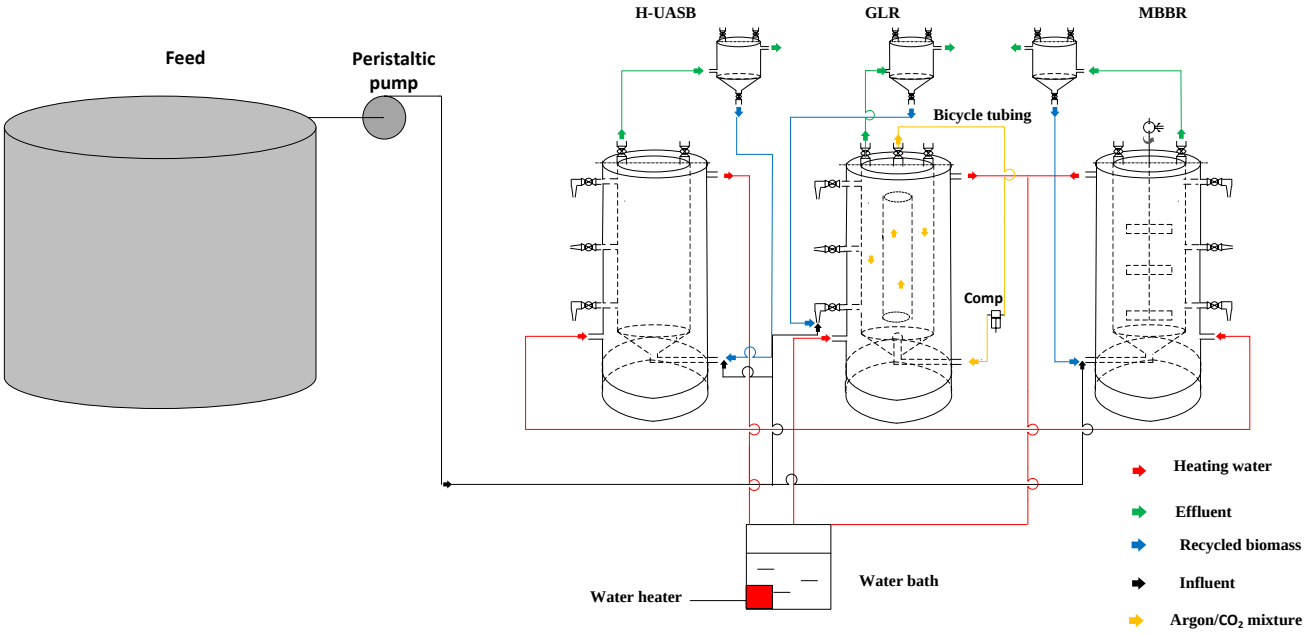

Figure 3. 2. Schematic diagram of the experimental set-up.

Figure 3. 3. Photographic image of K1-type bio-carriers used for biofilm development in the reactors.

3.2.4 Analysis of residence time distribution

The residence time distribution (RTD) was determined as previously described by Danckwerts (1953) and Scott (2016) modification. This was done by injecting a tracer (green food colouring) (*figure A. 3. 8, Appendix A*) at a constant rate (Q) of 10 ml per minute for 4 minutes at the inlet and then measuring the absorbance of the effluent samples from the reactors every 30 minutes for 15 hours. During the analysis of RTD, internal gas circulation in GLR was effected for the first three hours only, after which gas circulation was stopped. Tap water was pumped into and out of the reactors at the rate of 10 ml/min during the entire process of RTD analysis, and the working volume (V) was kept constant at 5L.

3.2.5 Analytical methods

The absorbance of the effluent samples during the analysis of RTD was measured on a DR 6000 (HACH, USA) (*figure A.3.4, appendix A*) at 680 nm using tap water as the reference. The concentrations of NO_2^-, NH_4^+, and NO_3^- were also measured colorimetrically three times a week using DR 6000 (HACH, USA) as described previously by Lotti *et al.* (2014b). The effluent samples were first filtered through 0.45 µm syringe filters before the analysis. Bacterial activities were monitored in the three reactors based on the ratios of NO_2^--N consumed to NH_4^+-N consumed ($\Delta NO_2^-/\Delta NH_4^+$) (*equation 3.1*) and NO_3^--N produced to NH_4^+-N consumed ($\Delta NO_3^-/\Delta NH_4^+$) (*equation 3.2*) (Lotti *et al.* 2014b). The DO and pH in the feed tank were measured using LabQuest 2 multiparameter device during feed preparation (Vernier, USA) (*figure A.3.5, appendix A*). The temperature of the reactors were maintained at 36±1ºC by continuously circulating warm water between the water jackets in the reactors and the water bath (Labcon Laboratory equipment, Johannesburg) (*figure A.3.6, Appendix A*), while the pH in the reactors was maintained between 7-7.5 with either HCl or $NAHCO_3$ using automatic pH controllers (Etatron, Italy) (*figure A.3.7, Appendix A*). Statistical analyses of reactor performance were performed in Microsoft excel using a single factor ANOVA (analysis of variance).

$$\Delta NO_2^-/\Delta NH_4^+ = \frac{(Influent\ NO_2^- - \text{Effluent } NO_2^-)\ (\frac{kg-N}{m^3})}{(Influent\ NH_4^+ - \text{Effluent } NH_4^+)\ (\frac{kg-N}{m^3})} \quad (3.1)$$

$$\Delta NO_3^-/\Delta NH_4^+ = \frac{(\text{Effluent } NO_3^-)\ (\frac{kg-N}{m^3})}{(Influent\ NH_4^+ - \text{Effluent } NH_4^+)\ (\frac{kg-N}{m^3})} \quad (3.2)$$

The NRR and NRE were calculated according to *equations 3.3 and 3.4*, respectively, (Li et al. 2017a):

$$NRR\ (\frac{kg-N}{m^3 day}) = \frac{(Total\ influent\ N - \text{Total effluent N})\ (\frac{kg-N}{m^3})}{HRT\ (day)} \quad (3.3)$$

$$NRE\ (\%) = \frac{(Total\ influent\ N - \text{Total effluent N})\ \left(\frac{kg-N}{m^3}\right)}{Total\ influent\ N\ \left(\left(\frac{kg-N}{m^3}\right)\right)} * 100 \quad (3.4)$$

Where, total (influent/effluent) nitrogen was determined as a summation of NH_4^+, NO_2^- and NO_3^- concentrations.

The concentrations of FA (free ammonia) and FNA (free nitrous acid) were calculated based on *equations 2.15 and 2.16* in *Chapter 2* (Anthonisen *et al.* 1976; Soliman and Eldyasti

2016). The calculations were based on the operational pH of 7.5 and the temperature of 36ºC in the reactors. In both MBBR and GLR, the calculations of FA and FNA were based on the effluent NO_2^- and NH_4^+ concentrations, while their calculations in H-UASB were based on the average concentrations of the effluent and influent concentrations of NO_2^- and NH_4^+.

3.3 Results

3.3.1 Operation of reactors

During the inoculation of the reactors, 150 K1-type carrier particles were added to each reactor (*figure 3.3*), and from 351st day, an additional 100 carrier particles were added to MBBR due to faster biofilm attachment in the MBBR than in the other reactors (*Chapter 5*). For the first 120 days of this study, GLR was pressurised with argon/CO_2 mixture that was continuously circulated at 35 L/minute within the loop by an air compressor (*figure 3.2*). However, from the 121st day, gas circulation in GLR was only maintained for three hours a day as continuous circulation of argon/CO_2 mixture caused frequent failure of air compressors necessitating frequent replacements.

According to the influent concentrations of the DO, NH_4^+ and NO_2^-, the operational period of the reactors could be divided into IX operational phases (*table 3.2*). The average influent NO_2^- and NH_4^+ concentrations ranged from 38 mg-N/L and 50 mg-N/L to 305 mg-N/L and 220 mg-N/L, respectively, during the study period (*table 3.2).*

Table 3. 2. The average concentrations of the influent DO, NO_2^- and NH_4^+ in the different phases of operation of the reactors.

Phase	Period (days)	Influent DO and N concentrations		
		DO (mg-O_2/L)	NH_4^+ (mg-N/L)	NO_2^- (mg-N/L)
I	0-45	0.5 ±0.1	50.0±1.0	56.0±4.0
II	46-86	8.5±0.3	69.0±10.0	38.0±10.0
III	87-186	0.3 ±0.2	74.0±11.0	51.0±10.0
IV	187-250	0.3 ±0.2	75.0±21.0	81.0±0.5
V	251-327	0.3 ±0.2	131.0±39.0	175.0±61.8
VI	328-355	0.3 ±0.2	220.0±0.0	305.0±7.0
VII	356-424	0.3 ±0.2	200.0±0.0	264.0±0.0
VIII	425-434	0.3 ±0.2	110.0±0.0	145.0±0.0
IX	435-535	0.3 ±0.2	200.0±0.0	264.0±0.0

3.3.2 Residence time distribution

The internal decay of the food colouring in the reactors was observed over time in the reactors (*figures 3.4 a-c*). During the first 30 minutes of the experiment, sharp increase in the absorbance of the effluent samples in MBBR was observed, which was then followed by gradual decrease until it reached zero (*figure 3.4a*). In the H-UASB, the absorbance of the effluent samples remained close to zero for 390 minutes before a spike was observed between this period and the 450th minute, which was then followed by gradual decrease until it reached zero (*figure 3.4b*). In the GLR, the absorbance of the effluent samples followed similar trend with MBBR within the first 240 minutes, beyond which the absorbance of the effluent samples dropped sharply from 0.172 absorbance units (abs) (on 240th minute) to 0.054 (on 300th minute). Following this decrease was a plateau on the curve between the 300th and 330th minute, which preceded a minor spike in the absorbance of the effluent samples, which then gradually decreased to zero (*figure 3.4c*).

Visual observations made in the course of RTD analysis revealed uniform distribution of light-green colour in the MBBR and GLR within the first minute, and a dark-green colour between the fourth minute and the 150th minute (*figures 3.5 a-d and 3.5 i-l*). However, the intensity of the green colour gradually decreased in the MBBR over time, and by the 720th minute, faint-green colour was distributed in this reactor (*figure 3.5d*). On the contrary, faint-green "plug" was observed hanging on the upper liquid level in the GLR by this time (*figure 3.5l*). In the H-UASB, some thread-like light-green colour was seen extending from the base of the reactor up to just above the middle section within the first minute, which then expanded to cover almost half a section of the bottom-half of the reactor by the fourth minute (*figure 3.5f*). By the 150th minute, the upper three-quarter of the H-UASB was covered in light-green colour, while the lower quarter was covered in some dark-green colour (*figures 3.5 g*). Over time, the dark-green "plug" rose up the reactor until it reached the top, which

then gradually disappeared. However, light-green colouring which covered almost the entire reactor after the dark-green colouring had disappeared, begun to clear at the lower section and by the 750th minute, only a small light-green "plug" hang on the upper liquid level (*figure 3.5h*).

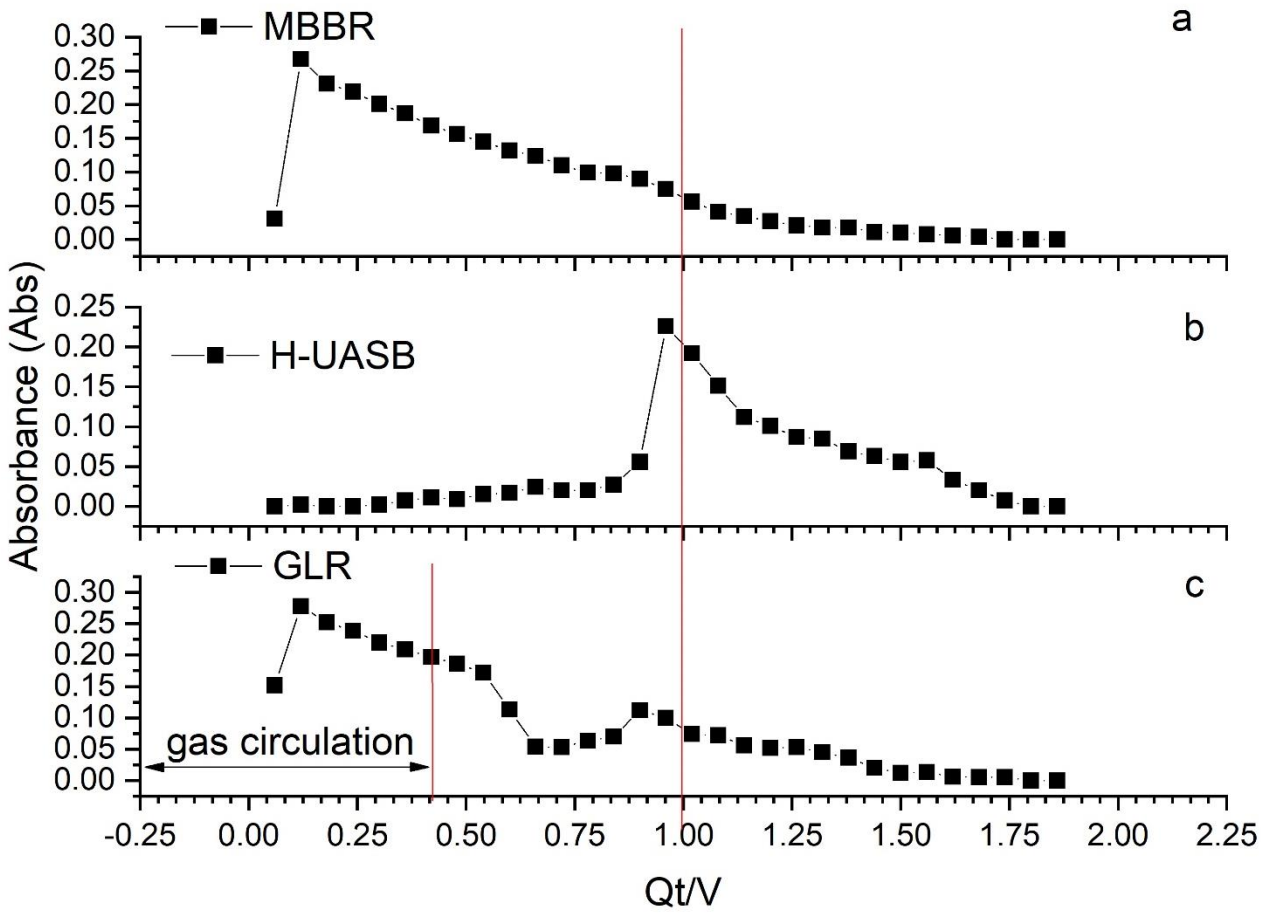

Figure 3. 4. Age distribution of the food colouring in the reactors during RTD analysis: a-MBBR; b-H-UASB and c-GLR. Q - flow rate; t - time (minutes); V - volume.

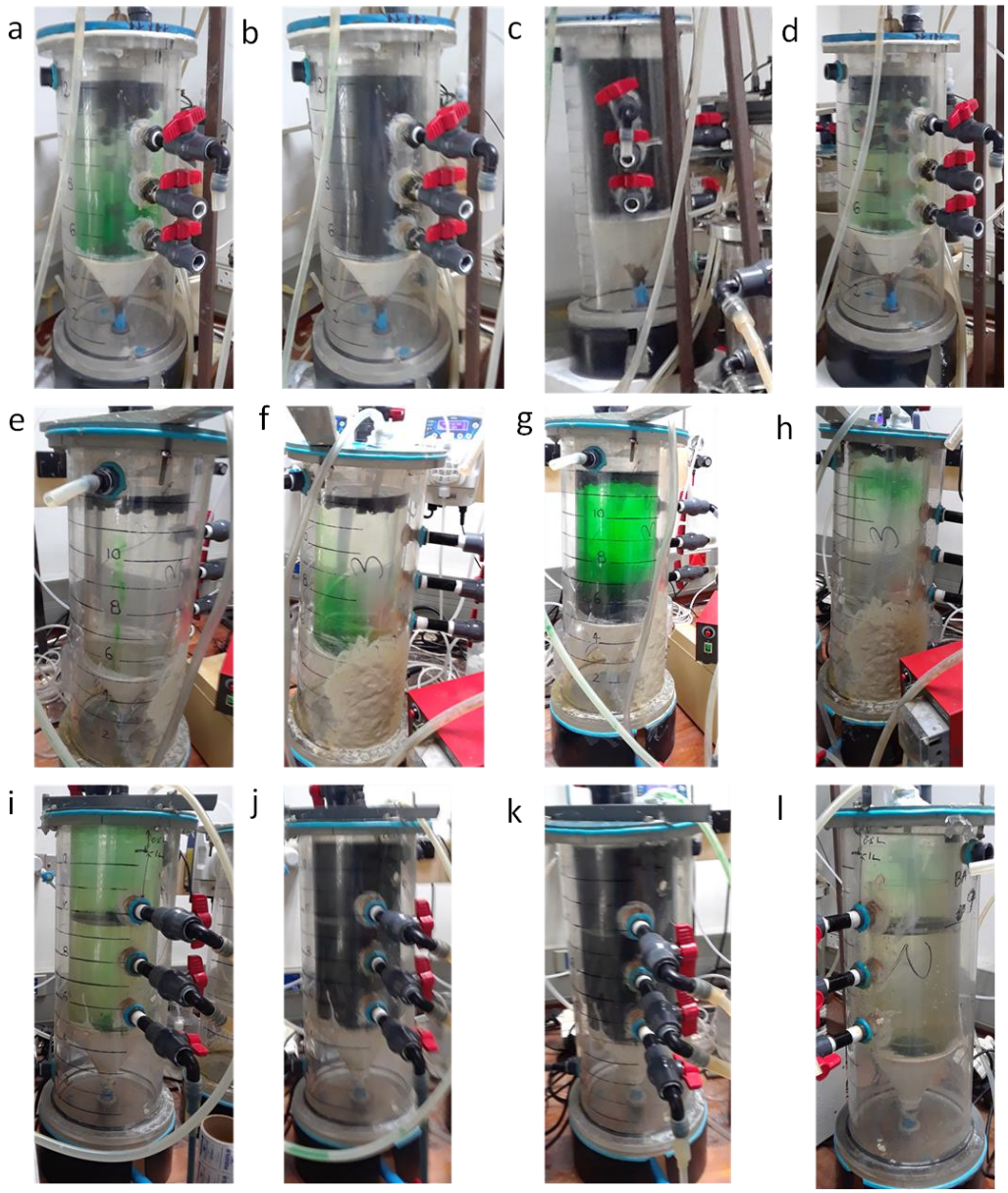

Figure 3. 5. Photographic images of the reactors upon injection of the food colouring: MBBR - a to d; H-UASB - e to h and GLR - i to l after 1 minute (a, e and i), 4 minutes (b, f and j), 150 minutes (c, g and k) and 720 minutes (d, h and l).

3.3.3 Stoichiometry of nitrite consumption and nitrate production per ammonium consumption

The ratios of NO_2^- consumed per NH_4^+ consumed ($\Delta NO_2^-/\Delta NH_4^+$) and NO_3^- produced per NH_4^+ ($\Delta NO_3^-/\Delta NH_4^+$) consumed significantly varied in the reactors during the study period (*figure 3.6*) (ANOVA, $p<0.005$). The $\Delta NO_2^-/\Delta NH_4^+$ and $\Delta NO_3^-/\Delta NH_4^+$ ratios during phase I (days 1-45) fluctuated from <-10 to >10 in all the reactors (*Figure 3.6*). In phases II (days 46-86), the $\Delta NO_2^-/\Delta NH_4^+$ and $\Delta NO_3^-/\Delta NH_4^+$ ratios in all the reactors ranged between -0.6 and 3, except on the 74th day in GLR when the $\Delta NO_3^-/\Delta NH_4^+$ was approximately 9.43 (*figure*

3.6). Towards the end of phase III, the calculated $\Delta NO_2^-/\Delta NH_4^+$ and $\Delta NO_3^-/\Delta NH_4^+$ ratios in the MBBR approached the stoichiometric ratios expected of ANAMMOX process (*figure 3.6a*). Conversely, in the H-UASB, the $\Delta NO_2^-/\Delta NH_4^+$ ratios in phase III were lower (0.42±0.29) than the stoichiometric ratios (1.32) expected of ANAMMOX process, while the $\Delta NO_3^-/\Delta NH_4^+$ ratios were close to the stoichiometric ratios of ANAMMOX process (*figure 3.6b*). In GLR, the $\Delta NO_2^-/\Delta NH_4^+$ ratios were also lower than the stoichiometric ratios of ANAMMOX process during this phase, while the $\Delta NO_3^-/\Delta NH_4^+$ ratios were higher (0.70±0.64) than the stoichiometric ratios expected of ANAMMOX process (*figure 3.6c*). However, at the beginning of phase IV, the $\Delta NO_2^-/\Delta NH_4^+$ and $\Delta NO_3^-/\Delta NH_4^+$ ratios in the H-UASB approached the stoichiometric ratios expected of ANAMMOX process (*figure 3.6b*), while in the GLR, the $\Delta NO_2^-/\Delta NH_4^+$ and $\Delta NO_3^-/\Delta NH_4^+$ ratios were only close to the stoichiometric ratios expected of ANAMMOX process towards the end of phase IV (*figure 3.6c*). Fluctuations in $\Delta NO_2^-/\Delta NH_4^+$ and $\Delta NO_3^-/\Delta NH_4^+$ ratios were observed in the MBBR in phase IV (*figure 3.6a*). During this period, the attachment of biomass on reactor wall in the MBBR was also observed, and the colour of the biomass turned dark brown (*Chapter 5*).

From phase V onwards, the $\Delta NO_2^-/\Delta NH_4^+$ ratios in all the reactors remained close to the stoichiometric ratios of ANAMMOX process, except in phase VIII in H-UASB when the $\Delta NO_2^-/\Delta NH_4^+$ ratios were 0.14±0.13 (*figure 3.6b*). The $\Delta NO_3^-/\Delta NH_4^+$ ratios were slightly lower than the stoichiometric ratio (0.26) in the MBBR and GLR between phases V and VII (0.06±0.03 and 0.11±0.08, respectively), while in the H-UASB, it was close to the stoichiometric ratio expected of ANAMMOX process (0.17±0.08) (*figure 3.6b*). In phase VIII, the $\Delta NO_3^-/\Delta NH_4^+$ ratios in the MBBR and GLR were 0.07±0.03 and 0.08±0.04, respectively, while in the H-UASB, it was 0.31±0.13. Decreases in the $\Delta NO_3^-/\Delta NH_4^+$ ratios were observed in all the reactors in the final phase (phase IX), reaching 0.03±0.02, 0.10±0.08 and 0.03±0.01 in the MBBR, H-UASB and GLR, respectively.

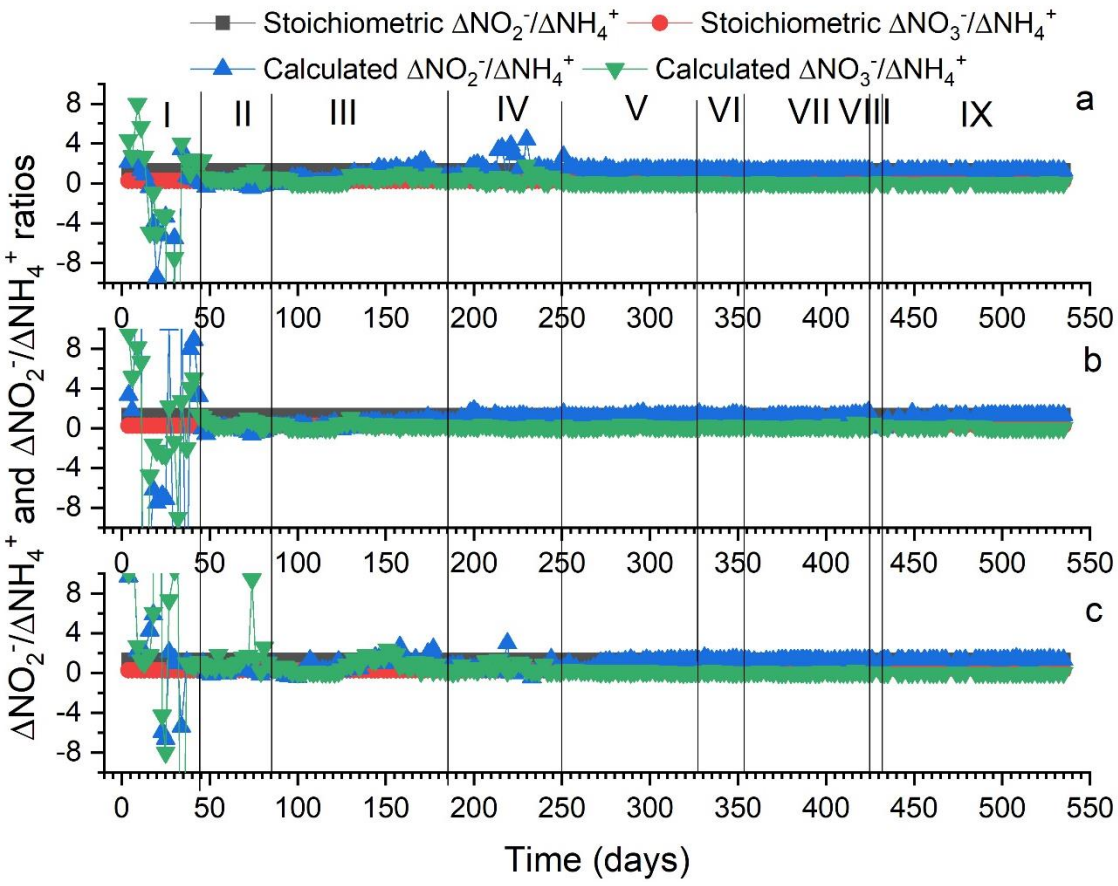

Figure 3. 6. Truncated $\Delta NO_2^-/\Delta NH_4^+$ and $\Delta NO_3^-/\Delta NH_4^+$ ratios in the reactors; a-MBBR, b-H-UASB and c-GLR.

3.3.4 Effluent nitrogen concentrations

Instances of higher concentrations of NH_4^+ in the effluent compared to the influent were observed in all the reactors in phase I (*figures 3.7 a-c*). The average effluent NH_4^+ concentration in all the reactors in phase I was above 40 mg-N/L. However, in phase II, more than 50% decrease in average effluent NH_4^+ concentrations were observed in both MBBR and H-UASB compared to phase I, while only a 2% decrease in the average effluent NH_4^+ concentrations were observed in GLR (*figures 3.7 a-c*). Conversely, in phase III, the average effluent NH_4^+ concentrations in MBBR increased by approximately 92%, while 18% and 1% decreases were recorded in H-UASB and GLR, respectively (*figures 3.7 a-c*). A further 3% increase in the effluent NH_4^+ concentrations were observed in the MBBR in phase IV, while approximately 62% and 22% decreases were observed in H-UASB and GLR, respectively, during the same period. Between phases IV and V, the effluent NH_4^+ concentrations decreased by approximately 75% in MBBR, and remained close to these concentrations until the end of the study (*figure 3.7c*). However, fluctuation in the effluent

NH_4^+ concentrations was observed in the H-UASB during this period (*figures 3.7a*), while gradual decreases in the effluent NH_4^+ concentrations were observed in the GLR during the same period (*figure 3.7b*). A 94% decrease in the effluent NH_4^+ concentrations were observed in the GLR between phases IV and IX (*figure 3.7b*), while a 386% increase in the effluent NH_4^+ concentrations was observed in the H-UASB between phases IV and VI, followed by a 43% decrease between phase VI and VII (*figure 3.7a*). The pH controller malfunctioned on the 425th day in the H-UASB, leading to a drop in the pH in the reactor to approximately 3, leading to a 268% jump in the average effluent NH_4^+ concentrations, which then decreased by 63% in the final phase (*figure 3.7a*).

Higher concentrations of NO_2^- in the effluent compared to the influent were also observed in the MBBR (phase I), H-UASB (phases II-III) and GLR (phases II-III), similar to the concentrations of NH_4^+ (*figures 3.7 a-c*). The average effluent NO_2^- concentrations ranged between 29 mg-N/L and 40 mg-N/L in phases I and II in both MBBR and GLR (*figures 3.7b and 3.7c*), while in the H-UASB, the average effluent NO_2^- concentrations during the same period ranged between 17 mg-N/L and 42 mg-N/L (*figures 3.7a*). In phase III, 35% and 28% decreases in the average effluent NO_2^- concentrations were observed in the MBBR and H-UASB (*figures 3.7a and 3.7c*), respectively, while 31% decrease was observed in the GLR (*figure 3.7b*). A further 68% increase in the average effluent NO_2^- concentration was observed in the GLR between phases III and IV, while 36% and 78% decreases were observed in MBBR and H-UASB, respectively. In phase V, 70% and 26% decreases in the average effluent NO_2^- concentrations were observed in the MBBR and GLR, respectively, while a 443% increase was observed in the H-UASB during this period (*figures 3.7 a-c*). In MBBR and H-UASB, 182% and 117% increases in the average effluent NO_2^- concentrations were observed between phases V and VI, followed by approximately 62% and 33% decreases between phases VI and VII, respectively (*figures 3.7a and 3.7c*). In the GLR, the average NO_2^- concentrations in the effluent decreased by ca. 24% between phases V and VI, before further decreasing by 46% between phases VI and VII (*figure 3.7b*). When the pH controller malfunctioned in phase VIII in H-UASB, an increase in the concentration of NO_2^- by 169% was observed in the effluent. An increase in the concentration of NO_2^- in the effluent was also observed in the MBBR by 229% during this phase, while a decrease by 75% was observed in the GLR (*figures 3.7 a-c*). In the final phase, the average effluent NO_2^- concentrations in the H-UASB decreased by approximately 66% (*figure 3.7a*), while in the MBBR and GLR, 77% and 75% decreases were observed (*figures 3.7b and 3.7c*).

The average effluent NO_3^- concentrations in phase I were approximately 23 mg-N/L, 14 mg-N/L and 23 mg-N/L in MBBR, H-UASB and GLR, respectively (*figures 3.7 a-c*). In phase II, approximately 41% and 36% increases in the effluent NO_3^- concentrations were observed in the MBBR and H-UASB, respectively, while only 8% increase was observed in GLR during this phase. However, in phase III, approximately 53%, 28% and 43% decreases in the average effluent NO_3^- concentrations were observed in MBBR, H-UASB and GLR, respectively (*figures 3.7 a-c*). The average effluent NO_3^- concentrations increased by approximately 14% in the MBBR in phase IV, and remained close to this concentration until the end of phase VI. Between phases VI and VII, the average effluent NO_3^- concentrations decreased by 37%, and remained close to this concentration until the end of the study. In the H-UASB, the average effluent NO_3^- concentrations decreased by approximately 31% in phase IV, followed by 69% increase between this phase and phase VII (*figure 3.7a*). In phase VIII, when the pH controller malfunctioned, the average effluent NO_3^- concentrations decreased by 69%, which then increased by 68% in the final phase (*figure 3.7a*). In the GLR, the average effluent NO_3^- concentrations increased by approximately 19% in phase IV, and remained close to this concentration until phase VII (*figure 3.7b*). In phase VIII, a 37% decrease in the effluent NO_3^- concentrations were recorded in the GLR, followed by a further 39% decrease in the final phase (*figure 3.7b*).

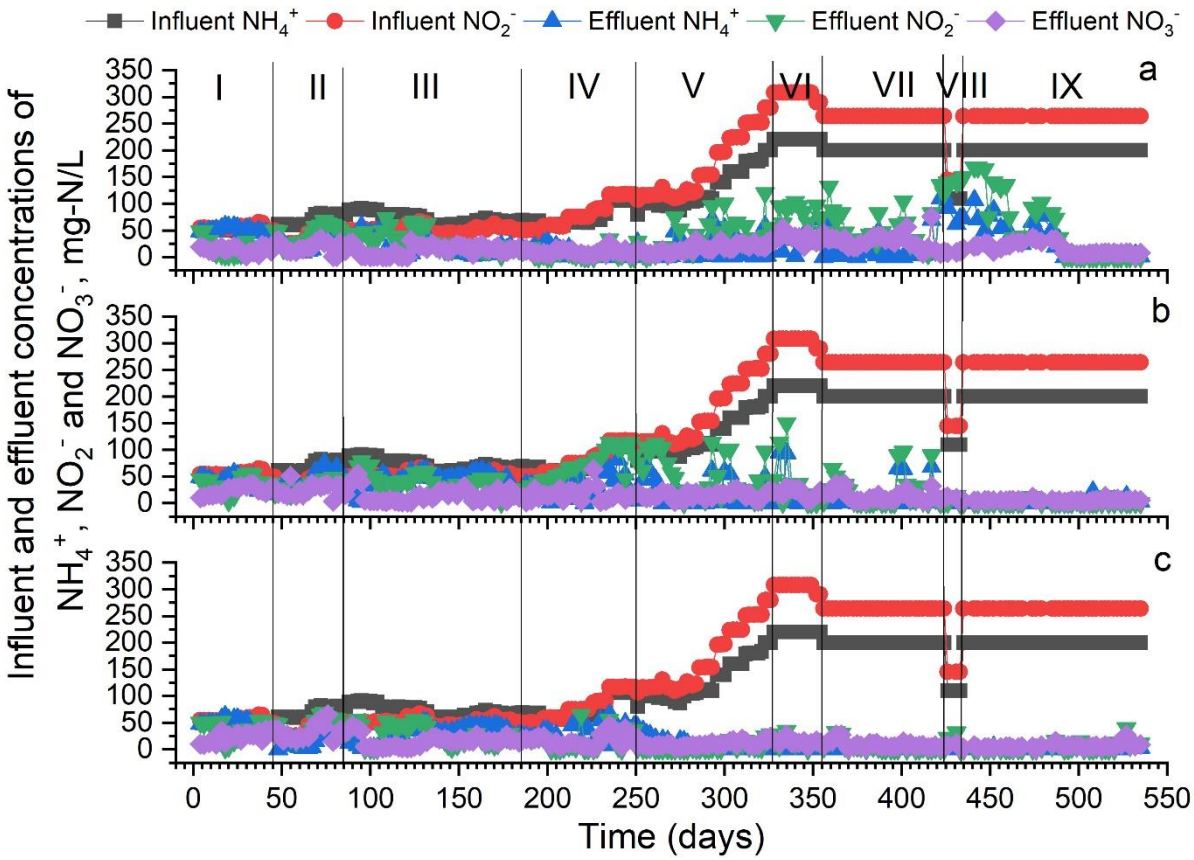

Figure 3. 7. Influent and effluent nitrogen concentrations in H-UASB (a), GLR (b) and MBBR (c).

3.3.5 Nitrogen loading and removal rates

The nitrogen loading rates (NLRs) in MBBR and H-UASB were gradually increased from 0.0192 kg-N/m^3-day in phase I to 1.056 kg-N/m^3-day in phase VI, while the NLRs in GLR were gradually increased from 0.0146 kg-N/m^3-day in phase I to 1.056 kg-N/m^3-day in phase VIII (*figure 3.8*). Beyond phase VI, the NLRs varied between 0.928 kg-N/m^3-day and 0.464 kg-N/m^3-day in all the reactors. The HRT in H-UASB ranged between 0.2 days and 4.4 days, while the HRT in MBBR and GLR ranged between 0.28 - 4.4 days and 0.28 - 5.8 days, respectively, during the study (*figure 3.8*).

Low NRRs (<0.04 kg-N/m^3-day) were observed in all the reactors in phases I and II (*figure 3.9*). However, between phases III and V, gradual increases in NRRs were observed in all the reactors from 0.056±0.023 kg-N/m^3-day, 0.073±0.043 kg-N/m^3-day and 0.030±0.025 kg-N/m^3-day to 0.468±0.230 kg-N/m^3-day, 0.427±0.191 kg-N/m^3-day and 0.382±0.263 kg-N/m^3-day in MBBR, H-UASB, and GLR, respectively (*figure 3.9*). The highest NRRs during the study of 0.992±0.031 kg-N/m^3-day, 0.750±0.065 kg-N/m^3-day and 0.907±0.171 kg-N/m^3-day were observed in phase VI in MBBR, H-UASB, and GLR, respectively. In

phase VII, the NRR decreased synchronously with NLR, reaching 0.900±0.028 kg-N/m^3-day, 0.722±0.127 and 0.848±0.105 kg-N/m^3-day in MBBR, H-UASB and GLR, respectively (*figures 3.8 and 3.9*). When the pH controller malfunctioned in H-UASB in phase VIII, the NRR decreased to an average of 0.097±0.049 kg-N/m^3-day, while in MBBR and GLR, decreases were observed in synchrony with NLR, reaching 0.764±0.065 kg-N/m^3-day and 0.805 kg-N/m^3-day, respectively (*figures 3.8 and 3.9*). In phase IX, the NRR initially decreased from approximately 0.751 kg-N/m^3-day and 0.808 kg-N/m^3-day on day 425 to approximately 0.458 kg-N/m^3-day and 0.441 kg-N/m^3-day on day 474, and then it gradually increased to reach 0.882 kg-N/m^3-day and 0.912 kg-N/m^3-day on the last day of study in MBBR and GLR, respectively, (*figures 3.8 and 3.9*). In H-UASB, following the malfunctioning of the pH controller, an approximate NRR of 0.05 kg-N/m^3-day was recorded on day 425, which then gradually increased to reach 0.911 kg-N/m^3-day on the last day of study, in synchrony with the gradual increase of NLR during the same period ((*figures 3.8 and 3.9*)). Overall, MBBR showed the highest average NRR (0.405±0.379 kg-N/m^3-day) during the entire study period, while the lowest average NRR was observed in H-UASB (0.358±0.320 kg-N/m^3-day) (*figure 3.9*). In comparison, the average NRR in GLR during the entire study period was 0.367±0.383 kg-N/m^3-day (*figure 3.9*).

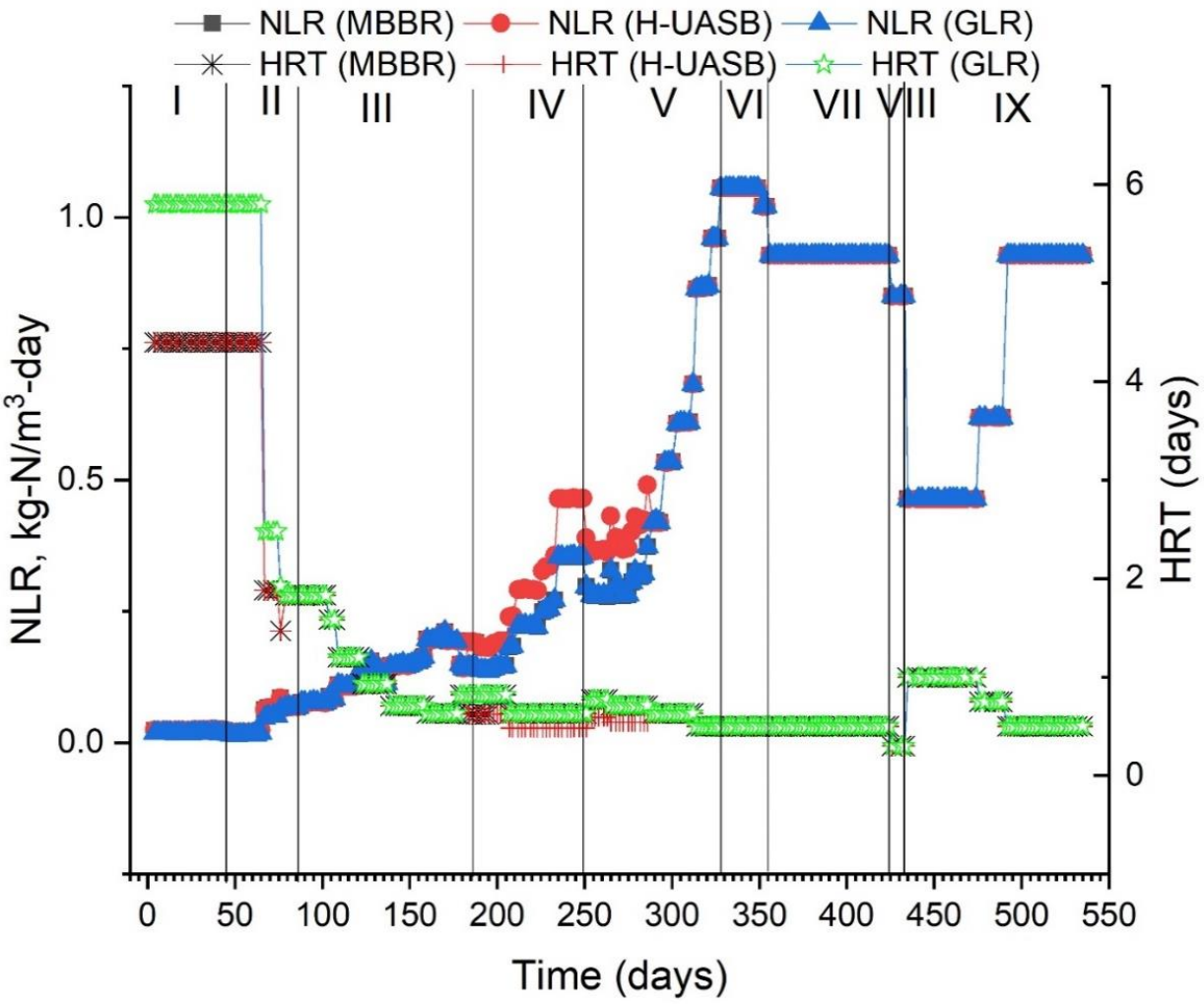

Figure 3. 8. The NLRs and the HRTs in the reactors during the study period.

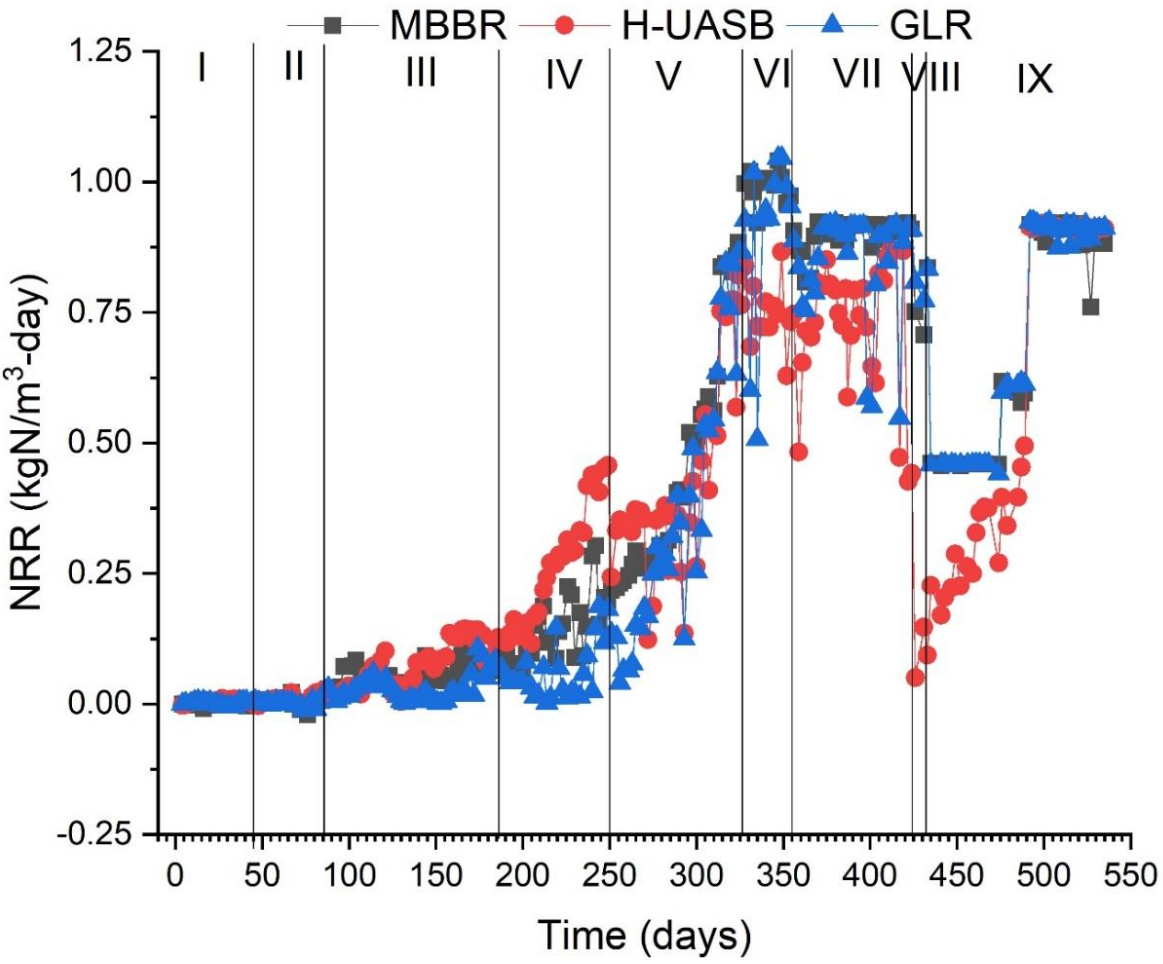

Figure 3. 9. The NRRs in the reactors during the study.

3.3.6 Nitrogen removal efficiencies in the reactors

NREs were low (<30%) in all the reactors in the first two phases (*figure 3.10*). During this period, instances of negative NREs were observed in the reactors when the nitrogen concentrations were higher in the effluent than in the influent (*figures 3.7 and 3.10*). Between phases III and IV, increases in average NREs were observed in all the reactors from 42%, 50% and 23% to 59%, 83% and 25% in MBBR, H-UASB and GLR (*figure 3.10*). In both phases III and IV, the highest average NRE was observed in H-UASB, while the lowest was observed in GLR. Conversely, from phase V onwards, the highest NREs were observed in the MBBR, except in the last two phases (during which the highest average NREs were observed in GLR). During this period (phases V-IX), the NREs in the H-UASB were the lowest (*figure 3.10*). Overall, significant variation in NREs was observed in the reactors during the study period (ANOVA, $p<0.005$), and the average NRE in the MBBR during the entire study period was the highest at 67±36%, while the average NRE in the GLR was the lowest (54±39%).

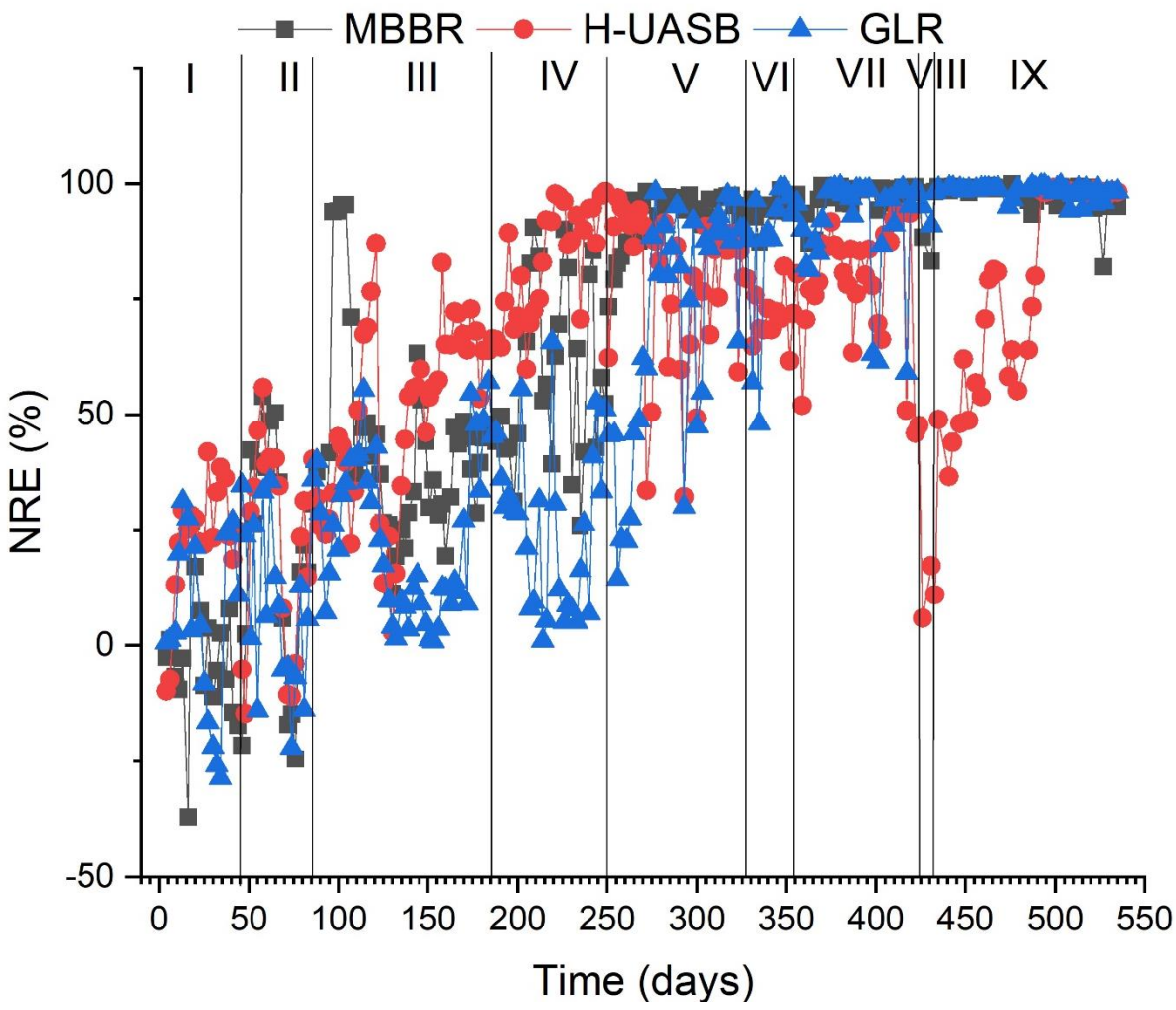

Figure 3. 10. Total nitrogen removal efficiencies in the reactors during the study.

3.3.7 Free ammonia and free nitrous acid

The average FA and FNA concentrations in the reactors in phase I ranged from 50 mg-N/L and 0.0021 mg-N/L to 61.5 mg-N/L and 0.0024 mg-N/L, respectively (*figures 3.11a and 3.11b*). The average FA concentrations in phase II in MBBR and H-UASB were estimated to have decreased by 68% and 7% from approximately 58 mg-N/L and 61 mg-N/L, respectively (*figure 3.11a*), while an increase from 51 mg-N/L by approximately 2% was estimated in GLR. On the contrary, the average FNA concentrations in MBBR and H-UASB were estimated to be 1.03-fold and 1.05-fold higher in phase II compared to phase I, while in the GLR, it was estimated to be only 0.8 times its concentration (*figure 3.11b*).

In phase III, the average FA was estimated to have increased 1.92-fold in MBBR, while its average concentrations in H-UASB and GLR were estimated to have remained close to those in phase II (*figures 3.11a*). The average FNA in phase III, on the other hand, was 0.65-fold, 1.03-fold and 1.31-fold its concentration in MBBR, H-UASB and GLR in phase III,

respectively, (*figure 3.11b*). A 3% increase in the average FA concentration was estimated in phase IV in MBBR, while 11% and 22% decreases were estimated in H-UASB and GLR, respectively (*figures 3.11a*). Conversely, the average FNA decreased by 36% in MBBR, while in H-UASB and GLR, it increased by 6% and 68%, respectively (*figure 3.11b*).

From phase V onwards, the average FA was estimated to be the lowest in MBBR (*figure 3.11a*), while the FNA was estimated to be the lowest in the MBBR in all but the last phase, in which the FNA in GLR was estimated to be the lowest (*figure 3.11b*). During this period, the FA and FNA were estimated to be the highest in H-UASB. The average FA and FNA were estimated to be 19.30±22.85 mg-N/L and 0.0010±0.0011 mg-N/L, respectively, in the MBBR for the entire study period, while their concentrations in H-UASB were estimated to be 91.51±41.74 mg-N/L and 0.0059±0.0037 mg-N/L, respectively. In comparison, the average FA and FNA in GLR during the entire study period were estimated to be 28.71±29.64 mg-N/L and 0.0020±0.0020 mg-N/L, respectively (*figures 3.11a and 3.11b*).

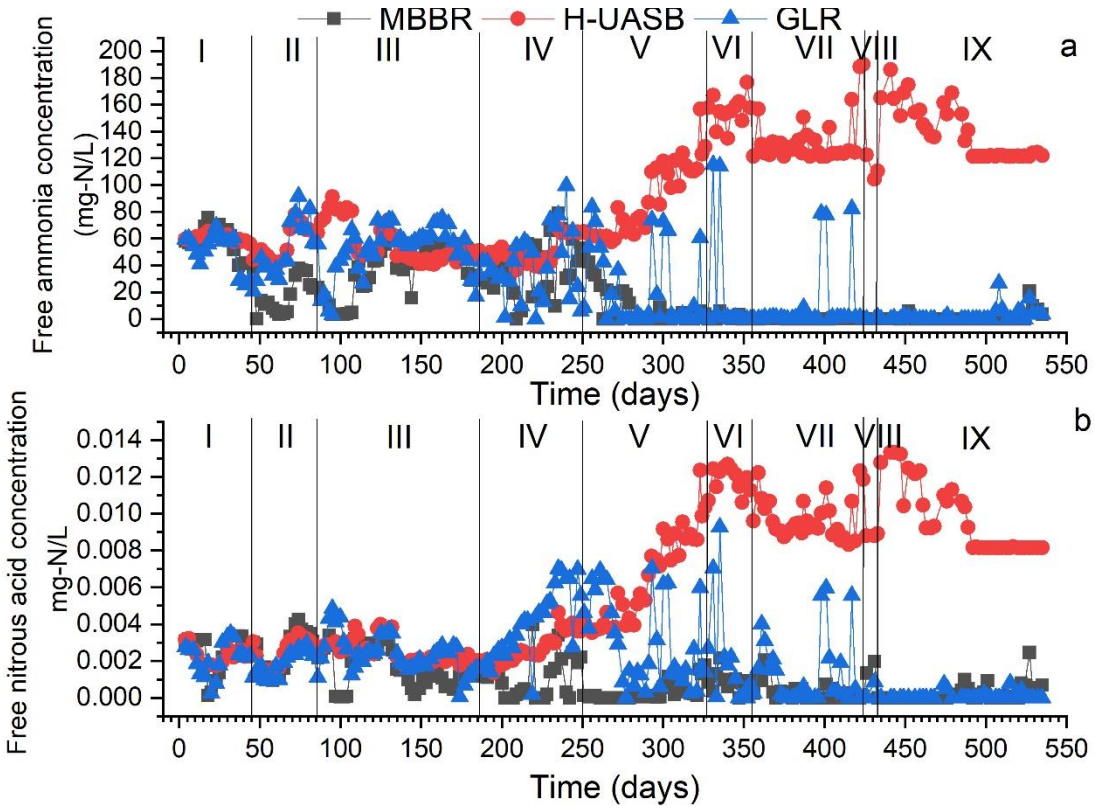

Figure 3. 11 Free ammonia (a) and free nitrous acid (b) concentrations in the reactors during the study.

3.4 Discussion

3.4.1 Residence time distribution

RTD analysis indicated that the MBBR either contained some "dead water" in the system whereby a good portion of the water in the system get trapped in the eddies and thus spend more time than the mean length of time in the system as was demonstrated by Danckwerts (1953), or there was bypassing within the reactor (Scott 2016). The long tail observed on the curve could indicate the presence of dead zones within which the food colouring slowly diffused in the MBBR (*figure 3.5 a*) (Scott 2016). On the other hand, the curve observed in the H-UASB was similar to *figure 2b* in a previous report by Danckwerts (1953) which was reported to belong to a plug-flow system with some longitudinal mixing. Indeed, visual inspection of H-UASB revealed longitudinal mixing in H-UASB as some green colour was seen extending from the base of the reactor up to just above the middle section of the reactor (*figure 3.5e*), which preceded some dark green "plug" which was observed after 150 minutes (*figure 3.5g*). In the GLR, the decaying of the colouring followed the same trend as the MBBR during the first 180 minutes of the experiment when gas was circulated in the reactor, which indicated that this reactor also either contained some "dead water" similar to MBBR (Danckwerts 1953), or there was bypassing within the reactor during this period (Scott 2016). After the circulation of gas in the reactor was stopped, the decaying of the food colouring followed similar trend as the H-UASB in which a spike preceded gradual decrease of the effluent's absorbance (*figure 3.4b*), an indication that this system displayed plug-flow characteristics with some longitudinal mixing from the 180th minute onwards (Danckwerts 1953). Indeed, the presence of plug-flow conditions could be determined from the captured photographic images of the GLR as a light green "plug" could be observed hanging on the upper liquid level on the 720th minute (*figure 3.5l*), similar to that observed in the H-UASB during the same period (*figure 3.5h*). On the contrary, a uniform variation in the intensity of the green colour was observed in the course of the experiment within the MBBR, an indication of better mixing (homogeneous colouring distribution) within this reactor (*figures 3.5 a-d*).

3.4.2 Process performance

A significant variation in process performance with reactor configuration was observed during the study (ANOVA, p<0.005). Changes in the NREs, NRRs and the effluent concentrations of NO_2^-, NH_4^+ and NO_3^- as well as the $\Delta NO_2^-/\Delta NH_4^+$ and $\Delta NO_3^-/\Delta NH_4^+$ ratios were observed in the course of study in all the reactors (*figures 3.6 -3.10*)

In the initial phase (phase I), there was low nitrogen removal in all the reactors (*figures 3.7-3.10*). This could have been because the ANAMMOX bacteria were still adapting to the operating conditions in the reactors (Zhao *et al.* 2018). However, during this period, heterotrophic bacteria could have been actively breaking down cellular organic material such as the cells of dead bacteria, leading to the release of NH_4^+ (Tang *et al.* 2009). Consequently, this could have resulted in the accumulation of NH_4^+ in the reactors, hence the observed presence of higher concentrations of NH_4^+ in the effluent than in the influent. Additionally, heterotrophic bacteria may have also competed for NO_2^- with ANAMMOX bacteria, further limiting ANAMMOX bacterial activities, and consequently, affecting the removal of nitrogen in the reactors (Li *et al.* 2018). This could have then led to the observed fluctuation of the $\Delta NO_2^-/\Delta NH_4^+$ and $\Delta NO_3^-/\Delta NH_4^+$ ratios from <-10 to >10 (*figures 3.6 a-c*). The negative $\Delta NO_2^-/\Delta NH_4^+$ and $\Delta NO_3^-/\Delta NH_4^+$ ratios, in particular, were due to the presence of NH_4^+ at higher concentrations in the effluent than in the influent (*figures 3.6-3.7*). Conversely, the $\Delta NO_2^-/\Delta NH_4^+$ ratios higher than the stoichiometric 1.32 ratio (expected of ANAMMOX process) could have been because of high consumption rates of NO_2^- than the consumption of NH_4^+ in the reactors, possibly by the heterotrophic bacteria and/or NOB (Laureni *et al.* 2015). On the other hand, the $\Delta NO_3^-/\Delta NH_4^+$ ratios higher than 0.26 (expected of ANAMMOX process) may be as a result of higher activities of NOB in the reactors, leading to NO_3^- accumulation (Christensson *et al.* 2013). Similar trends in $\Delta NO_2^-/\Delta NH_4^+$ and $\Delta NO_3^-/\Delta NH_4^+$ ratios were previously reported during the start-up of lab-scale ANAMMOX-mediated reactors (Tang *et al.* 2009; Jin *et al.* 2013), and full-scale ANAMMOX-mediated system (van der Star *et al.* 2007).

In phase II, the $\Delta NO_2^-/\Delta NH_4^+$ and $\Delta NO_3^-/\Delta NH_4^+$ ratios fluctuated over a smaller range than in phase I (*figure 3.6*). An improvement in nitrogen removal was also observed in all the reactors during this period (*figures 3.7 and 3.10*), possibly because of acclimatization of the bacterial communities to the operating conditions in the reactors. However, the average $\Delta NO_2^-/\Delta NH_4^+$ ratios were still negative in this phase in the MBBR and the H-UASB as the effluent NO_2^- concentrations were higher than in the influent. It is thus possible that the activities of the AOB were enhanced during this phase since the DO concentration in the influent was not regulated and was approximately 8.5±0.3 mg-O_2/L (*table 3.2*). On the contrary, in the GLR, both the average $\Delta NO_2^-/\Delta NH_4^+$ and $\Delta NO_3^-/\Delta NH_4^+$ ratios were positive, probably because the circulation of argon/CO_2 mixture removed oxygen from the bulk liquid, limiting the AOB activities. However, despite the observed accumulation of NO_2^- in

the MBBR and H-UASB, nitrogen removal in all the reactors was higher in phase II compared to phase I (*figures 3.7 a-c and 3.10*). Zhao *et al.* (2018) reported similar NRRs within the first 77 days (lag phase) of reactor operation in their study, an indication that phases I and II in this study represented the lag phase.

In phase III, when the DO concentration in the influent was maintained below 0.5 mg-O_2/L (*table 3.2*), the $\Delta NO_2^-/\Delta NH_4^+$ and $\Delta NO_3^-/\Delta NH_4^+$ ratios in the MBBR approached the stoichiometric ratios expected of ANAMMOX process. However, the $\Delta NO_2^-/\Delta NH_4^+$ and $\Delta NO_3^-/\Delta NH_4^+$ ratios were still fluctuating in both GLR and H-UASB during this period (*figures 3.10 a-c*), an indication that the bacterial communities had not stabilised in these reactors during this period (Jin *et al.* 2013). This could suggest that the maintenance of low DO concentration in the influent favoured ANAMMOX bacterial activities, leading to the observed improvement in nitrogen removal as well as less fluctuations in the ratios of $\Delta NO_2^-/\Delta NH_4^+$ and $\Delta NO_3^-/\Delta NH_4^+$ (*figures 3.6, 3.9 and 3.10*). The gradual increases in the NLRs in the reactors could have also stimulated the activities of ANAMMOX bacteria, leading to the improvements in the process performance (*figures 3.8, 3.9 and 3.10*) (Sun *et al.* 2018).

The $\Delta NO_2^-/\Delta NH_4^+$ and the $\Delta NO_3^-/\Delta NH_4^+$ ratios close to the stoichiometric ratios expected of ANAMMOX process were observed in both GLR and H-UASB in phase IV, when the influent NO_2^- and NH_4^+ concentrations averaged 81 mg-N/L and 75 mg-N/L *(table 3.2*). However, in the MBBR, $\Delta NO_2^-/\Delta NH_4^+$ ratios higher than 1.32 (expected of ANAMMOX process) was observed, probably because of competition for NO_2^- between ANAMMOX bacteria, heterotrophic bacteria and NOB (Laureni *et al.* 2015). Therefore, to recover ANAMMOX bacterial activities, the biomass attaching on the walls of MBBR were scrubbed with a brush every week as previously suggested by Laureni *et al.* (2015) (*Chapter 5*). Following these interventions, ANAMMOX bacterial activities were recovered as evidenced by the $\Delta NO_2^-/\Delta NH_4^+$ ratios re-aligning once again with the stoichiometric ratios expected of ANAMMOX process. Despite the fluctuation of $\Delta NO_2^-/\Delta NH_4^+$ ratios in the MBBR, an improvement in the nitrogen removal (NRR and NRE) was observed in the MBBR during this period compared to phase III. However, the NRRs and the NREs in the MBBR were still lower than those in the H-UASB (*figures 3.9a, 3.9c and 3.10*), probably because plug-flow in the H-UASB favoured ANAMMOX bacterial growth than complete mixing in the MBBR (*Chapter 4*). Similarly, the average NRRs and the NREs in the GLR were also lower than in the H-UASB, possibly because plug-flow in the H-UASB favoured

ANAMMOX bacterial growth better than the sequential circulation of argon/CO_2 gas mixture (in the GLR) (*Chapter 4*). This was a new finding and has not been reported in any previous study.

With further increases in the NLRs, improvements in the NRRs and the NREs were observed in all the reactors in phase V (*figures 3.9 and 3.10*). However, in this phase, higher average NRRs and NREs were observed in the MBBR compared to the H-UASB for the first time during the study. Less fluctuation in nitrogen removal was also observed in the MBBR than in the H-UASB and GLR during this period (*figures 3.9 and 3.10*), possibly because of lower concentrations of both FA and FNA in the MBBR compared to GLR and H-UASB (*figures 3.11a and 3.11b*) (Fernández *et al.* 2012; Jaroszynski *et al.* 2012). It is thus possible that continuous mixing in the MBBR improved mass transfer, leading to higher nitrogen removal compared to plug-flow in H-UASB and internal gas circulation in GLR (*figures 3.9 and 3.10*). It is also possible that the heterotrophic bacteria were more active in the MBBR than they were in both GLR and H-UASB as the $\Delta NO_3^-/\Delta NH_4^+$ were lower than the stoichiometric ratios during this phase (Kindaichi *et al.* 2007). Several researchers including Kindaichi *et al.* (2007), Dapena-Mora *et al.* (2004d), Liu *et al.* (2016) and Zhang *et al.* (2016b) have indicated that heterotrophic bacteria can grow on the NO_3^- (produced through ANAMMOX activities) and the organic carbon in form of EPS, dead bacterial biomass and EDTA (present in the synthetic feed). The consumption of NO_3^- by these bacteria could have thus led to the observed lower $\Delta NO_3^-/\Delta NH_4^+$ ratios than the stoichiometric ratio of 0.26 expected of ANAMMOX process. Based on the $\Delta NO_3^-/\Delta NH_4^+$ ratios, it is therefore likely that the MBBR had higher heterotrophic bacterial activities than the H-UASB and GLR during this period. This, in turn, could have enhanced nitrogen removal (Gu *et al.* 2018), leading to higher NRRs and NREs in MBBR compared to H-UASB and GLR during this phase (*figures 3.9 and 3.10*).

In phase VI, the influent $\Delta NO_2^-/\Delta NH_4^+$ ratio was kept at 1.4 in the feed (*figures 3.7 a-c*), which was higher than the ideal ratio for the ANAMMOX process. This was done in order to limit the growth of NOB while favouring the enrichment of ANAMMOX bacteria as previously suggested by Gasa *et al.* (2019). With these changes, the NRRs increased to 0.99 ± 0.03, 0.75 ± 0.06 and 0.91 ± 0.17 kg-N/m^3-day in MBBR, H-UASB and GLR, respectively, which were within the range of ANAMMOX-mediated full-scale systems reported by (Lackner *et al.* 2014; Shi, Wells and Morgenroth 2016). However, in this phase, it was observed that the nitrogen removal in H-UASB and GLR was still fluctuating (*figures*

3.9 and 3.10), possibly because of FA and FNA inhibition of ANAMMOX activities (Fernández *et al.* 2012; Jaroszynski *et al.* 2012). In comparison, the estimated concentration of FA in the MBBR in phase VI was non-inhibitory as it was less than the inhibitory concentration of 2 mg/L reported by Jaroszynski *et al.* (2012), while its concentration in the H-UASB and GLR was estimated to be above this inhibitory threshold (*figure 3.11a*). Similarly, the concentration of FNA was estimated to be close to the non-inhibitory concentrations of 0.5 μg-N/L in the MBBR, while that in both GLR and H-UASB were estimated to be considerably higher (*figures 3.11b*) (Fernández *et al.* 2012). Therefore, as a result of the observed fluctuations in the nitrogen removal in the GLR and H-UASB, the NLRs were decreased from an average of 1.05 kg-N/m^3-day to 0.93 kg-N/m^3-day in phase VII in all the reactors (*figures 3.8*). The $\Delta NO_2^-/\Delta NH_4^+$ ratio was also reduced to 1.32 in the influent (*figures 3.7 a-c*). Since the average NRRs and NREs increased further in both H-UASB and GLR when these interventions were effected (*figures 3.9 and 3.10*), it indicates that the FA and FNA were inhibiting bacterial activities in the H-UASB and GLR in phases V and VI (*figures 3.11a and 3.11b*). Similar to phase V, the $\Delta NO_3^-/\Delta NH_4^+$ ratios in the MBBR were lower compared to H-UASB and GLR between phases VI and VII, an indication of higher heterotrophic activities in this reactor (Kindaichi *et al.* 2007). It is possible that stirring in the MBBR stimulated higher EPS generation compared to GLR and H-UASB that were not subjected to continuous shear forces (Wu *et al.* 2009). The heterotrophic bacteria could have then used the secreted EPS as a source of carbon and energy, in addition to EDTA (in the feed) and the dead bacterial cells, to reduce the NO_3^- produced by ANAMMOX bacteria (Liu *et al.* 2016; Zhang *et al.* 2016b).

When the pH controller malfunctioned on the 425th day (phase VIII) leading to a decrease in the pH to below 3 in H-UASB, a drop in the NRE and NRR to about 5 % and 0.05 kg-N/m^3-day, respectively, was observed, indicating possible deactivation of bacteria (*figures 3.9 and 3.10*) (Egli *et al.* 2001). Similarly, the $\Delta NO_2^-/\Delta NH_4^+$ ratios were lower than the stoichiometric ratio of 1.32 expected of ANAMMOX bacteria during this phase, an indication of a drop in the consumption of NO_2^- compared to that of NH_4^+, possibly also due to the deactivation of the ANAMMOX bacteria. On the contrary, the $\Delta NO_2^-/\Delta NH_4^+$ ratios were close to the stoichiometric ratios in the GLR and MBBR, which suggest that both the NO_2^- and the NH_4^+ were mainly removed through the ANAMMOX pathway. However, the $\Delta NO_3^-/\Delta NH_4^+$ ratios in both GLR and MBBR were still lower than the

stoichiometric ratios expected of ANAMMOX process (*figure 3.6*), which indicate that the heterotrophic bacteria were actively removing NO_3^-, similar to phases VI-IX.

In the final phase (phase IX), the H-UASB reactor recovered, leading to an improvement in nitrogen removal (*Figures 3.9 and 3.10*), possibly because the microbial communities had re-established after a possible de-activation in phase VIII. However, the $\Delta NO_3^-/\Delta NH_4^+$ ratio in the H-UASB was much lower than the stoichiometric ratio during the final phase (*figure 3.6b*), possibly because of the malfunctioning of the pH led to mass bacterial death, leading to accumulation of dead bacterial cells in the reactor. Heterotrophic bacterial communities, in turn, could have consumed the NO_3^- produced by the ANAMMOX bacteria, leading to a decrease in $\Delta NO_3^-/\Delta NH_4^+$ ratio. The NREs, NRRs and the $\Delta NO_3^-/\Delta NH_4^+$ ratios in both MBBR and GLR were comparable during this phase. However, the $\Delta NO_3^-/\Delta NH_4^+$ ratios in both reactors were also still lower than the stoichiometric ratio, also an indication of the presence of active heterotrophic bacterial communities (Agrawal *et al.* 2017; Zhao *et al.* 2018). During this phase, the GLR also displayed stable performance, similar to MBBR, which coincided with low concentrations of FA and FNA (*figures 3.11a and 3.11b*), in agreement with the findings from previous phases indicating that high concentrations of these compounds led to fluctuation in process performance in the reactors.

3.5 Conclusion

Gradual increases in NRRs and NREs were observed in all the reactors during the study, which corroborated the gradual increments of NLRs. MBBR displayed higher and more stable NRRs and NREs than both GLR and H-UASB during the study, while the GLR had the lowest average NREs, and the H-UASB had the lowest average NRRs during the study. The highest average FA and FNA concentrations were estimated in H-UASB, while their lowest average concentrations were observed in the MBBR during the study. Based on the $\Delta NO_2^-/\Delta NH_4^+$ and $\Delta NO_3^-/\Delta NH_4^+$ ratios, start-up of ANAMMOX process in the MBBR was faster than in the H-UASB and GLR, while the start-up of H-UASB was faster than GLR. The drop in the pH in phase X led to bacterial de-activation in the H-UASB, which affected nitrogen removal. Overall, the nitrogen removal in the reactors is comparable to the performance of full-scale systems reported in previous studies.

CHAPTER 4

4 DYNAMICS OF NITRIFYING AND ANAMMOX BACTERIAL COMMUNITIES IN THE ANAMMOX-MEDIATED SYSTEMS

4.1 Introduction

To date, the complete characterization of ANAMMOX bacteria has not been achieved due to the difficulty in isolating them in pure culture (Kartal *et al.* 2013). All the ANAMMOX bacterial species, therefore, have the taxonomical status 'Candidatus' (Kartal *et al.* 2013). Besides ANAMMOX bacteria, it has been reported that AOB, NOB, and heterotrophic bacteria are core community members of ANAMMOX-mediated systems (Agrawal *et al.* 2017; Zhao *et al.* 2018). Apart from this, other microbial groups such as viruses, archaea and protozoans have also been reported in ANAMMOX-mediated systems (Suarez, Persson and Hermansson 2015; Li *et al.* 2017b). The activities of AOB and AOA (ammonia oxidising archaea) could benefit the ANAMMOX process as both groups could generate NO_2^-, while the activities of heterotrophic bacteria and NOB could be detrimental to ANAMMOX process as they present competition to ANAMMOX bacteria for NO_2^-, which acts as an electron acceptor (Agrawal *et al.* 2017; Li *et al.* 2017b). On the other hand, some of the protozoans present in ANAMMOX-mediated systems could graze on autotrophic bacteria, consequently influencing nitrogen removal (Suarez, Persson and Hermansson 2015).

Characterisation of bacterial communities in biological systems could thus be an important step in the description of process performance in ANAMMOX-mediated systems. To date, several techniques have been employed for characterising microbial communities from ANAMMOX-mediated reactors, including polymerase chain reaction (PCR), quantitative polymerase chain reaction (qPCR), 16S rRNA sequencing and *fluorescence in situ hybridization* (FISH) (Vlaeminck *et al.* 2010; Bhattacharjee *et al.* 2017; Park, Park and Chandran 2017; Zhang *et al.* 2017c).

Microbial analyses that were done in previous studies provide crucial information relating to the impact of growth morphology and inoculum on microbial community richness, structures and diversities in ANAMMOX-mediated systems (Date *et al.* 2009; Park *et al.* 2010a). However, more studies under baseline conditions are still necessary to understand

the impact of reactor configuration on the prevailing microbial communities and their impact on nitrogen removal performance.

In this Chapter, changes in bacterial community structures within the reactors during the study period are presented. Bacterial communities in the biomass samples collected from the inoculum and from the reactors in the different phases were characterised through high-throughput sequencing using Illumina MiSeq platform.

4.2 Methodology

4.2.1 DNA extraction

Genomic DNA (gDNA) was extracted from the inoculum and the suspended biomass from each reactor in phases III (day 125), phase IV (day 192), phase V (days 260 and 309) and phase IX (day 535). Approximately 50 ml of mixed liquors were collected from each reactor and centrifuged at 4ºC to obtain pellets. Additionally, in phase IX (day 535), the biomass from five carrier materials which were randomly collected from each reactor was scrubbed off using sterile pipette tips into sterile Eppendorf tubes. Genomic DNA (gDNA) was then extracted from the biomass samples using the Qiagen extraction kit (Qiagen, Denmark) as per the manufacturer's instructions. The quality of DNA was ascertained with Implen NanoPhotometer® and stored at -20ºC until further analysis. The samples were subsequently labelled with reactor name followed by the date of collection. For instance, MBBR125 indicates that the sample was collected on the day 125 (phase III) from MBBR.

4.2.2 Illumina sequencing and phylogenetic characterization of bacterial communities

Multiplexed paired-end (2×300 bp) libraries were prepared using the Nextera XT DNA sample preparation kit (Illumina, San Diego, CA, USA). The gDNA was sequenced on an Illumina MiSeq platform at the Sequencing Core Facility, National Institute for Communicable Diseases (Johannesburg, South Africa). The obtained paired-end reads were analysed using sequence-based ultra-rapid pathogen identification (SURPI) pipeline, a computational pipeline for rapid classification of next-generation sequencing reads according to their origin (Naccache *et al.* 2014). The raw sequencing data were further analysed using CLC microbial genomics module (Qiagen, Germany) to uncover and compare the taxonomic and functional composition of microbial communities in each

sample. Sequencing reads produced during this study have been deposited in the NCBI Short-Read Archive under SRA accession: PRJNA526389.

4.2.3 Statistical analyses

Bacterial diversity, evenness and richness were assessed using R Package Vegan version 2.5-2 for each reactor sample (Oksanen *et al.* 2015), including; rarefaction curves at cut-off levels 3%, Shannon–Weiner diversity index, Pielou's evenness index, observed species, and Simpson diversity index, abundance-based coverage estimators (ACE) and Chao1 estimates of alpha diversity (number of bacterial operational taxonomic units (OTUs)).

4.3 Results

4.3.1 Bacterial diversity, richness, and evenness

The metagenomic analysis of the biomass samples was carried out to profile the microbial community of the different reactors. The rarefaction curves of the sequences at 3% genetic distance suggested that the sequencing depths for the samples were sufficient and therefore, the actual taxonomic diversity was fully covered (*figures A.4.3 a-s, appendix B*). About 123,033 - 1,325,481 effective reads were generated from the inoculum and from the reactor samples after filtering the low-quality reads and trimming using CLC microbial genomics module (Qiagen, Germany). The Chao 1 and ACE at a cut-off level of 3 % are shown in *table 4.1*. The Shannon and Simpson diversity indices ranged from 2.089 (H-UASB260) to 6.261 (H-UASB535BIOFILM) and 0.453 (H-UASB260) to 0.990 (H-UASB535BIOFILM), respectively. The Pielou's Evenness varied from 0.057 (H-UASB260) to 0.124 (H-UASB535BIOFILM) (*table 4.1*). Comparison of the rarefaction analyses with the number of OTUs determined by Chao1 and ACE richness estimators revealed that an average of 70% of the estimated taxonomic richness was covered by the surveying effort (*table 4.1 and figures A.4.3 a-s*), hence a significant fraction of the bacterial diversity within the bioreactor samples was assessed at species and genus level.

The comparison of Chao1 estimates for the suspended biomass samples from the reactors indicated a high level variation in species richness at different phases of the reactors. The lowest species richness of the suspended biomass in the MBBR and GLR was observed in phase V (day 309), while the lowest richness in the H-UASB was observed in phase IX (day 535). On the other hand, the highest species richness of the suspended biomass was observed in the H-UASB in phase III (day 125), whilst the highest in the MBBR and GLR was observed in phases IV (day 192) and III (days 125), respectively (*table 4.1*). Similar

trends in the ACE richness estimator compared to that of Chao 1 was also observed in the reactors (*table 4.1*).

The Shannon index of diversity (H'), Simpson index and the Pielou's Evenness (J) were also determined for the suspended biomass samples (*table 4.1*). The Shannon indices of the suspended biomass ranged from 4.208 to 5.446 in the MBBR, while for the suspended biomass in the H-UASB and GLR, it ranged from 2.086 to 4.789, and from 3.741 to 5.240, respectively. The estimated Simpson index for the suspended biomass in the MBB, H-UASB and GLR were within 0.864 - 0.971, 0.453 - 0.907 and 0.755 - 0.960 ranges, respectively (*table 4.1*). The estimated Pielou's Evenness (J) for the suspended biomass in the MBBR, H-UASB and the GLR were estimated to range from 0.108, 0.057 and 0.094, to 0.121, 0.113 and 0.120, respectively (*table 4.1*).

Following the development of the biofilms on the carrier materials towards the end of the study (*Chapter 5*), microbial analyses of the biomass in the biofilms was done on the last day of reactor operation (day 535). It was found that the biofilms in the H-UASB supported the most diverse (H'=6.261 and Simpson index=0.990) and even bacterial communities (J=0.124), while GLR supported the least diverse (H'=4.209 and Simpson index=0.829) and even communities (J=0.105) (*table 4.1*). In comparison, the H' index, Simpson index and the J index of the biomass growing in the biofilms in the MBBR were estimated to be 4.806, 0.914 and 0.115, respectively (*table 4.1*). The bacterial communities growing in the biofilms in the MBBR were estimated to have the highest Chao 1 richness (3668.000) and ACE (3619.646) richness, while the communities in the biofilms in GLR were estimated to have the least ACE (3426.022) and Chao 1 richness (3560.059) (*table 4.1*).

Table 4.1. Diversity, richness and evenness of bacterial communities in the inoculum and the different reactor samples.

	S.chao1	S.ACE	Shannon index (H')	Simpson index	Pielou's Evenness (J)
	Biomass samples collected from the suspended biomass				
INOCULUM	4649.150	4666.748	3.952	0.808	0.0990
MBBR125 (phase III)	4075.780	4039.519	4.208	0.864	0.108
H-UASB125 (phase III)	4928.696	4870.179	4.506	0.907	0.111
GLR125 (phase III)	4379.860	4267.266	4.379	0.949	0.117
MBBR192 (phase IV)	4597.166	4644.319	4.763	0.925	0.114
H-UASB192 (phase IV)	4551.230	4537.018	4.151	0.884	0.109
GLR192 (phase IV)	4012.627	4054.199	5.240	0.960	0.120
MBBR260 (phase V)	4091.571	4055.756	5.078	0.965	0.121
H-UASB260 (phase V)	3876.061	3705.665	2.089	0.453	0.0570
GLR260 (phase V)	3673.500	3602.112	4.931	0.940	0.119
MBBR309 (phase V)	3481.626	3344.757	4.991	0.946	0.120
H-UASB309 (phase V)	4176.555	4106.805	2.660	0.566	0.0710
GLR309 (phase V)	3641.539	3453.884	4.741	0.924	0.117
MBBR535SUSPENSION (phase IX)	3845.278	3764.317	5.446	0.971	0.121
H-UASB535SUSPENSION (phase IX)	3188.179	3148.390	4.789	0.885	0.113
GLR535SUSPENSION (phase IX)	3778.003	3682.642	3.741	0.755	0.094
	Biomass samples collected from the biofilms				
MBBR535BIOFILM (phase IX)	3668.000	3619.646	4.806	0.914	0.115
H-UASB535BIOFILM (phase IX)	3566.021	3561.002	6.261	0.990	0.124
GLR535BIOFILM (phase IX)	3560.059	3426.022	4.209	0.829	0.105

4.3.2 Microbial community structure of seed inoculum

At the phylum level, Planctomycetes accounted for 45.13% relative abundance, whilst Proteobacteria, the second most abundant phylum, was present at 38.85% relative abundance (*figure 4.1*). The relative abundance of Bacteroidetes Chloroflexi, Actinobacteria and Nitrospirae in the inoculum was 1.49%, 1.52%, 2.28% and 7.32%, respectively (*figure 4.1*).

The relative abundance of the other bacterial phyla (Acidobacteria, Aquificae, Armatimonadetes, Berkelbacteria, Chlamydiae, Chlorobi, Chrysiogenetes, Cyanobacteria, Deferribacteres, Deinococcus-Thermus, Elusimicrobia, Fibrobacteres, Firmicutes, Gemmatimonadetes, Ignavibacteriae, Kiritimatiellaeota, Spirochaetes, Synergistetes, Tenericutes, Thermotogae, Verrucomicrobia) and the unclassified Bacteria was ≤0.93%.

Among the Planctomycetes, ANAMMOX bacteria dominated at 99.99% (*figures 4.2*), with *Candidatus* Kuenenia stuttgartiensis dominating at 99.99 % of the total ANAMMOX bacterial population. *Candidatus* Kuenenia sp. enrichment culture clone hzsB K and *Candidatus* Brocadia sp. 40 were both present at 0.00024% relative abundance, while the relative abundance of ANAMMOX-like bacteria was 0.004% in the inoculum (*figures 4.2*). *Nitrosomonas europaea* and *Nitrospira moscoviensis* were the most dominant species within the AOB and NOB communities, respectively. *Nitrolancea, Nitrosococcus, Ca. Nitrosoglobus, Nitrosospira, Nitrosovibrio* were all present in trace concentrations (<0.093%) *(figures 4.3 and 4.4).* The only COMAMMOX bacterial species detected were *Candidatus* Nitrospira inopinata, which were present at 0.9% relative abundance.

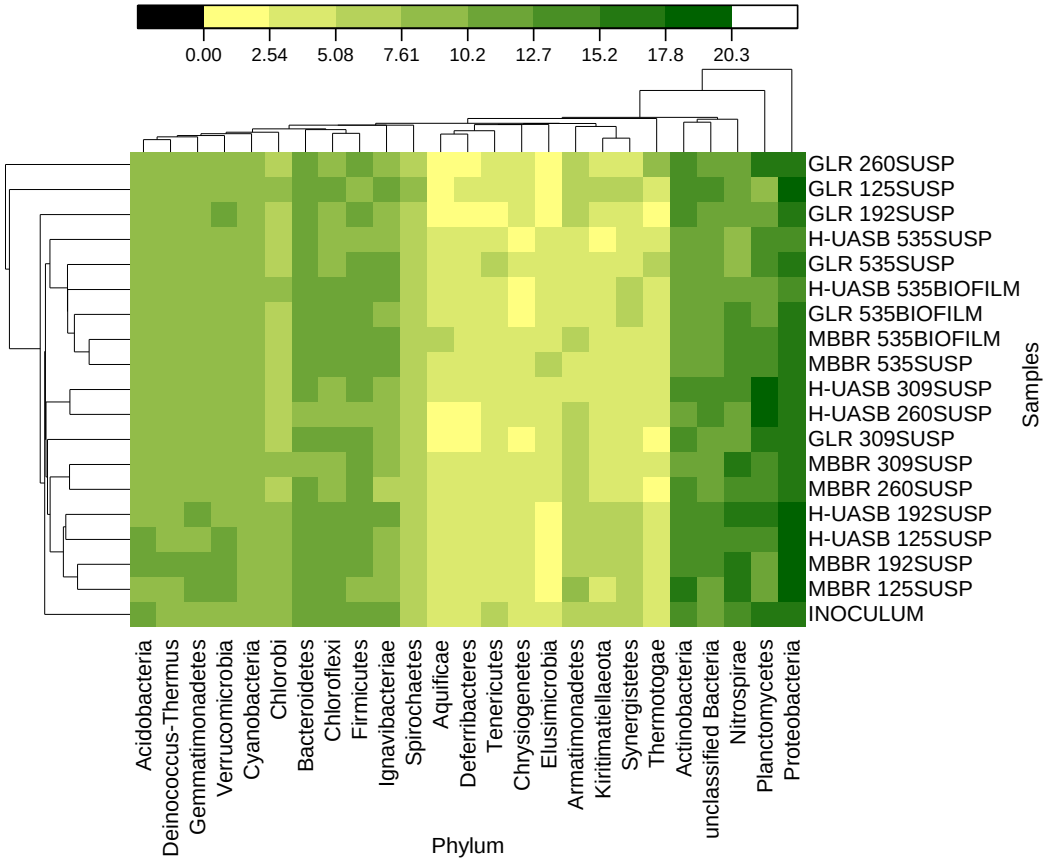

Figure 4. 1. Heatmap of the most abundant bacterial phyla in the different reactor samples and the inoculum. Hierarchical clustering was done on log-transformed abundances using Euclidean distances. The relative values of the bacterial phyla are depicted by colour intensity from yellow (lowest concentration) to green (highest concentration).

4.3.3 Microbial community structures of the suspended biomass in the reactors

4.3.3.1 Population dynamics of ANAMMOX bacteria in the reactors

The relative abundance of ANAMMOX bacteria remained consistently higher in H-UASB throughout the study period compared to MBBR and GLR (*figure 4.2*). On day 125 (phase III), the relative abundance of ANAMMOX bacteria in H-UASB had dropped from ca. 45% in the inoculum to approximately 5%, before gradually increasing to ca. 74% by day 260 (phase V). On the contrary, the relative abundance of ANAMMOX bacteria in MBBR and GLR was below 1% in the first 192 days (first four phases), but by day 260 (phase V), their relative abundance had increased to approximately 14% and 23%, respectively *(figure 4.2*). However, between days 260 and 309 (phase V), there was approximately

11%, 50% and 3% decrease in the relative abundance of ANAMMOX bacteria in H-UASB, MBBR and GLR, respectively (*figure 4.2*). On the last day of study (day 535), the relative abundance of ANAMMOX bacteria in the suspended biomass was approximately 11%, 33% and 4% in MBBR, H-UASB and GLR, respectively (*figure 4.2*).

Candidatus Kuenenia stuttgartiensis dominated over all the other ANAMMOX bacterial species throughout the study period in all the reactors, while *Candidatus* Scalindua spp. were not detected in GLR during the study (*figure 4.2*). In the MBBR, *Candidatus* Scalindua spp. were only detected on days 260 and 535 at 0.00043% and 0.002%, respectively, while in the H-UASB, their relative abundance was approximately 0.002% (*figure 4.2*). On the other hand, *Candidatus* Brocadia spp. were only detected in the H-UASB from day 192 onwards, while in the MBBR and GLR, they were only detected from day 260 onwards (*figure 4.2*). The presence of *Candidatus* Jettenia spp. was detected from day 260 onwards in all the reactors (*figure 4.2*). However, the relative abundance of *Candidatus* Brocadia spp. and *Candidatus* Jettenia spp. remained below 0.4% in all the reactors during the study.

Candidatus Kuenenia stuttgartiensis were the only species detected in all the reactors on day 125 (phase III). However, on day 192 (phase IV), both uncultured *Ca.* Brocadia spp. and *Candidatus* Kuenenia stuttgartiensis were detectable in H-UASB, while in the MBBR and GLR, only *Candidatus* Kuenenia stuttgartiensis was detectable during this period (*table A.4.1*). On day 260 (phase V), a total of eight, seven and four species belonging to either *Candidatus* Kuenenia, *Candidatus* Brocadia or *Candidatus* Jettenia genera were detected in the MBBR, H-UASB and GLR, respectively. Nine species affiliated to ANAMMOX bacteria were present in both MBBR and H-UASB on day 309 (phase V), while eight species were present in GLR during this period (*table A.4.1*). On the last day of study (day 535), the number of species affiliated to ANAMMOX bacteria had increased

to nine in GLR, similar to MBBR, while in the H-UASB, the number of species had increased to eleven (*table A.4.1*).

The presence of ANAMMOX-like bacteria was also detected in all the reactors throughout the study period (*figure 4.2*). However, their relative abundance in the reactors was ≤0.76% (*figure 4.2*). In all the reactors, their relative abundance was consistently higher than that of *Candidatus* Brocadia spp. and *Candidatus* Jettenia spp. (*figure 4.2*).

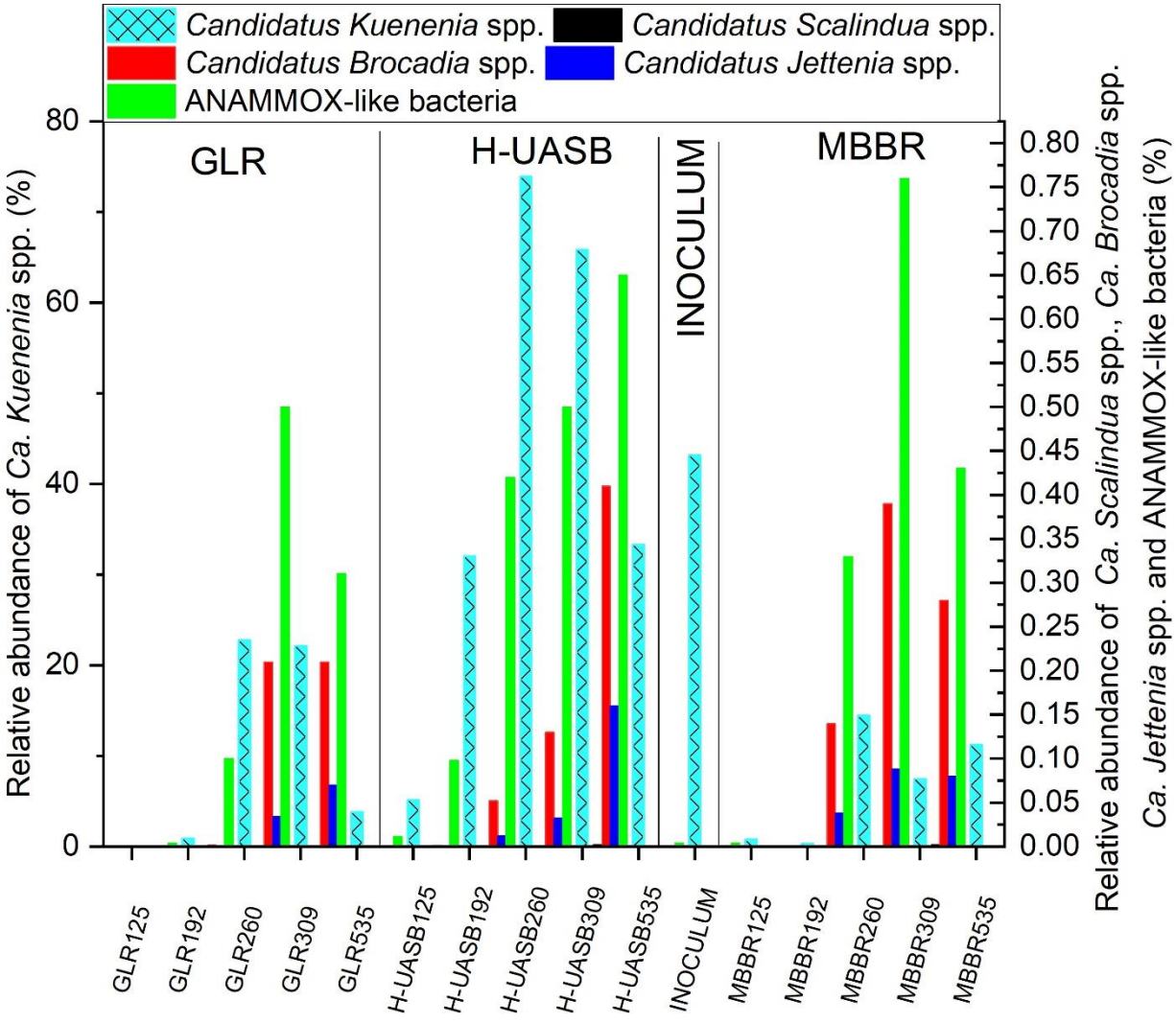

Figure 4. 2. The relative abundance of ANAMMOX bacteria and ANAMMOX-like bacteria in the suspended biomass in the reactors on days 125, 192, 260, 309 and 535.

4.3.3.2 Population dynamics of AOB in the suspended biomass

Between the inoculum and day 125 (phase III), the relative abundance of *Nitrosomonas* spp. increased 8 and 7 times in the MBBR and H-UASB, respectively, while a 0.08-times

decrease in their relative abundance was observed in the GLR (*figure 4.3*). However, on day 192 (phase IV), approximately 27% and 30% decreases in the relative abundance of *Nitrosomonas* spp. was observed in the MBBR and H-UASB, while a 5000% increase in their abundance was observed in the GLR (*figure 4.3*). A further decrease in the relative abundance of *Nitrosomonas* spp. in both MBBR and H-UASB was observed between days 192 - 260 to <1%, and remained in this range until the end of the study (*figure 4.3*). Conversely, in the GLR, the relative abundance of *Nitrosomonas* spp. decreased between days 192 -260 by approximately 1500%, before increasing by approximately 1200% between days 260- 309 (phase V). However, their relative abundance had decreased to below 1% on day 535, similar to both MBBR and H-UASB (*figure 4.3*).

The relative abundance of *Nitrosospira* spp. remained below 1% in all the reactors during the first 125 days, but then increased between days 125 - 192 to reach ca. 2.5%, ca. 2.4% and 2% in MBBR, H-UASB and GLR, respectively (*figure 4.3*). In the MBBR and H-UASB, *Nitrosospira* spp. dominated over all the other AOB-affiliated bacteria between days 260 - 535. In the GLR, *Nitrosospira* spp. were dominant on day 260, after which *Nitrosomonas* spp. emerged as the dominant AOB-affiliated bacteria once again on day 309, but then *Nitrosospira* spp. re-emerged once again as the dominant species on the last day of study (day 535) (*figure 4.3*).

At species level, *Nitrosomonas europaea* dominated over all the other AOB-affiliated bacterial species during first 192 days (four phases) (*table A.4.2*). However, from day 260 onwards, the dominance of *Nitrosospira multiformis* was observed in both MBBR and H-UASB, while their dominance in GLR was observed on day 260, before the re-emergence of *Nitrosomonas europaea* as the dominant species on day 309. On the last day of study, *Nitrosospira multiformis* were once again the dominant AOB-affiliated species in the GLR, similar to H-UASB and MBBR (*table A.4.2*). The relative abundance of *Ca. Nitrosoglobus* spp., *Nitrosococcus* spp. and *Nitrosovibrio* spp. remained below 0.035% throughout the study in all the reactors (*figure 4.3*).

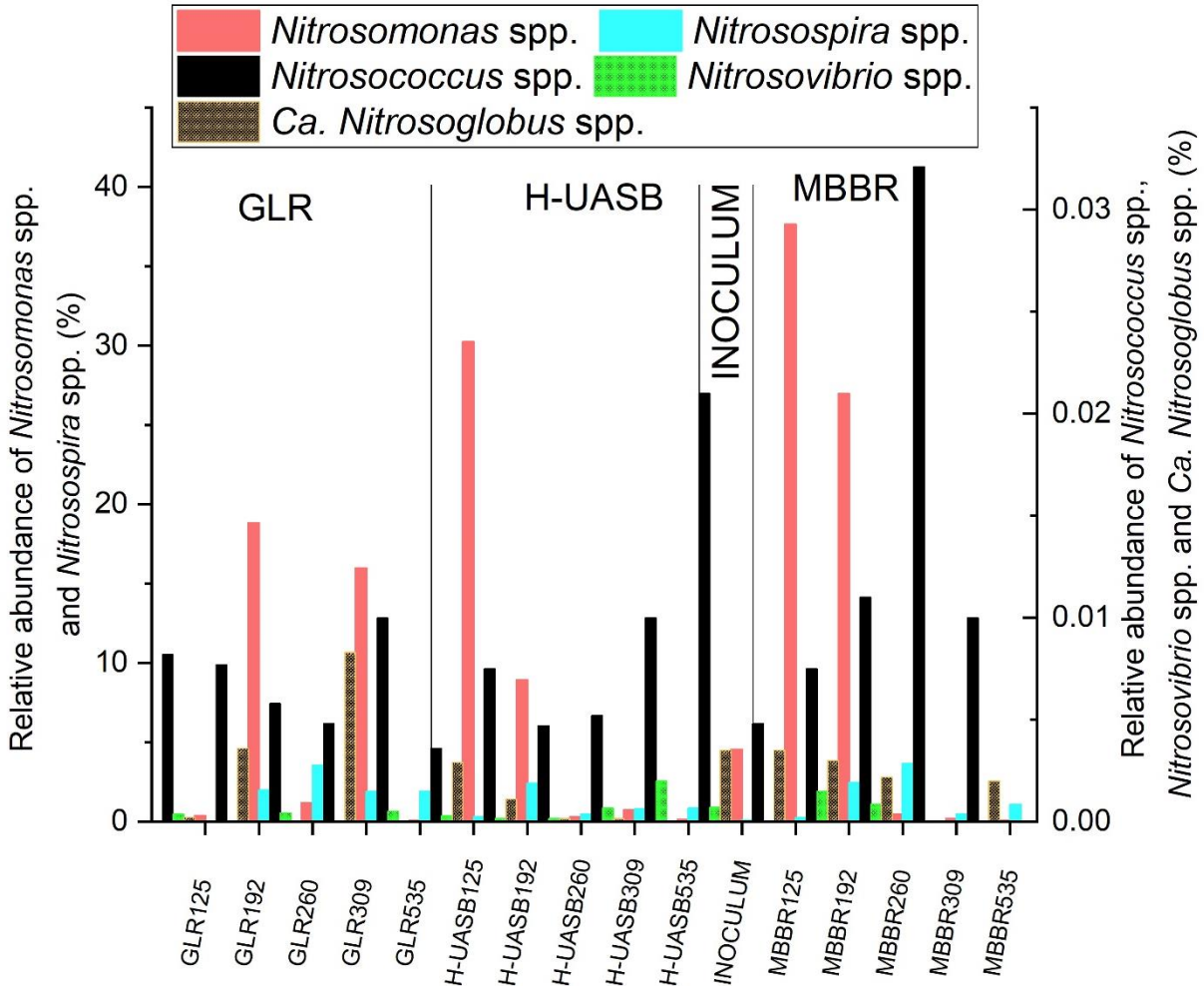

Figure 4. 3. The relative abundance of AOB in the suspended biomass in the reactors on days 125, 192, 260, 309 and 535.

4.3.3.3 Population dynamics of NOB in the suspended biomass

Nitrospira spp. remained the most dominant NOB-affiliated genera in H-UASB and MBBR during the study, while *Nitrospira* spp. only dominated in the first 192 days (four phases) in the GLR before *Nitrobacter* spp. emerged as the dominant NOB between days 260 - 309 (phase V) (*figure 6*). However, *Nitrospira*-affiliated NOB remained below 10% throughout the study period in H-UASB, while their relative abundance increased to 30.7% between the inoculum and day 309 in MBBR (*figure 4.4*), before decreasing to ca. 4.5% between days 309 - 535. In contrast, the relative abundance of NOB in GLR remained below 3% in suspended biomass during the study (*figure 4.4*). The highest relative abundance of *Nitrobacter*-affiliated NOB in the MBBR was observed on day 260 at ca.

8.6%, while their highest relative abundance in the H-UASB was observed on day 192 at ca. 1.4% (*figure 4.4*). in the GLR, the highest relative abundance of *Nitrobacter*-affiliated NOB was observed on day 260 at ca. 1.3% (*figure 4.4*).

At species level, *Nitrospira defluvii* were the dominant species throughout the study in H-UASB and MBBR, while *Nitrospira defluvii* only dominated in the first three phases in the GLR before *Nitrobacter hamburgensis* emerged as the dominant species between days 260 -309 (phase V) (*table A.4.2, Appendix B*). On the last day of study (day 535), *Nitrospira moscoviensis* were the dominant NOB-affiliated species in GLR (*table A.4.2, Appendix B*). The relative abundance of NOB affiliated to *Nitrolancea hollandica* was ≤0.02% in all the reactors during the study (*figure 4.4*).

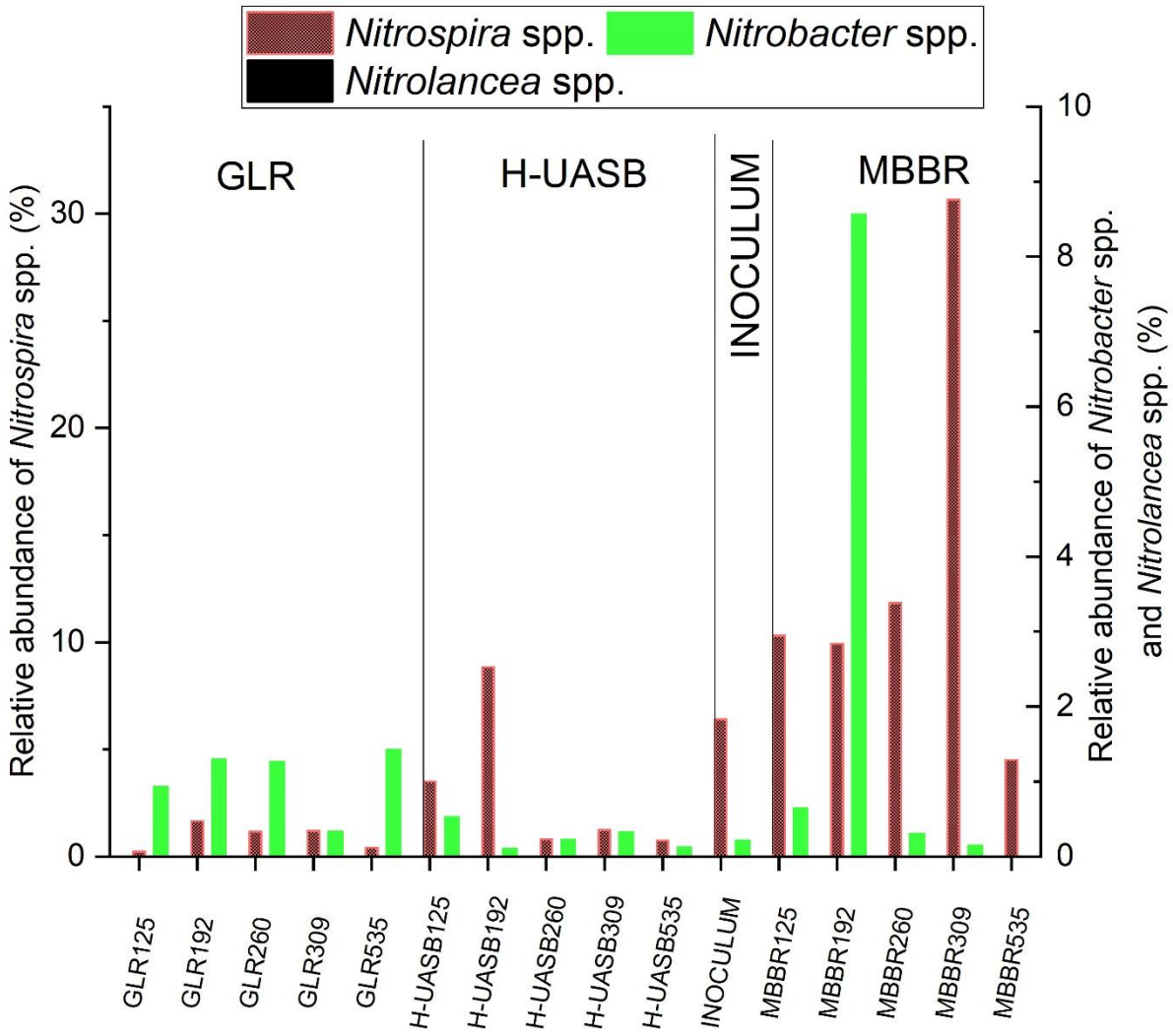

Figure 4. 4. The relative abundance of NOB in the suspended biomass in the reactors on days 125, 192, 260, 309 and 535.

4.3.3.4 Population dynamics of COMAMMOX bacteria in the suspended biomass

The relative abundance of COMAMMOX bacteria was consistently higher in suspended biomass throughout the study in the MBBR compared to H-UASB and GLR (*figure 7*), similar to *Nitrospira* spp. (*figure 4.5*). However, their relative abundance remained below 5% in the MBBR during the study, while their abundance in the suspended biomass in both H-UASB and GLR remained ≤0.11% (*figure 4.5*). The highest relative abundance of COMAMMOX bacteria was observed on day 309 in both GLR and MBBR at ca. 4.5% and 0.11%, while their highest abundance was observed in the H-UASB on day 125 at 0.15% (*figure 4.5*). In all the reactors, *Candidatus* Nitrospira inopinata were the only

species within the COMAMMOX bacterial community detected during the study in the reactors (*table A.4.3, Appendix B*).

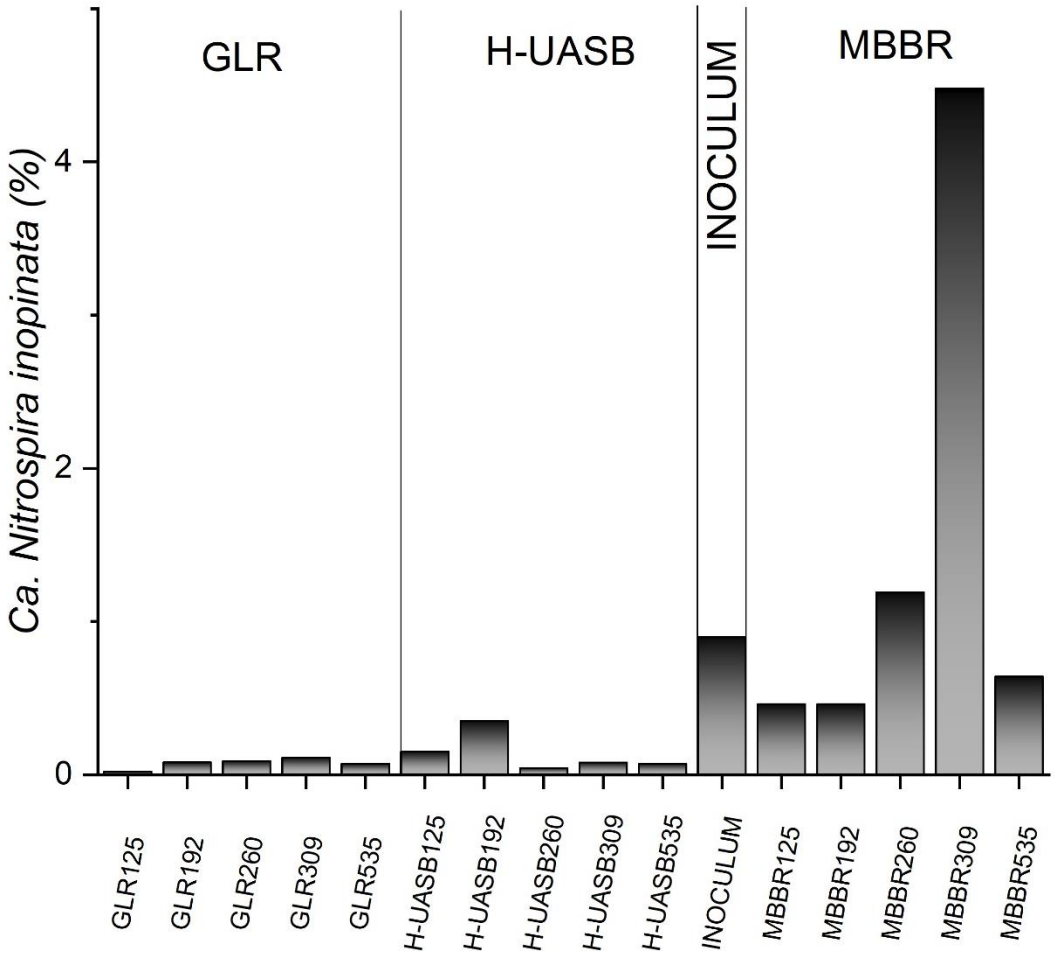

Figure 4. 5. The relative abundance of COMAMMOX bacteria in the suspended biomass in the reactors on days 125, 192, 260, 309 and 535.

4.3.4 Microbial community structures of the biofilms

4.3.4.1 Abundance of ANAMMOX bacteria in the biofilms

On day 535 (final day of study), the relative abundance of ANAMMOX bacteria in the biofilms was approximately 4.5%, 5.7% and 4.4% in the MBBR, H-UASB and GLR, respectively (*figure 4.6*). This represented approximately 0.4, 0.2 and 1.1 times their relative abundance in the suspended biomass in the MBBR, H-UASB and GLR, respectively (*figure 4.6*). At species level, *Candidatus* Kuenenia spp. were the most dominant species affiliated to the ANAMMOX bacteria in all the reactors in the biofilms, similar to the suspended biomass (*figure 4.6*). *Candidatus* Scalindua spp. were not detected in the biofilms in the GLR and H-UASB, while their relative abundance in the MBBR was approximately

0.0007%. The relative abundance of *Candidatus* Jettenia spp. and *Candidatus* Brocadia spp. in the biofilms and the suspended biomass was ≤0.41% (*figure 4.6*). ANAMMOX-like bacteria were also detected in the biofilms in all the reactors, similar to the suspended biomass (*figure 4.6*). However, their relative abundance was ≤0.46% in the biofilms in all the reactors (*figure 4.6*).

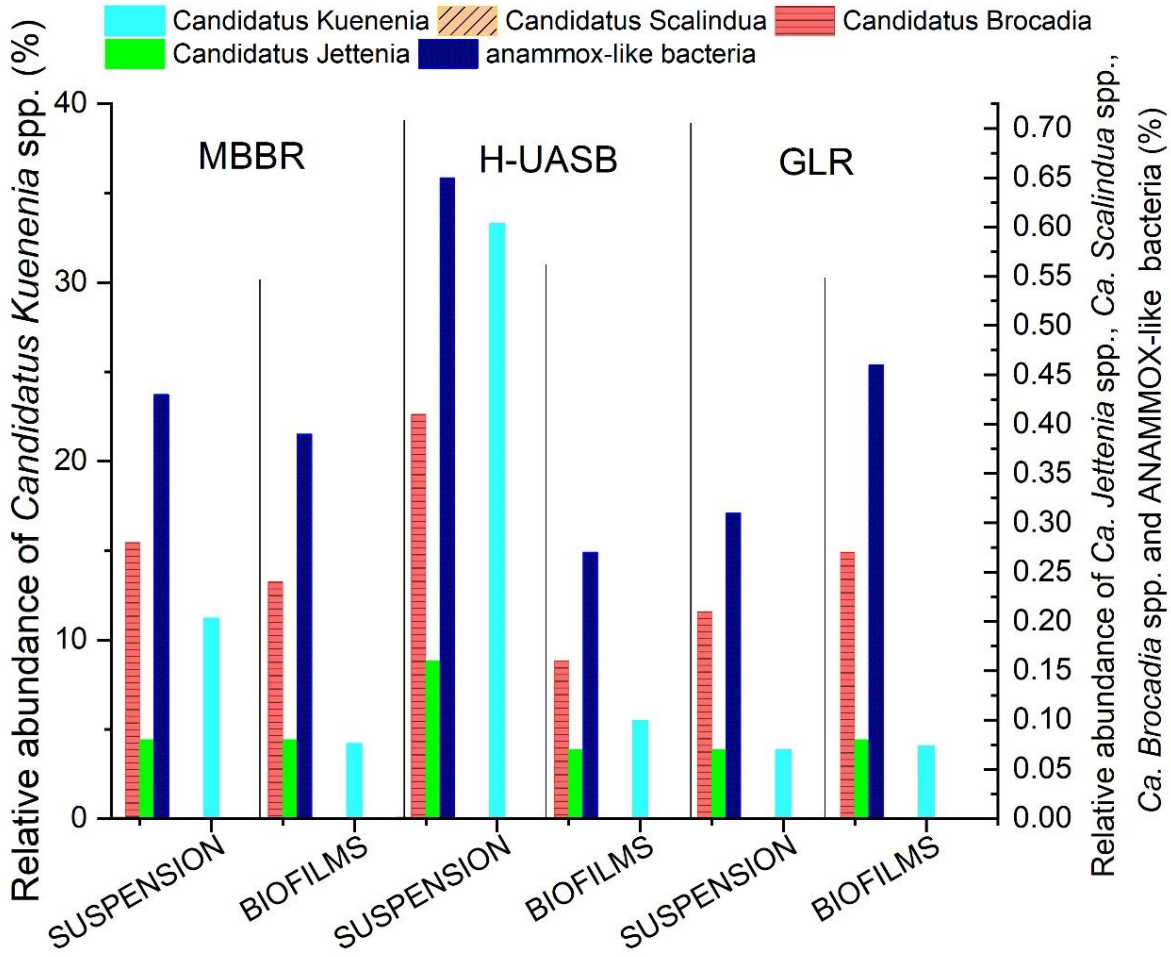

Figure 4. 6. The relative abundance of ANAMMOX bacteria and ANAMMOX-like bacteria in the biofilms and suspended biomass on day 535.

4.3.4.2 Abundance of AOB in the biofilms

The relative abundance of AOB was below 1% in the biofilms in all the reactors on day 535 (*figure 4.7*). On the contrary, the relative abundance of AOB was approximately 2.0% and 1.2% in the suspended biomass in the GLR and MBBR, respectively, while their abundance in the H-UASB was <1% in the suspended biomass (*figure 4.7*). At species level, *Nitrosospira* spp. were the most dominant AOB-affiliated bacteria in the biofilms in the MBBR and H-UASB (similar to the suspended biomass), while *Nitrosomonas* spp. were the most dominant in the biofilms in the GLR (unlike the suspended biomass that was dominated

by the *Nitrosospira* spp.) (*figure 4.7*). *Nitrosovibrio* spp. and *Candidatus* Nitrosoglobus spp. were not detected in the biofilms in the MBBR, while their relative abundance in the GLR was approximately 0.0008% (*figure 4.7*). In the H-UASB, the presence of *Nitrosovibrio* spp. was also not detected in the biofilms (similar to MBBR), while the relative abundance of *Candidatus* Nitrosoglobus spp. was approximately 0.003% (*figure 4.7*). Although *Nitrosococcus* spp. were detected at approximately 0.01% in the suspended biomass in all the reactors, their relative abundance was 0.02% in the biofilms in both GLR and H-UASB, and their abundance was 0.01% in the biofilms in MBBR (similar to suspended biomass) (*figure 4.7*).

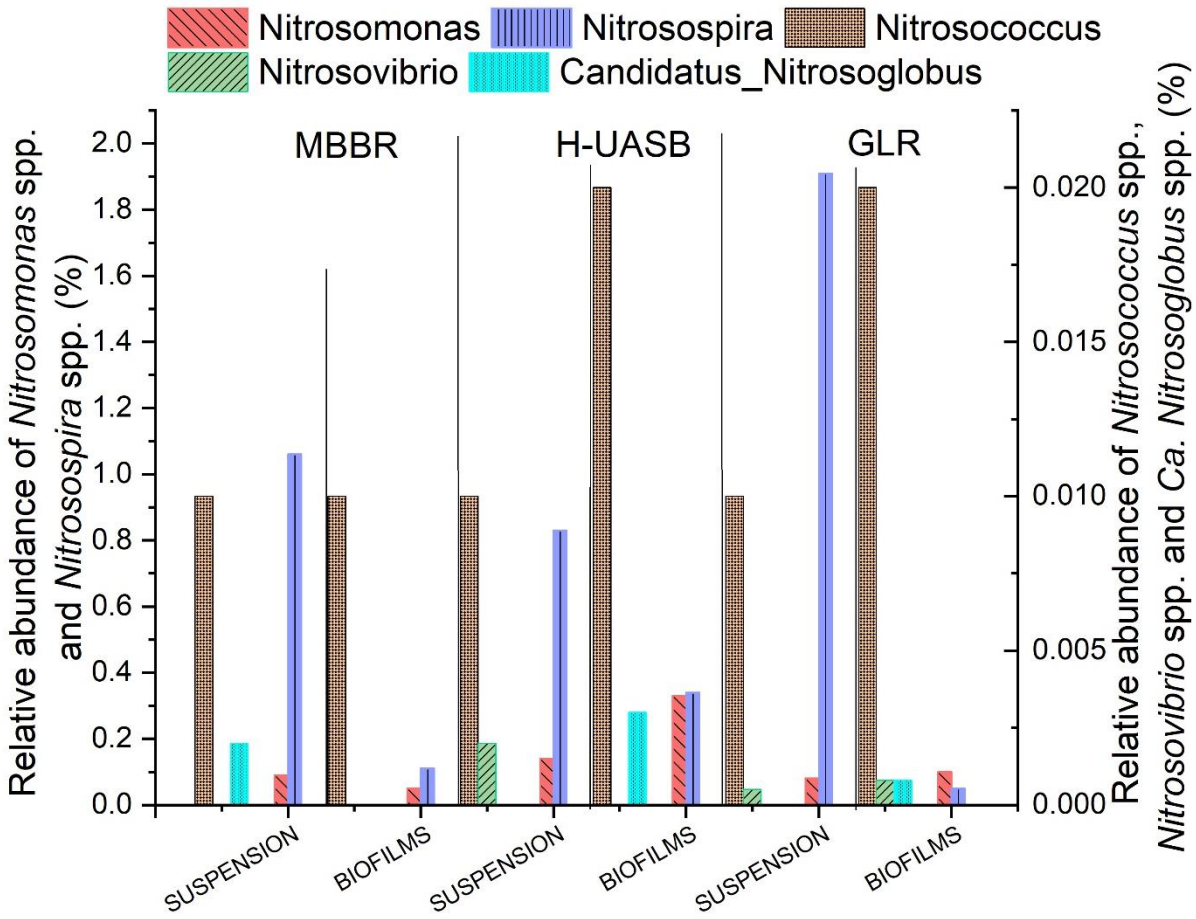

Figure 4. 7. The relative abundance of AOB in the biofilms and suspended biomass on day 535.

4.3.4.3 Abundance of NOB in the biofilms

The relative abundance of NOB in the biofilms in GLR and H-UASB was approximately 7.3% and 7.8%, respectively, which was approximately 10 times and 7 times their abundance in the suspended biomass (*figure 4.8*). On the contrary, the relative abundance of NOB in the suspended biomass in the MBBR was only 1.1 times its abundance in the biofilms (*figure*

4.8). In all the reactors, the relative abundance of *Nitrolancea* spp. was ≤0.02% in the suspended biomass and the biofilms (*figure 4.8*). *Nitrospira* spp. were the most dominant NOB-affiliated bacteria in the biofilms in all the reactors, similar to the suspended biomass (*figure 4.8*). On the other hand, the relative abundance of *Nitrobacter* spp. was ≤0.36% in the biofilms in all the reactors, while their abundance in the suspended biomass was ≤0.34% in all the reactors (*figure 4.8*).

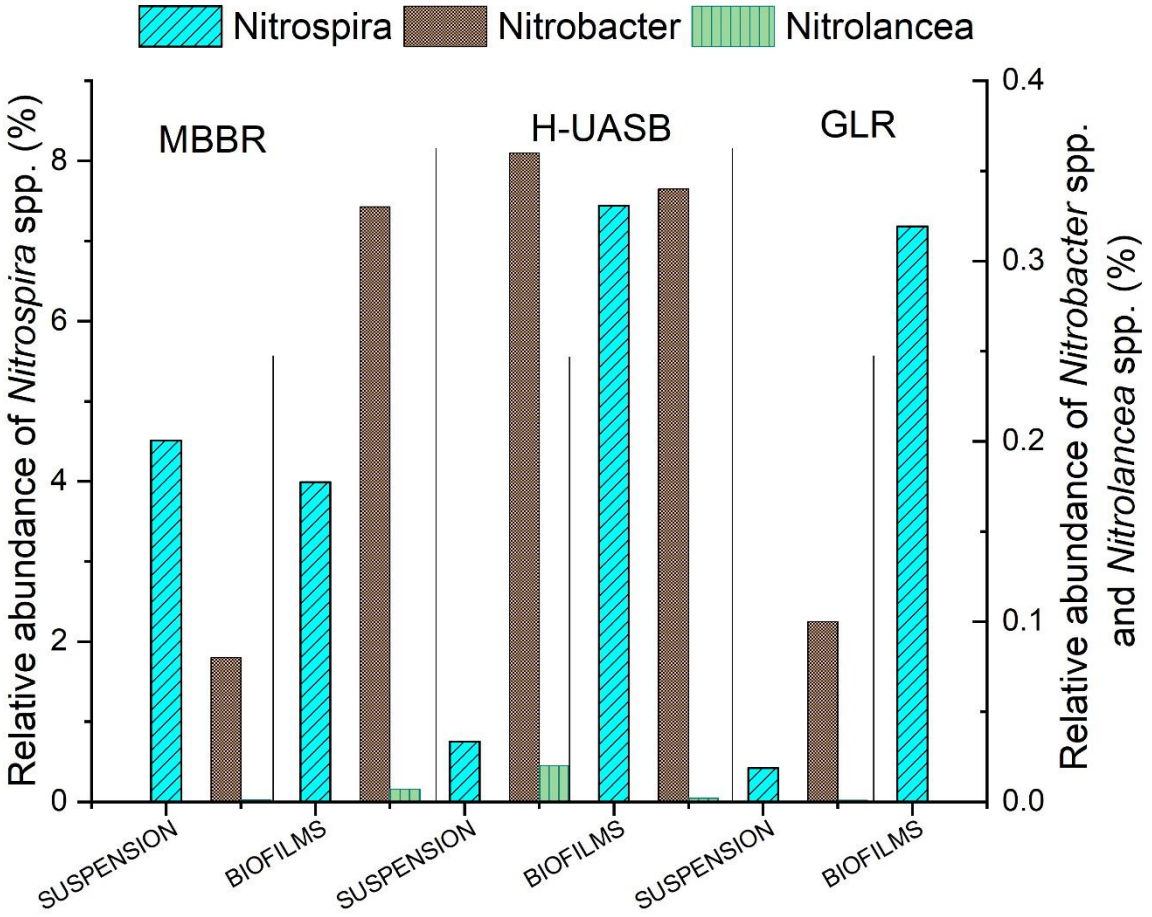

Figure 4. 8. The relative abundance of NOB in the biofilms and suspended biomass on day 535.

4.3.4.4 Abundance of COMAMMOX bacteria in the biofilms

The relative abundance of COMAMMOX bacteria in the biofilms on day 535 in all the reactors was ≤0.71%, with *Candidatus* Nitrospira inopinata being the only species affiliated to COMAMMOX bacteria that were detected (*figure 4.9*). However, their relative abundance in the biofilms in both GLR and H-UASB was ≥8 times their relative abundance in the suspended biomass, while their abundance in the suspended biomass in the MBBR was approximately 1.3 times their abundance in the biofilms (*figure 4.9*).

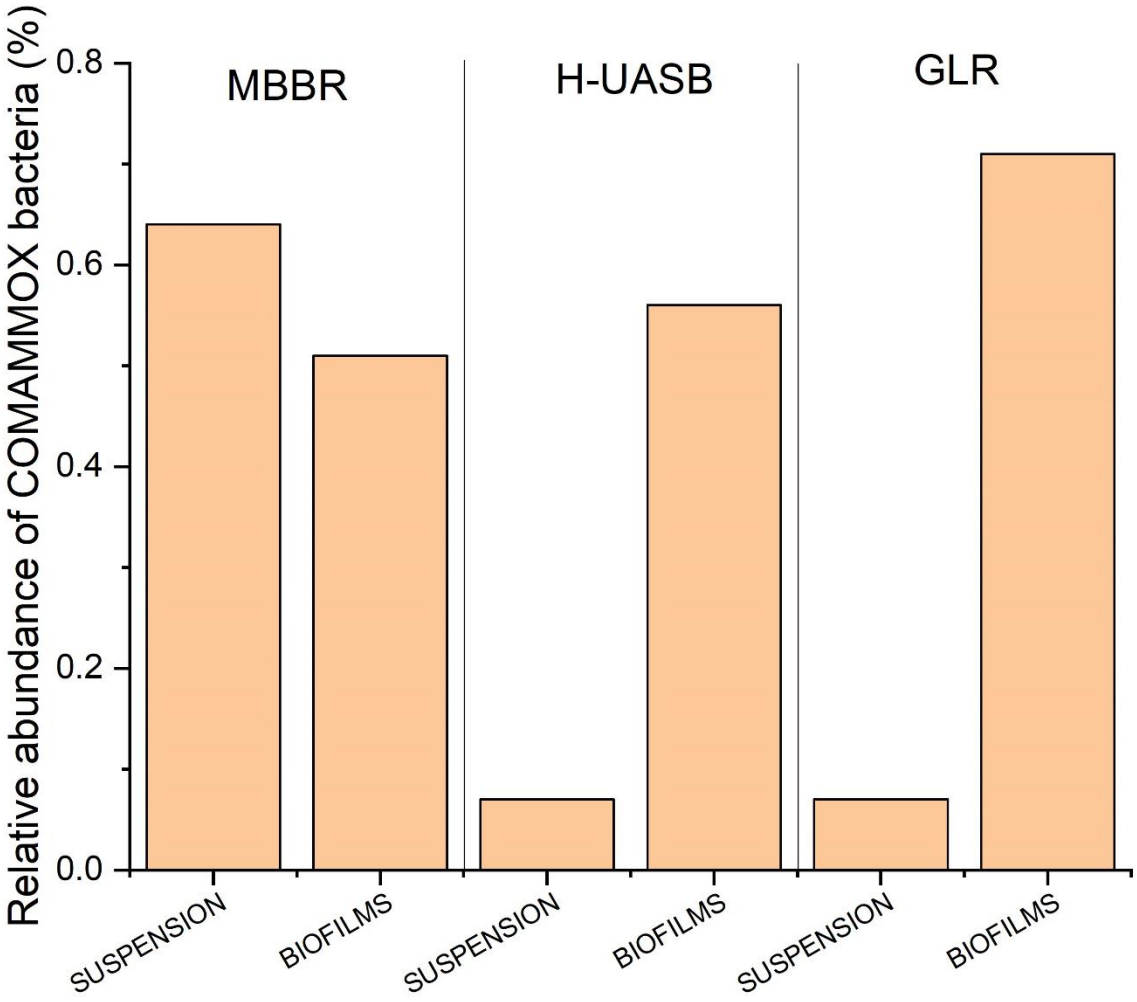

Figure 4. 9. The relative abundance of COMAMMOX bacteria in the biofilms and suspended biomass on day 535.

4.4 Discussion

Proteobacteria represents the largest and the most diverse phylogenetic lineage within the bacterial domain (Kersters *et al.* 2006), and are also frequently reported among the most abundant phyla in ANAMMOX-mediated systems (Liang *et al.* 2014; Gu *et al.* 2018). Many bacterial groups including all the known AOB and NOB (*Nitrobacter* spp. and *Nitrococcus* spp.) as well as many classes affiliated to heterotrophic bacteria belong to this phylum (Kersters *et al.* 2006; Peng and Zhu 2006). In this study, bacteria belonging to Proteobacteria were the most dominant throughout the study in the suspended biomass in MBBR and GLR, while their dominance in the H-UASB was only observed in phases III, IV and IX when the relative abundance of ANAMMOX bacteria was below 50% (*figure 4.1*). On the other hand, the relative abundance of bacteria belonging to Planctomycetes phylum fluctuated

synchronously in the suspended biomass with the relative abundance of ANAMMOX bacteria in the reactors (*figures 4.1 and 4.2*). This could be because ANAMMOX bacteria were the most dominant planctomycetes detected within these reactors throughout the study period (*figures 4.1 and 4.2*). The heterotrophic nitrate-reducing denitrifying bacteria (such as bacteria belonging to Acidobacteria, Firmicutes, Bacteroidetes, Actinobacteria and Gemmatimonadetes) could have been responsible for NO_3^- reduction in the reactors, while COMAMMOX bacteria and *Nitrospira*-afffiliated NOB, both of which belong to the Nitrospirae phylum, could have contributed in the production of the NO_3^- (Prosser 2007; Daims *et al.* 2015; Speth *et al.* 2016). *Nitrolancea hollandica*, which belongs to Chloroflexi phylum, has previously been reported to be able to oxidise NO_2^- to NO_3^-, while other members of this phylum are known to be heterotrophic in nature (Sorokin *et al.* 2014; Awolusi *et al.* 2015; Zhao *et al.* 2018). The presence of bacteria belonging to all these phyla in the reactors throughout the study was thus in the line with literature (Kartal *et al.* 2013; Lawson *et al.* 2017; Zhao *et al.* 2018). This is because cross-feeding and sharing of substrate amongst the ANAMMOX bacteria, nitrifying and heterotrophic bacteria make it difficult to culture ANAMMOX bacteria in pure cultures (Zhao *et al.* 2018).

Between the inoculum and phase III, there was a decrease in the relative abundance of ANAMMOX bacteria in the suspended biomass, possibly because the ANAMMOX bacteria had not acclimatised to the operating conditions in the reactors (Tang *et al.* 2009; Jin *et al.* 2013). During this period, heterotrophic nitrite- or nitrate-reducing denitrifying bacteria could have degraded organic carbon from dead bacterial cells using NO_2^- or NO_3^- as the electron acceptor (Kindaichi *et al.* 2007; Tang *et al.* 2009). The consumption of NO_2^- by the heterotrophic nitrite-reducing denitrifying bacteria, in turn, could have limited ANAMMOX bacterial growth, leading to a decrease in their relative abundance as well as a decrease in the nitrogen removal in the reactors (*Chapter 3*). The high DO in the influent in phase II (*table 3.2*) may have limited the growth of ANAMMOX bacteria as it could have favoured the growth of AOB and NOB, leading to competition for NH_4^+ and NO_2^-, respectively, or could have inhibited their activities as previously demonstrated by Carvajal-Arroyo *et al.* (2013) and (Strous *et al.* 1997a). The sequencing results also revealed the presence AOB and NOB in phase III (day 125) at a relative abundance >5% in both H-UASB and MBBR (*figures 4.2 and 4.3*). In the GLR, continuous circulation of argon/CO_2 gas mixture during the first 121 days may have limited the growth of AOB and NOB in the reactor due to maintenance of anaerobic conditions. However, gas circulation did not favour the growth of

ANAMMOX bacteria either in the GLR as their relative abundance was low (<1%) during this phase (*figure 4.2*). It is thus possible that internal gas circulation in the GLR made it impossible for ANAMMOX bacterial communities to establish in the reactor due to frequent fluctuations in the pH within the reactor that led to activation of the pH controller on regular basis. Amongst the three reactors, the abundance of ANAMMOX bacteria was the highest in the H-UASB during phase III at ca. 5%, and remained the highest throughout the study (*figure 4.2*), possibly because plug-flow in the H-UASB favoured ANAMMOX bacterial growth better than mixed conditions in the MBBR, and sequential plug-flow-internal gas circulation in the GLR. This is a new finding and has not been reported previously.

Between phases III and IV, an increase in the relative abundance of ANAMMOX bacteria was observed in both H-UASB (5% to 32%) and GLR (0.0004% to 0.9%) in the suspended biomass, while a decrease from 0.7% to 0.3% was observed in the MBBR (*figure 4.2*). It is possible that the presence of substrate gradients in the H-UASB (due to plug-flow) and the alternation of gas circulation with plug-flow conditions in the GLR favoured ANAMMOX bacterial growth compared to better-mixing in the MBBR. Since most of the biomass in the H-UASB was observed to settle in the lower sections (conical base) of the reactor that was receiving fresh feed (*figure 3.1*), the substrate gradient existing in this reactor could have favoured ANAMMOX bacterial growth in the lower section, possibly because of better access to NO_2^- and NH_4^+. On the contrary, better-mixing in the MBBR could have lowered the spatial substrate gradient within this reactor, favouring organisms with low Ks (affinity for substrate) values such as *Nitrospira* spp. at the detriment of organisms with high Ks values. Since plug-flow conditions prevailed for 21 hours a day from 121st day onwards in the GLR (compared to gas circulation which was only done for 3 hours a day), bacterial growth patterns similar to those in the H-UASB was possible. In addition, stirring and gas circulation could have also led to the growth of biofilms on the reactor walls (*figure 5.2, Chapter 5*), which may have supported the growth of heterotrophic bacteria within the MBBR and the GLR (Laureni *et al.* 2015), which could have, in turn, competed with ANAMMOX bacteria for NO_2^-. Since fluctuations in the $\Delta NO_2^-/\Delta NH_4^+$ ratios and the attachment of biomass on the reactor wall were observed during this phase in the MBBR, it indicates that the mixing in the MBBR favoured the growth of heterotrophic nitrite-reducing denitrifying bacteria, leading to competition for NO_2^- with ANAMMOX bacteria (*Chapter 3*). However, when the biomass growing on the reactor wall was scrubbed every week using a brush, the $\Delta NO_2^-/\Delta NH_4^+$ re-aligned with the stoichiometric ratios expected of

ANAMMOX bacteria (*Chapter 3*), an indication of a possible re-establishment of ANAMMOX bacterial populations in the reactors. Moreover, it is also possible that the concentration of FA and FNA in the reactors influenced the growth of the ANAMMOX bacteria in the reactors (*Chapter 3*). Since the concentration of FA and FNA was estimated to be the highest in the H-UASB during the study, it could indicate that these compounds favoured the growth of ANAMMOX bacteria (Gasa *et al.* 2019). This could be because other bacteria that compete for the substrate with ANAMMOX bacteria could be more sensitive to FA and FNA concentrations than the ANAMMOX bacteria. Indeed, a higher inhibitory concentration of FA for ANAMMOX bacteria (2 mg-N/L) compared to that of NOB (0.1–1.0 mg/L) were reported by Jaroszynski *et al.* (2012) and Fernández *et al.* (2012), respectively. However, the inhibitory concentration of FNA of ANAMMOX bacteria (0.0005 mg-N/L) reported by Fernández *et al.* (2012) is lower than the inhibitory concentration of NOB (0.026–0.22 mg/L) and AOB (0.42–1.72 mg/L) reported by Soliman and Eldyasti (2016). Therefore, it is possible that the presence of NO_2^- and NH_4^+ in the feed limited the effect of FNA on ANAMMOX bacteria, in agreement with Lotti *et al.* (2012b).

At the early stages of phase V (day 260), the highest relative abundance of ANAMMOX bacteria was observed in all the reactors, possibly because this stage represented propagation phase as the NRRs increased sharply with the NLRs (*figures 3.6 and 3.7, Chapter 3*) (Zhao *et al.* 2018). However, towards the end of this phase (day 309), synchronous decrease in the relative abundance of ANAMMOX bacteria was observed in all the reactors, probably because further increments of the NLRs led to the inhibition of ANAMMOX bacterial activities by FA and FNA (Zhao *et al.* 2018) (*Chapter, 3*). Another possibility is that the indefinite retention of biomass in the reactors could have led to the accumulation of none-ANAMMOX bacteria and none-active (dead) cells in the reactors as previously suggested by Hoekstra *et al.* (2018). Indeed, further decreases in the relative abundance of ANAMMOX bacteria in the suspended biomass were observed in the H-UASB and GLR between phases V and IX, while an increase was observed in the MBBR (*figure 4.2*).

Molecular analyses of the biomass in the biofilms was only performed at the end of the study due to the slow biofilm development on carrier materials (*Chapter 5*). The lower relative abundance of ANAMMOX bacteria in the biofilms than in the suspended biomass in the H-UASB was in contrast to Park *et al.* (2015), who reported better ANAMMOX bacterial enrichment in the biofilms compared to the suspended biomass of MBBR system. This is probably because the biomass growing in the biofilms had limited access to the substrate (as

they were floating) compared to the suspended biomass that was receiving fresh feed (*figure A.4.1, appendix B*). It is noteworthy here that the feed was introduced at the bottom of each reactor and was withdrawn at the top, which means that the biomass settling within the conical base was receiving fresh feed (highest substrate concentrations), while the biomass floating on the surface (biofilms) was receiving lower concentrations of substrate (*figure 3.2*). These findings corroborated the modelling results in *table A.6.1 in Appendix D*, which indicated faster growth of ANAMMOX bacteria in the lowest section of H-UASB compared to the highest section. On the contrary, comparable abundance of ANAMMOX bacteria was observed in the biofilms and suspended biomass in the GLR (*figures 4.2 and 4.7*), possibly because the alternation of gas circulation with plug-flow conditions led to similar growth patterns of ANAMMOX bacteria within the biofilms and the suspended biomass. However, in the MBBR, better accessibility to substrate in the suspended biomass compared to the biofilms could have led to better enrichment of ANAMMOX bacteria in the suspended biomass than in the biofilms.

The dominance of *Candidatus* Kuenenia stuttgartiensis over other ANAMMOX bacterial species in all the reactors could have been influenced by the operating conditions, including substrate concentrations and loading rates (van der Star *et al.* 2008; Park *et al.* 2015). It is possible that *Candidatus* Kuenenia spp. can adapt well to a wider range of operating conditions than the other ANAMMOX bacterial species as has been reported in previous studies (Lin *et al.* 2018; Yang *et al.* 2018; Lu *et al.* 2019). On the contrary, *Candidatus* Brocadia spp. have been reported to dominate in systems with high substrate concentrations (Park *et al.* 2015), which is in agreement with this study as they were only detected in phase V when the NLRs were ≥0.38 kg-N/m^3-day. The factors driving the growth of *Candidatus* Jettenia spp. are not as well articulated in scientific literature as those of *Candidatus* Kuenenia spp. and *Candidatus* Brocadia spp. A review of reports by Bae *et al.* (2017), Ma *et al.* (2017) and Li *et al.* (2017b) in which the dominance of *Candidatus* Jettenia spp. was reported, indicated that these bacteria could dominate in systems fed with low-strength wastewaters. However, in this study, they were detected from the beginning of phase V onwards, when the influent NO_2^- and NH_4^+ concentrations were each >100 mg-N/L (*figures 4.2*). The suggestion by Zhang *et al.* (2017a) that *Candidatus* Jettenia spp. are sensitive to oxygen is thus in agreement with the findings in this study as they were first detected towards the end of phase V when the anaerobic conditions had been maintained for over 5 months in the reactor.

Candidatus Scalindua spp. were detected in the MBBR between phase V (260th day) and IX (535th day) (both in suspended biomass and in the biofilms) at low relative abundance ≤0.002%, while in the H-UASB, they were detected in the suspended biomass on the last day of study, and none at all in the GLR. Since these species are well adapted to marine conditions, the limited growth observed in the reactors could thus indicate that the operating conditions did not favour their growth (van de Vossenberg *et al.* 2013). The operation of reactors at 36±1ºC could have also limited their growth as their optimal growth has been reported at lower temperatures (<30ºC) (Awata *et al.* 2012).

Although the relative abundance of ANAMMOX-like bacteria was low (≤0.76) during the entire study period in all the reactors (*figure 4.2*), an over 10-fold increase in their concentrations was observed between phases III and IX, probably a response to the increasing NLRs. These bacteria were closely related to those previously reported by Park *et al.* (2017a). Since Park *et al.* (2017a) reported the presence of ANAMMOX-like bacteria as well as the dominance of *Candidatus* Kuenenia stuttgartiensis in their systems, these two bacterial groups may have similar growth patterns. However, this is hypothetical and could only be ascertained through rigorous experimentation in future studies.

There was a better selection of COMAMMOX bacteria in the suspended biomass in MBBR compared to GLR and H-UASB during the study (*figure 4.9*), probably because better-mixed conditions and the presence of flocculent biomass (*Chapter 5*) favoured their growth. The presence of flocculent biomass in the MBBR, in particular, could have also enabled COMAMMOX bacteria to easily access any residual oxygen in the bulk liquid, unlike in the GLR and H-UASB which contained granular suspended biomass (*Chapter 5*). In addition, lower spatial gradients and lower substrate concentrations due to better-mixed conditions in the MBBR could have enabled the fast growth of COMAMMOX bacteria due to their high affinity for NH_4^+. Conversely, since the relative abundance of COMAMMOX bacteria in the biofilms in GLR and H-UASB was over 8-fold their abundance in suspended biomass (*figures 4.5 and 4.9*), it suggests that the substrate gradient in the H-UASB and GLR led to selection of different bacterial groups at different sections with the reactors. It is also possible that the growth of these bacteria in the biofilms was favoured to their growth in the suspended biomass, because they have a high affinity for NH_4^+ (and could thus grow at low substrate concentrations), as previously demonstrated by Kits *et al.* (2017). It could also be possible that their growth in the biofilms was favoured compared to their growth in

suspended biomass because they are sensitive to the SRT, in line with Annavajhala *et al.* (2018) and Cotto *et al.* (2020).

Better selection of *Nitrospira* spp. in the suspended biomass in MBBR compared to the suspended biomass in GLR and H-UASB was also observed during the study (*figure 4.8*). However, the relative abundance of *Nitrospira* spp. was approximately six times lower on the last day of study in the MBBR than on the 309th day (phase V). In addition, while the abundance of *Nitrospira* spp. in the suspended biomass in MBBR was comparable to that in the biofilms on the last day of study, their abundance in the biofilms in the H-UASB and GLR was approximately 10-fold their abundance in the suspended biomass. This is probably because better-mixed conditions in the MBBR led to lower spatial substrate distribution and lower substrate concentrations favoured their growth as K-strategists compared to H-UASB and GLR in which plug-flow conditions and a mix of plug-flow conditions/mixed conditions prevailed, respectively. Indeed, there was better selection of *Nitrospira* spp. in the biofilms than in the suspended biomass in both GLR and H-UASB, an indication that the substrate distribution influenced their growth. Additionally, their growth in the biofilms could have also been favoured due to the confluence of other factors including sensitivity to FA and FNA (Blackburne *et al.* 2007), since in the biofilms they were better protected from inhibition (Trojanowicz, Plaza and Trela 2016).

Within the NOB community, better selection of *Nitrospira* spp. than *Nitrobacter* spp. in both the MBBR and H-UASB throughout the study could have been because *Nitrospira* spp. have higher affinities for oxygen and substrate than *Nitrobacter* spp. (Park, Park and Chandran 2017). Park *et al.* (2015) previously demonstrated that under micro-aerobic conditions (DO<1 mg-O_2/L) and NO_2^- concentrations below 10 mg-N/L, the *Nitrospira*-affiliated NOB could be selected over *Nitrobacter*-affiliated NOB. However, in phase V in GLR, *Nitrobacter* spp. were the dominant NOB in the suspended biomass, which differed from MBBR and H-UASB (*figure 4.4* and *table A.4.2, Appendix B*). This could have been due to the increased NLRs (*figure 3.6, Chapter 3*), which could have favoured their growth as *r*-strategists (Blackburne *et al.* 2007). However, on the last day of study (535th day), *Nitrospira* spp. dominated over *Nitrobacter* spp. in all the reactors, possibly because of the decrease in the NLRs in the reactors (between phases VI and the beginning of phase IX (*figure 3.6, Chapter 3*)), which might have favoured the *Nitrospira* spp. as *K*-strategists (Park, Park and Chandran 2017).

The population dynamics observed within the AOB communities during the study may have also been influenced by the DO concentration in the influent and the NLRs. Although *Nitrosomonas* spp. have been reported to be able to adapt to diverse environments with complex substrates (Park *et al.* 2010a), including adaptation to oxygen-limiting conditions (Cabezas *et al.* 2006; Rodriguez-Sanchez *et al.* 2016), in this study, fluctuation in their concentrations was observed in all the reactors. Their dominance in all the reactors in the first four phases may have been driven by the high DO concentration in the influent in phase II (*Chapter 3*), in agreement with Awolusi, Kumari and Bux (2015). On the other hand, the dominance of *Nitrosospira* spp. observed from the early stages of phase V (day 260) in both MBBR and H-UASB, could indicate that they have better adaptabilities to oxygen-limiting conditions than other species within the AOB community, as previously suggested by Awolusi, Kumari and Bux (2015). However, in the GLR, *Nitrosomonas* spp. re-emerged as the dominant AOB bacteria towards the end of phase V (day 309), at a time when *Nitrobacter* spp. were also dominating over *Nitrospira* spp, an indication that the NLR favoured their growth in GLR as *r*-strategists (Awolusi, Kumari and Bux 2015; Park, Park and Chandran 2017). Indeed, during this phase, the effluent NH_4^+ concentrations in GLR (16±23 mg-N/L) were higher than in the MBBR (7±11 mg-N/L) and H-UASB (15±19 mg-N/L). Conversely, the low abundance of *Nitrosococcus*, *Nitrosovibrio* and *Candidatus* Nitrosoglobus in all the reactors during the study could be as a result of their inability to adapt to extreme conditions maintained in the reactors and/or low growth rates (Gu, Yang and Liu 2018; Pichel *et al.* 2019).

Overall, MBBR supported the most diverse bacterial communities in suspended biomass in phases V and IX, while H-UASB and GLR supported the most diverse bacterial communities in phases III and IV, respectively (*table 4.1*). According to Fernández *et al.* (1999) and Hashsham *et al.* (2000), diverse microbial communities have higher abilities to absorb perturbations resulting from fluctuations in operating conditions in biological systems. This is because, in diverse microbial communities, parallel substrate utilization is possible, unlike in less diverse systems where serial processing of substrate could be expected to occur (Hashsham *et al.* 2000). As a result of high bacterial diversities, better functional stability during periods of transient perturbations could be expected of diverse communities than of less diverse communities. The molecular studies in this work were based on microbial structure and inferred functionality. The impact of potential and extant

functionality could also be beneficial toward the same objective in future studies, as shown recently by Brotto, Annavajhala and Chandran (2018).

4.5 Conclusion

Plug-flow conditions in the H-UASB and the alternation of plug-flow conditions with gas circulation in the GLR led to better selection of ANAMMOX bacteria compared to better-mixed conditions in the MBBR. However, the better-mixed conditions in the MBBR favoured the growth of COMAMMOX bacteria and *Nitrospira* spp. compared to the plug-flow conditions in the H-UASB and the alternation of plug-flow conditions with gas circulation in the GLR. In addition, plug-flow conditions in the H-UASB and the alternation of plug-flow conditions with gas circulation in the GLR favoured the growth of *Nitrospira* spp. in the biofilms compared to the suspended biomass, while better-mixed conditions in the MBBR led to comparable abundance of these bacteria in the biofilms and the suspended biomass. Furthermore, there was a better adaptation of *Nitrosospira* spp. to limited oxygen conditions compared to *Nitrosomonas* spp. in all the reactors. MBBR supported the most diverse bacterial communities during the study.

CHAPTER 5

5 PHYSICAL PROPERTIES OF THE BIOMASS IN THE ANAMMOX-MEDIATED SYSTEMS

5.1 Introduction

Physical properties of biomass are of paramount importance in ANAMMOX-mediated systems as they influence not only the process performance but also biomass retention in the reactors (Winkler *et al.* 2013; Zhao *et al.* 2013). Biofilm thickness and aggregate sizes have both been associated with process performance (Terada *et al.* 2007), while biomass densities and shapes have been associated with biomass settleability (Wang and Zheng 2017).

In ANAMMOX-mediated systems, poor biomass settleability leading to washout is a matter of concern as it could seriously affect process performance (Dapena-Mora *et al.* 2004a). Among the factors affecting biomass settleability are mineral content of the biomass, shapes of biomass aggregates, their compactness and sizes (Green *et al.* 1994; Dapena-Mora *et al.* 2004a; Winkler *et al.* 2013; Wang and Zheng 2017). Granulation of biomass within the ANAMMOX-mediated systems would be desirable as granules have better settleabilities than the flocculent biomass (Schmidt and Ahring 1996). However, granule overgrowth could be undesirable as granules bigger than the critical sizes could experience mass transfer limitations (Dapena-Mora *et al.* 2004a; Ni *et al.* 2019).

Although mixing within the reactors would be desirable to enhance mass transfer of substrate to the bacteria, mixing forces could shear off biomass from the granule and biofilm surfaces or lead to granule and biofilm disintegration (Strous *et al.* 1998; Arrojo *et al.* 2006). Moderate mixing forces could lead to the continuous exchange of bacteria on the surfaces with the suspension. However, since the ANAMMOX bacteria grow in the inner anoxic layers of granules and biofilms, they benefit from the protection of the outer layers against the detachment by external forces (Strous *et al.* 1998). The shearing of the biomass from the granule or biofilm surfaces followed by re-growth would be particularly important in NOB control as they grow close to the AOB within the outer layers, while the protection of ANAMMOX bacteria from these forces is important as they have slow growth rates (Strous *et al.* 1998; Kartal *et al.* 2013).

In this chapter, the morphologies, sizes and elemental composition of biomass obtained from the three reactors are presented. The impact of these physical properties on the overall process performance are also discussed.

5.2 Methodology

5.2.1 Determination of biomass aggregate sizes

Approximately 0.5 L suspended biomass samples were collected from all the reactors for aggregate size analysis in phase V (day 256). The aggregate sizes of the suspended biomass in the MBBR were analysed using Mastersizer (Malvern Instruments, UK), while the sizes of biomass aggregates in H-UASB and GLR could only be analysed through stereo microscopy (Nikon AZ100) owing to their large sizes.

5.2.2 Determination of biomass concentration on the bio-carriers and suspension

The concentration of biomass in the biofilms formed on the carrier particles was by scrubbing the biomass from 5 carrier particles from each reactor using pipette tips and washing the biomass off the carrier particles with de-ionised water. Approximately 50 ml of mixed liquors were also collected from each reactor. The biomass scrubbed from the carrier materials and the mixed liquors were then dried at 105ºC overnight in an oven on pre-weighed crucibles as described in APHA (1998). After drying, the crucibles were cooled to room temperature in a desiccator before their masses were determined. The concentration of the biomass in suspension and the carrier materials were determined as the difference between the masses of the crucibles containing the biomass and the masses of the empty crucibles (APHA 1998).

5.2.3 Scanning electron microscopy (SEM) and energy dispersive X-ray (EDX)

Mixed liquor samples from each reactor were collected for analysis through scanning electron microscopy – energy dispersive X-ray (SEM-EDX). The preparation of samples for SEM-EDX (washing, dehydration and seasoning) was done as previously described with modification (Sondi and Salopek-Sondi 2004; Gao *et al.* 2014). The mixed liquors were centrifuged and the supernatant discarded, followed by washing with distilled water three times before air-drying. Air-dried samples were then dehydrated by soaking in 30%, 50% and 75% for 5 minutes each, followed by 10 minutes in 100% ethanol. The pre-treated samples were thereafter gold sputter-coated in a Quorum Q150RES and viewed with Carl Zeiss Ultra Plus Field Emission Scanning Electron Microscope (FEGSEM). Different portions of the images obtained were subjected to energy dispersive X-ray (EDX) with

Oxford EDX detector (UK) coupled to Aztec software (UK) for identity and quantification of elements.

5.2.4 Microwave plasma – atomic emission spectroscopy

Approximately 200 ml of suspended biomass from MBBR, H-UASB and GLR reactor were collected, centrifuged and the supernatant discarded. The biomass from 20 bio-carriers from each reactor was also collected by scrubbing with pipette tips into Falcon tubes and the remaining biomass on the bio-carriers was washed off into the Falcon tubes using deionised water. The suspended biomass and the biomass collected from the bio-carriers from each reactor was then separately dried at 105ºC in an oven. Dried biomass was further ground into fine powder in a mortar using a pestle.

The powdered biomass samples were then digested in 6 ml of 65% nitric acid (HNO_3) and 4 ml of 30% hydrogen peroxide (H_2O_2) in Milestone Start D labstation (Milestone S.R.L., Italy, output power 1200 W). The digestion protocol involved 20 minutes of ramping to 180ºC, digestion at 180ºC for 15 minutes at 500 W, followed by cooling to room temperature (Ramsundar *et al.* 2017). The digested samples were then filtered through glass fibre filters with 1.2 µm-pore sizes before quantification of Fe, Zn, Co, Cu, Mn, Mo, Ni and Mg through Microwave plasma – atomic emission spectroscopy (MP-AES) (Agilent 4200, USA).

5.3 Results

5.3.1 Physical appearance and the aggregate sizes of suspended biomass in the reactors

The seed sludge used for the inoculation of the reactors was brown in colour (*figure 5.1*). However, after inoculating the reactors, the biomass in all the reactors turned creamy within the first phase (*figure 5.2 a, f & k*), and remained creamy during the second phase. In phase III (day 125), the biomass in the MBBR had turned brown in colour, while the biomass in H-UASB and GLR was tawny and dark-tawny, respectively (*figures 5.1 and 5.2 b, g & l*). In phase IV (day 192), the suspended biomass in MBBR had turned dark-brown in colour, while the suspended biomass in H-UASB and GLR had turned brown and tawny, respectively (*figures 5.1 and 5.2 c, h & m*). Towards the end of phase V (day 309), the biomass in MBBR had turned red, and the biomass in H-UASB and GLR contained red dense sphere-like aggregates and brown-tawny film-shaped aggregates (*figure 5.1*). From this phase onwards, there was no noticeable change in the colour of the biomass in MBBR and GLR (*figures 5.2 and 5.5*). However, in the H-UASB, when the pH controller

malfunctioned on the 425th day, the colour of the biomass changed from red to creamy, before gradually turning red (*figure 5.2j, 5.5f and A.4.2, appendix B*).

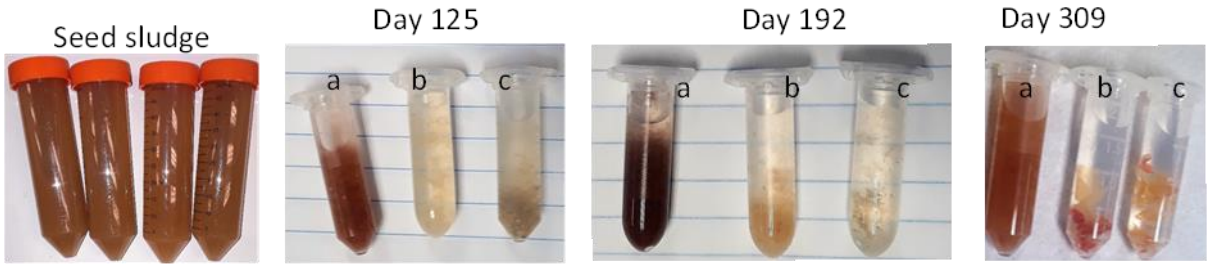

Figure 5. 1. The photographic images of the inoculum and suspended biomass collected from the MBBR (a), H-UASB (b) and GLR (c) in phases III (day 125), IV (day 192) and V (day 309).

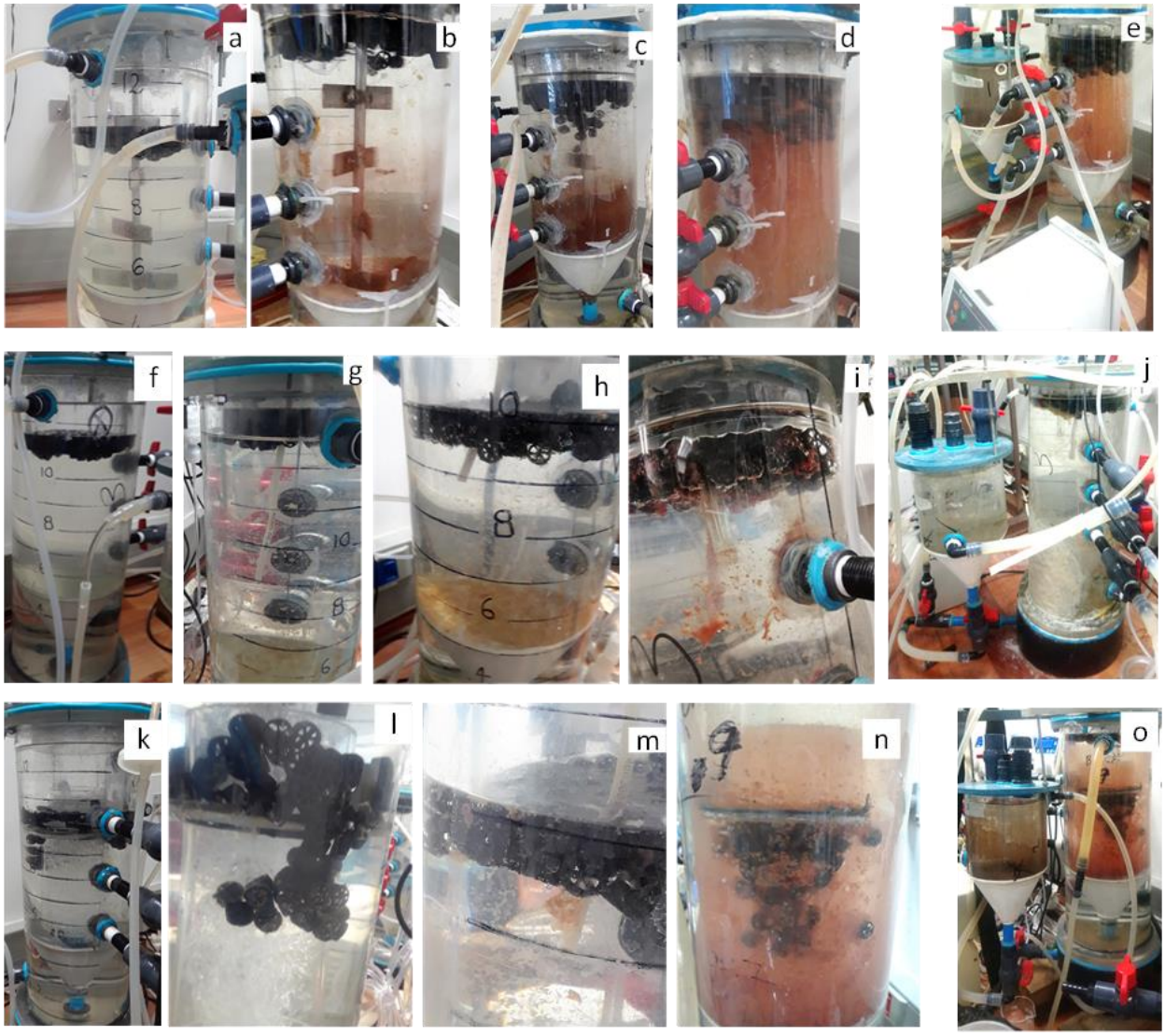

Figure 5. 2. Photographic images of the reactors in phases I (a, f&k), III (b, g&i), IV (c, h&m), VII (d, i&n) and IX (e, j&o): a-e (MBBR); f-j (H-UASB); and k-o (GLR).

The biomass aggregates in MBBR were ≤310 µm in diameter, with all the particles falling within 1.45 - 310 µm-diameter range (*figure 5.3*). The suspended biomass in MBBR formed a homogeneous layer on the petri dish upon settling (*figures 5.4a and 5.5a-c*). The largest portion of the biomass aggregates in the MBBR was approximately 144 µm big, and constituted approximately 9.39 % of the total biomass volume (*figure 5.3*). The volume densities of suspended biomass in both GLR and H-UASB could not be determined as the particle size analyser could measure up to 350 µm only. Therefore, the biomass aggregates in these reactors were approximated through stereo microscopy, as well as using a ruler placed on petri-dishes containing biomass (*figures 5.4 and 5.5*).

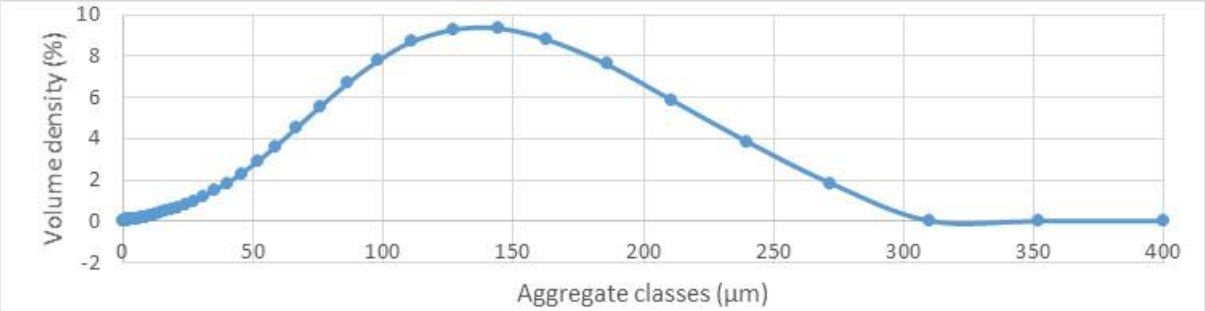

Figure 5. 3. Distribution of aggregate sizes of suspended biomass in MBBR as determined in a particle size analyser in phase V (day 256).

Between phases I and III, there were no noticeable changes in the biomass aggregate sizes in all the reactors. However, in phase IV, the biomass aggregates in H-UASB and GLR were noticed to have increased in sizes, while there were no noticeable changes in the sizes of biomass aggregates in MBBR during the study (*figures 5.4 and 5.5*). During this period (phase IV), the biomass aggregates in H-UASB contained sphere-like red biomass aggregates, with the largest aggregates measuring about 5 mm in diameter (*figure 5.5d*). However, towards the end of phase V, bigger red biomass aggregates compared to phase IV were observed in H-UASB, with the biggest aggregates measuring about 8 mm in length (*figure 5.5e*). In the final phase, dense red sphere-like biomass aggregates were present in the H-UASB, with the largest aggregates measuring approximately 10 mm in diameter (*figure 5.5f*). The largest brown film-like aggregates observed in the H-UASB were even bigger than the sphere-like aggregates, measuring about 15 mm in length. Contrary to H-UASB, most of the biomass aggregates in GLR were film-shaped (*figures 5.5 g-i*). However, some sparsely distributed dense sphere-like red biomass aggregates were observed in GLR during the study. In phase IV, the biomass aggregates in GLR were almost similar to those

in MBBR as the boundaries of the individual aggregates was hard to determine since the aggregates formed macroscopic layers upon settling (*figure 5.5g*). However, towards the end of phase V, large brown film-shaped aggregates were observed in the GLR, with the largest aggregates measuring about 25 mm in length, while red smaller (ca. 5mm in diameter) aggregates were sparsely distributed within the biomass (*figure 5.5h*). In the final phase, larger (ca. 10 mm in diameter) red dense sphere-like aggregates were sparsely distributed within the film-shaped brown biomass aggregates in GLR (*figure 5.5i*).

Through stereomicroscopy, the MBBR biomass was also observed to form macroscopic layers on petri dishes (*figure 5.4 a & d*), corroborating the observations made on the images captured on the normal camera (Samsung J3) in *figures 5.5 a-c*. Similarly, the presence of film-shaped aggregates and dense red aggregates in H-UASB and GLR was also confirmed through stereomicroscopy (*figures 5.4 b-c&e-f*).

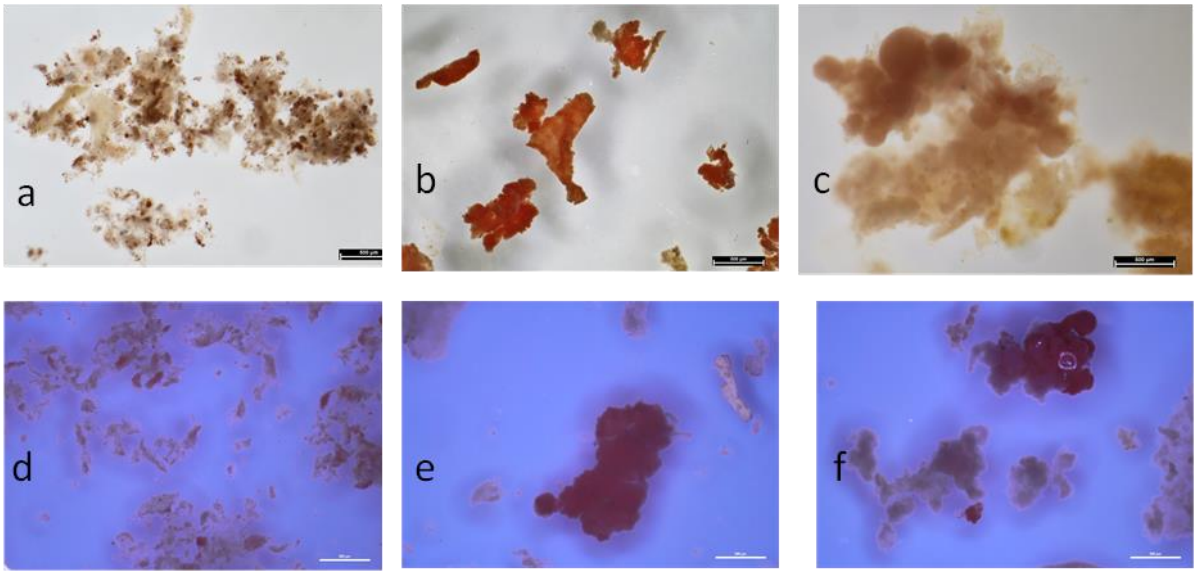

Figure 5. 4. Stereo microscopy images of suspended biomass in MBBR (a&d), H-UASB (b&e) and GLR (c&f) in phase V (day 256 - a-c) and phase IX (day 519 - d-f). Scale bars: 500 µm.

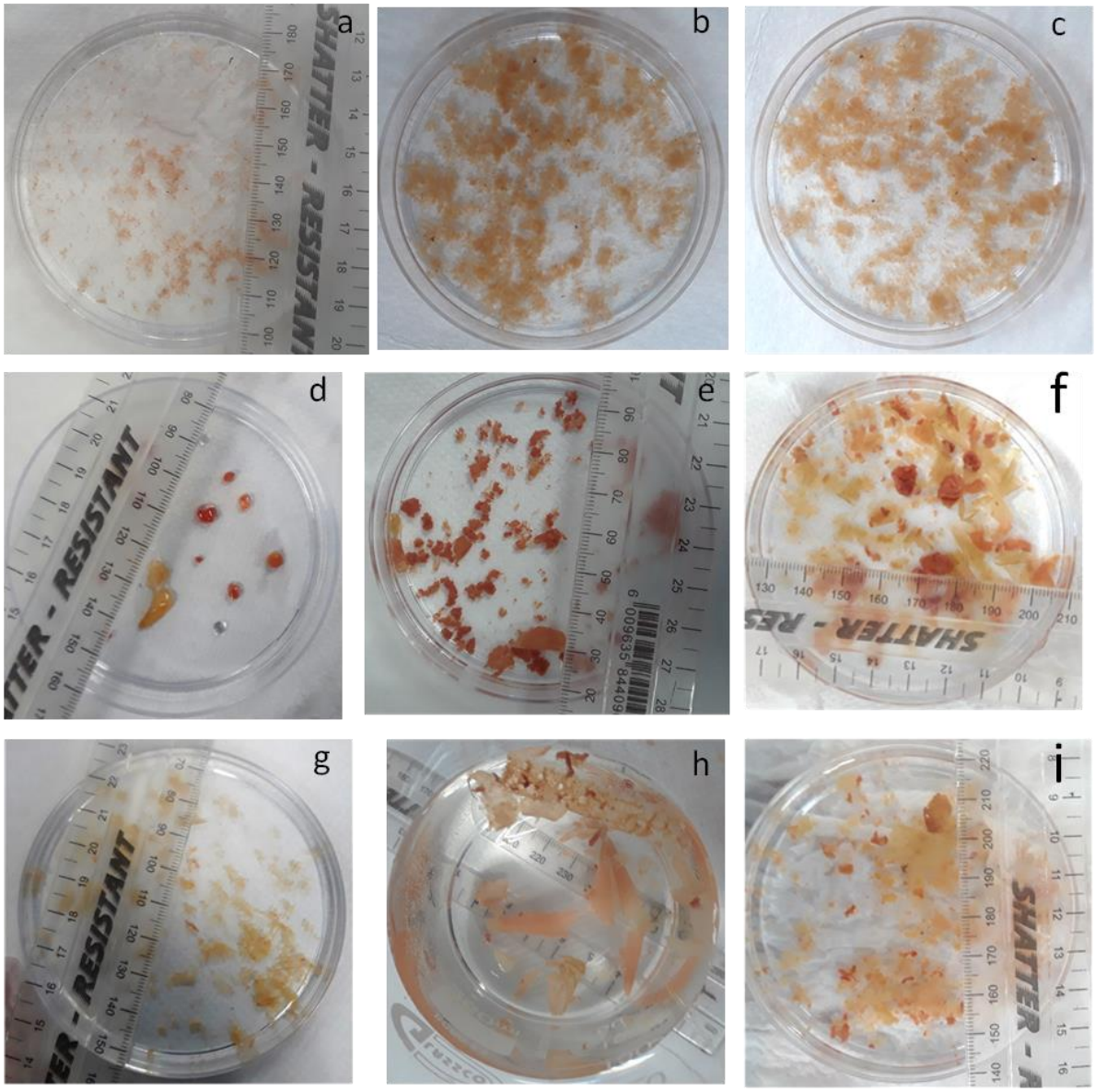

Figure 5. 5. Photographic images of the suspended biomass in phases IV (a, d & g), V (b, e & h) and IX (c, f & i) in MBBR (a-c), H-UASB (d-f) and GLR (g-i). Images in phase IV, V and IX were taken on days 246, 309 and 513, respectively.

5.3.2 Biofilm development

Slow development of biofilms on carrier particles was observed in all the reactors during the study, which begun in phase V (days 250-327), at a time when the biomass concentration in suspension ranged between 1.3 g/L and 2.1 g/L in the reactors. During the biofilm development process, thin biofilms were first observed to cover the surfaces of the sections within the carrier materials before gradually developing to cover most of the surface of the carrier materials by seventh phase (*figures 5.6 a, d & g*). The biofilms were observed to form

both on the outer surfaces and the inner surfaces of the carrier materials in H-UASB (*figure 5.6 f*), while in the MBBR and GLR, the biofilms only formed in the inner protected sections (*figure 5.5 c & j*).

The colour of the biomass in the biofilms during the early stages (phase V) of development was brown in H-UASB and MBBR, and tawny in GLR (*figures 5.6 a, d & g*). In phase VII, the colour of the biomass in the biofilms was red (*figures 5.6 c, f & i)*, similar to the suspended biomass (*figure 5.2*). However, following the malfunctioning of the pH controller in phase X, the colour of the biomass in H-UASB changed from bright red to tawny, similar to the suspended biomass (*figure A.4.2, Appendix B*), while the biomass in both MBBR and GLR remained reddish until the end of the study. In the final phase (phase IX), the average biomass concentration on the bio-carriers in the MBBR, H-UASB and GLR was 11.59 mg/carrier, 7.8 mg/carrier and 9.5 mg/carrier, while the approximate concentration of the suspended biomass during this period was 2.0 mg/L, 2.5 mg/L and 2.3 mg/L (*figure A.5.1, appendix C*).

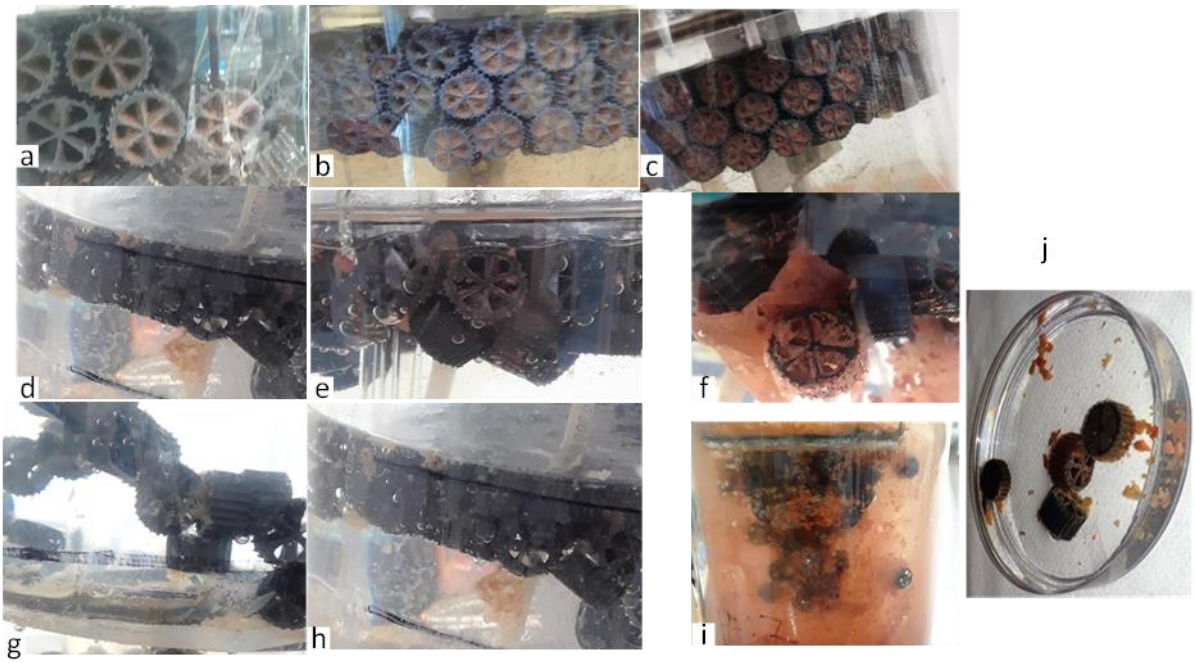

Figure 5. 6. Photographic images of the biofilms on carrier materials in MBBR (a - c), H-UASB (d - f) and GLR (g - j) in phases V (a, d & g), VI (b, e & h) and VII (c, f, i & j).

5.3.3 Morphologies of biomass aggregates

Stereomicroscopic images revealed the presence of irregularly shaped film-like aggregates in GLR and H-UASB (*figures 5.4 b-c and e-f*). Because the suspended MBBR biomass flocculated on the petri dishes (forming homogeneous macroscopic layer) upon collection

(*figures 5.4 a & d, and 5.5 a-c*), its morphology was not assessable through stereomicroscopy, unlike the biomass from H-UASB and GLR (*figures 5.4 b-c & e-f, and 5.5 d-i*). However, SEM revealed the presence of cauliflower-shaped aggregates on which spherical particles dominated on the MBBR biomass, similar to the H-UASB and GLR biomass (*figure 5.7*). The spherical particles had varying diameters, ranging from below 1 µm to above 1 µm.

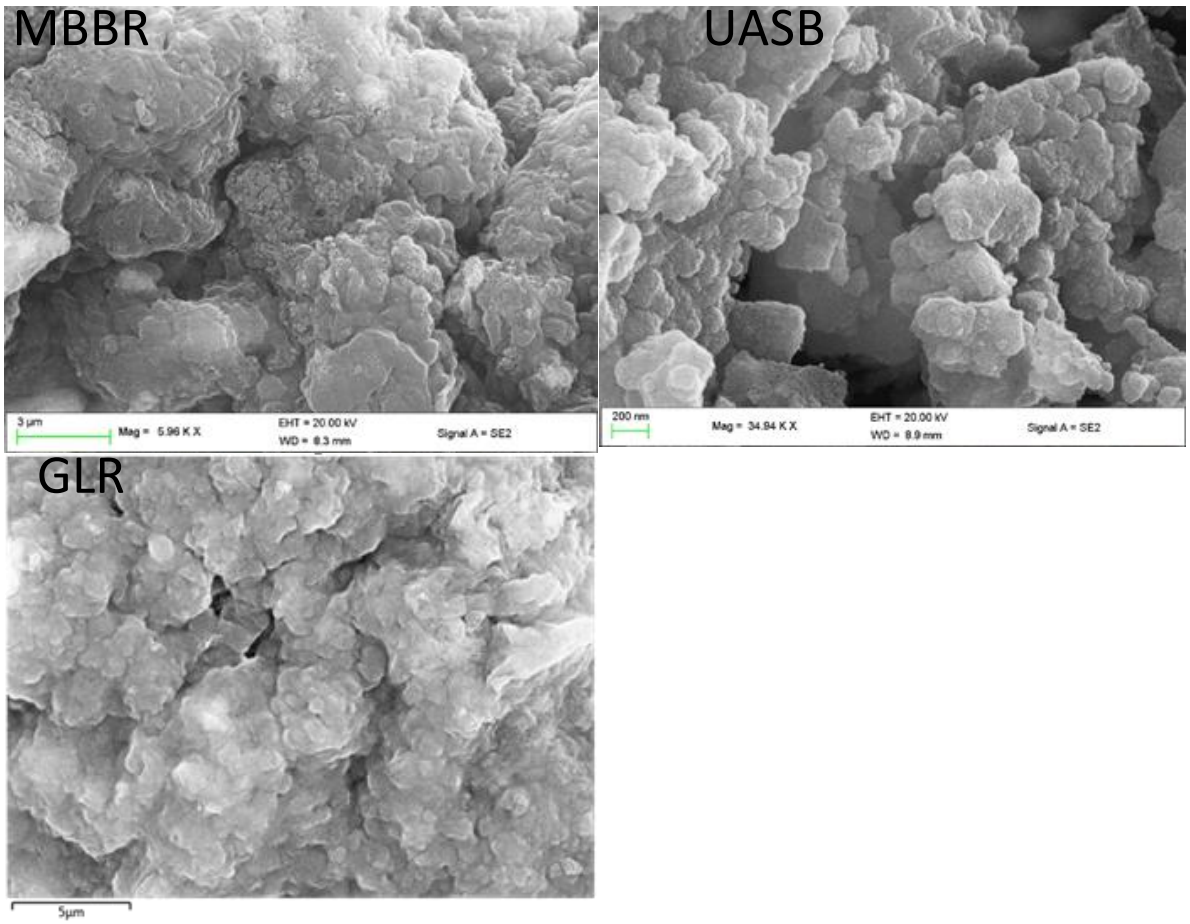

Figure 5. 7. SEM images of suspended biomass from MBBR, H-UASB and GLR in phase V. Scale bars: 3 µm (MBBR), 200 nm (H-UASB) and 5 µm (GLR).

5.3.4 Elemental composition

The elemental analysis was done in phase V and the final phase (IX) through SEM-EDX and MP-AES, respectively. The concentrations of Iron (Fe), magnesium (Mg), phosphorus (P), calcium (Ca), nickel (Ni), cobalt (Co), manganese (Mn), molybdenum (Mo), sodium (Na) and copper (Cu) in biomass samples are presented in *table 5.1*. Other elements detected in the biomass samples through SEM-EDX are presented on *figures 5.8-5.10*. It was determined through SEM-EDX that MBBR suspended biomass had the highest concentration of Fe at

approximately 5.92±9.54 *wt*% Fe (*table 5.1 and figure 5.8*), while the suspended biomass in H-UASB and GLR contained lower Fe concentrations (2.75±5.37 *wt*% and 2.05±1.89 *wt*%, respectively) compared to MBBR biomass *(table 5.1* and *figures 5.9 and 5.10*). The suspended biomass from MBBR, H-UASB and GLR contained 0.45 ± 0.42 *wt*% P, 1.10 ± 1.52 *wt*% P and 2.12±0.71 *wt*% P, and 0.65 ± 0.67 *wt*% Ca, 1.63 ± 1.01 *wt*% Ca and 1.92±0.63 *wt*% Ca, respectively. Cu, Co and Ni were detected through SEM-EDX in all the suspended biomass samples, albeit in low concentrations (≤0.11 *wt*%). Mo was not detected in all the biomass samples through SEM-EDX. Furthermore, Na and Mg in H-UASB suspended biomass were determined through SEM-EDX to be present at higher concentrations (0.57 ± 0.24 *wt*% and 2.83 ± 1.06 *wt*%, respectively) than in MBBR biomass (0.06 ± 0.05 *wt*% and 0.13 ± 0.11 *wt*%, respectively) and GLR biomass (0.336±0.16 *wt*% and 0.7±0.18 *wt*%, respectively). The concentrations of Mn in all the biomass samples were also found to be low (≤1 *wt*%) (*figures 5.8-5.10*).

Mg, Fe, Co, Cu, Mn and Ni were also detected in the biomass samples through MP-AES in the final phase (*table 5.1*). Since the biofilms had developed on the carrier materials had developed in all the reactors during this period, the elemental composition was determined for both suspended biomass and the biomass growing in the biofilms. The highest concentration of Mn, Fe and Co was found in MBBR biofilms at 0.43 mg/g-dry-weight, 122.95 mg/g-dry-weight and 0.62 mg/g-dry-weight, whilst the highest concentration of Mg was found in GLR suspended biomass at 13.22 mg/g-dry-weight biomass. The highest concentration of Cu and Ni were found in MBBR suspended biomass and in the GLR biofilms at 0.29 mg/g-dry weight and 0.28 mg/g-dry weight, respectively (*table 5.1*). Mo was not detected in all the biomass samples through MP-AES, similar to SEM-EDX.

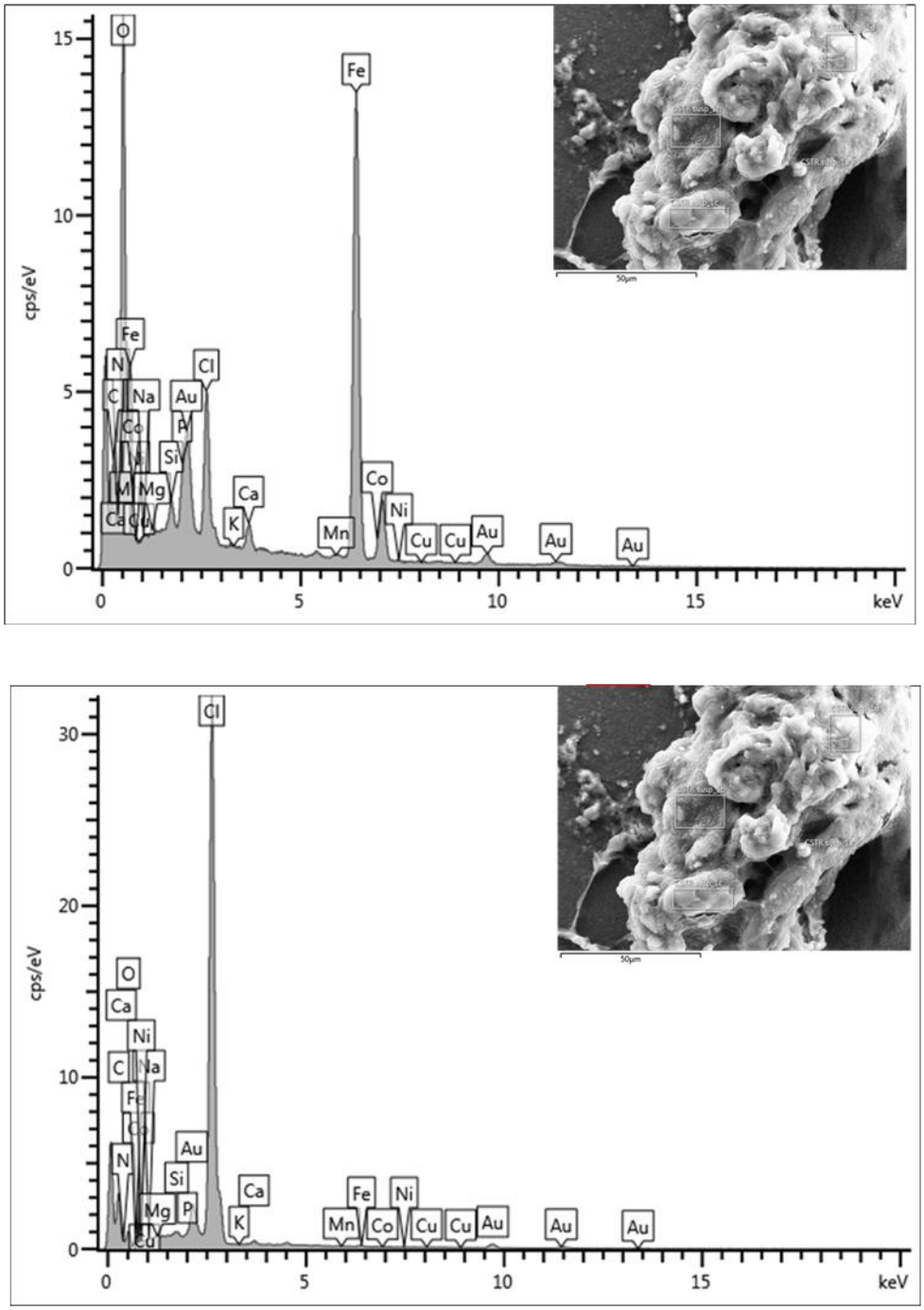

Figure 5. 8. EDX spectra of MBBR suspended biomass in phase V. Scale bars: 50 µm.

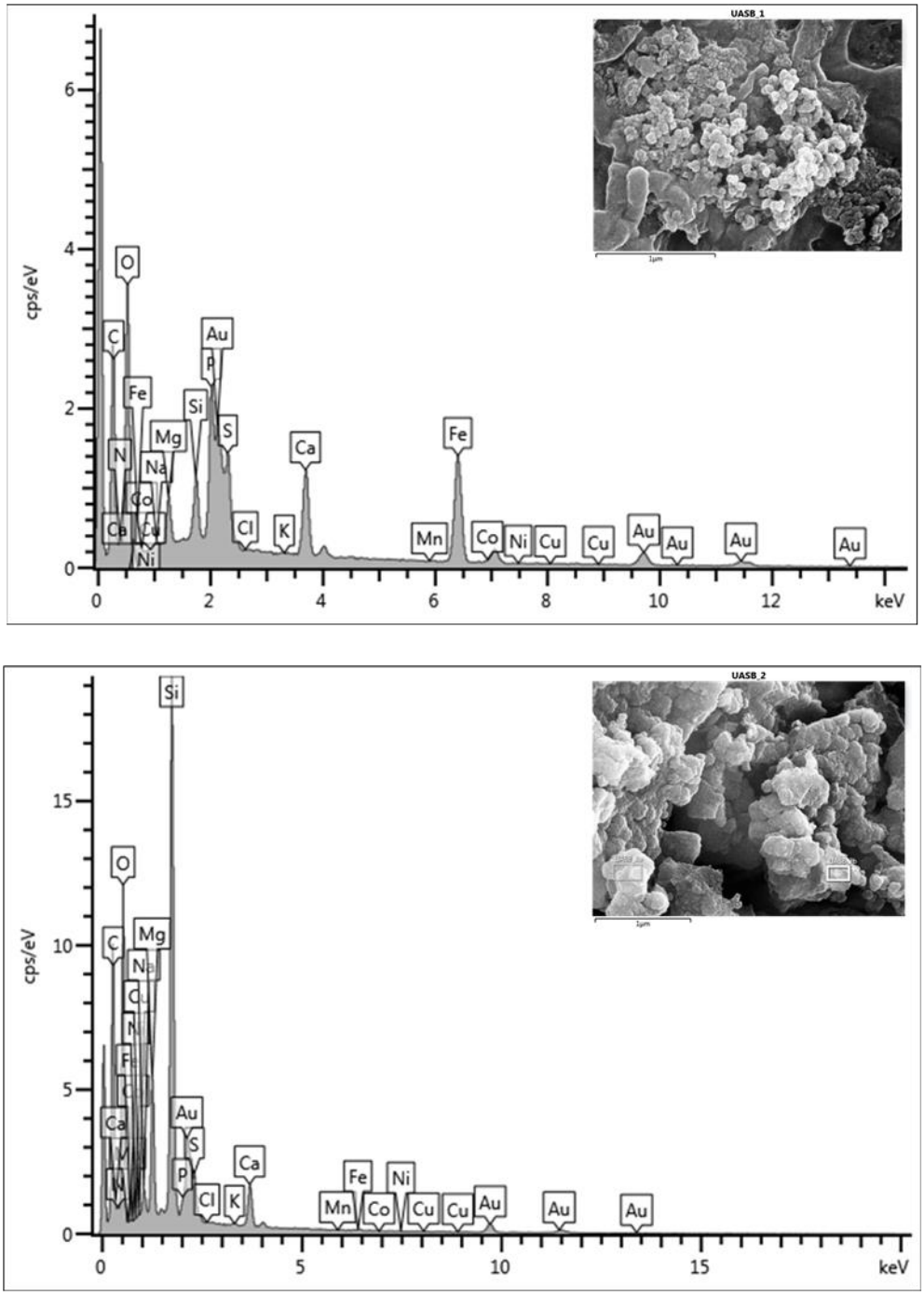

Figure 5. 9. EDX spectra of H-UASB suspended biomass in phase V. Scale bars: 1 µm.

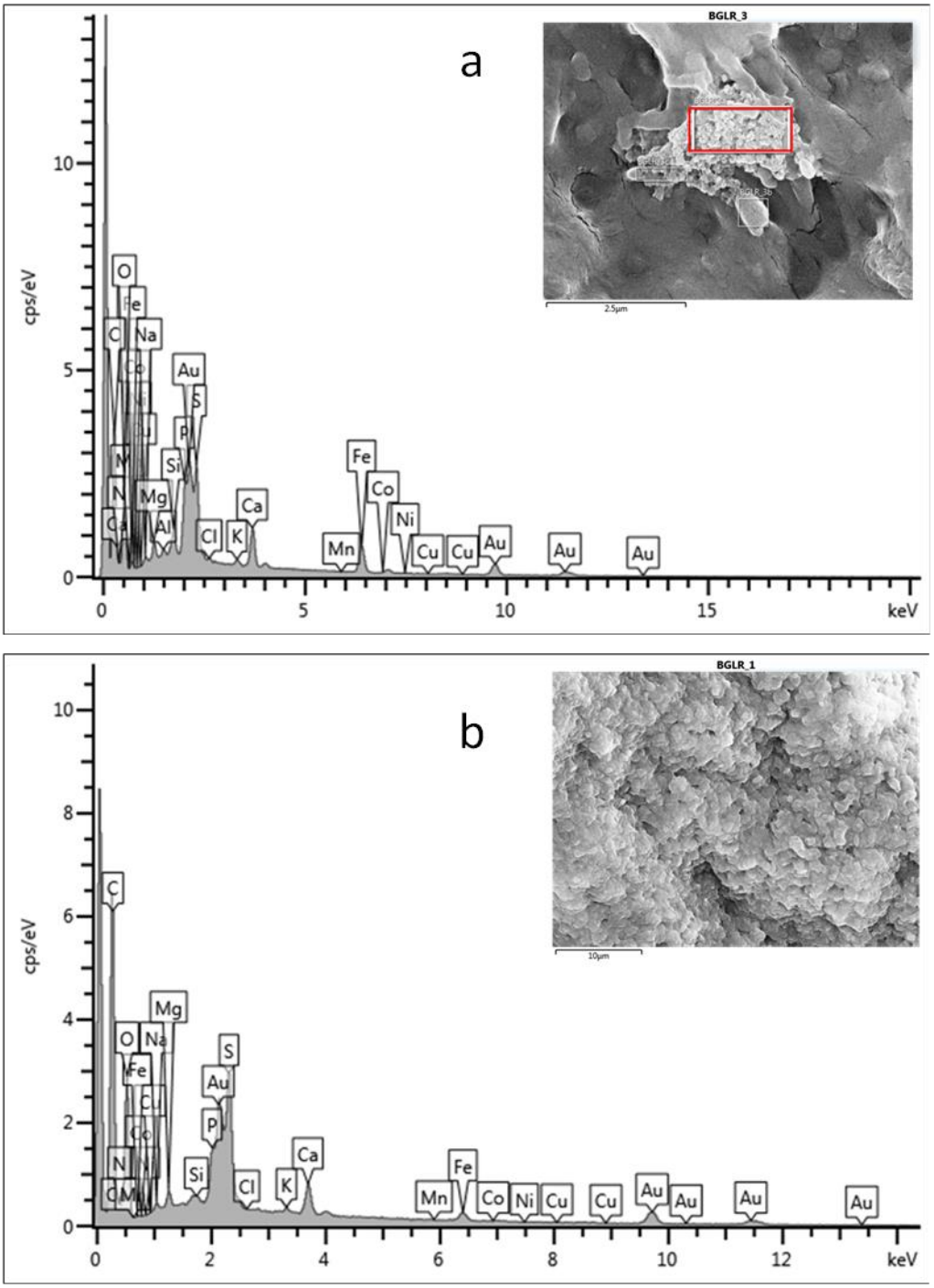

Figure 5. 10. EDX spectra of GLR suspended biomass in phase V. Scale bars: 2.5 µm (a) and 10 µm (b).

Table 5. 1. Concentration of phosphorus and metallic elements in the biomass: SEM – EDX (*wt*%), MP – AES (mg/g-dry weight).

SEM-EDX										
ELEMENT	**P**	**Ca**	**Mg**	**Fe**	**Na**	**Ni**	**Mn**	**Co**	**Cu**	**Mo**
H-UASB	1.10 ± 1.52	1.63 ± 1.01	2.83 ± 1.06	2.75 ± 5.37	0.57 ± 0.24	0.020 ± 0.030	0.020 ± 0.010	0.020 ± 0.030	0.040 ± 0.020	0.000 ± 0.000
MBBR	0.45 ± 0.42	0.65 ± 0.67	0.13 ± 0.11	5.92 ± 9.54	0.060 ± 0.050	0.020 ± 0.040	0.040 ± 0.060	0.050 ± 0.090	0.020 ± 0.020	0.000± 0.000
GLR	2.12±0.71	1.92±0.63	0.70±0.18	2.05±1.89	0.34±0.16	0.030±0.040	0.020±0.030	0.020±0.040	0.070±0.040	0.000± 0.000
MP-AES										
MBBR Suspension	N/A	N/A	9.37	74.47	N/A	0.10	0.40	0.37	0.29	N/D
MBBR Biofilm	N/A	N/A	11.11	122.95	N/A	0.10	0.43	0.62	0.27	N/D
H-UASB Suspension	N/A	N/A	11.73	12.39	N/A	0.07	0.28	0.040	0.21	N/D
H-UASB Biofilm	N/A	N/A	11.67	21.01	N/A	0.10	0.49	0.040	0.22	N/D
GLR Suspension	N/A	N/A	13.22	14.97	N/A	0.04	0.23	0.030	0.21	N/D
GLR Biofilm	N/A	N/A	9.28	16.70	N/A	0.28	0.28	0.000	0.37	N/D

N/A – not applicable, N/D – not detected

5.4 Discussion

Biofilm development, aggregate sizes and morphologies as well as the elemental composition of the biomass were assessed during the study. The physical properties of the biomass were based on the stereomicroscopy, particle size analysis, SEM-EDX, MP-AES as well as visual inspection of the photographic images captured during the study. However, biomass could not be collected from the reactors in all the phases as this could have destabilised the reactors. Therefore, analyses of the physical properties using the aforementioned techniques were alternated in the different phases.

The aggregation of biomass in ANAMMOX-mediated systems are of huge significance since granules have good settling properties and are not easily washed out of the reactors like the flocculent biomass (Wang and Zheng 2017). Similarly, when the biomass grow on the carrier materials or any other support materials within the reactors, they are not easily washed out of the reactors (Ødegaard 2006), which would be desirable in systems mediated by the ANAMMOX processes because of the slow growth rates of ANAMMOX bacteria. However, the settleability of granules could be compromised if their mineral contents are low, contain gas pockets or have irregular shapes (Green *et al.* 1994; Dapena-Mora *et al.* 2004a; Winkler *et al.* 2013; Wang and Zheng 2017). Therefore, the properties of biomass in the reactors were analysed in order to understand the impact of reactor configuration on them.

According to Lemaire, Webb and Yuan (2008) and Schmidt and Ahring (1996), the dense and compact microbial aggregates with spherical external appearance are granules, while the aggregates with loose structures that form homogeneous macroscopic layer upon settling are flocs. Based on these definitions, the suspended biomass in GLR and H-UASB were granular, while the biomass in the MBBR was flocculent (*figures 5.4-5.5*). This indicates that the shear forces due to mixing within the MBBR prevented the biomass from granulating as the stirrer blades could have sheared any granulating biomass. On the contrary, lower shear forces in both the H-UASB and the GLR compared to the MBBR could have favoured biomass granulation. Besides the shear forces, it is also possible that the gradual increase in the NLRs in the reactors could have stimulated EPS secretion by bacteria leading to biomass granulation, as previously suggested by Kwok *et al.* (1998). According to van Loosdrecht *et al.* (1995) and Van Loosdrecht and Heijnen (1993), bacteria can naturally granulate if the dilution rates are higher than the doubling rate of the bacteria (as a way of protecting themselves from wash-out).

However, biofilm development on the carrier materials was faster in the MBBR compared to H-UASB and UASB, possibly because the carrier materials and the biomass were constantly in contact due to stirring (Fernández *et al.* 2008). In comparison, the carrier materials in the H-UASB was floating on the surface throughout the study, while most of the suspended biomass was located in the lower sections (*figure 5.2h*), which could have limited the attachment on the carrier materials. In the GLR, although gas circulation could bring the biomass and the carrier materials in contact, the biofilm development on the carrier materials could have been limited by the high shear forces due to the violent mixing regime during gas circulation. In spite of the variation in the mixing conditions in the reactors, biofilm development was observed in all the reactors, from the beginning of phase V (*figure 5.6*). After thin films formed on the surfaces of the carrier materials, fast growth of the biofilms was witnessed in the reactors, with the biofilms in the MBBR growing faster compared to H-UASB and GLR (*figure 5.5*), possibly because the stirring enhanced the transfer of biomass from the suspension to the carrier materials (Fernández *et al.* 2008). It is also possible that the stirring stimulated higher EPS secretion in the MBBR compared to the H-UASB and GLR Kwok *et al.* (1998), leading to faster development of the biofilms in the MBBR as well as the presence of higher biomass concentration per unit carrier. Literature survey revealed that Kowalski, Devlin and Oleszkiewicz (2018) also reported slow biofilm development on carrier materials, starting with a thin film of biomass on the carrier materials before gradually increasing in thickness to fill up the available spaces after approximately 320 days, which was within the range observed in this study (*figure 5.6*). However, the concentration of biomass on the carrier materials in all the reactors were lower than the 19 ± 1 mg-total suspended solids per carrier reported by Kowalski *et al.* (2019), possibly because of variation in the available surface for biomass attachment since the carrier materials were manufactured by different companies.

SEM revealed the presence of cauliflower - shaped biomass aggregates in all the reactors (*figure 5.7*), which is typical of biomass from ANAMMOX-mediated systems (Ni *et al.* 2015; Han *et al.* 2018). All the biomass aggregates were covered with spherical particles on the captured SEM images (*figures 5.7*), which were presumed to be the cells of bacteria, possibly the cells of ANAMMOX bacteria, AOB or NOB since they have been reported to have similar shapes (Prosser 2007; Erdim *et al.* 2018). The interspaces observed on the biomass aggregates could be beneficial to the bacteria as it could be used in nutrient transport

into inner lying layers as well as in the escape of products of bacterial activities (Han *et al.* 2012).

During the study, the relative abundance of ANAMMOX bacteria, AOB and NOB fluctuated in all the reactors (*Chapter 4*), which coincided with the change of colour of the biomass (*figures 5.4 and A.4.2, appendix*). According to Alleman and Preston (1991) and Li and Sung (2015), reddish-brown colour could be an indication of either the presence of nitrifying bacteria or ANAMMOX bacteria. Therefore, the brown colour observed in MBBR biomass in phase III (day 125) at a time when the ANAMMOX bacterial abundance was below 1% could have been due to AOB and NOB as their relative abundance during this period was ≥10% (*Chapter 4*). On the contrary, the biomass in both H-UASB and GLR was tawny, coinciding with lower relative abundance of AOB and NOB compared to MBBR. However, after this period, the relative abundance of ANAMMOX bacteria increased in all the reactors, coinciding with the change in colour from tawny to red in H-UASB and GLR, and from brown to red in MBBR, in agreement with Li and Sung (2015) and Podmirseg *et al.* (2015).

The growth of different bacterial groups in the reactors was also expected to influence the elemental composition of the biomass, in line with Winkler *et al.* (2013) and Lin *et al.* (2013). Indeed, SEM-EDX and MP-AES analyses revealed variation in the elemental composition with the reactor configuration in phases V and IX, respectively (*table 5.1*). The biomass extracted from the MBBR had the highest Fe concentrations of all the biomass samples (*table 5.1*). However, the Fe concentrations in the MBBR biomass were higher than the values reported from other studies, while those of H-UASB and GLR biomass samples were comparable to those reported previously (*tables 5.1 and 5.2*). It is thus possible that Fe-containing minerals accumulated in the MBBR, probably due to oxidation of Fe^{2+} to Fe^{3+}, leading to precipitation of ferric hydroxide, as previously suggested by Oshiki *et al.* (2013) and Kappler, Schink and Newman (2005). Therefore, it is possible that the small particles (<120 nm) captured through SEM (*figures 5.7-5.9*), were mineral precipitates as these particles might be smaller than ANAMMOX bacterial cells (Erdim *et al.* 2018), and cells of many other microorganisms (Lebedeva *et al.* 2008; Sauder *et al.* 2017). This finding could thus be investigated in future studies.

The accumulation of Ca-, P- and Mg-containing minerals has been reported in many previous studies to influence biomass settleabilities and granulation (Lin *et al.* 2013; Winkler *et al.* 2013; Johansson, Ruscalleda and Colprim 2017). Apatite (Ca-P mineral), in particular,

has been suggested to precipitate due to the variation in conditions as a result of microbial activities which, in turn, lead to the variation of pH (Lin *et al.* 2013; Johansson, Ruscalleda and Colprim 2017; Ma *et al.* 2018). This mineral is known to have a theoretical Ca/P ratio of 1.67, and is also known to contain Na, Fe and Mg in different concentrations (Johansson, Ruscalleda and Colprim 2017). Since ANAMMOX bacteria are known to raise the pH through the consumption of acidity, while the AOB are known to reduce the pH through the consumption of alkalinity (Daigger *et al.* 2011), the variation in pH as a result of bacterial activities could have led to the precipitation of Ca- and P-containing apatite (Winkler *et al.* 2013). Indeed, the Ca/P ratios of H-UASB biomass (1.48) and MBBR biomass (1.44) were close to the theoretical Ca/P ratio of 1.67 in apatite, while that of GLR biomass was much lower (0.91), possibly because of variations in operational conditions or the microbial community structures within the reactors.

The presence of Na bearing minerals in the biomass could have been due to its presence in the feed as $NaNO_2$, NaCl and $NaHCO_3$ (*Chapter 3*). The addition of NaCl in the feed follows from Fernández *et al.* (2008) who asserted that its addition increases salinity, in turn inducing granulation of bacterial biomass in the reactors as the precipitates of low solubility salts such as $Ca_3(PO_4)_2$ provide nuclei on which granules form. It is thus possible that the observed granulation in the reactors could have been influenced by the NaCl salt added in the feed (Fernández *et al.* 2008). Ma *et al.* (2018) also reported concentrations of Na within the range of those observed in the reactors.

Table 5. 2. Documented concentrations of phosphorus and metallic elements in ANAMMOX-mediated systems.

Source of biomass	Elemental composition, *wt* (%)							Analytical technique	Reference
	Fe	Ca	Mg	P	Na	K	Ni		
Granular plug-flow AMX[a] reactor	0.57	28.9	0.51	13.4	0.36	0.19	-	ICP-OES[b]	(Ma *et al.* 2018)
Centrate fed PNA[c] SBR	878[d]	33.5 ±1.94	0.24± 0.00	15.8± 0.99	-	0.12±0.004	8.5E-6	ICP-OES[b]	(Johansson, Ruscalleda and Colprim 2017)
Anaerobic AMX landfill bioreactor	1.33	2.44	0.74	0.49	0.23	0.48	-	SEM-EDX	(Sri Shalini and Joseph 2013)
Anaerobic MBBR	2.01	-	0.020	0.14	3.30	-	-	SEM-EDX	(Gao *et al.* 2014)

[a]ANAMMOX;[b]Inductively coupled plasma optical emission spectroscopy; [c]partial nitrification/ANAMMOX; [d]mg/kg-dry wt

5.5 Conclusions

Variation in physical properties of the biomass with reactor configuration was observed during the study. Plug flow conditions in H-UASB and the sequencing of gas circulation in the GLR favoured biomass granulation, while continuous mixing in the MBBR limited biomass granulation, leading to the formation of flocculent biomass. However, continuous mixing led to faster biofilm development in the MBBR compared to H-UASB and GLR.

The colour of the biomass changed during the study because of the change in the bacterial composition of the biomass. The change in the colour of biomass from brown to creamy in phase I represented a decrease in the relative abundance of the ANAMMOX bacteria, while the gradual change in colour from creamy, then to brown, and finally to red signified the presence of ANAMMOX bacteria in high concentrations.

The accumulation of metallic elements and P in the reactors was influenced by the bacterial activities in the reactors. The high concentration of Fe in the MBBR biomass was due to the precipitation of iron-containing minerals in the reactors, while the high Ca/P ratios in H-UASB and MBBR was due to the precipitation of apatite.

CHAPTER SIX

6 MODEL-BASED DESCRIPTION OF PROCESS PERFORMANCE IN THE ANAMMOX-MEDIATED SYSTEMS

6.1 Introduction

The importance of mathematical modelling in undertaking studies relating to complex processes such as biological nitrogen removal processes that are carried out by several competing microorganisms has been demonstrated previously (Ni, Joss and Yuan 2014; Liu *et al.* 2016; Trojanowicz, Plaza and Trela 2017). These processes are determined not only by the concentration profiles of electron donors and acceptors, but also by other factors such as bacterial population shifts (Nielsen *et al.* 2005; Kindaichi *et al.* 2007). Concentration profiles, in turn, could be influenced by several interlinked factors such as diffusion coefficients, biomass spatial distribution and the physical properties of biomass (Terada *et al.* 2007; Ni, Ruscalleda and Smets 2012). Therefore, model-based description of process performance could provide useful insights pertaining the bacterial communities and NRRs in the ANAMMOX-mediated systems.

In this chapter, extended ASM 1 (activated sludge model number 1) has been applied to describe the performance of the reactors. The ASM 1 described in Henze *et al.* (1987) was modified with the inclusion of ANAMMOX and COMAMMOX bacterial activities. In addition, the NOB were split into two groups (*Nitrobacter* and *Nitrospira*) in the modified ASM 1 model. It is noteworthy here that this is a novel approach in the modelling of ANAMMOX-mediated systems, as this has not been done in any other study previously. This has been necessitated by the fact that the three groups have recently been reported to have distinct kinetic properties (Kits *et al.* 2017; Park, Park and Chandran 2017), requiring their separation in kinetic models.

The modified model was calibrated with the experimental data from the H-UASB, and validated with experimental data from MBBR and GLR. The modelling period covered the entire study period (535 days of study). Following from the process performance observed in *Chapter 3* and the bacterial population dynamics observed in *Chapter 4*, the concentration of oxygen at the gas-liquid interface as well as the concentration of biodegradable substrate in the reactors were adjusted after model calibration.

6.2 Methodology

6.2.1 Model description

ASM 1 described in Henze *et al.* (1987) was modified with the inclusion of *Nitrobacter* spp., *Nitrospira* spp., ANAMMOX bacteria and COMAMMOX bacteria (*tables 6.1 and 6.2*). The modified model incorporates a switching function to account for oxygen inhibition of both ANAMMOX bacterial and anaerobic heterotrophic bacterial activities as described in Henze *et al.* (1987) (*equation 6.1*). In addition, in the modified model, anoxic reduction factor η in ASM 1 was retained to account for the possible reduction in activities under anaerobic conditions (Henze *et al.* 1987). The reduction factor η for NO_3^- and NO_2^- were assumed to be the same (Hao, Heijnen and Van Loosdrecht 2002).

All the expected processes of nitrification, denitrification and carbon oxidation as well as the stoichiometric coefficients are presented in a matrix format in *table 6.1*. The corresponding conversion rate expressions are listed on *table 6.2*. The process within the blank cells have no impact on the corresponding component. To account for the conversion of a component *i*, the product of process rates ρ_j ($gm^{-3}day^{-1}$) in *table 6.2* and the stoichiometric coefficients v_{ij} in *table 6.1* are summed up according to *equation 6.2*.

$$\frac{C_{O_2}}{K_O + C_{O_2}} \tag{6.1}$$

Where C_{O_2} is the oxygen concentration in the bulk liquid and K_O is the oxygen inhibition coefficient.

$$r_i = \sum_j v_{ij}\rho_j \tag{6.2}$$

Where ρ_j is the rate of process and v_{ij} is the stoichiometric coefficient.

Table 6. 1. Model stoichiometry (*continued in the next page*)

Component (j) →	1	2	3	4	5	6	7	8	9	10	12	13
Process (i) ↓	X_{AOB}	X_{Nb}	X_{Nsp}	X_{CMX}	X_{AMX}	X_H	X_S	S_{NO2}	S_{NO3}	S_{NH4}	S_{O2}	S_S
1. AOB growth	1							$\frac{1}{Y_{AOB}}$		$-i_{NXB}-\frac{1}{Y_{AOB}}$	$-\frac{3.43-Y_{AOB}}{Y_{AOB}}$	
2. *Nitrobacter* growth		1						$-\frac{1}{Y_{nsp/nb}}$	$\frac{1}{Y_{nsp/nb}}$	$-i_{NXB}$	$-\frac{1.14-Y_{nsp/nb}}{Y_{nsp/nb}}$	
3. *Nitrospira* growth			1					$-\frac{1}{Y_{nsp}}$	$\frac{1}{Y_{nsp}}$	$-i_{NXB}$	$-\frac{1.14-Y_{nsp}}{Y_{nsp}}$	
4. CMX bacterial growth				1				$-\frac{1}{Y_{CMX}}$	$\frac{1}{Y_{CMX}}$	$-i_{NXB}-\frac{1}{Y_{CMX}}$	$-\frac{4.57-Y_{CMX}}{Y_{CMX}}$	
5. AMX bacterial growth	1				1			$-\frac{1}{1.14}-\frac{1}{Y_{AMX}}$	$\frac{1}{1.14}$	$-i_{NXB}-\frac{1}{Y_{AMX}}$		
6. Anaerobic growth of heterotrophic bacteria on nitrite						1		$-\frac{1-Y_{ANA,H}}{1.71Y_{ANA,H}}$		$-i_{NXB}$		$-\frac{1}{Y_{ANA,H}}$
7. Anaerobic growth of heterotrophic bacteria on nitrate						1			$-\frac{1-Y_{ANA,H}}{2.86Y_{ANA,H}}$	$-i_{NXB}$		$-\frac{1}{Y_{ANA,H}}$
8. aerobic growth of heterotrophic bacteria						1				$-i_{NXB}$	$-\frac{1-Y_{AER.H}}{Y_{AER,H}}$	$-\frac{1}{Y_{AER,H}}$
9. Aerobic endogenous respiration of AOB	-1									i_{NBM}-$f_I i_{NXI}$	-(1- f_I)	
10. Aerobic endogenous respiration of *Nitrobacter*		-1								i_{NBM}-$f_I i_{NXI}$	-(1- f_I)	
11. Aerobic endogenous respiration of *Nitrospira*			-1							i_{NBM}-$f_I i_{NXI}$	-(1- f_I)	

Process (i) ↓	X_{AOB}	X_{Nb}	X_{Nsp}	X_{CMX}	X_{AMX}	X_H	X_S	S_{NO2}	S_{NO3}	S_{NH4}	S_{O2}	S_S
12. Aerobic endogenous respiration of CMX				-1						i_{NBM}-$f_I i_{NXI}$	-(1- f_I)	
13. Aerobic endogenous respiration of AMX					-1					i_{NBM}-$f_I i_{NXI}$	-(1- f_I)	
14. Aerobic endogenous respiration of heterotrophic bacteria						-1				i_{NBM}-$f_I i_{NXI}$	-(1- f_I)	
15. Anoxic endogenous respiration of X_{AOB}									-(1- f_I)/2.86	i_{NBM}-$f_I i_{NXI}$		
16. Anoxic endogenous respiration of X_{nb}									-(1- f_I)/2.86	i_{NBM}-$f_I i_{NXI}$		
17. Anoxic endogenous respiration of X_{nsp}									-(1- f_I)/2.86	i_{NBM}-$f_I i_{NXI}$		
18. Anoxic endogenous respiration of X_{CMX}									-(1- f_I)/2.86	i_{NBM}-$f_I i_{NXI}$		
19. Anoxic endogenous respiration of X_{AMX}									-(1- f_I)/2.86	i_{NBM}-$f_I i_{NXI}$		
20. Anoxic endogenous respiration of X_H									-(1- f_I)/2.86	i_{NBM}-$f_I i_{NXI}$		
21. Hydrolysis							-1					1

Table 6. 2. Process rate equations (*continued in the next page*)

Process	Rate
1. Growth of AOB	$\mu_{AOB}^{MAX}(\frac{S_{O2}}{K_{O2,AOB}+S_{O2}})(\frac{S_{NH}}{K_{NH,AOB}+S_{NH}})\eta_{AOB}X_{AOB}$
2. Growth of *Nitrospira*	$\mu_{Nb}^{MAX}(\frac{S_{O2}}{K_{O2,NOB}+S_{O2}})(\frac{S_{NO2}}{K_{NO2,Nb}+S_{NO2}})\eta_{Nb}X_{Nb}$
3. Growth of *Nitrobacter*	$\mu_{Nsp}^{MAX}(\frac{S_{O2}}{K_{O2,Nsp}+S_{O2}})(\frac{S_{NO2}}{K_{NO2,Nsp}+S_{NO2}})\eta_{Nsp}X_{Nsp}$
4. Growth of CMX	$\mu_{CMX}^{MAX}[(\frac{S_{O2}}{K_{O2,CMX}+S_{O2}})(\frac{S_{NO2}}{K_{NO2,CMX}+S_{NO2}})+(\frac{S_{O2}}{K_{O2,CMX}+S_{O2}})(\frac{S_{NH}}{K_{NH,CMX}+S_{NH}})]\eta_{CMX}X_{CMX}$
5. Growth of AMX	$\mu_{AMX}^{MAX}(\frac{K_{O2,AMX}}{K_{O2,AMX}+S_{O2}})(\frac{S_{NO2}}{K_{NO2,AN}+S_{NO2}})(\frac{S_{NH}}{K_{NH,AOB}+S_{NH}})X_{AMX}$
6. Growth of anaerobic heterotrophic bacteria on nitrite	$\mu_{H}^{MAX}\eta_{H}[\left(\frac{K_{O2,H}}{K_{O2,H}+S_{O}}\right)\left(\frac{S_{NO2}}{K_{NO3H}+S_{NO2}}\right)\left(\frac{S_{S}}{K_{S\,H}+S_{S}}\right)]X_{H}$
7. Growth of anaerobic heterotrophic bacteria on nitrate	$\mu_{H}^{MAX}\eta_{ANA.H}(\frac{K_{O2,H}}{K_{O2,H}+S_{O}})(\frac{S_{NO3}}{K_{NO3,H}+S_{NO3}})(\frac{S_{S}}{K_{S,H}+S_{S}})X_{H}$
8. Growth of aerobic heterotrophic bacteria	$\mu_{H}^{MAX}(\frac{S_{O2}}{K_{O2,H}+S_{O2}})(\frac{S_{S}}{K_{S,H}+S_{S}})\eta_{H}X_{H}$
9. Aerobic endogenous respiration of AOB	$b_{AOB}\frac{S_{O_2}}{K_{O_2}^{AOB}+S_{O_2}}X_{AOB}$
10. Aerobic endogenous respiration of *Nitrobacter*	$b_{nb}\frac{S_{O_2}}{K_{O_2}^{nb}+S_{O_2}}X_{nb}$
11. Aerobic endogenous respiration of *Nitrospira*	$b_{nsp}\frac{S_{O_2}}{K_{O_2}^{nsp}+S_{O_2}}X_{nsp}$
12. Aerobic endogenous respiration of CMX	$b_{CMX}\frac{S_{O_2}}{K_{O_2}^{CMX}+S_{O_2}}X_{CMX}$

Process	Rate
13. Aerobic endogenous respiration of AMX	$b_{AMX}\frac{S_{O_2}}{K_{O_2}^{AMX}+S_{O_2}}X_{AMX}$
14. Aerobic endogenous respiration of heterotrophic bacteria	$b_H\frac{S_{O_2}}{K_{O_2}^{H}+S_{O_2}}X_H$
15. Anoxic endogenous respiration of X_{AOB}	$b_{AOB}\eta_{AOB}\frac{K_{O_2}^{AOB}}{K_{O_2}^{AOB}+S_{O_2}}\frac{S_{NO_2}+S_{NO_3}}{K_{O_2}^{AOB}+S_{NO_2}+S_{NO_3}}X_{AOB}$
16. Anoxic endogenous respiration of X_{nb}	$b_{nb}\eta_{nb}\frac{K_{O_2}^{nb}}{K_{O_2}^{nb}+S_{O_2}}\frac{S_{NO_2}+S_{NO_3}}{K_{O_2}^{nb}+S_{NO_2}+S_{NO_3}}X_{nb}$
17. Anoxic endogenous respiration of X_{nsp}	$b_{nsp}\eta_{nsp}\frac{K_{O_2}^{nsp}}{K_{O_2}^{nsp}+S_{O_2}}\frac{S_{NO_2}+S_{NO_3}}{K_{O_2}^{nsp}+S_{NO_2}+S_{NO_3}}X_{nsp}$
18. Anoxic endogenous respiration of X_{CMX}	$b_{CMX}\eta_{CMX}\frac{K_{O_2}^{CMX}}{K_{O_2}^{CMX}+S_{O_2}}\frac{S_{NO_2}+S_{NO_3}}{K_{O_2}^{CMX}+S_{NO_2}+S_{NO_3}}X_{CMX}$
19. Anoxic endogenous respiration of X_{AMX}	$b_{AMX}\eta_{AMX}\frac{K_{O_2}^{AMX}}{K_{O_2}^{AMX}+S_{O_2}}\frac{S_{NO_2}+S_{NO_3}}{K_{O_2}^{AMX}+S_{NO_2}+S_{NO_3}}X_{AMX}$
20. Anoxic endogenous respiration of X_H	$b_H\eta_H\frac{K_{O_2}^{,H}}{K_{O_2}^{H}+S_{O_2}}\frac{S_{NO_2}+S_{NO_3}}{K_{O_2}^{H}+S_{NO_2}+S_{NO_3}}X_H$
21. Hydrolysis	$K_H\frac{{X_S}/{(X_H+X_H)}}{K_X+{X_S}/{(X_H+X_H)}}(X_H)$

6.2.2 Definition and specification of model kinetic and stoichiometric parameters

The literature-obtained maximum specific growth rates (μ_{max}) of AOB, *Nitrobacter*, *Nitrospira*, COMAMMOX bacteria, ANAMMOX bacteria, anaerobic heterotrophic bacteria and aerobic heterotrophic bacteria as well as the biomass yields of each of these bacterial groups, their decay coefficients (*b*) and affinities for electron donors and acceptors are presented in *table 6.4*. Since the *b*, μ_{max} and K_H *(hydrolysis saturation constant)* are temperature-dependent, their values at the operational temperature of approximately 36ºC were estimated using Arrhenius-type equation (Cema *et al.* 2012) (*equation 6.3*):

$$k(T) = k(T_r)e^{\theta(T-T_r)} \quad (6.3)$$

Where k(T) and k(T_r) are the parameters (*b*, K_H and μ_{max}) at 36ºC (temperature within the reactors) and 20ºC (reference temperature), respectively. The Arrhenius constant θ for AOB, *Nitrobacter*, *Nitrospira*, COMAMMOX bacteria, ANAMMOX bacteria and heterotrophic bacteria was calculated according to *equation 6.4* (Wyffels *et al.* 2004):

$$\theta = E_{act}/(R * 293(T + 273)) \quad (6.4)$$

Where *R* is the universal gas constant (8.31 J/mol-K) and E_{act} is the activation energy (AOB=68, NOB (*Nitrobacter*, *Nitrospira*) = 44 kJ/mol, ANAMMOX bacteria=71 kJ/mol). The activation energy of COMAMMOX bacteria was assumed to be equal to that of *Nitrospira*. The heterotrophs' θ values for *b* and μ_{max} were assumed to be 0.11 and 0.069 (Wyffels *et al.* 2004; Reino *et al.* 2018). The oxygen transfer coefficient (K_La) was estimated according to *equation 6.5* at 36ºC, which was the operational temperature of the reactors *(Wyffels et al. 2004):*

$$K_La(T) = K_La(T_r)\varphi^{(T-T_r)} \quad (6.5)$$

Where φ(=1.04) is the temperature correction factor (Wyffels *et al.* 2004).

Table 6. 3. Definition of model kinetic and stoichiometric parameters and terms

	Symbol	Definition	Units
1	$X_{i,in}, X_{i,out}$	Concentration of bacterial group *i* in the influent and in the effluent	gCOD/m^3
2	μ_i	Maximum growth rate of bacterial group *i*	day^{-1}
3	$S_{i,in}, S_{i,out}$	Concentration of component *j* in the influent and effluent streams	gN/m^3 (NO_3^-, NO_2^-, NH_4^+), gCOD/m^3 (organic substrate) or gO_2/m^3
4	$K_{j,i}$	Half-saturation coefficient of component *j* for bacterial group *i*	gN/ m^3 or gCOD/ m^3
5	K_{SO2}^i	Oxygen inhibiting coefficient for bacterial group *i*	gO_2/ m^3
6	Y_i	Yield coefficient for bacterial group *i*	gCOD/gN or gCOD/gCOD
7	Q_W, Q_{in}, Q_{out}	Biomass washout rate, influent and effluent flow rates, respectively	m^3/day
8	$K_L a_{O2}$	Oxygen mass transfer coefficient	day^{-1}
9	S_{O2}^G	Concentration of oxygen in air	g/m^3
10	m_{O2}	Partition coefficient for component *i*	mol/mol
11	*H*	Heterotrophic bacteria	-
13	*AMX*	ANAMMOX bacteria	-
14	X_I, X_S	Inert (non-biodegradable organics), slowly biodegradable substrate	gCOD/m^3
15	f_I	Fraction of X_I in decaying biomass	gCOD/gCOD
16	i_{NBM}	Concentration of nitrogen in biomass	gN/gCOD
17	i_{NXI}	Nitrogen content of non-biodegradable organics	gN/gCOD
18	η	Anoxic reduction factor	-
19	K_X, K_H	Hydrolysis saturation constant and hydrolysis rate constant	day^{-1} and gCOD/gCOD, respectively

Table 6. 4. Average stoichiometric and kinetic parameters of AOB, NOB, ANAMMOX and heterotrophic bacteria at 20ºC.

Bacterial group	**μ_{max} (day^{-1})**	**Y**	**b (day^{-1})**	**e$^-$ donor**	**K_S^* (gN/ m^3 or gCOD/ m^3)**	**e$^-$ acceptor**	**$K_{O/N}^{**}$ (gN/ m^3 or gCOD/ m^3)**	**References**
1. AOB	1.443	0.150	0.130	NH_4^+	2.400	O_2	0.594	(Hellinga, van Loosdrecht and Heijnen 1999; Ahn, Yu and Chandran 2008; Wett *et al.* 2013; Ni, Joss and Yuan 2014)
2. *Nitrobacter*	0.480	0.130	0.069	NO_2^-	1.375	O_2	0.430	(Blackburne *et al.* 2007; Ni, Joss and Yuan 2014; Park, Park and Chandran 2017)
3. *Nitrospira*	0.690	0.140	0.060	NO_2^-	0.760	O_2	0.435	
4. COMAMMOX bacteria	0.720	0.470	0.060	NH_4^+	0.0118	O_2	0.430$^{\#}$	(Kits *et al.* 2017)
		0.140$^{\#}$	0.060	NO_2^-	6.290	O_2	0.430$^{\#}$	
3. ANAMMOX bacteria	0.066	0.159	0.00312	NH_4^+	0.185	NO_2^-	0.175	(Dapena-Mora *et al.* 2004c; Ni, Joss and Yuan 2014)
4. Heterotrophic bacteria	7.20	0.490	0.192	Organic substrate	2.000	NO_2^-	0.500	(Hellinga, van Loosdrecht and Heijnen 1999; Ni, Joss and Yuan 2014)
		0.79 0		Organic substrate		NO_3^-	0.320	(Hellinga, van Loosdrecht and Heijnen 1999; Ni, Joss and Yuan 2014)
		0.370		Organic substrate		O_2	0.200	(Henze *et al.* 1987; Hellinga, van Loosdrecht and Heijnen 1999; Ni, Joss and Yuan 2014)

Other model parameters

$K_L a_{O2}$-222 day^{-1}, i_{NBM}-0.0583 gN/gCOD, f_I-0.080, i_{NXI}-0.02, K_{O2}^{AMX} -0.010 gO^2/m^3, $K_{O2}^{H,AN}$-0.200 gO^2/m^3, η~0.600 (Heterotrophic bacteria), η ~0.500 (ANAMMOX bacteria), K_{NO3}^{AMX}=0.500, K_X=0.030, K_H=3.000 (Hellinga, van Loosdrecht and Heijnen 1999; Wyffels *et al.* 2004; Ni, Joss and Yuan 2014)

K_S^*-affinity for electron donor, $K_{O/N}^{**}$-affinity for electron acceptor, $^{\#}$estimated based on reported values for *Nitrospira.* $^{a\ and\ b}$anoxic reduction factors

6.2.3 Simulation of process performance and bacterial population dynamics in the reactors

Process performance and bacterial population dynamics in the reactors were simulated in *MATLAB 2019b* using *ode15s solver* (*figure A.6.4, Appendix D*). The simulations were done for 535 days, thus covering the entire study period. The following assumptions were made during the simulation:

1. Organic carbon concentration in the influent was approximately 2 mg/L throughout the study (Dapena-Mora *et al.* 2004c)
2. No other inhibition other than the inhibition of ANAMMOX and anoxic heterotrophic bacterial activities by oxygen
3. Anoxic heterotrophic bacteria used both nitrite and nitrate
4. The MBBR was homogeneously mixed
5. The GLR was homogeneously mixed during gas circulation
6. The solids retention time (SRT) in all the reactors was constant at 250 days
7. Ammonium oxidation by AOB, and the reduction of both nitrate and nitrite by anoxic heterotrophic bacteria, were complete
8. The chemical oxygen demand (COD)-equivalent of 1 g of suspended solids (SS) was 1.20g.

The following were the initial conditions:

1. NH_4^+, NO_3^- and NO_2^- concentrations were 50 mg-N/L, 0.005 mg-N/L and 55 mg-N/L, respectively.
2. DO and organic substrate concentrations were 0.5 mg-O_2/L and 2 mg-COD/L, respectively.
3. The mixed liquor suspended solids (MLSS) concentrations in the reactors was 200 mg/L. Of these, the concentration of AOB, *Nitrobacter* spp., *Nitrospira* spp., COMAMMOX bacteria, ANAMMOX bacteria and heterotrophic bacteria were taken to be 4.54%, 0.13%, 6.14%, 0.9%, 45.15% and 44.87%, respectively (based on the shotgun sequencing).

The modelling equations for NH_4^+, NO_2^-, NO_3^- and COD in the MBBR followed *equation 6.6*, while the modelling equations for oxygen followed *equation 6.7 (Hellinga, van Loosdrecht and Heijnen 1999; Batstone et al. 2002; Scott 2016)*:

$$\left(\frac{dC}{dt}\right)V = Q_{in}C_{in} - Q_{out}C_{out} + r_iV \quad (6.6)$$

$$\left(\frac{dC}{dt}\right)V = Q_{in}C_{in} - Q_{out}C_{out} + K_La(C_S - C_{O_2}) + r_iV \quad (6.7)$$

Where r_i was determined according to *equation 6.2*, Q_{in} and Q_{out} were the influent and effluent concentrations, C_{in} and C_{out} were the component concentrations in the influent and effluent streams, C_{O_2} were the oxygen concentration in the bulk liquid and C_S was the gas-liquid interface oxygen concentration.

The H-UASB was divided into 5 continuously stirred tank reactors (CSTRs) of equal volumes, in which the effluent from the first (lower) CSTR was feeding the second CSTR right above it, and the effluent from the second CSTR fed the third CSTR, etc. (*figure 6.1*) as previously described by Rodríguez-Gómez *et al.* (2014). The volume of each CSTR was assumed to be a fifth of the total working volume.

Two approaches were employed in the modelling of the GLR. During the first 121 days when the argon/CO_2 mixture was continuously recycled in the reactor, the reactor was assumed to be completely mixed and was thus modelled as a CSTR. From the 122nd day onwards when gas circulation was sequenced, the GLR was modelled similar to H-UASB, by dividing the reactor into five CSTRs (*figure 6.1*).

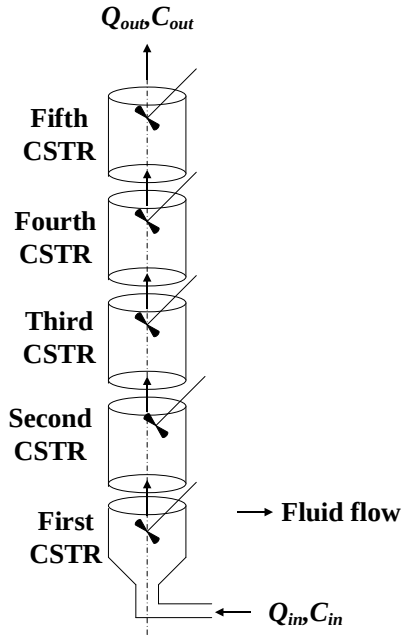

Figure 6. 1. Schematic diagram of H-UASB depicted as a series of 5 CSTRs.

6.2.4 Calibration and validation of the model

Model calibration was undertaken in two steps: simulation with default (literature-obtained) parameters, and parameter adjustments based on H-UASB performance. The values of specific growth rates, yield and affinities for the electron donors and acceptors of AOB, *Nitrobacter*, *Nitrospira*, COMAMMOX bacteria, ANAMMOX bacteria and heterotrophic bacteria were adjusted during model calibration. The selection of these parameters was based on the sensitivity of the model to their adjustments, one at a time as previously suggested (Cema *et al.* 2012). The parameter estimations were done through the minimization of the sum of squares of the deviations of the model predictions from the experimental data from H-UASB (*equation 6.8*) (Trojanowicz, Plaza and Trela 2017).

$$Root\ mean\ squared\ error = \sqrt{(\frac{1}{n}\sum_{i=1}^{n}(observed\ value - predicted\ value)^2)} \quad (6.8)$$

The calibrated model was then validated with long-term experimental data of effluent NH_4^+, NO_3^- and NO_2^- concentrations from the MBBR and GLR.

6.2.5 Model testing at baseline conditions

The calibrated model was tested in all the reactors at baseline conditions (similar conditions across all the reactors). Since the influent and effluent flow rates as well as the feed composition were similar in all the reactors during the study (*Chapter 3*), the working volumes in MBBR and GLR during model testing were kept similar to that in H-UASB in order for the NLRs to be similar in all the reactors. In addition, the gas-liquid interface concentration of oxygen (Cs) was fixed at 0.1 mg-O_2/L in the reactors.

6.2.6 Verification of model accuracy

The accuracy of the coding in *MATLAB* was checked by simulating the process performance in *Simulink* under similar conditions (as in *MATLAB*) (*figures A.6.4 - A.6.5 and A.6.8 - A.6.9, Appendix D*). Based on the output of both *Simulink* and *MATLAB*, the accuracy of coding in *MATLAB* was determined.

6.3 Results

6.3.1 Model Calibration

The model was calibrated using the relative abundance of AOB, *Nitrospira* spp., *Nitrobacter* spp., COMAMMOX bacteria and ANAMMOX bacteria as well as the effluent concentrations of NH_4^+, NO_2^- and NO_3^- in the H-UASB. During calibration, the model

parameters were adjusted through the reduction of RMSE. The final kinetic parameters obtained after model calibration are presented on *table 6.5*.

Table 6. 5. Calibrated kinetic and stoichiometric parameters

Bacterial group	**μ_{max} (day^{-1})**	**Y (gCOD/gN or gCOD/gCOD)**	**b (day^{-1})**	**e^- donor**	**K_S (gN/m^3 or $gCOD/m^3$)**	**e^- acceptor**	**$K_{O/N}$ (gN/m^3, $gCOD/m^3$ or gO^2/m^3)**
1. AOB	1.443	0.450	0.130	NH_4^+	1.32	O_2	0.505
2. *Nitrobacter*	0.864	0.143	0.069	NO_2^-	0.825	O_2	0.426
3. *Nitrospira*	0.690	0.140	0.060	NO_2^-	0.760	O_2	0.413
4. COMAMMOX bacteria	0.360	0.047	0.060	NH_4^+	0.770	O_2	0.421
		0.094	0.060	NO_2^-	0.944	O_2	0.421
3. ANAMMOX bacteria	0.0797	0.151	0.00312	NH_4^+	0.370	NO_2^-	0.210
4. Heterotrophic bacteria	7.200	0.882	0.192	Organic substrate	2.000	NO_2^-	0.500
		0.790		Organic substrate		NO_3^-	0.320
		0.666		Organic substrate		O_2	0.200

6.3.2 Model simulation of effluent concentrations of NO_2^-, NO_3^- and NH_4^+

6.3.2.1 H-UASB

The model predicted the trends in the effluent concentrations of NO_2^-, NO_3^- and NH_4^+ in the reactor during the study period (*figures 6.2 a-c*). However, the model was limited in the prediction of fluctuations in the effluent concentrations of NO_2^-, NO_3^- and NH_4^+. During the first 90 days, the effluent NO_3^- concentrations predicted by the model were higher than the measured concentrations (*figure 6.2a*), while the effluent NH_4^+ concentrations were lower than the measured concentrations. From day 492 onwards, the effluent NO_3^- and NO_2^- concentrations predicted by the model were higher than the measured values (*figures 6.2a and 6.2b*).

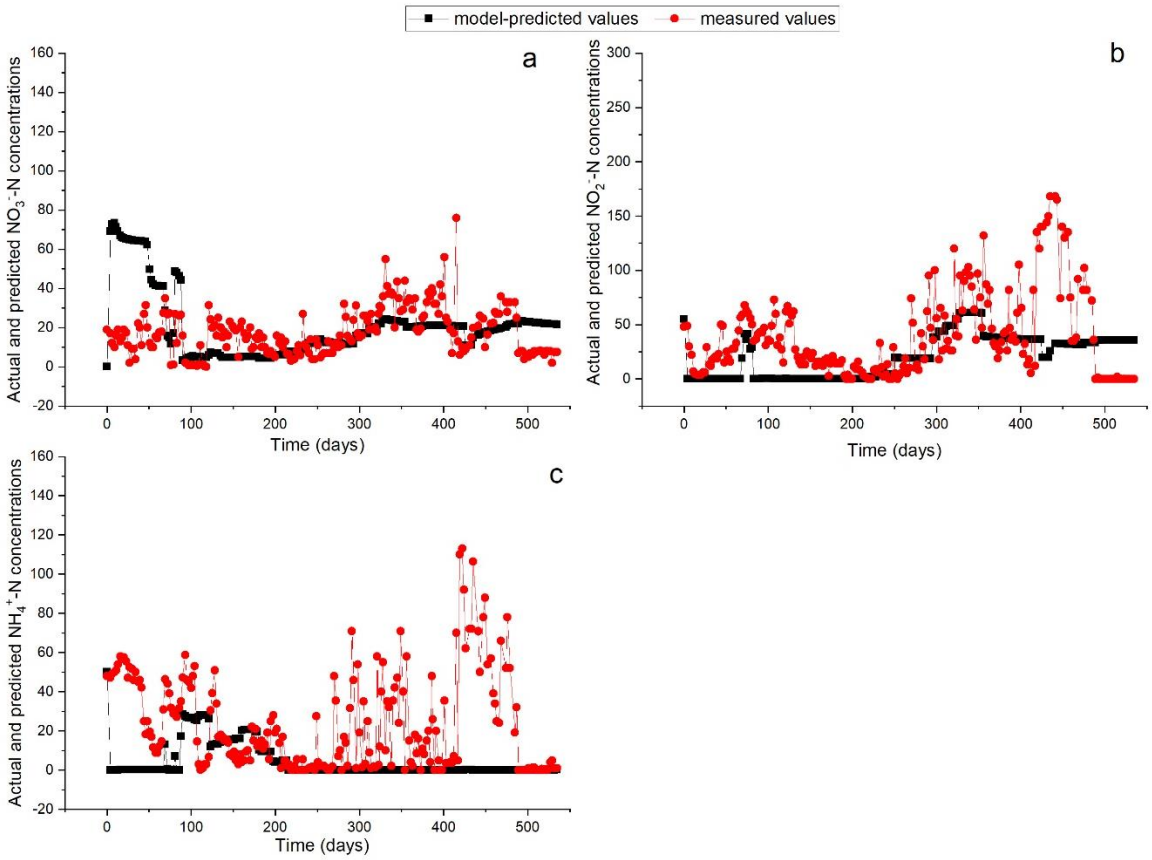

Figure 6. 2. Measured and model-predicted effluent concentrations of NO_3^- (a), NO_2^- (b) and NH_4^+ (c) in H-UASB during the study period.

6.3.2.2 MBBR

At baseline conditions with H-UASB, the effluent concentrations of NO_2^-, NO_3^- and NH_4^+ in MBBR were comparable to those in H-UASB and GLR (*figure A.6.1, Appendix D*). However, when the working volumes were adjusted in line with the actual working volumes used, there were variations in the predicted process performance between the reactors (*figures 6.2 and 6.3*). With the actual working volume in the MBBR, the model was able to predict the trends in the effluent concentrations of NO_2^- and NH_4^+ (*figures 6.3c and 6.3d*). However, the model-predicted effluent concentrations of NO_3^- were consistently higher than the measured concentrations (*figure 6.3 a*). Adjustment of the concentration of biodegradable substrate by a value equivalent to 36% of the total biomass in the reactor led to a decrease in the effluent NO_3^- concentrations predicted by the model, approaching the measured concentrations (*figure 6.3 b*). The model predicted an increase in the effluent concentrations of NH_4^+ and NO_2^- around the 250th day in line with the predicted increase in the abundance of AOB around this time (*figures 6.3c and 6.3d*).

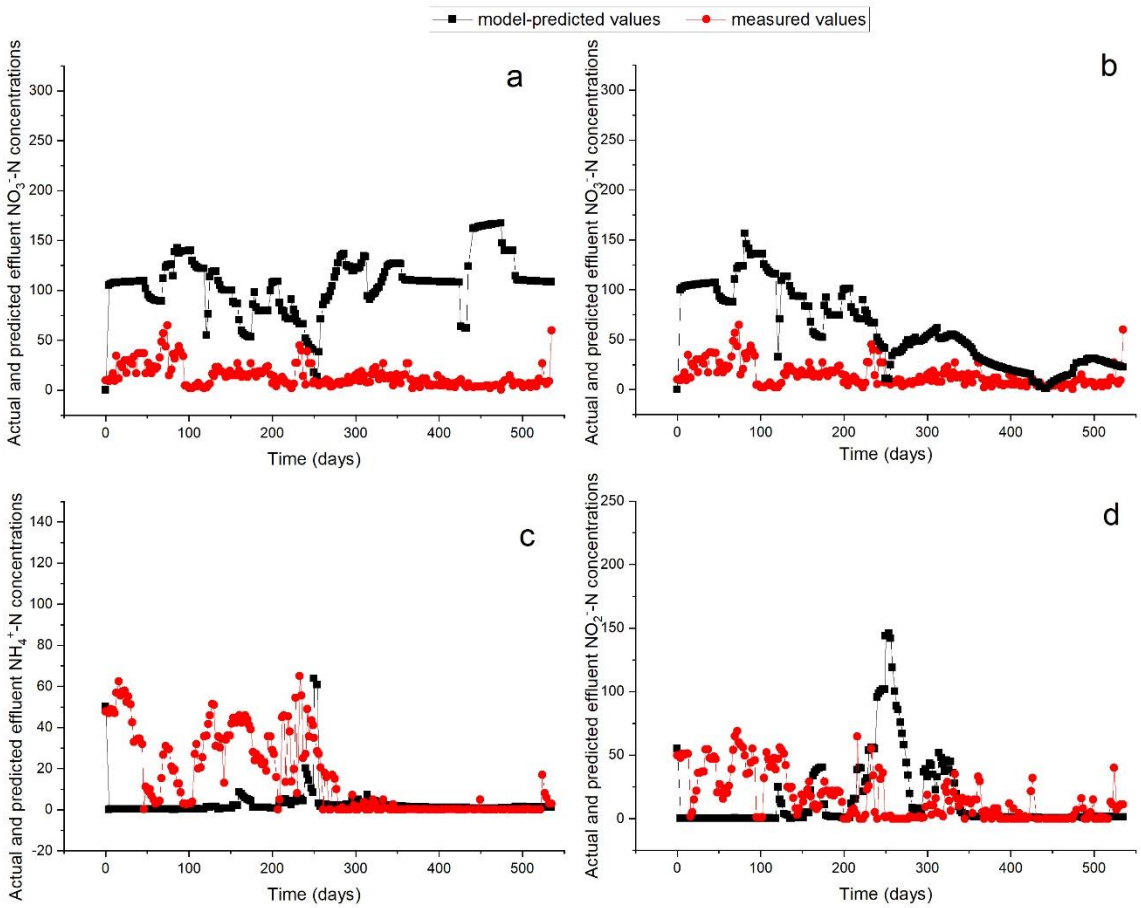

Figure 6. 3. Measured and model-predicted effluent concentrations of NH_4^+, NO_2^- and NO_3^- in MBBR: a, c & d-effluent concentrations at biodegradable substrate described on *table 6.1*, b - effluent NO_3^- concentrations on adjustment of the biodegradable substrate in the model equations by 36% of the total biomass.

6.3.2.3 GLR

Similar to both H-UASB and MBBR, the model was able to predict the trends in the effluent concentrations of NO_2^-, NO_3^- and NH_4^+ (*figures 6.4 a-c*). However, the effluent concentrations of NO_3^- predicted by the model were higher than the measured concentrations during most of the study period (*figure 6.4c*). Adjustment of the concentration of biodegradable substrate by a value equivalent 20% of the total biomass in the reactor led to a decrease in the predicted effluent concentrations of NO_3^-, approaching the measured concentrations (*figure 6.4 d*). The model was limited in predicting the fluctuations in the effluent concentrations of NO_2^-, NO_3^- and NH_4^+ (*figures 6.4 a-c*).

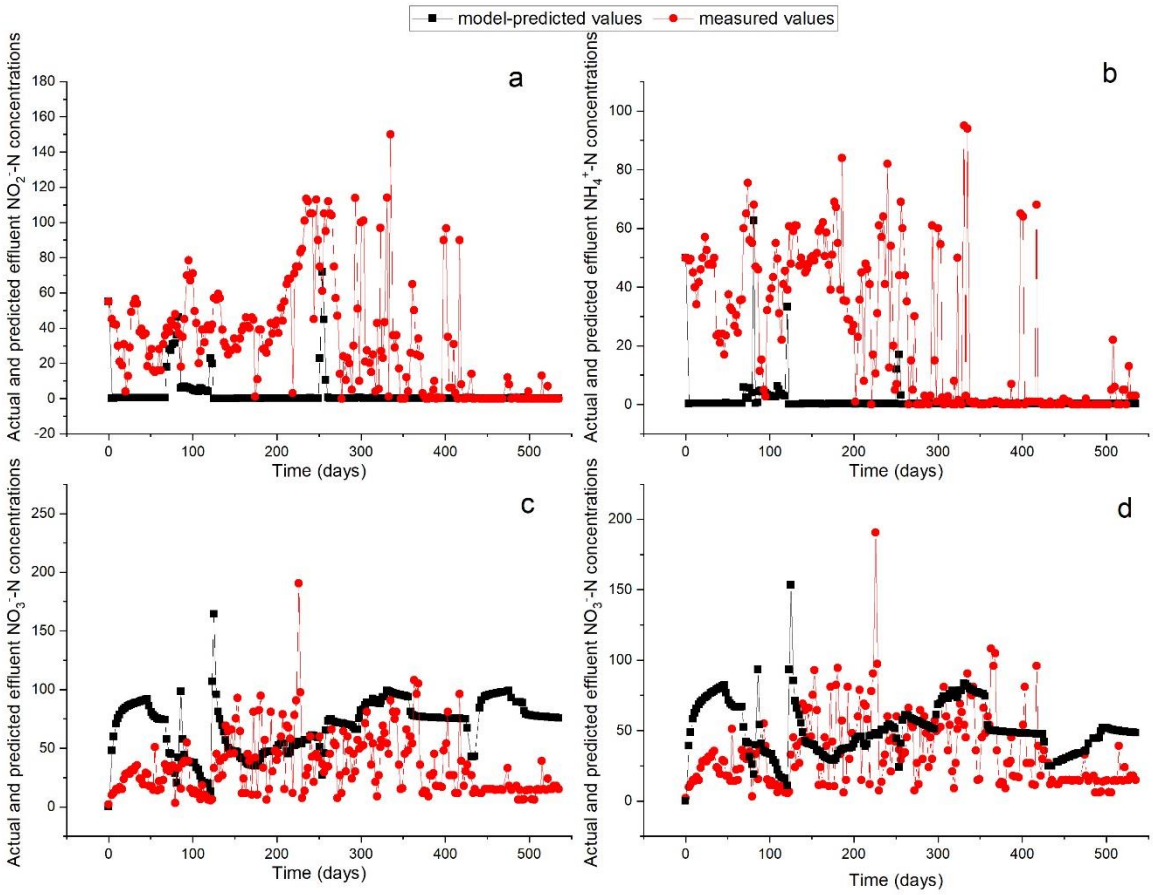

Figure 6. 4. Measured and model-predicted effluent concentrations of NH_4^+, NO_2^- and NO_3^- in GLR: a, b & c-effluent concentrations at biodegradable substrate described on *table 6.1*, d - effluent NO_3^- concentrations on increasing the biodegradable substrate by 20% of the total biomass in the model equations.

6.3.3 Model simulation of nitrifying and ANAMMOX bacterial populations in the reactors

6.3.3.1 H-UASB

In H-UASB, since the reactor was modelled with five CSTRs connected in series (*figure 6.1*), the average concentrations obtained in the five CSTRs were used to calibrate the model. The model predicted the highest concentration of ANAMMOX bacteria in the lowest compartment (first CSTR) throughout the study period, while its abundance was predictably the lowest on days 125 and 192 in the fourth and third CSTRs, respectively, and in the second CSTR on days 260, 309 and 535 (*table A.6.1, Appendix D*). On the contrary, the abundance of *Nitrobacter* spp. were predicted to increase with the reactor height during the study, while the abundance of AOB, COMAMMOX bacteria and *Nitrospira* spp. fluctuated along the reactor height during the study (*table A.6.1, Appendix D*).

The correlation coefficients of the predicted relative abundance of all the bacterial species were positive *figures 6.5 a-e*. The correlations coefficients (R^2) of the predicted verses the actual relative abundance ranged between 2% and 88.5% (*figures 6.5 a-e*). The highest correlation coefficient was found between the predicted and the actual relative abundance of COMAMMOX bacteria, while the lowest was between the predicted and the actual relative abundance of *Nitrobacter* spp. (*figure 6.5*).

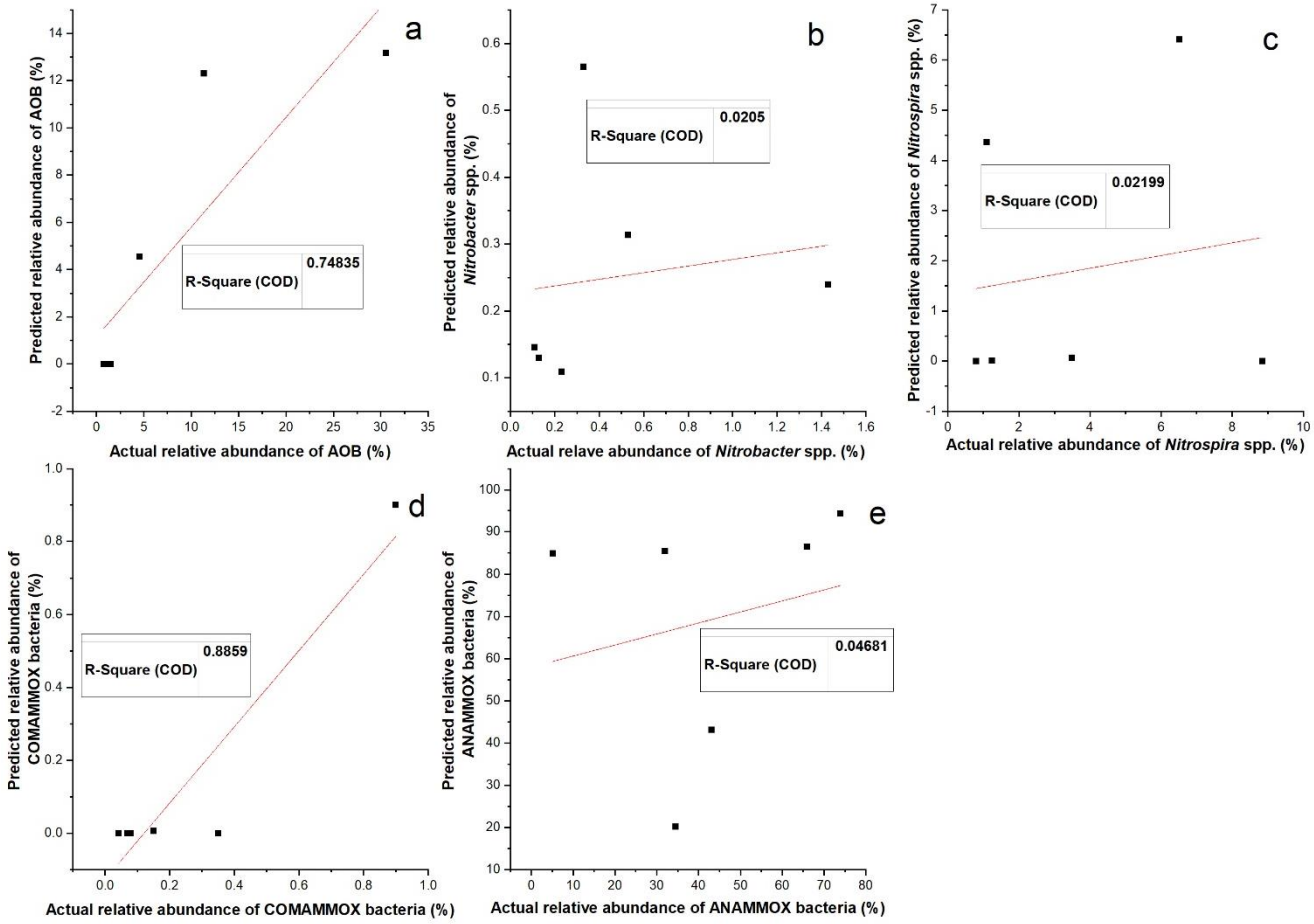

Figure 6. 5. Correlation of the model-predicted relative abundance of AOB (a), *Nitrobacter* spp. (b), *Nitrospira* spp. (c), COMAMMOX bacteria (d) and ANAMMOX bacteria (e) with the measured relative abundance in H-UASB.

6.3.3.2 MBBR

After the model was calibrated in H-UASB, it was validated with the experimental data in MBBR. When the gas-liquid interface oxygen concentration (Cs) was kept at 0.1 mg-O_2/L, the model predicted the dominance of ANAMMOX bacteria throughout the study (*table A.6.3, Appendix D*). In addition, under these conditions, the model predicted constant decrease in the abundance of nitrifying bacteria (*table A.6.3, Appendix D*). Furthermore, the

correlation of the predicted relative abundance of *Nitrospira* spp., *Nitrobacter* spp., COMAMMOX bacteria and ANAMMOX bacteria to their actual relative abundance was negative, while the predicted relative abundance of AOB positively correlated with the actual relative abundance (*figure A.6.2, Appendix D*). On the contrary, when the gas-liquid interface oxygen concentration was increased to 1 mg-O_2/L between days 87-535 (phase III onwards), there was a positive correlation of the model predicted relative abundance of nitrifying and ANAMMOX bacteria with the actual relative abundance (*figures 6.6 a-e*). The correlation coefficient (R^2) of *Nitrobacter* spp., *Nitrospira* spp., COMAMMOX bacteria, ANAMMOX bacteria and AOB was 2.02%, 00.01%, 0.058%, 7.47% and 69.51% respectively (*figures 6.6 a-e*).

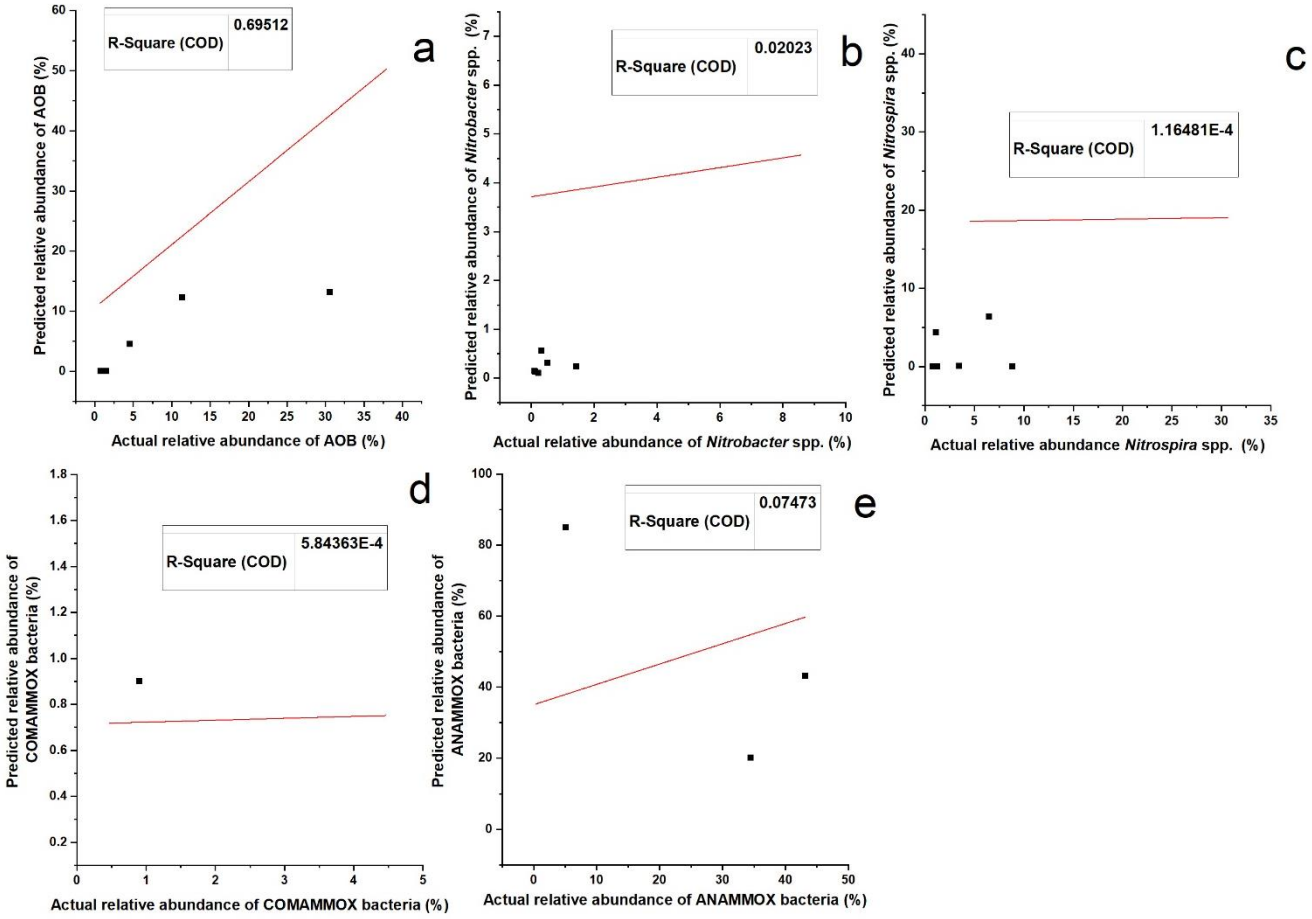

Figure 6. 6. Correlation of the model-predicted relative abundance of AOB (a) *Nitrobacter* spp. (b), *Nitrospira* spp. (c), COMAMMOX bacteria (d) and ANAMMOX bacteria (e) with the measured relative abundance in MBBR during the study.

6.3.3.3 GLR

At 0.1 mg-O_2/L gas-liquid interface concentration in all the phases, the correlation of model-predicted relative abundance of *Nitrospira* spp., *Nitrobacter* spp., COMAMMOX bacteria and ANAMMOX bacteria with the actual relative abundance was negative, while the correlation of only AOB was positive (*figure A.6.3*). Under these conditions, the model predicted the dominance of ANAMMOX bacteria during most of the study period, while the relative abundance of COMAMMOX bacteria was predicted to constantly decrease throughout the study period (*table A.6.4, Appendix D*). On the contrary, the relative abundance of AOB, *Nitrobacter* spp. and *Nitrospira* spp. was predicted to fluctuate during the study period under similar conditions (*table A.6.4, Appendix D*). However, when the gas-liquid interface concentration was increased to 1 mg-O_2/L between days 87-535 (phase III onwards), the model prediction of the relative abundance of nitrifying and ANAMMOX bacteria improved, leading to positive correlation with the actual relative abundance (*figures 6.7 a-e*). The highest correlation coefficient (R^2) was found between the predicted relative abundance of COMAMMOX bacteria and the actual relative abundance (at 95.30%) (*figure 6.7d*), while the lowest correlation coefficient was observed between the predicted and the actual relative abundance of *Nitrospira* spp. (at ca. 0.53%, *figure 6.7c*) . The correlation coefficients of the predicted relative abundance of AOB, *Nitrobacter* spp. and ANAMMOX bacteria to the actual relative abundance were 50.00%, 26.57% and 6.87%, respectively (*figures 6.7a, 6.7b and 6.7e*).

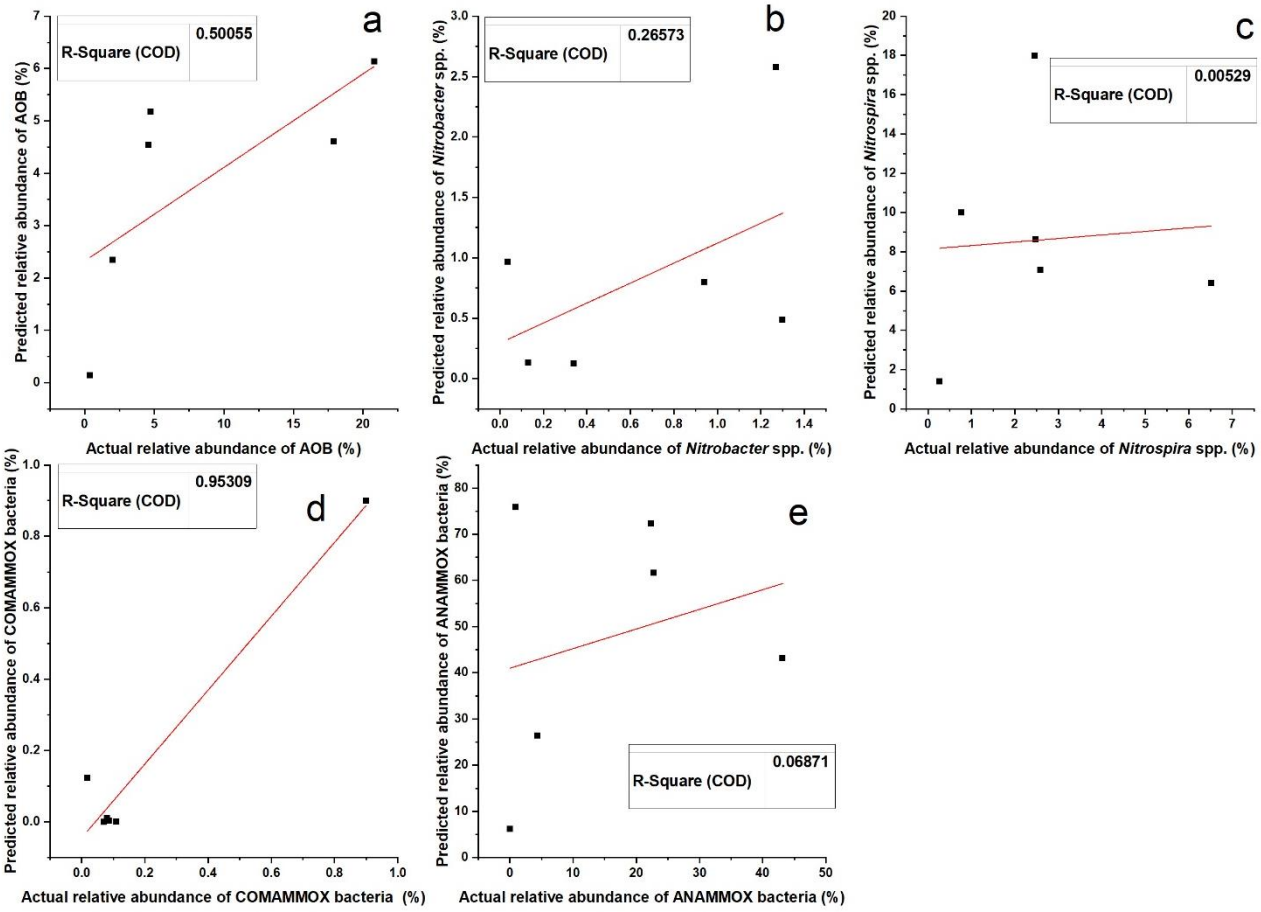

Figure 6. 7. Correlation of the model-predicted relative abundance of AOB (a), *Nitrobacter* spp. (b), *Nitrospira* spp. (c), COMAMMOX bacteria (d) and ANAMMOX bacteria (e) with the measured relative abundance in GLR.

6.4 Discussion

The model predicted the trends of the effluent concentrations of NO_2^-, NO_3^- and NH_4^+ in all the reactors as well as the trends in the relative abundance of AOB, *Nitrospira* spp., *Nitrobacter* spp., COMAMMOX bacteria and ANAMMOX bacteria (*figures 6.2-6.7*). Since the hydrodynamics of each reactor varied (*section 6.2.3*) as well as the working volumes between days 1 and 289 (*Chapter 3, figure 3.6*), there were variations in the model-output among the reactors (*figures 6.2-6.7*). However, when the model was tested at baseline conditions, comparable effluent concentrations of NO_2^-, NO_3^- and NH_4^+ in all the reactors was observed (*figure A.6.1, Appendix D*). Despite this observation at baseline conditions, there were variations in the relative abundance of nitrifying and ANAMMOX bacteria, with better selection of ANAMMOX bacteria being predicted in MBBR, while the lowest relative abundance was predicted in H-UASB in the course of the study (*table A.6.2, Appendix D*). On the contrary, when the working volumes of the reactors were adjusted in line with the

actual working volumes used, variations in process performance and bacterial community structure among the reactors were observed (*figures 6.2-6.7*), an indication that the NLR had an influence on the bacterial community structures, in line with Park *et al.* (2015).

The model-predicted effluent concentrations of NO_3^- in both GLR and MBBR were higher than the measured values (*figures 6.3a and 6.4c*), possibly because the actual concentrations of biodegradable substrate (COD) in these reactors were higher than the values used in the model, which could have led to higher heterotrophic bacterial activities in the reactors. Indeed, on increasing the concentration of biodegradable substrate during simulation by 36% and 20% of the total biomass in the MBBR and GLR, respectively, a drop in the effluent NO_3^- concentrations was observed, coming close to the measured values (*figures 6.3b and 6.4d*). This finding thus indicate that the concentrations of biodegradable substrate in the reactors were higher than the values indicated on *table 6.1*. It is possibly that shear stress due to stirring and gas circulation in MBBR and GLR, respectively, stimulated the secretion of EPS (extracellular polymeric substances) by bacteria as previously demonstrated by Wu *et al.* (2009), which in turn provided organic carbon for heterotrophic bacterial growth (Ni *et al.* 2011a; Liu *et al.* 2016). According to Wu *et al.* (2009), the rate of EPS secretion was directly correlated to the amount of shear force. Therefore, since mixing was not implemented in H-UASB, lower EPS secretion compared to MBBR and GLR could have occurred (Wu *et al.* 2009), in turn leading to lower activities of heterotrophic bacteria, and consequently, lower rate of NO_3^- reduction compared to MBBR and GLR. In addition, stirring in MBBR and gas circulation in GLR could have led to biofilm development on the walls of these reactors (*figure A.4.1, appendix B*), which could have also promoted the heterotrophic bacterial growth (Laureni *et al.* 2015), subsequently leading to higher rate of NO_3^- removal than it was accounted for in the model. The addition of 36% and 20% biodegradable substrate in the models for MBBR and GLR, respectively, was necessary to account for the activities of heterotrophic bacteria. These values were based on Liu *et al.* (2016) who previously reported that EPS in the biofilms within ANAMMOX-mediated systems could be as high as 50% of the total bacterial biomass.

The model predicted faster growth of ANAMMOX bacteria in the lower compartment (first CSTR) in HUASB than in the other compartments (*table A.6.1, Appendix D*). This is because this compartment received fresh feed, which enabled prediction of fast growth of ANAMMOX bacteria in the lower compartment. On the contrary, their relative abundance in the upper compartments (second CSTR through the fifth) received lower substrate

concentrations leading to lower growth rates of ANAMMOX bacteria compared to the first CSTR (*table A.6.1, Appendix D*). The variation in the growth of AOB, COMAMMOX bacteria, *Nitrospira* spp. and *Nitrobacter* spp. with the height of H-UASB during the study could have been influenced by the variation in the substrate concentrations. However, since fluidisation in H-UASB could have occurred due to liquid flow and nitrogen gas generation, mixing of biomass within the different compartments could have taken place (Cao *et al.* 2016; Chen *et al.* 2016). Therefore, since the actual relative abundance of the nitrifying and ANAMMOX bacteria used in this study represented the average abundance in the reactors (*Chapter 4*), the average relative abundance of the model-predicted abundance in the CSTRs within the H-UASB and GLR were also used.

At baseline conditions (keeping NLR and liquid-gas interface oxygen concentration similar in all the reactors), the model predicted the fastest growth of ANAMMOX bacteria in MBBR, while their growth in H-UASB and GLR was predicted to gradually increase between days 1 and 260, thereafter decreasing gradually until the end of the study (*table A.6.2, Appendix D*). However, the actual NLRs were not similar throughout the study (*Chapter 3, figure 3.6*), and were adjusted in MBBR and H-UASB by keeping the working volume at either 3.8L or 5L between days 1 and 289 based on the NREs, while the working volume of GLR was kept constant at 5L throughout the study. From day 289 onwards, the working volumes and consequently the NLRs of all the reactors were kept similar (*Chapter 3, figure 3.6*). When the reactor volumes were adjusted in line with the actual volumes used, the model predicted variations in the relative abundance of ANAMMOX bacteria with the reactor configuration, an indication that the NLR influenced bacterial structures and abundance, as previously demonstrated by Park *et al.* (2015). In addition to the adjustment of the working volumes, the adjustment of Cs in GLR and MBBR between days 87-535 led to positive correlation of the model-predicted relative abundance of nitrifying and ANAMMOX bacteria in these reactors (*figures 6.5-6.7*). This finding thus indicate that oxygen could have leaked into the MBBR and GLR in the course of study, in turn limiting ANAMMOX bacterial growth while promoting the growth of NOB and AOB. It is possible that the bearings used in MBBR could have allowed oxygen to leak into the reactors, while in GLR, oxygen could have leaked through the joints connecting different pieces of equipment used in the circulation of gas. Therefore, the Cs in MBBR and GLR was increased to 1 mg-O_2/L between days 87 and 535, leading to positive correlations of the relative abundance of nitrifying and ANAMMOX bacteria (*figures 6.6 and 6.7*).

Although some of the R^2 values were low, all the correlation coefficients between the predicted relative abundance and the actual relative abundance were positive. Since the relative abundance of nitrifying and ANAMMOX bacteria was based on the genomic DNA (gDNA), it is possible that a portion of these population was not active (redundant), as metagenomics analyses based on gDNA cannot differentiate between life and dead cells, unlike RNA based analyses (Habtewold *et al.* 2015). It is noteworthy that it was possible to improve R^2 values in the reactors through further parameter calibration, but it was observed that these further modifications were causing huge deviations between the predicted effluent concentrations and the actual measured concentrations. Therefore, model calibration based on the reduction of RMSE between the predicted and the actual effluent concentrations of NO_2^-, NO_3^- and NH_4^+ was favoured to high R^2 values. Future model calibration based on RNA could thus be important if high R^2 values were to be achieved. This is because RNA-based analyses would indicate the fraction of active biomass as well as bacterial affiliations and nitrogen, carbon or energy pathways (Habtewold *et al.* 2015).

6.5 Conclusion

The modified model was able to predict the trends in effluent concentrations of NO_2^-, NO_3^- and NH_4^+ as well as the population dynamics of AOB, NOB, COMAMMOX bacteria and ANAMMOX bacteria in the reactors. At baseline conditions, it was evident that the reactor configuration had minimal influence on the effluent concentrations of NO_2^-, NO_3^- and NH_4^+. However, it was determined through mathematical modelling that constant adjustments of NLR through the alterations of the working volumes had an impact on process performance and bacterial growth. In addition, the model predicted oxygen consumption in GLR and MBBR compared to H-UASB. The model also predicted higher heterotrophic bacterial activities in GLR and MBBR compared to H-UASB, which was attributed to higher EPS secretion in these reactors as a result of stimulation by the shear forces (stirring and gas circulation).

7 GENERAL CONCLUSIONS

Different reactor configurations have been applied in full-scale installations of ANAMMOX-mediated systems. However, system operation and stability are still affected by sensitivity of ANAMMOX bacteria to operational and environmental parameters. In addition, performance of ANAMMOX-mediated systems is influenced by; (I) the growth of different microorganisms competing for substrate with ANAMMOX bacteria, (II) reactor hydrodynamics which affect substrate distribution and biomass retention in the reactors.

This study evaluated the impact of mixing conditions on nitrogen removal, physical properties of biomass and microbial community structures in MBBR, H-UASB and GLR over 535 days. The growth of nitrifying and ANAMMOX bacteria in the reactors was also simulated using a calibrated mechanistic model for the duration of the study period. Based on the observations, the following conclusions have been drawn from this study.

Higher substrate utilisation was observed in the MBBR during the study compared to the H-UASB and GLR. This could have been due to better mixing in the MBBR compared to plug flow conditions in H-UASB, and the alternation of internal circulation with plug-flow conditions in the GLR. Based on the $\Delta NO_2^-/\Delta NH_4^+$ and $\Delta NO_3^-/\Delta NH_4^+$ ratios, the start-up period of ANAMMOX process in MBBR was shorter than in the GLR and H-UASB. Lower concentrations of FA and FNA in the MBBR led to more stable process performance compared to GLR and H-UASB, while higher FA and FNA concentrations in the H-UASB and GLR compared to MBBR led to fluctuations in nitrogen removal.

Plug-flow conditions in H-UASB and the alternation of internal circulation with plug-flow conditions in GLR favoured granulation of biomass, while the shear forces due to mixing in the MBBR led to the formation of flocculent biomass as expected. The colour of the biomass in all the reactors changed in the course of the study, corroborating with the nitrogen removal performance and the shifts in the bacterial community structures in the reactors. Better-mixed conditions in the MBBR led to faster development of the biofilms on the carrier materials compared to the H-UASB and GLR. Better-mixed conditions in MBBR also led to comparable abundance of nitrifying and ANAMMOX bacteria in the biofilms and suspended biomass, while plug-flow conditions in the H-UASB favoured the growth of ANAMMOX bacteria in the suspended biomass (lower section), and nitrifying bacteria in the upper section (biofilms). The alternation of plug-flow conditions with internal gas circulation in the GLR also led to comparable abundance of ANAMMOX bacteria between

the suspended biomass and the biofilms similar to MBBR, while the growth of nitrifying bacteria in the GLR was favoured in the biofilms compared to the suspended biomass. In combination, the microbial ecology and performance profiles show that nitrogen removal in H-UASB was likely dominated by ANAMMOX process, while nitrogen removal in MBBR and GLR was as a result of combined ANAMMOX and sequential nitrification-denitrification processes.

ASM 1, which was modified by separating the activities of *Nitrospira* spp. and *Nitrobacter* spp. as well as by adding ANAMMOX and COMAMMOX bacterial activities, was used to describe process performance in the reactors. Modelling results revealed that constant adjustments of NLR through the alterations of the working volumes had an impact on process performance and bacterial growth in the reactors. Modelling also predicted higher oxygen consumption in GLR and MBBR compared to H-UASB, as well as higher heterotrophic bacterial activities in GLR and MBBR compared to H-UASB, corroborating the experimental results. However, the model was limited in predicting process performance during the start-up period of the reactors when nitrogen removal was low.

8 RECOMMENDATIONS

- It is recommended that the modelling-predicted variation in bacterial communities with the reactor height in H-UASB be determined experimentally in future studies.
- It is also recommended that the impact of potential and extant functionality be further explored in future studies.
- The impact of mixing conditions on the growth of ANAMMOX and nitrifying bacteria in aerated systems could also be further explored.
- Future applications of the presented model in full-scale systems is recommended for better understanding of the model's versatility in predicting process performance in systems with complex substrates.

9 REFERENCES

Abbas, G., Wang, L., Li, W., Zhang, M. and Zheng, P. 2015. Kinetics of nitrogen removal in pilot-scale internal-loop airlift bio-particle reactor for simultaneous partial nitrification and anaerobic ammonia oxidation. *Ecological Engineering*, 74: 356-363.

Agrawal, S., Karst, S. M., Gilbert, E. M., Horn, H., Nielsen, P. H. and Lackner, S. 2017. The role of inoculum and reactor configuration for microbial community composition and dynamics in mainstream partial nitritation anammox reactors. *MicrobiologyOpen*, 6 (4): e00456.

Ahn, J. H., Yu, R. and Chandran, K. 2008. Distinctive microbial ecology and biokinetics of autotrophic ammonia and nitrite oxidation in a partial nitrification bioreactor. *Biotechnology and Bioengineering*, 100 (6): 1078-1087.

Ali, M. and Okabe, S. 2015. Anammox-based technologies for nitrogen removal: Advances in process start-up and remaining issues. *Chemosphere*, 141: 144-153.

Ali, M., Oshiki, M., Awata, T., Isobe, K., Kimura, Z., Yoshikawa, H., Hira, D., Kindaichi, T., Satoh, H., Fujii, T. and Okabe, S. 2015a. Physiological characterization of anaerobic ammonium oxidizing bacterium 'Candidatus Jettenia caeni'. *Environ Microbiol*, 17 (6): 2172-2189.

Ali, M., Oshiki, M., Rathnayake, L., Ishii, S., Satoh, H. and Okabe, S. 2015b. Rapid and successful start-up of anammox process by immobilizing the minimal quantity of biomass in PVA-SA gel beads. *Water Research*, 79 (Supplement C): 147-157.

Alleman, J. E. and Preston, K. 1991. Behavior and physiology of nitrifying bacteria. In: Proceedings of *Proceedings of the second annual conference on commercial aquaculture, CES*. 1-13.

Almstrand, R., Persson, F., Daims, H., Ekenberg, M., Christensson, M., Wilén, B.-M., Sörensson, F. and Hermansson, M. 2014. Three-Dimensional Stratification of Bacterial Biofilm Populations in a Moving Bed Biofilm Reactor for Nitritation-Anammox. *International Journal of Molecular Sciences*, 15 (2): 2191-2206.

Annavajhala, M. K., Kapoor, V., Santo-Domingo, J. and Chandran, K. 2018. Comammox Functionality Identified in Diverse Engineered Biological Wastewater Treatment Systems. *Environmental Science & Technology Letters*, 5 (2): 110-116.

Anthonisen, A. C., Loehr, R. C., Prakasam, T. and Srinath, E. 1976. Inhibition of nitrification by ammonia and nitrous acid. *Journal (Water Pollution Control Federation)*: 835-852.

APHA. 1998. Standard methods for the examination of water and wastewater: Washington. *DC, American Public Health Association, American Water Works Association, and Water Environment Federation*: 3-37.

Arbib, Z., Ruiz, J., Álvarez-Díaz, P., Garrido-Pérez, C. and Perales, J. A. 2014. Capability of different microalgae species for phytoremediation processes: Wastewater tertiary treatment, CO2 bio-fixation and low cost biofuels production. *Water Research*, 49: 465-474.

Arnaldos, M., Rehman, U., Naessens, W., Amerlinck, Y. and Nopens, I. 2017. Understanding the effects of bulk mixing on the determination of the affinity index: consequences for process operation and design. *Water Science and Technology*, 77 (3): 576-588.

Arrojo, B., Mosquera-Corral, A., Campos, J. L. and Méndez, R. 2006. Effects of mechanical stress on Anammox granules in a sequencing batch reactor (SBR). *Journal of Biotechnology*, 123 (4): 453-463.

Augusto, M. R., Camiloti, P. R. and Souza, T. S. O. d. 2018. Fast start-up of the single-stage nitrogen removal using anammox and partial nitritation (SNAP) from conventional activated sludge in a membrane-aerated biofilm reactor. *Bioresource Technology*, 266: 151-157.

Awata, T., Kindaichi, T., Ozaki, N. and Ohashi, A. 2015. Biomass yield efficiency of the marine anammox bacterium, "Candidatus Scalindua sp.," is affected by salinity. *Microbes and environments*, 30 (1): 86-91.

Awata, T., Tanabe, K., Kindaichi, T., Ozaki, N. and Ohashi, A. 2012. Influence of temperature and salinity on microbial structure of marine anammox bacteria. *Water Science and Technology*, 66 (5): 958-964.

Awolusi, O. O., Enitan, A. M., Kumari, S. and Bux, F. 2015. Nitrification efficiency and community structure of municipal activated sewage sludge. *International Journal of Environmental, Chemical, Ecological, Geological and Geophysical Engineering*, 9 (9): 996-1003.

Awolusi, O. O., Kumari, S. K. S. and Bux, F. 2015. Ecophysiology of nitrifying communities in membrane bioreactors. *International Journal of Environmental Science and Technology*, 12 (2): 747-762.

Bae, H., Choi, M., Chung, Y.-C., Lee, S. and Yoo, Y. J. 2017. Core-shell structured poly(vinyl alcohol)/sodium alginate bead for single-stage autotrophic nitrogen removal. *Chemical Engineering Journal*, 322 (Supplement C): 408-416.

Bae, H., Choi, M., Lee, C., Chung, Y.-C., Yoo, Y. J. and Lee, S. 2015. Enrichment of ANAMMOX bacteria from conventional activated sludge entrapped in poly(vinyl alcohol)/sodium alginate gel. *Chemical Engineering Journal*, 281 (Supplement C): 531-540.

Bae, H., Chung, Y.-C. and Jung, J.-Y. 2010. Microbial community structure and occurrence of diverse autotrophic ammonium oxidizing microorganisms in the anammox process. *Water Science and Technology*, 61 (11): 2723-2732.

Batstone, D. J., Keller, J., Angelidaki, I., Kalyuzhnyi, S., Pavlostathis, S., Rozzi, A., Sanders, W., Siegrist, H. and Vavilin, V. 2002. The IWA anaerobic digestion model no 1 (ADM1). *Water Science and technology*, 45 (10): 65-73.

Beun, J. J., Hendriks, A., van Loosdrecht, M. C. M., Morgenroth, E., Wilderer, P. A. and Heijnen, J. J. 1999. Aerobic granulation in a sequencing batch reactor. *Water Research*, 33 (10): 2283-2290.

Bhattacharjee, A. S., Wu, S., Lawson, C. E., Jetten, M. S. M., Kapoor, V., Domingo, J. W. S., McMahon, K. D., Noguera, D. R. and Goel, R. 2017. Whole-Community Metagenomics in Two Different Anammox Configurations: Process Performance and Community Structure. *Environmental Science & Technology*, 51 (8): 4317-4327.

Blackburne, R., Vadivelu, V. M., Yuan, Z. and Keller, J. 2007. Kinetic characterisation of an enriched Nitrospira culture with comparison to Nitrobacter. *Water Research*, 41 (14): 3033-3042.

Boltz, J. P., Smets, B. F., Rittmann, B. E., van Loosdrecht, M. C. M., Morgenroth, E. and Daigger, G. T. 2017. From biofilm ecology to reactors: a focused review. *Water Sci Technol*, 75 (7-8): 1753-1760.

Bowden, G., Stensel, H. D. and Tsuchihashi, R. 2015. *Technologies for Sidestream nitrogen removal*. Water Environment Research Foundation.

Breisha, G. Z. and Winter, J. 2010. Bio-removal of nitrogen from wastewaters-A review. *Journal of American Science*, 6 (12): 508-528.

Broda, E. 1977. Two kinds of lithotrophs missing in nature. *Zeitschrift für allgemeine Mikrobiologie*, 17 (6): 491-493.

Brookes, P. R. and Livingston, A. G. 1994. Biotreatment of a point-source industrial wastewater arising in 3,4-dichloroaniline manufacture using an extractive membrane bioreactor. *Biotechnology Progress*, 10 (1): 65-75.

Brotto, A. C., Annavajhala, M. K. and Chandran, K. 2018. Metatranscriptomic Investigation of Adaptation in NO and N2O Production From a Lab-Scale Nitrification Process Upon Repeated Exposure to Anoxic–Aerobic Cycling. *Frontiers in Microbiology*, 9 (3012)

Burmolle, M., Ren, D., Bjarnsholt, T. and Sorensen, S. J. 2014. Interactions in multispecies biofilms: do they actually matter? *Trends Microbiol*, 22 (2): 84-91.

Cabezas, A., Draper, P., Muxí, L. and Etchebehere, C. 2006. Post-treatment of a slaughterhouse wastewater: stability of the microbial community of a sequencing batch reactor operated under oxygen limited conditions. *Water Science and Technology*, 54 (2): 215-221.

Cao, S., Li, B., Du, R., Ren, N. and Peng, Y. 2016. Nitrite production in a partial denitrifying upflow sludge bed (USB) reactor equipped with gas automatic circulation (GAC). *Water Research*, 90: 309-316.

Carvajal-Arroyo, J. M., Sun, W., Sierra-Alvarez, R. and Field, J. A. 2013. Inhibition of anaerobic ammonium oxidizing (anammox) enrichment cultures by substrates, metabolites and common wastewater constituents. *Chemosphere*, 91 (1): 22-27.

Castro-Barros, C. M., Daelman, M. R. J., Mampaey, K. E., van Loosdrecht, M. C. M. and Volcke, E. I. P. 2015. Effect of aeration regime on N2O emission from partial nitritation-anammox in a full-scale granular sludge reactor. *Water Research*, 68: 793-803.

Cema, G., Sochacki, A., Kubiatowicz, J., Gutwiński, P. and Surmacz-Górska, J. 2012. Start-up, modelling and simulation of the anammox process in a membrane bioreactor. *Chemical and Process Engineering*, 33 (4): 639-650.

Chang, W.-S., Tran, H.-T., Park, D.-H., Zhang, R.-H. and Ahn, D.-H. 2009. Ammonium nitrogen removal characteristics of zeolite media in a Biological Aerated Filter (BAF) for the treatment of textile wastewater. *Journal of Industrial and Engineering Chemistry*, 15 (4): 524-528.

Chen, C.-j., Huang, X.-x., Lei, C.-x., Zhu, W.-j., Chen, Y.-x. and Wu, W.-x. 2012. Improving Anammox start-up with bamboo charcoal. *Chemosphere*, 89 (10): 1224-1229.

Chen, X., Dai, R., Ni, S., Luo, Y., Ma, P., Xiang, X. and Li, G. 2016. Super-high-rate performance and its mechanisms of a spiral symmetry stream anaerobic bioreactor. *Chemical Engineering Journal*, 295: 237-244.

Cheng, J., Zhang, L., Yang, Y., Zhang, S., Han, X. and Peng, Y. 2017. Promotion of partial nitritation-anammox process by improving granule proportion. *Water Science and Technology*, 75 (11): 2580-2585.

Cho, K., Choi, M., Jeong, D., Lee, S. and Bae, H. 2017. Comparison of inoculum sources for long-term process performance and fate of ANAMMOX bacteria niche in poly(vinyl alcohol)/sodium alginate gel beads. *Chemosphere*, 185 (Supplement C): 394-402.

Cho, K., Shin, S. G., Lee, J., Koo, T., Kim, W. and Hwang, S. 2016. Nitrification resilience and community dynamics of ammonia-oxidizing bacteria with respect to ammonia loading shock in a nitrification reactor treating steel wastewater. *Journal of Bioscience and Bioengineering*, 122 (2): 196-202.

Cho, S., Fujii, N., Lee, T. and Okabe, S. 2011. Development of a simultaneous partial nitrification and anaerobic ammonia oxidation process in a single reactor. *Bioresource Technology*, 102 (2): 652-659.

Choi, M., Cho, K., Lee, S., Chung, Y.-C., Park, J. and Bae, H. 2018. Effective seeding strategy using flat type poly (vinyl alcohol) cryogel for anammox enrichment. *Chemosphere*, 205: 88-97.

Choi, N. C., Choi, J. W., Kim, S. B. and Kim, D. J. 2008. Modeling of growth kinetics for Pseudomonas putida during toluene degradation. *Applied Microbiology and Biotechnology*, 81 (1): 135-141.

Christensson, M., Ekstrom, S., Andersson Chan, A., Le Vaillant, E. and Lemaire, R. 2013. Experience from start-ups of the first ANITA Mox plants. *Water Sci Technol*, 67 (12): 2677-2684.

Chu, K. H., van Veldhuizen, H. M. and van Loosdrecht, M. C. M. 2003. Respirometric measurement of kinetic parameters: effect of activated sludge floc size. *Water Science and Technology*, 48 (8): 61-68.

Clark, J. H., Moseng, E. M. and Asano, T. 1978. Performance of a Rotating Biological Contactor under Varying Wastewater Flow. *Journal (Water Pollution Control Federation)*, 50 (5): 896-911.

Collison, R. and Grismer, M. 2018. Upscaling the Zeolite-Anammox Process: Treatment of Secondary Effluent. *Water*, 10 (3): 236.

Constantine, T., Sandino, J., Houweling, D., Stephan, S., Yin, H. and Nielsen, P. 2016. Incorporating Leading Edge Mainstream Deammonification into Full-scale Advanced BNR Facilities. *Proceedings of the Water Environment Federation*, 2016 (7): 1007-1018.

Cordero, O. X. and Datta, M. S. 2016. Microbial interactions and community assembly at microscales. *Current Opinion in Microbiology*, 31: 227-234.

Costa, E., Pérez, J. and Kreft, J.-U. 2006. Why is metabolic labour divided in nitrification? *Trends in Microbiology*, 14 (5): 213-219.

Cotto, I., Dai, Z., Huo, L., Anderson, C. L., Vilardi, K. J., Ijaz, U., Khunjar, W., Wilson, C., De Clippeleir, H., Gilmore, K., Bailey, E. and Pinto, A. J. 2020. Long solids retention times and attached growth phase favor prevalence of comammox bacteria in nitrogen removal systems. *Water Research*, 169: 115268.

Daigger, G. T., Sanjines, P., Pallansch, K., Sizemore, J. and Wett, B. 2011. Implementation of a full-scale anammox-based facility to treat an anaerobic digestion sidestream at the Alexandria sanitation authority water resource facility. *Water Practice and Technology*, 6 (2): wpt2011033.

Daims, H., Lebedeva, E. V., Pjevac, P., Han, P., Herbold, C., Albertsen, M., Jehmlich, N., Palatinszky, M., Vierheilig, J., Bulaev, A., Kirkegaard, R. H., von Bergen, M., Rattei, T., Bendinger, B., Nielsen, P. H. and Wagner, M. 2015. Complete nitrification by Nitrospira bacteria. *Nature*, 528: 504.

Danckwerts, P. V. 1953. Continuous flow systems: Distribution of residence times. *Chemical Engineering Science*, 2 (1): 1-13.

Dapena-Mora, A., Arrojo, B., Campos, J. L., Mosquera-Corral, A. and Méndez, R. 2004a. Improvement of the settling properties of Anammox sludge in an SBR. *Journal of Chemical Technology & Biotechnology*, 79 (12): 1417-1420.

Dapena-Mora, A., Campos, J. L., Mosquera-Corral, A., Jetten, M. S. M. and Méndez, R. 2004b. Stability of the ANAMMOX process in a gas-lift reactor and a SBR. *Journal of Biotechnology*, 110 (2): 159-170.

Dapena-Mora, A., Fernández, I., Campos, J. L., Mosquera-Corral, A., Méndez, R. and Jetten, M. S. M. 2007. Evaluation of activity and inhibition effects on Anammox process by batch tests based on the nitrogen gas production. *Enzyme and Microbial Technology*, 40 (4): 859-865.

Dapena-Mora, A., Van Hulle, S. W., Luis Campos, J., Méndez, R., Vanrolleghem, P. A. and Jetten, M. 2004c. Enrichment of Anammox biomass from municipal activated sludge: experimental and modelling results. *Journal of Chemical Technology & Biotechnology*, 79 (12): 1421-1428.

Dapena-Mora, A., Van Hulle, S. W. H., Luis Campos, J., Méndez, R., Vanrolleghem, P. A. and Jetten, M. 2004d. Enrichment of Anammox biomass from municipal activated sludge: experimental and modelling results. *Journal of Chemical Technology & Biotechnology*, 79 (12): 1421-1428.

Date, Y., Isaka, K., Ikuta, H., Sumino, T., Kaneko, N., Yoshie, S., Tsuneda, S. and Inamori, Y. 2009. Microbial diversity of anammox bacteria enriched from different types of seed sludge in an anaerobic continuous-feeding cultivation reactor. *Journal of Bioscience and Bioengineering*, 107 (3): 281-286.

Desloover, J., De Clippeleir, H., Boeckx, P., Du Laing, G., Colsen, J., Verstraete, W. and Vlaeminck, S. E. 2011. Floc-based sequential partial nitritation and anammox at full scale with contrasting N2O emissions. *Water Research*, 45 (9): 2811-2821.

Di Capua, F., Pirozzi, F., Lens, P. N. L. and Esposito, G. 2019. Electron donors for autotrophic denitrification. *Chemical Engineering Journal*, 362: 922-937.

Dolfing, J. 1986. Granulation in UASB Reactors. *Water Science and Technology*, 18 (12): 15-25.

Dzionek, A., Wojcieszyńska, D. and Guzik, U. 2016. Natural carriers in bioremediation: A review. *Electronic Journal of Biotechnology*, 23: 28-36.

Egli, K., Fanger, U., Alvarez, P. J. J., Siegrist, H., van der Meer, J. R. and Zehnder, A. J. B. 2001. Enrichment and characterization of an anammox bacterium from a rotating biological contactor treating ammonium-rich leachate. *Archives of Microbiology*, 175 (3): 198-207.

Erdim, E., Özkan, Z. Y., Kurt, H. and Kocamemi, B. A. 2018. Overcoming challenges in mainstream Anammox applications: Utilization of nanoscale zero valent iron (nZVI). *Science of The Total Environment*,

Fernández, A., Huang, S., Seston, S., Xing, J., Hickey, R., Criddle, C. and Tiedje, J. 1999. How stable is stable? Function versus community composition. *Applied and environmental microbiology*, 65 (8): 3697-3704.

Fernández, I., Dosta, J., Fajardo, C., Campos, J. L., Mosquera-Corral, A. and Méndez, R. 2012. Short- and long-term effects of ammonium and nitrite on the Anammox process. *Journal of Environmental Management*, 95: S170-S174.

Fernández, I., Mosquera-Corral, A., Campos, J. L. and Méndez, R. 2009. Operation of an Anammox SBR in the presence of two broad-spectrum antibiotics. *Process Biochemistry*, 44 (4): 494-498.

Fernández, I., Vázquez-Padín, J. R., Mosquera-Corral, A., Campos, J. L. and Méndez, R. 2008. Biofilm and granular systems to improve Anammox biomass retention. *Biochemical Engineering Journal*, 42 (3): 308-313.

Foglar, L. and Briški, F. 2003. Wastewater denitrification process—the influence of methanol and kinetic analysis. *Process Biochemistry*, 39 (1): 95-103.

Fumasoli, A., Bürgmann, H., Weissbrodt, D. G., Wells, G. F., Beck, K., Mohn, J., Morgenroth, E. and Udert, K. M. 2017. Growth of Nitrosococcus-Related Ammonia Oxidizing Bacteria Coincides with Extremely Low pH Values in Wastewater with High Ammonia Content. *Environmental Science & Technology*, 51 (12): 6857-6866.

Gao, F., Zhang, H., Yang, F., Li, H. and Zhang, R. 2014. The effects of zero-valent iron (ZVI) and ferroferric oxide (Fe3O4) on anammox activity and granulation in anaerobic continuously stirred tank reactors (CSTR). *Process Biochemistry*, 49 (11): 1970-1978.

Gasa, N. P., Nnadozie, C. F., Kosgey, K., Bux, F. and Kumari, S. 2019. Effect of ammonium to nitrite ratio on reactor performance and microbial population structure in anammox reactors. *Environmental Technology*: 1-16.

Giustinianovich, E. A., Campos, J.-L., Roeckel, M. D., Estrada, A. J., Mosquera-Corral, A. and Val del Río, Á. 2018. Influence of biomass acclimation on the performance of a partial nitritation-anammox reactor treating industrial saline effluents. *Chemosphere*, 194: 131-138.

Gonzalez-Martinez, A., Rodriguez-Sanchez, A., Garcia-Ruiz, M. J., Muñoz-Palazon, B., Cortes-Lorenzo, C., Osorio, F. and Vahala, R. 2016. Performance and bacterial community dynamics of a CANON bioreactor acclimated from high to low operational temperatures. *Chemical Engineering Journal*, 287: 557-567.

Grady Jr, C. L., Daigger, G. T., Love, N. G. and Filipe, C. D. 2011. *Biological wastewater treatment*. CRC press.

Green, M., Tarre, S., Schnizer, M., Bogdan, B., Armon, R. and Shelef, G. 1994. Groundwater denitrification using an upflow sludge blanket reactor. *Water Research*, 28 (3): 631-637.

Grismer, M. and Collison, R. 2017. The Zeolite-Anammox Treatment Process for Nitrogen Removal from Wastewater—A Review. *Water*, 9 (11): 901.

Gu, J., Yang, Q. and Liu, Y. 2018. Mainstream anammox in a novel A-2B process for energy-efficient municipal wastewater treatment with minimized sludge production. *Water research*, 138: 1-6.

Gu, Z., Li, Y., Yang, Y., Xia, S., Hermanowicz, S. W. and Alvarez-Cohen, L. 2018. Inhibition of anammox by sludge thermal hydrolysis and metagenomic insights. *Bioresource Technology*, 270: 46-54.

Guo, J., Peng, Y., Fan, L., Zhang, L., Ni, B. J., Kartal, B., Feng, X., Jetten, M. S. and Yuan, Z. 2016. Metagenomic analysis of anammox communities in three different microbial aggregates. *Environ Microbiol*, 18 (9): 2979-2993.

Güven, D., Dapena, A., Kartal, B., Schmid, M. C., Maas, B., van de Pas-Schoonen, K., Sozen, S., Mendez, R., Op den Camp, H. J. M., Jetten, M. S. M., Strous, M. and Schmidt, I. 2005. Propionate Oxidation by and Methanol Inhibition of Anaerobic Ammonium-Oxidizing Bacteria. *Applied and Environmental Microbiology*, 71 (2): 1066-1071.

Habtewold, T., Groom, Z., Duchateau, L. and Christophides, G. K. 2015. Detection of viable Plasmodium ookinetes in the midguts of Anopheles coluzzi using PMA-qrtPCR. *Parasites & Vectors*, 8 (1): 455.

Han, L., Zhang, Y., Kang, J., Tang, J. and Zhang, Y. 2012. Chemiluminescence determination of terbutaline sulfate in bovine urine and pharmaceutical preparations based on enhancement of the 2-phenyl-4, 5-di (2-furyl) imidazole–potassium ferricyanide system. *Journal of Pharmaceutical and Biomedical Analysis*, 58: 141-145.

Han, M., Vlaeminck, S. E., Al-Omari, A., Wett, B., Bott, C., Murthy, S. and De Clippeleir, H. 2016. Uncoupling the solids retention times of flocs and granules in mainstream deammonification: A screen as effective out-selection tool for nitrite oxidizing bacteria. *Bioresource Technology*, 221: 195-204.

Han, Y.-m., Liu, F.-x., Xu, X.-f., Yan, Z. and Liu, Z.-j. 2018. Nitrogen removal via a single-stage PN–Anammox process in a novel combined biofilm reactor. *Water Science and Technology*, 77 (6): 1483-1492.

Hao, X., Heijnen, J. J. and Van Loosdrecht, M. C. M. 2002. Model-based evaluation of temperature and inflow variations on a partial nitrification–ANAMMOX biofilm process. *Water Research*, 36 (19): 4839-4849.

Hashsham, S. A., Fernandez, A. S., Dollhopf, S. L., Dazzo, F. B., Hickey, R. F., Tiedje, J. M. and Criddle, C. S. 2000. Parallel Processing of Substrate Correlates with Greater Functional Stability in

Methanogenic Bioreactor Communities Perturbed by Glucose. *Applied and Environmental Microbiology*, 66 (9): 4050-4057.

He, S., Chen, Y., Qin, M., Mao, Z., Yuan, L., Niu, Q. and Tan, X. 2018. Effects of temperature on anammox performance and community structure. *Bioresource Technology*, 260: 186-195.

Hellinga, C., Schellen, A. A. J. C., Mulder, J. W., van Loosdrecht, M. C. M. and Heijnen, J. J. 1998. The sharon process: An innovative method for nitrogen removal from ammonium-rich waste water. *Water Science and Technology*, 37 (9): 135-142.

Hellinga, C., van Loosdrecht, M. C. M. and Heijnen, J. J. 1999. Model Based Design of a Novel Process for Nitrogen Removal from Concentrated Flows. *Mathematical and Computer Modelling of Dynamical Systems*, 5 (4): 351-371.

Hendrickx, T. L. G., Kampman, C., Zeeman, G., Temmink, H., Hu, Z., Kartal, B. and Buisman, C. J. N. 2014. High specific activity for anammox bacteria enriched from activated sludge at 10°C. *Bioresource Technology*, 163: 214-221.

Henze, M., Grady Jr, C. L., Gujer, W., Marais, G. and Matsuo, T. 1987. A general model for single-sludge wastewater treatment systems. *Water research*, 21 (5): 505-515.

Hira, D., Aiko, N., Yabuki, Y. and Fujii, T. 2018. Impact of aerobic acclimation on the nitrification performance and microbial community of landfill leachate sludge. *Journal of Environmental Management*, 209: 188-194.

Hoekstra, M., de Weerd, F. A., Kleerebezem, R. and van Loosdrecht, M. C. M. 2018. Deterioration of the anammox process at decreasing temperatures and long SRTs. *Environmental Technology*, 39 (5): 658-668.

Hu, Z., Lotti, T., de Kreuk, M., Kleerebezem, R., van Loosdrecht, M., Kruit, J., Jetten, M. S. and Kartal, B. 2013. Nitrogen removal by a nitritation-anammox bioreactor at low temperature. *Appl Environ Microbiol*, 79 (8): 2807-2812.

Innerebner, G., Insam, H., Franke-Whittle, I. H. and Wett, B. 2007. Identification of anammox bacteria in a full-scale deammonification plant making use of anaerobic ammonia oxidation. *Systematic and Applied Microbiology*, 30 (5): 408-412.

Isaka, K., Date, Y., Kimura, Y., Sumino, T. and Tsuneda, S. 2008. Nitrogen removal performance using anaerobic ammonium oxidation at low temperatures. *FEMS Microbiology Letters*, 282 (1): 32-38.

Isaka, K., Date, Y., Sumino, T. and Tsuneda, S. 2007. Ammonium removal performance of anaerobic ammonium-oxidizing bacteria immobilized in polyethylene glycol gel carrier. *Applied Microbiology and Biotechnology*, 76 (6): 1457-1465.

Isaka, K., Itokawa, H., Kimura, Y., Noto, K. and Murakami, T. 2011. Novel autotrophic nitrogen removal system using gel entrapment technology. *Bioresource Technology*, 102 (17): 7720-7726.

Isaka, K., Kimura, Y., Matsuura, M., Osaka, T. and Tsuneda, S. 2017. First full-scale nitritation-anammox plant using gel entrapment technology for ammonia plant effluent. *Biochemical Engineering Journal*, 122 (Supplement C): 115-122.

Jaroszynski, L. W., Cicek, N., Sparling, R. and Oleszkiewicz, J. A. 2012. Impact of free ammonia on anammox rates (anoxic ammonium oxidation) in a moving bed biofilm reactor. *Chemosphere*, 88 (2): 188-195.

Jeanningros, Y., Vlaeminck, S. E., Kaldate, A., Verstraete, W. and Graveleau, L. 2010. Fast start-up of a pilot-scale deammonification sequencing batch reactor from an activated sludge inoculum. *Water Science and Technology*, 61 (6): 1393-1400.

Jin, R.-C., Xing, B.-S., Yu, J.-J., Qin, T.-Y. and Chen, S.-X. 2013. The importance of the substrate ratio in the operation of the Anammox process in upflow biofilter. *Ecological Engineering*, 53: 130-137.

Jin, Y., Wang, D. and Zhang, W. 2016. Use of bamboo charcoal reduced the cultivated anammox seed sludge dosage during the start-up period. *Desalination and Water Treatment*, 57 (43): 20248-20253.

Johansson, S., Ruscalleda, M. and Colprim, J. 2017. Phosphorus recovery through biologically induced precipitation by partial nitritation-anammox granular biomass. *Chemical Engineering Journal*, 327: 881-888.

Joss, A., Derlon, N., Cyprien, C., Burger, S., Szivak, I., Traber, J., Siegrist, H. and Morgenroth, E. 2011. Combined Nitritation–Anammox: Advances in Understanding Process Stability. *Environmental Science & Technology*, 45 (22): 9735-9742.

Joss, A., Salzgeber, D., Eugster, J., König, R., Rottermann, K., Burger, S., Fabijan, P., Leumann, S., Mohn, J. and Siegrist, H. 2009. Full-Scale Nitrogen Removal from Digester Liquid with Partial Nitritation and Anammox in One SBR. *Environmental Science & Technology*, 43 (14): 5301-5306.

Kanders, L., Areskoug, T., Schneider, Y., Ling, D., Punzi, M. and Beier, M. 2014. Impact of seeding on the start-up of one-stage deammonification MBBRs. *Environ Technol*, 35 (21-24): 2767-2773.

Kappler, A., Schink, B. and Newman, D. K. 2005. Fe(III) mineral formation and cell encrustation by the nitrate-dependent Fe(II)-oxidizer strain BoFeN1. *Geobiology*, 3 (4): 235-245.

Kartal, B., de Almeida, N. M., Maalcke, W. J., Op den Camp, H. J. M., Jetten, M. S. M. and Keltjens, J. T. 2013. How to make a living from anaerobic ammonium oxidation. *FEMS Microbiology Reviews*, 37 (3): 428-461.

Kartal, B. and Keltjens, J. T. 2016. Anammox Biochemistry: a Tale of Heme c Proteins. *Trends Biochem Sci*, 41 (12): 998-1011.

Kartal, B., Koleva, M., Arsov, R., van der Star, W., Jetten, M. S. M. and Strous, M. 2006. Adaptation of a freshwater anammox population to high salinity wastewater. *Journal of Biotechnology*, 126 (4): 546-553.

Kartal, B., Rattray, J., van Niftrik, L. A., van de Vossenberg, J., Schmid, M. C., Webb, R. I., Schouten, S., Fuerst, J. A., Damsté, J. S., Jetten, M. S. M. and Strous, M. 2007. Candidatus "Anammoxoglobus propionicus" a new propionate oxidizing species of anaerobic ammonium oxidizing bacteria. *Systematic and Applied Microbiology*, 30 (1): 39-49.

Kartal, B., van Niftrik, L., Rattray, J., van de Vossenberg, J. L., Schmid, M. C., Sinninghe Damste, J., Jetten, M. S. and Strous, M. 2008. Candidatus 'Brocadia fulgida': an autofluorescent anaerobic ammonium oxidizing bacterium. *FEMS Microbiol Ecol*, 63 (1): 46-55.

Kawagoshi, Y., Fujisaki, K., Tomoshige, Y., Yamashiro, K. and Qiao, Y. 2012. Temperature effect on nitrogen removal performance and bacterial community in culture of marine anammox bacteria derived from sea-based waste disposal site. *Journal of Bioscience and Bioengineering*, 113 (4): 515-520.

Kersters, K., De Vos, P., Gillis, M., Swings, J., Vandamme, P. and Stackebrandt, E. 2006. Introduction to the Proteobacteria. In: Dworkin, M., Falkow, S., Rosenberg, E., Schleifer, K.-H. and Stackebrandt, E. eds. *The Prokaryotes: Volume 5: Proteobacteria: Alpha and Beta Subclasses*. New York, NY: Springer New York, 3-37. Available: https://doi.org/10.1007/0-387-30745-1_1 (Accessed

Kester, R. A., De Boer, W. and Laanbroek, H. J. 1997. Production of NO and N(inf2)O by Pure Cultures of Nitrifying and Denitrifying Bacteria during Changes in Aeration. *Applied and Environmental Microbiology*, 63 (10): 3872-3877.

Kimura, Y. and Isaka, K. 2014. Evaluation of inhibitory effects of heavy metals on anaerobic ammonium oxidation (anammox) by continuous feeding tests. *Applied Microbiology and Biotechnology*, 98 (16): 6965-6972.

Kindaichi, T., Tsushima, I., Ogasawara, Y., Shimokawa, M., Ozaki, N., Satoh, H. and Okabe, S. 2007. In Situ Activity and Spatial Organization of Anaerobic Ammonium-Oxidizing (Anammox) Bacteria in Biofilms. *Applied and Environmental Microbiology*, 73 (15): 4931-4939.

Kits, K. D., Sedlacek, C. J., Lebedeva, E. V., Han, P., Bulaev, A., Pjevac, P., Daebeler, A., Romano, S., Albertsen, M., Stein, L. Y., Daims, H. and Wagner, M. 2017. Kinetic analysis of a complete nitrifier reveals an oligotrophic lifestyle. *Nature*, 549: 269.

Klaus, S., Baumler, R., Rutherford, B., Thesing, G., Zhao, H. and Bott, C. 2017. Startup of a Partial Nitritation-Anammox MBBR and the Implementation of pH-Based Aeration Control. *Water Environment Research*, 89 (6): 500-508.

Kotay, S. M., Mansell, B. L., Hogsett, M., Pei, H. and Goel, R. 2013. Anaerobic ammonia oxidation (ANAMMOX) for side-stream treatment of anaerobic digester filtrate process performance and microbiology. *Biotechnology and Bioengineering*, 110 (4): 1180-1192.

Kowalski, M. S., Devlin, T. R., di Biase, A. and Oleszkiewicz, J. A. 2019. Effective nitrogen removal in a two-stage partial nitritation-anammox reactor treating municipal wastewater – Piloting PN-MBBR/AMX-IFAS configuration. *Bioresource Technology*, 289: 121742.

Kowalski, M. S., Devlin, T. R. and Oleszkiewicz, J. A. 2018. Start-up and long-term performance of anammox moving bed biofilm reactor seeded with granular biomass. *Chemosphere*, 200: 481-486.

Kwok, W. K., Picioreanu, C., Ong, S. L., van Loosdrecht, M. C. M., Ng, W. J. and Heijnen, J. J. 1998. Influence of biomass production and detachment forces on biofilm structures in a biofilm airlift suspension reactor. *Biotechnology and Bioengineering*, 58 (4): 400-407.

Lackner, S., Gilbert, E. M., Vlaeminck, S. E., Joss, A., Horn, H. and van Loosdrecht, M. C. M. 2014. Full-scale partial nitritation/anammox experiences – An application survey. *Water Research*, 55: 292-303.

Lackner, S. and Horn, H. 2013. Comparing the performance and operation stability of an SBR and MBBR for single-stage nitritation-anammox treating wastewater with high organic load. *Environmental Technology*, 34 (10): 1319-1328.

Lackner, S., Welker, S., Gilbert, E. M. and Horn, H. 2015. Influence of seasonal temperature fluctuations on two different partial nitritation-anammox reactors treating mainstream municipal wastewater. *Water Science and Technology*, 72 (8): 1358-1363.

Laureni, M., Weissbrodt, D. G., Szivák, I., Robin, O., Nielsen, J. L., Morgenroth, E. and Joss, A. 2015. Activity and growth of anammox biomass on aerobically pre-treated municipal wastewater. *Water Research*, 80: 325-336.

Lawson, C. E., Wu, S., Bhattacharjee, A. S., Hamilton, J. J., McMahon, K. D., Goel, R. and Noguera, D. R. 2017. Metabolic network analysis reveals microbial community interactions in anammox granules. *Nature Communications*, 8: 15416.

Lebedeva, E., Alawi, M., Maixner, F., Jozsa, P.-G., Daims, H. and Spieck, E. 2008. Physiological and phylogenetic characterization of a novel lithoautotrophic nitrite-oxidizing bacterium,'Candidatus Nitrospira bockiana'. *International journal of systematic and evolutionary microbiology*, 58 (1): 242-250.

Lemaire, R., Webb, R. I. and Yuan, Z. 2008. Micro-scale observations of the structure of aerobic microbial granules used for the treatment of nutrient-rich industrial wastewater. *Isme j*, 2 (5): 528-541.

Li, J., Zhang, L., Peng, Y., Yang, S., Wang, X., Li, X. and Zhang, Q. 2019. NOB suppression in partial nitritation-anammox (PNA) process by discharging aged flocs: Performance and microbial community dynamics. *Chemosphere*, 227: 26-33.

Li, J., Zhang, L., Peng, Y. and Zhang, Q. 2017a. Effect of low COD/N ratios on stability of single-stage partial nitritation/anammox (SPN/A) process in a long-term operation. *Bioresource Technology*, 244: 192-197.

Li, X., Klaus, S., Bott, C. and He, Z. 2018. Status, Challenges, and Perspectives of Mainstream Nitritation‐Anammox for Wastewater Treatment. *Water Environment Research*, 90 (7): 634-649.

Li, X., Sun, S., Badgley, B. D., Sung, S., Zhang, H. and He, Z. 2016. Nitrogen removal by granular nitritation–anammox in an upflow membrane-aerated biofilm reactor. *Water Research*, 94: 23-31.

Li, X., Sun, S., Yuan, H., Badgley, B. D. and He, Z. 2017b. Mainstream upflow nitritation-anammox system with hybrid anaerobic pretreatment: Long-term performance and microbial community dynamics. *Water Research*, 125: 298-308.

Li, X. and Sung, S. 2015. Development of the combined nitritation–anammox process in an upflow anaerobic sludge blanket (UASB) reactor with anammox granules. *Chemical Engineering Journal*, 281: 837-843.

Liang, Y., Li, D., Zhang, X., Zeng, H., Yang, Z. and Zhang, J. 2014. Microbial characteristics and nitrogen removal of simultaneous partial nitrification, anammox and denitrification (SNAD) process treating low C/N ratio sewage. *Bioresource Technology*, 169: 103-109.

Lin, L., Pratt, S., Rattier, M. and Ye, L. 2020. Individual and combined effect of salinity and nitrite on freshwater Anammox bacteria (FAB). *Water Research*, 169: 114931.

Lin, X., Wang, Y., Ma, X., Yan, Y., Wu, M., Bond, P. L. and Guo, J. 2018. Evidence of differential adaptation to decreased temperature by anammox bacteria. *Environ Microbiol*,

Lin, Y. M., Lotti, T., Sharma, P. K. and van Loosdrecht, M. C. M. 2013. Apatite accumulation enhances the mechanical property of anammox granules. *Water Research*, 47 (13): 4556-4566.

Liu, Y., Sun, J., Peng, L., Wang, D., Dai, X. and Ni, B.-J. 2016. Assessment of Heterotrophic Growth Supported by Soluble Microbial Products in Anammox Biofilm using Multidimensional Modeling. *Scientific Reports*, 6 (1): 27576.

Loick, N., Dixon, E. R., Abalos, D., Vallejo, A., Matthews, G. P., McGeough, K. L., Well, R., Watson, C. J., Laughlin, R. J. and Cardenas, L. M. 2016. Denitrification as a source of nitric oxide emissions from incubated soil cores from a UK grassland soil. *Soil Biology and Biochemistry*, 95: 1-7.

Lotti, T., Cordola, M., Kleerebezem, R., Caffaz, S., Lubello, C. and van Loosdrecht, M. C. M. 2012a. Inhibition effect of swine wastewater heavy metals and antibiotics on anammox activity. *Water Science and Technology*, 66 (7): 1519-1526.

Lotti, T., Kleerebezem, R., Hu, Z., Kartal, B., de Kreuk, M. K., van Erp Taalman Kip, C., Kruit, J., Hendrickx, T. L. and van Loosdrecht, M. C. 2015. Pilot-scale evaluation of anammox-based mainstream nitrogen removal from municipal wastewater. *Environ Technol*, 36 (9-12): 1167-1177.

Lotti, T., Kleerebezem, R., Hu, Z., Kartal, B., Jetten, M. S. M. and van Loosdrecht, M. C. M. 2014a. Simultaneous partial nitritation and anammox at low temperature with granular sludge. *Water Research*, 66: 111-121.

Lotti, T., Kleerebezem, R., van Erp Taalman Kip, C., Hendrickx, T. L. G., Kruit, J., Hoekstra, M. and van Loosdrecht, M. C. M. 2014b. Anammox Growth on Pretreated Municipal Wastewater. *Environmental Science & Technology*, 48 (14): 7874-7880.

Lotti, T., Kleerebezem, R. and van Loosdrecht, M. C. M. 2015. Effect of temperature change on anammox activity. *Biotechnology and Bioengineering*, 112 (1): 98-103.

Lotti, T., van der Star, W. R. L., Kleerebezem, R., Lubello, C. and van Loosdrecht, M. C. M. 2012b. The effect of nitrite inhibition on the anammox process. *Water Research*, 46 (8): 2559-2569.

Lu, H., Li, Y., Shan, X., Abbas, G., Zeng, Z., Kang, D., Wang, Y., Zheng, P. and Zhang, M. 2019. A holistic analysis of ANAMMOX process in response to salinity: From adaptation to collapse. *Separation and Purification Technology*, 215: 342-350.

Lucker, S., Wagner, M., Maixner, F., Pelletier, E., Koch, H., Vacherie, B., Rattei, T., Damste, J. S., Spieck, E., Le Paslier, D. and Daims, H. 2010. A Nitrospira metagenome illuminates the physiology and evolution of globally important nitrite-oxidizing bacteria. *Proc Natl Acad Sci U S A*, 107 (30): 13479-13484.

Ma, B., Qian, W., Yuan, C., Yuan, Z. and Peng, Y. 2017. Achieving Mainstream Nitrogen Removal through Coupling Anammox with Denitratation. *Environmental Science & Technology*, 51 (15): 8405-8413.

Ma, H., Zhang, Y., Xue, Y. and Li, Y.-Y. 2018. A new process for simultaneous nitrogen removal and phosphorus recovery using an anammox expanded bed reactor. *Bioresource technology*, 267: 201-208.

Ma, L., Dai, M., Tan, S., Xia, X. and Liu, H. 2016. Potential nitrous oxide yield of AOA vs. AOB and utilization of carbon and nitrogen in the ammonia oxidizing process in the Pearl River Estuary. Paper presented at the *AGU Fall Meeting Abstracts*. December 01, 2016. Available: https://ui.adsabs.harvard.edu/abs/2016AGUFM.B23E0631M (Accessed

Magrí, A., Vanotti, M. B. and Szögi, A. A. 2012. Anammox sludge immobilized in polyvinyl alcohol (PVA) cryogel carriers. *Bioresource Technology*, 114 (Supplement C): 231-240.

Malovanyy, A., Trela, J. and Plaza, E. 2015. Mainstream wastewater treatment in integrated fixed film activated sludge (IFAS) reactor by partial nitritation/anammox process. *Bioresource Technology*, 198: 478-487.

Montalvo, S., Guerrero, L., Borja, R., Sánchez, E., Milán, Z., Cortés, I. and Angeles de la la Rubia, M. 2012. Application of natural zeolites in anaerobic digestion processes: A review. *Applied Clay Science*, 58 (Supplement C): 125-133.

Mulder, A., Graaf, A. A., Robertson, L. A. and Kuenen, J. G. 1995. Anaerobic ammonium oxidation discovered in a denitrifying fluidized bed reactor. *FEMS Microbiology Ecology*, 16 (3): 177-184.

Murthy, S. N., Giraldo, E., Dockett, N. D., De Clippeleir, H., Wett, B. and Bailey Jr, W. F. 2014. *Method and apparatus for water treatment using screens*: Google Patents.

Naccache, S. N., Federman, S., Veeraraghavan, N., Zaharia, M., Lee, D., Samayoa, E., Bouquet, J., Greninger, A. L., Luk, K.-C. and Enge, B. 2014. A cloud-compatible bioinformatics pipeline for ultrarapid pathogen identification from next-generation sequencing of clinical samples. *Genome research*, 24 (7): 1180-1192.

Nejidat, A., Diaz-Reck, D., Massalha, N., Arbiv, A., Dawas, A., Dosoretz, C. and Sabbah, I. 2018. Abundance and diversity of anammox bacteria in a mainstream municipal wastewater treatment plant. *Applied Microbiology and Biotechnology*, 102 (15): 6713-6723.

Ni, B.-J., Joss, A. and Yuan, Z. 2014. Modeling nitrogen removal with partial nitritation and anammox in one floc-based sequencing batch reactor. *Water Research*, 67: 321-329.

Ni, B.-J., Ruscalleda, M. and Smets, B. F. 2012. Evaluation on the microbial interactions of anaerobic ammonium oxidizers and heterotrophs in Anammox biofilm. *Water Research*, 46 (15): 4645-4652.

Ni, B.-J., Xie, W.-M., Chen, Y.-P., Fang, F., Liu, S.-Y., Ren, T.-T., Sheng, G.-P., Yu, H.-Q., Liu, G. and Tian, Y.-C. 2011a. Heterotrophs grown on the soluble microbial products (SMP) released by autotrophs are responsible for the nitrogen loss in nitrifying granular sludge. *Biotechnology and Bioengineering*, 108 (12): 2844-2852.

Ni, L., Lin, X., Yan, H. and Wang, Y. 2019. A novel anammox granules-circulating expanded granular sludge bed reactor for the efficient circulation and retention of floating anammox granules. *Chemosphere*, 235: 316-326.

Ni, S.-Q., Sun, N., Yang, H., Zhang, J. and Ngo, H. H. 2015. Distribution of extracellular polymeric substances in anammox granules and their important roles during anammox granulation. *Biochemical Engineering Journal*, 101: 126-133.

Ni, S. Q., Gao, B. Y., Wang, C. C., Lin, J. G. and Sung, S. 2011b. Fast start-up, performance and microbial community in a pilot-scale anammox reactor seeded with exotic mature granules. *Bioresour Technol*, 102 (3): 2448-2454.

Nielsen, M., Bollmann, A., Sliekers, O., Jetten, M., Schmid, M., Strous, M., Schmidt, I., Larsen, L. H., Nielsen, L. P. and Revsbech, N. P. 2005. Kinetics, diffusional limitation and microscale distribution of chemistry and organisms in a CANON reactor. *FEMS Microbiology Ecology*, 51 (2): 247-256.

O'Shaughnessy, M. 2015. *Mainstream deammonification*. Water Environment Research Foundation Alexandria, VA.

Ochoa-Herrera, V., León, G., Banihani, Q., Field, J. A. and Sierra-Alvarez, R. 2011. Toxicity of copper(II) ions to microorganisms in biological wastewater treatment systems. *Science of The Total Environment*, 412-413: 380-385.

Ødegaard, H. 2006. Innovations in wastewater treatment: –the moving bed biofilm process. *Water Science and Technology*, 53 (9): 17-33.

Ødegaard, H., Mende, U., Skjerping, E. O., Simonsen, S., Strube, R. and Bundgaard, E. 2012. Compact tertiary treatment based on the combination of MBBR and contained hollow fibre UF-membranes. *Desalination and Water Treatment*, 42 (1-3): 80-86.

Oksanen, J., Blanchet, F., Kindt, R., Legendre, P., Minchin, P., O'Hara, R., Simpson, G., Solymos, P., Stevens, M. and Wagner, H. 2015. Vegan: community ecology package. R package vegan, vers. 2.2-1. *World Agroforestry Centre, Nairobi, Kenya. Published online.[Google Scholar]*,

Oshiki, M., Ishii, S., Yoshida, K., Fujii, N., Ishiguro, M., Satoh, H. and Okabe, S. 2013. Nitrate-dependent Ferrous Iron Oxidation by Anaerobic Ammonium Oxidation (anammox) Bacteria. *Applied and Environmental Microbiology*,

Oshiki, M., Shimokawa, M., Fujii, N., Satoh, H. and Okabe, S. 2011. Physiological characteristics of the anaerobic ammonium-oxidizing bacterium 'Candidatus Brocadia sinica'. *Microbiology*, 157 (Pt 6): 1706-1713.

Park, G., Takekawa, M., Soda, S., Ike, M. and Furukawa, K. 2017a. Temperature dependence of nitrogen removal activity by anammox bacteria enriched at low temperatures. *Journal of Bioscience and Bioengineering*, 123 (4): 505-511.

Park, H., Brotto, A. C., van Loosdrecht, M. C. M. and Chandran, K. 2017b. Discovery and metagenomic analysis of an anammox bacterial enrichment related to Candidatus "Brocadia caroliniensis" in a full-scale glycerol-fed nitritation-denitritation separate centrate treatment process. *Water Research*, 111: 265-273.

Park, H., Rosenthal, A., Jezek, R., Ramalingam, K., Fillos, J. and Chandran, K. 2010a. Impact of inocula and growth mode on the molecular microbial ecology of anaerobic ammonia oxidation (anammox) bioreactor communities. *Water Res*, 44 (17): 5005-5013.

Park, H., Rosenthal, A., Ramalingam, K., Fillos, J. and Chandran, K. 2010b. Linking Community Profiles, Gene Expression and N-Removal in Anammox Bioreactors Treating Municipal Anaerobic Digestion Reject Water. *Environmental Science & Technology*, 44 (16): 6110-6116.

Park, H., Sundar, S., Ma, Y. and Chandran, K. 2015. Differentiation in the microbial ecology and activity of suspended and attached bacteria in a nitritation-anammox process. *Biotechnology and Bioengineering*, 112 (2): 272-279.

Park, M.-R., Park, H. and Chandran, K. 2017. Molecular and Kinetic Characterization of Planktonic Nitrospira spp. Selectively Enriched from Activated Sludge. *Environmental Science & Technology*, 51 (5): 2720-2728.

Pellicer-Nàcher, C., Sun, S., Lackner, S., Terada, A., Schreiber, F., Zhou, Q. and Smets, B. F. 2010. Sequential Aeration of Membrane-Aerated Biofilm Reactors for High-Rate Autotrophic Nitrogen Removal: Experimental Demonstration. *Environmental Science & Technology*, 44 (19): 7628-7634.

Peng, Y. and Zhu, G. 2006. Biological nitrogen removal with nitrification and denitrification via nitrite pathway. *Applied Microbiology and Biotechnology*, 73 (1): 15-26.

Persson, F., Sultana, R., Suarez, M., Hermansson, M., Plaza, E. and Wilén, B.-M. 2014. Structure and composition of biofilm communities in a moving bed biofilm reactor for nitritation–anammox at low temperatures. *Bioresource Technology*, 154: 267-273.

Petersen, E. E. 1965. *Chemical reaction analysis*. Prentice-Hall.

Pichel, A., Moreno, R., Figueroa, M., Campos, J. L., Mendez, R., Mosquera-Corral, A. and del Rio, A. V. 2019. How to cope with NOB activity and pig manure inhibition in a partial nitritation-anammox process? *Separation and Purification Technology*, 212: 396-404.

Pietri, R., Román-Morales, E. and López-Garriga, J. 2011. Hydrogen sulfide and hemeproteins: knowledge and mysteries. *Antioxidants & redox signaling*, 15 (2): 393-404.

Podmirseg, S. M., Pümpel, T., Markt, R., Murthy, S., Bott, C. and Wett, B. 2015. Comparative evaluation of multiple methods to quantify and characterise granular anammox biomass. *Water research*, 68: 194-205.

Prosser, J. I. 2005. NITROGEN IN SOILS | Nitrification. In: Hillel, D. ed. *Encyclopedia of Soils in the Environment*. Oxford: Elsevier, 31-39. Available: http://www.sciencedirect.com/science/article/pii/B0123485304005129 (Accessed

Prosser, J. I. 2007. Chapter 15 - The Ecology of Nitrifying Bacteria. In: Bothe, H., Ferguson, S. J. and Newton, W. E. eds. *Biology of the Nitrogen Cycle*. Amsterdam: Elsevier, 223-243. Available: http://www.sciencedirect.com/science/article/pii/B9780444528575500163 (Accessed

Puyol, D., Carvajal-Arroyo, J. M., Sierra-Alvarez, R. and Field, J. A. 2014. Nitrite (not free nitrous acid) is the main inhibitor of the anammox process at common pH conditions. *Biotechnology Letters*, 36 (3): 547-551.

Quan, L. M., Khanh, D. P., Hira, D., Fujii, T. and Furukawa, K. 2011. Reject water treatment by improvement of whole cell anammox entrapment using polyvinyl alcohol/alginate gel. *Biodegradation*, 22 (6): 1155-1167.

Ramsundar, P., Guldhe, A., Singh, P., Pillay, K. and Bux, F. 2017. Evaluation of waste activated sludge as a potential nutrient source for cultivation of Chlorella sorokiniana. *Algal Research*, 28: 108-117.

Regmi, P., Miller, M. W., Holgate, B., Bunce, R., Park, H., Chandran, K., Wett, B., Murthy, S. and Bott, C. B. 2014. Control of aeration, aerobic SRT and COD input for mainstream nitritation/denitritation. *Water Res*, 57: 162-171.

Reij, M. W., de Bont, J. A. M., Hartmans, S. and de Gooijer, K. D. 1995. Membrane bioreactor with a porous hydrophobic membrane as a gas–liquid contactor for waste gas treatment. *Biotechnology and Bioengineering*, 45 (2): 107-115.

Reino, C. and Carrera, J. 2017. Low-strength wastewater treatment in an anammox UASB reactor: Effect of the liquid upflow velocity. *Chemical Engineering Journal*, 313: 217-225.

Reino, C., Suarez-Ojeda, M. E., Perez, J. and Carrera, J. 2018. Stable long-term operation of an upflow anammox sludge bed reactor at mainstream conditions. *Water Res*, 128: 331-340.

Rodríguez-Gómez, R., Renman, G., Moreno, L. and Liu, L. 2014. A model to describe the performance of the UASB reactor. *Biodegradation*, 25 (2): 239-251.

Rodriguez-Sanchez, A., Purswani, J., Lotti, T., Maza-Marquez, P., van Loosdrecht, M. C. M., Vahala, R. and Gonzalez-Martinez, A. 2016. Distribution and microbial community structure analysis of a single-stage partial nitritation/anammox granular sludge bioreactor operating at low temperature. *Environmental Technology*, 37 (18): 2281-2291.

Rosenwinkel, K. H. and Cornelius, A. 2005. Deammonification in the Moving-Bed Process for the Treatment of Wastewater with High Ammonia Content. *Chemical Engineering & Technology*, 28 (1): 49-52.

Rysgaard, S., Glud, R. N., Risgaard-Petersen, N. and Dalsgaard, T. 2004. Denitrification and anammox activity in Arctic marine sediments. *Limnology and Oceanography*, 49 (5): 1493-1502.

Sauder, L. A., Albertsen, M., Engel, K., Schwarz, J., Nielsen, P. H., Wagner, M. and Neufeld, J. D. 2017. Cultivation and characterization of Candidatus Nitrosocosmicus exaquare, an ammonia-oxidizing archaeon from a municipal wastewater treatment system. *The Isme Journal*, 11: 1142.

Schmidt, J. E. and Ahring, B. K. 1996. Granular sludge formation in upflow anaerobic sludge blanket (UASB) reactors. *Biotechnology and Bioengineering*, 49 (3): 229-246.

Scott, H. F. 2016. *Elements of chemical reaction engineering*. Prentice Hall.

Shi, Y., Hu, S., Lou, J., Lu, P., Keller, J. and Yuan, Z. 2013. Nitrogen Removal from Wastewater by Coupling Anammox and Methane-Dependent Denitrification in a Membrane Biofilm Reactor. *Environmental Science & Technology*, 47 (20): 11577-11583.

Shi, Y., Wells, G. and Morgenroth, E. 2016. Microbial activity balance in size fractionated suspended growth biomass from full-scale sidestream combined nitritation-anammox reactors. *Bioresource Technology*, 218: 38-45.

Sliekers, A. O., Derwort, N., Gomez, J. L. C., Strous, M., Kuenen, J. G. and Jetten, M. S. M. 2002. Completely autotrophic nitrogen removal over nitrite in one single reactor. *Water Research*, 36 (10): 2475-2482.

Smith, K. A. 2010. *Nitrous oxide and climate change*. Earthscan.

Soliman, M. and Eldyasti, A. 2016. Development of partial nitrification as a first step of nitrite shunt process in a Sequential Batch Reactor (SBR) using Ammonium Oxidizing Bacteria (AOB) controlled by mixing regime. *Bioresource Technology*, 221: 85-95.

Sondi, I. and Salopek-Sondi, B. 2004. Silver nanoparticles as antimicrobial agent: a case study on E. coli as a model for Gram-negative bacteria. *Journal of Colloid and Interface Science*, 275 (1): 177-182.

Sorokin, D. Y., Vejmelkova, D., Lucker, S., Streshinskaya, G. M., Rijpstra, W. I., Sinninghe Damste, J. S., Kleerbezem, R., van Loosdrecht, M., Muyzer, G. and Daims, H. 2014. Nitrolancea hollandica gen. nov., sp. nov., a chemolithoautotrophic nitrite-oxidizing bacterium isolated from a bioreactor belonging to the phylum Chloroflexi. *Int J Syst Evol Microbiol*, 64 (Pt 6): 1859-1865.

Speth, D. R., in 't Zandt, M. H., Guerrero-Cruz, S., Dutilh, B. E. and Jetten, M. S. M. 2016. Genome-based microbial ecology of anammox granules in a full-scale wastewater treatment system. *Nature Communications*, 7: 11172.

Sri Shalini, S. and Joseph, K. 2013. Start-up of the SHARON and ANAMMOX process in landfill bioreactors using aerobic and anaerobic ammonium oxidising biomass. *Bioresource technology*, 149: 474-485.

Strous, M., Heijnen, J. J., Kuenen, J. G. and Jetten, M. S. M. 1998. The sequencing batch reactor as a powerful tool for the study of slowly growing anaerobic ammonium-oxidizing microorganisms. *Applied Microbiology and Biotechnology*, 50 (5): 589-596.

Strous, M., Van Gerven, E., Kuenen, J. G. and Jetten, M. 1997a. Effects of aerobic and microaerobic conditions on anaerobic ammonium-oxidizing (anammox) sludge. *Applied and Environmental Microbiology*, 63 (6): 2446-2448.

Strous, M., Van Gerven, E., Zheng, P., Kuenen, J. G. and Jetten, M. S. M. 1997b. Ammonium removal from concentrated waste streams with the anaerobic ammonium oxidation (Anammox) process in different reactor configurations. *Water Research*, 31 (8): 1955-1962.

Su, J., Liang, D. and Lian, T. 2018. Comparison of denitrification performance by bacterium Achromobacter sp. A14 under different electron donor conditions. *Chemical Engineering Journal*, 333: 320-326.

Suarez, C., Persson, F. and Hermansson, M. 2015. Predation of nitritation–anammox biofilms used for nitrogen removal from wastewater. *FEMS Microbiology Ecology*, 91 (11)

Sumino, T., Nakamura, H., Mori, N. and Kawaguchi, Y. 1992. Immobilization of nitrifying bacteria by polyethylene glycol prepolymer. *Journal of Fermentation and Bioengineering*, 73 (1): 37-42.

Sun, S., Song, Y., Yang, X. J., Hu, H., Wu, S., Qi, W.-k. and Li, Y.-Y. 2018. Strategies for improving nitrogen removal under high sludge loading rate in an anammox membrane bioreactor operated at 25 °C. *Chemical Engineering Science*, 183: 106-114.

Syron, E. and Casey, E. 2008. Membrane-Aerated Biofilms for High Rate Biotreatment: Performance Appraisal, Engineering Principles, Scale-up, and Development Requirements. *Environmental Science & Technology*, 42 (6): 1833-1844.

Tang, C.-J., Zheng, P., Wang, C.-H., Mahmood, Q., Zhang, J.-Q., Chen, X.-G., Zhang, L. and Chen, J.-W. 2011. Performance of high-loaded ANAMMOX UASB reactors containing granular sludge. *Water Research*, 45 (1): 135-144.

Tang, C. J., Zheng, P., Mahmood, Q. and Chen, J. W. 2009. Start-up and inhibition analysis of the Anammox process seeded with anaerobic granular sludge. *J Ind Microbiol Biotechnol*, 36 (8): 1093-1100.

Tao, Y., Gao, D.-W., Fu, Y., Wu, W.-M. and Ren, N.-Q. 2012. Impact of reactor configuration on anammox process start-up: MBR versus SBR. *Bioresource Technology*, 104: 73-80.

Terada, A., Lackner, S., Tsuneda, S. and Smets, B. F. 2007. Redox-stratification controlled biofilm (ReSCoBi) for completely autotrophic nitrogen removal: The effect of co- versus counter-diffusion on reactor performance. *Biotechnology and Bioengineering*, 97 (1): 40-51.

Third, K. A., Paxman, J., Schmid, M., Strous, M., Jetten, M. S. M. and Cord-Ruwisch, R. 2005. Enrichment of Anammox from Activated Sludge and Its Application in the CANON Process. *Microbial Ecology*, 49 (2): 236-244.

Tomaszewski, M., Cema, G. and Ziembińska-Buczyńska, A. 2017. Significance of pH control in anammox process performance at low temperature. *Chemosphere*, 185: 439-444.

Trimmer, M., Chronopoulou, P.-M., Maanoja, S. T., Upstill-Goddard, R. C., Kitidis, V. and Purdy, K. J. 2016. Nitrous oxide as a function of oxygen and archaeal gene abundance in the North Pacific. *Nature Communications*, 7 (1): 13451.

Trojanowicz, K., Plaza, E. and Trela, J. 2016. Pilot scale studies on nitritation-anammox process for mainstream wastewater at low temperature. *Water Science and Technology*, 73 (4): 761-768.

Trojanowicz, K., Plaza, E. and Trela, J. 2017. Model extension, calibration and validation of partial nitritation-anammox process in moving bed biofilm reactor (MBBR) for reject and mainstream wastewater. *Environ Technol*: 1-22.

Tsushima, I., Ogasawara, Y., Kindaichi, T., Satoh, H. and Okabe, S. 2007. Development of high-rate anaerobic ammonium-oxidizing (anammox) biofilm reactors. *Water Research*, 41 (8): 1623-1634.

Val del Río, Á., Campos Gómez, J. L. and Mosquera Corral, A. 2016. *Technologies for the Treatment and Recovery of Nutrients from Industrial Wastewater*. IGI Global.

van de Graaf, A. A., de Bruijn, P., Robertson, L. A., Jetten, M. S. M. and Kuenen, J. G. 1996. Autotrophic growth of anaerobic ammonium-oxidizing micro-organisms in a fluidized bed reactor. *Microbiology*, 142 (8): 2187-2196.

Van De Vossenberg, J., Rattray, J. E., Geerts, W., Kartal, B., Van Niftrik, L., Van Donselaar, E. G., Sinninghe Damsté, J. S., Strous, M. and Jetten, M. S. M. 2008. Enrichment and characterization of marine anammox bacteria associated with global nitrogen gas production. *Environmental Microbiology*, 10 (11): 3120-3129.

van de Vossenberg, J., Woebken, D., Maalcke, W. J., Wessels, H. J. C. T., Dutilh, B. E., Kartal, B., Janssen-Megens, E. M., Roeselers, G., Yan, J., Speth, D., Gloerich, J., Geerts, W., van der Biezen, E., Pluk, W., Francoijs, K.-J., Russ, L., Lam, P., Malfatti, S. A., Tringe, S. G., Haaijer, S. C. M., Op den Camp, H. J. M., Stunnenberg, H. G., Amann, R., Kuypers, M. M. M. and Jetten, M. S. M. 2013. The metagenome of the marine anammox bacterium 'Candidatus Scalindua profunda' illustrates the versatility of this globally important nitrogen cycle bacterium. *Environmental Microbiology*, 15 (5): 1275-1289.

van der Star, W. R., Miclea, A. I., van Dongen, U. G., Muyzer, G., Picioreanu, C. and van Loosdrecht, M. C. 2008. The membrane bioreactor: a novel tool to grow anammox bacteria as free cells. *Biotechnol Bioeng*, 101 (2): 286-294.

van der Star, W. R. L., Abma, W. R., Blommers, D., Mulder, J.-W., Tokutomi, T., Strous, M., Picioreanu, C. and van Loosdrecht, M. C. M. 2007. Startup of reactors for anoxic ammonium oxidation: Experiences from the first full-scale anammox reactor in Rotterdam. *Water Research*, 41 (18): 4149-4163.

van Dongen, U., Jetten, M. S. and van Loosdrecht, M. C. 2001. The SHARON-Anammox process for treatment of ammonium rich wastewater. *Water Sci Technol*, 44 (1): 153-160.

van Kempen, R., Mulder, J. W., Uijterlinde, C. A. and Loosdrecht, M. C. 2001a. Overview: full scale experience of the SHARON process for treatment of rejection water of digested sludge dewatering. *Water Sci Technol*, 44 (1): 145-152.

van Kempen, R., Mulder, J. W., Uijterlinde, C. A. and Loosdrecht, M. C. M. 2001b. Overview: full scale experience of the SHARON® process for treatment of rejection water of digested sludge dewatering. *Water Science and Technology*, 44 (1): 145-152.

van Loosdrecht, M. C. M., Eikelboom, D., Gjaltema, A., Mulder, A., Tijhuis, L. and Heijnen, J. J. 1995. Biofilm structures. *Water Science and Technology*, 32 (8): 35-43.

Van Loosdrecht, M. C. M. and Heijnen, S. J. 1993. Biofilm bioreactors for waste-water treatment. *Trends in Biotechnology*, 11 (4): 117-121.

Vanotti, M. and Hunt, P. 2000. Nitrification treatment of swine wastewater with acclimated nitrifying sludge immobilized in polymer pellets. *Transactions of the ASAE*, 43 (2): 405.

Vázquez-Padín, J. R., Morales, N., Gutiérrez, R., Fernández, R., Rogalla, F., Barrio, J. P., Campos, J. L., Mosquera-Corral, A. and Méndez, R. 2013. Implications of full-scale implementation of an anammox-based process as post-treatment of a municipal anaerobic sludge digester operated with co-digestion. *Water Science and Technology*, 69 (6): 1151-1158.

Veuillet, F., Lacroix, S., Bausseron, A., Gonidec, E., Ochoa, J., Christensson, M. and Lemaire, R. 2013. Integrated fixed-film activated sludge ANITA™Mox process – a new perspective for advanced nitrogen removal. *Water Science and Technology*, 69 (5): 915-922.

Veuillet, F., Lacroix, S., Bausseron, A., Gonidec, E., Ochoa, J., Christensson, M. and Lemaire, R. 2014. Integrated fixed-film activated sludge ANITAMox process--a new perspective for advanced nitrogen removal. *Water Sci Technol*, 69 (5): 915-922.

Veys, P., Vandeweyer, H., Audenaert, W., Monballiu, A., Dejans, P., Jooken, E., Dumoulin, A., Meesschaert, B. D. and Van Hulle, S. W. 2010. Performance analysis and optimization of autotrophic nitrogen removal in different reactor configurations: a modelling study. *Environ Technol*, 31 (12): 1311-1324.

Vlaeminck, S. E., Terada, A., Smets, B. F., De Clippeleir, H., Schaubroeck, T., Bolca, S., Demeestere, L., Mast, J., Boon, N., Carballa, M. and Verstraete, W. 2010. Aggregate Size and Architecture Determine Microbial Activity Balance for One-Stage Partial Nitritation and Anammox. *Applied and Environmental Microbiology*, 76 (3): 900-909.

Wang, H., Xu, G., Qiu, Z., Zhou, Y. and Liu, Y. 2019. NOB suppression in pilot-scale mainstream nitritation-denitritation system coupled with MBR for municipal wastewater treatment. *Chemosphere*, 216: 633-639.

Wang, S., Zhu, G., Peng, Y., Jetten, M. S. M. and Yin, C. 2012a. Anammox Bacterial Abundance, Activity, and Contribution in Riparian Sediments of the Pearl River Estuary. *Environmental Science & Technology*, 46 (16): 8834-8842.

Wang, T., Zhang, H., Gao, D., Yang, F. and Zhang, G. 2012b. Comparison between MBR and SBR on Anammox start-up process from the conventional activated sludge. *Bioresource Technology*, 122: 78-82.

Wang, Y., Fang, H., Zhou, D., Han, H. and Chen, J. 2016. Characterization of nitrous oxide and nitric oxide emissions from a full-scale biological aerated filter for secondary nitrification. *Chemical Engineering Journal*, 299: 304-313.

Wang, Z. and Zheng, P. 2017. Predicting settling performance of ANAMMOX granular sludge based on fractal dimensions. *Water Research*, 120 (Supplement C): 222-228.

Wei, Q., Kawagoshi, Y., Huang, X., Hong, N., Van Duc, L., Yamashita, Y. and Hama, T. 2016. Nitrogen removal properties in a continuous marine anammox bacteria reactor under rapid and extensive salinity changes. *Chemosphere*, 148: 444-451.

Wells, G. F., Shi, Y., Laureni, M., Rosenthal, A., Szivák, I., Weissbrodt, D. G., Joss, A., Buergmann, H., Johnson, D. R. and Morgenroth, E. 2017. Comparing the Resistance, Resilience, and Stability of Replicate Moving Bed Biofilm and Suspended Growth Combined Nitritation–Anammox Reactors. *Environmental Science & Technology*, 51 (9): 5108-5117.

Wen, J., Liu, Y., Tu, Y. and LeChevallier, M. W. 2015. Energy and chemical efficient nitrogen removal at a full-scale MBR water reuse facility. *AIMS Environmental Science*, 2 (1): 42-55.

Wenjie, Z., Huaqin, W., Joseph, D. and Yue, J. 2015. Granular activated carbon as nucleus for formation of Anammox granules in an expanded granular-sludge-bed reactor. *Global NEST Journal*, 17 (3): 508-514.

Wett, B. 2007. Development and implementation of a robust deammonification process. *Water Sci Technol*, 56 (7): 81-88.

Wett, B., Nyhuis, G., Takács, I. and Murthy, S. 2010. Development of Enhanced Deammonification Selector. *Proceedings of the Water Environment Federation*, 2010 (10): 5917-5926.

Wett, B., Omari, A., Podmirseg, S., Han, M., Akintayo, O., Gómez Brandón, M., Murthy, S., Bott, C., Hell, M. and Takács, I. 2013. Going for mainstream deammonification from bench to full scale for maximized resource efficiency. *Water Sci. Technol*, 68 (2): 283-289.

Wett, B., Podmirseg, S. M., Gomez-Brandon, M., Hell, M., Nyhuis, G., Bott, C. and Murthy, S. 2015. Expanding DEMON Sidestream Deammonification Technology Towards Mainstream Application. *Water Environ Res*, 87 (12): 2084-2089.

Wiesmann, U. 1994. Biological nitrogen removal from wastewater. In: *Biotechnics/Wastewater*. Berlin, Heidelberg: Springer Berlin Heidelberg, 113-154. Available: https://doi.org/10.1007/BFb0008736 (Accessed 23/05/2019).

Winkler, M.-K. H., Kleerebezem, R., Strous, M., Chandran, K. and van Loosdrecht, M. C. M. 2013. Factors influencing the density of aerobic granular sludge. *Applied Microbiology and Biotechnology*, 97 (16): 7459-7468.

Winkler, M. K. H., Kleerebezem, R. and van Loosdrecht, M. C. M. 2012. Integration of anammox into the aerobic granular sludge process for main stream wastewater treatment at ambient temperatures. *Water Research*, 46 (1): 136-144.

Wu, J., Zhou, H.-m., Li, H.-z., Zhang, P.-c. and Jiang, J. 2009. Impacts of hydrodynamic shear force on nucleation of flocculent sludge in anaerobic reactor. *Water Research*, 43 (12): 3029-3036.

Wu, L., Yan, Z., Li, J., Huang, S., Li, Z., Shen, M. and Peng, Y. 2020. Low temperature advanced nitrogen and sulfate removal from landfill leachate by nitrite-anammox and sulfate-anammox. *Environmental Pollution*, 259: 113763.

Wyffels, S., Van Hulle, S. W., Boeckx, P., Volcke, E. I., Van Cleemput, O., Vanrolleghem, P. A. and Verstraete, W. 2004. Modeling and simulation of oxygen-limited partial nitritation in a membrane-assisted bioreactor (MBR). *Biotechnol Bioeng*, 86 (5): 531-542.

Xie, G.-J., Cai, C., Hu, S. and Yuan, Z. 2017. Complete Nitrogen Removal from Synthetic Anaerobic Sludge Digestion Liquor through Integrating Anammox and Denitrifying Anaerobic Methane Oxidation in a Membrane Biofilm Reactor. *Environmental Science & Technology*, 51 (2): 819-827.

Xu, X., Wang, G., Zhou, L., Yu, H. and Yang, F. 2018. Start-up of a full-scale SNAD-MBBR process for treating sludge digester liquor. *Chemical Engineering Journal*, 343: 477-483.

Yang, Y., Zhang, L., Cheng, J., Zhang, S., Li, X. and Peng, Y. 2018. Microbial community evolution in partial nitritation/anammox process: From sidestream to mainstream. *Bioresource Technology*, 251: 327-333.

Yang, Y., Zhang, L., Han, X., Zhang, S., Li, B. and Peng, Y. 2016. Determine the operational boundary of a pilot-scale single-stage partial nitritation/anammox system with granular sludge. *Water Science and Technology*, 73 (9): 2085-2092.

Zekker, I., Rikmann, E., Tenno, T., Lemmiksoo, V., Menert, A., Loorits, L., Vabamäe, P., Tomingas, M. and Tenno, T. 2012. Anammox enrichment from reject water on blank biofilm carriers and carriers containing nitrifying biomass: operation of two moving bed biofilm reactors (MBBR). *Biodegradation*, 23 (4): 547-560.

Zhang, L., Narita, Y., Gao, L., Ali, M., Oshiki, M., Ishii, S. and Okabe, S. 2017a. Microbial competition among anammox bacteria in nitrite-limited bioreactors. *Water Research*, 125: 249-258.

Zhang, L., Narita, Y., Gao, L., Ali, M., Oshiki, M. and Okabe, S. 2017b. Maximum specific growth rate of anammox bacteria revisited. *Water Research*, 116: 296-303.

Zhang, L., Narita, Y., Gao, L., Ali, M., Oshiki, M. and Okabe, S. 2017c. Maximum specific growth rate of anammox bacteria revisited. *Water Research*, 116 (Supplement C): 296-303.

Zhang, L. and Okabe, S. 2017. Rapid cultivation of free-living planktonic anammox cells. *Water Research*, 127 (Supplement C): 204-210.

Zhang, L. and Okabe, S. 2020. Ecological niche differentiation among anammox bacteria. *Water Research*, 171: 115468.

Zhang, L., Zhang, S., Peng, Y., Han, X. and Gan, Y. 2015. Nitrogen removal performance and microbial distribution in pilot- and full-scale integrated fixed-biofilm activated sludge reactors based on nitritation-anammox process. *Bioresource Technology*, 196: 448-453.

Zhang, Q., De Clippeleir, H., Su, C., Al-Omari, A., Wett, B., Vlaeminck, S. E. and Murthy, S. 2016a. Deammonification for digester supernatant pretreated with thermal hydrolysis: overcoming inhibition through process optimization. *Applied Microbiology and Biotechnology*, 100 (12): 5595-5606.

Zhang, Q., Vlaeminck, S. E., DeBarbadillo, C., Su, C., Al-Omari, A., Wett, B., Pümpel, T., Shaw, A., Chandran, K., Murthy, S. and De Clippeleir, H. 2018. Supernatant organics from anaerobic digestion after thermal hydrolysis cause direct and/or diffusional activity loss for nitritation and anammox. *Water Research*, 143: 270-281.

Zhang, X., Chen, Z., Zhou, Y., Ma, Y., Ma, C., Li, Y., Liang, Y. and Jia, J. 2019. Impacts of the heavy metals Cu (II), Zn (II) and Fe (II) on an Anammox system treating synthetic wastewater in low ammonia nitrogen and low temperature: Fe (II) makes a difference. *Science of The Total Environment*, 648: 798-804.

Zhang, Y., Ma, H., Niu, Q., Chen, R., Hojo, T. and Li, Y.-Y. 2016b. Effects of soluble microbial products (SMP) on the performance of an anammox attached film expanded bed (AAFEB) reactor: Synergistic interaction and toxic shock. *Bioresource Technology*, 222: 261-269.

Zhang, Z.-Z., Xu, J.-J., Hu, H.-Y., Shi, Z.-J., Ji, Z.-Q., Deng, R., Shi, M.-L. and Jin, R.-C. 2016c. Insight into the short- and long-term effects of inorganic phosphate on anammox granule property. *Bioresource Technology*, 208: 161-169.

Zhang, Z.-Z., Zhang, Q.-Q., Xu, J.-J., Deng, R., Ji, Z.-Q., Wu, Y.-H. and Jin, R.-C. 2016d. Evaluation of the inhibitory effects of heavy metals on anammox activity: A batch test study. *Bioresource Technology*, 200: 208-216.

Zhao, H., Lemaire, R., Christensson, M., Thesing, G., Veuillet, F., Ochoa, J., Lamarre, D. and Gadbois, A. 2013. Single-stage deammonification process performance-MBBR versus IFAS configurations. *Proceedings of the Water Environment Federation*, 2013 (4): 1-17.

Zhao, Y., Liu, S., Jiang, B., Feng, Y., Zhu, T., Tao, H., Tang, X. and Liu, S. 2018. Genome-Centered Metagenomics Analysis Reveals the Symbiotic Organisms Possessing Ability to Cross-Feed with Anammox Bacteria in Anammox Consortia. *Environmental Science & Technology*, 52 (19): 11285-11296.

Zhu, G. L., Hu, Y. Y. and Wang, Q. R. 2009. Nitrogen removal performance of anaerobic ammonia oxidation co-culture immobilized in different gel carriers. *Water Sci Technol*, 59 (12): 2379-2386.

APPENDICES

10 APPENDIX A

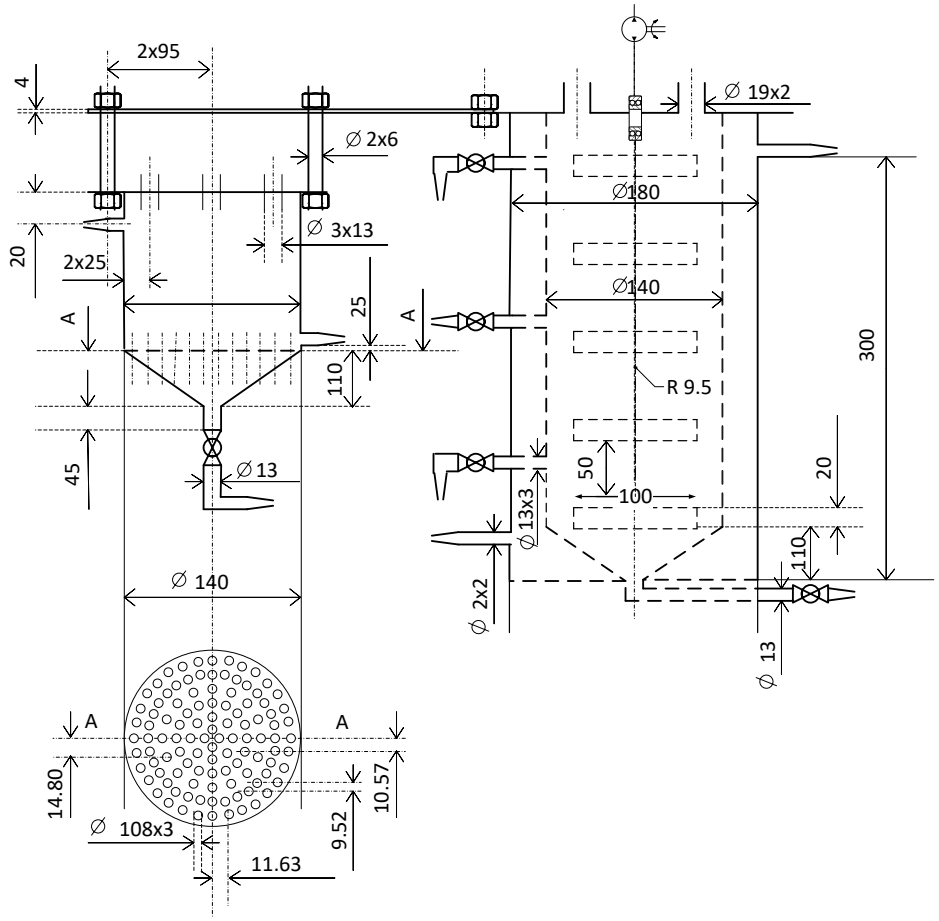

Figure A. 3. 1. Schematic diagram of MBBR. Units: mm.

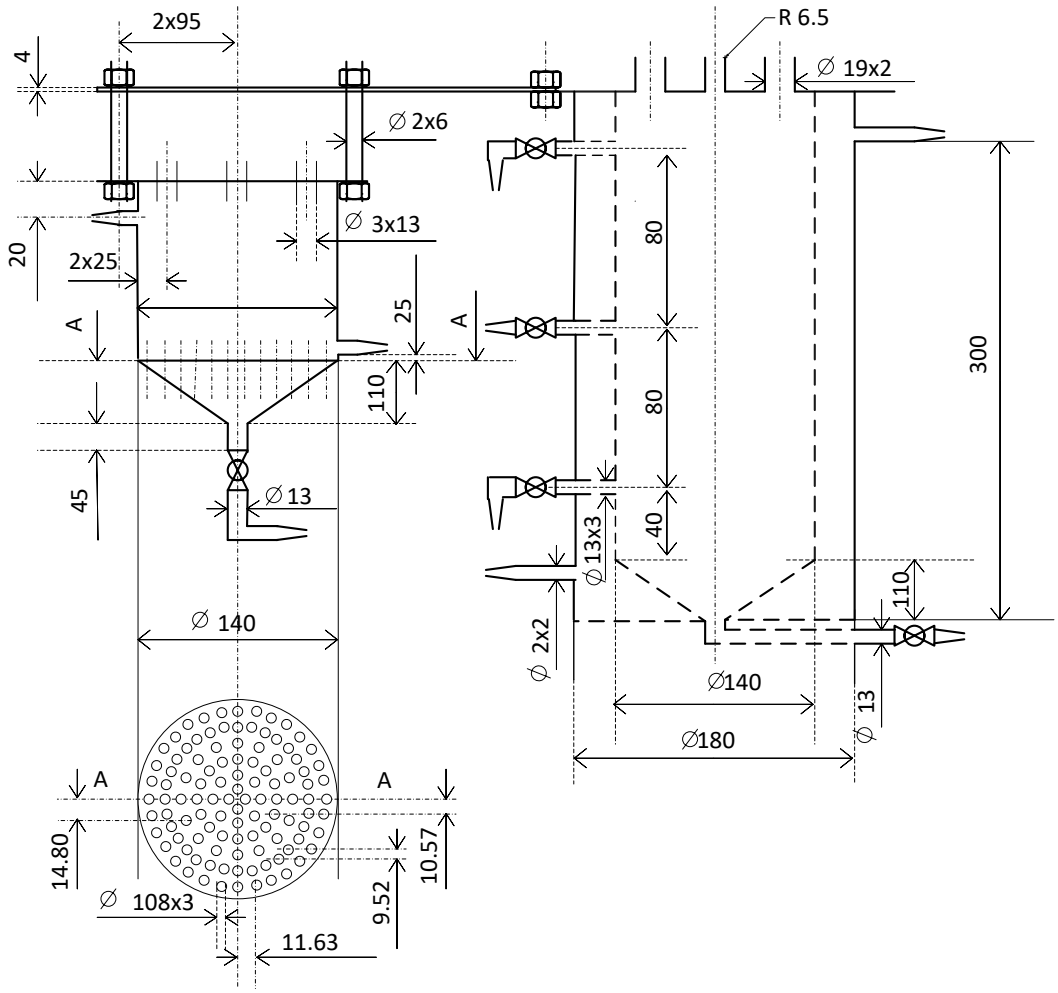

Figure A. 3. 2. Schematic diagram of H-UASB. Units: mm.

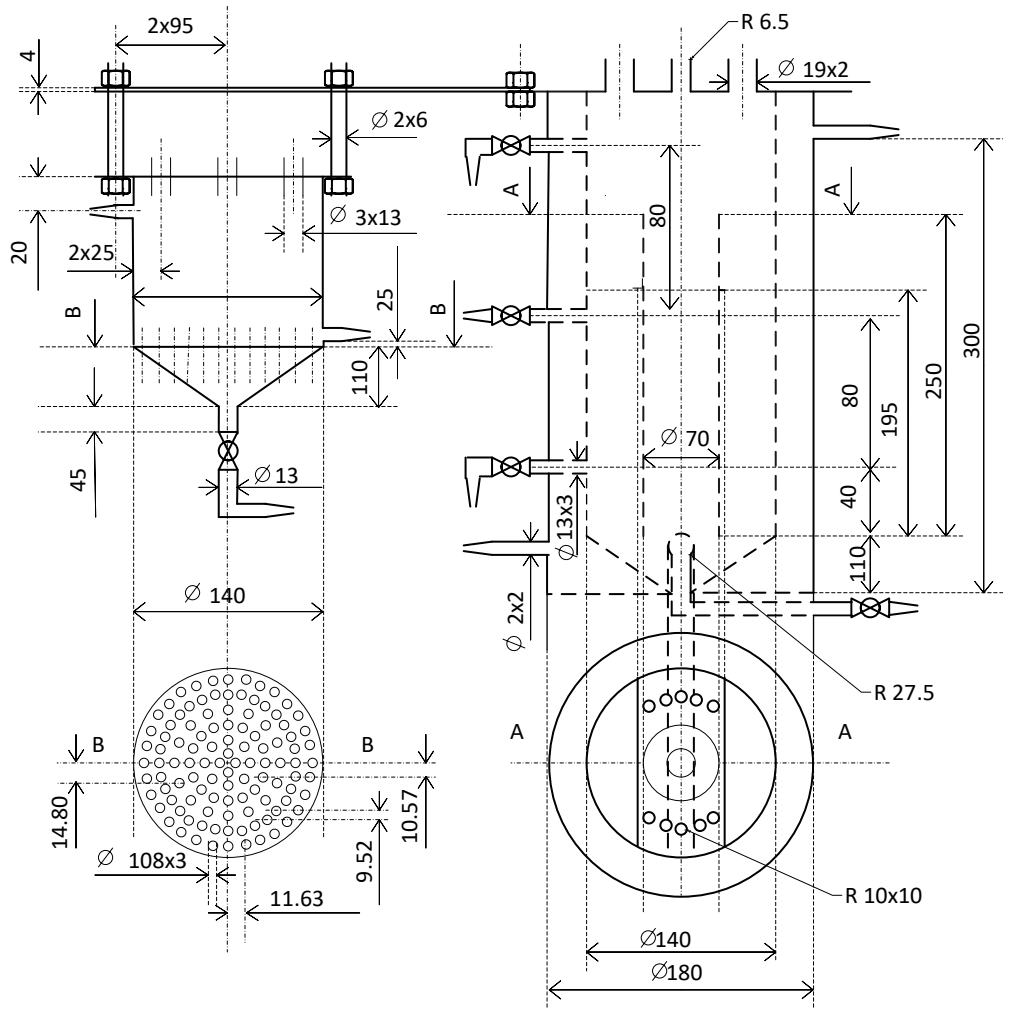

Figure A. 3. 3. Schematic diagram of GLR. Units: mm.

Figure A. 3. 4. Photographic image of DR 6000

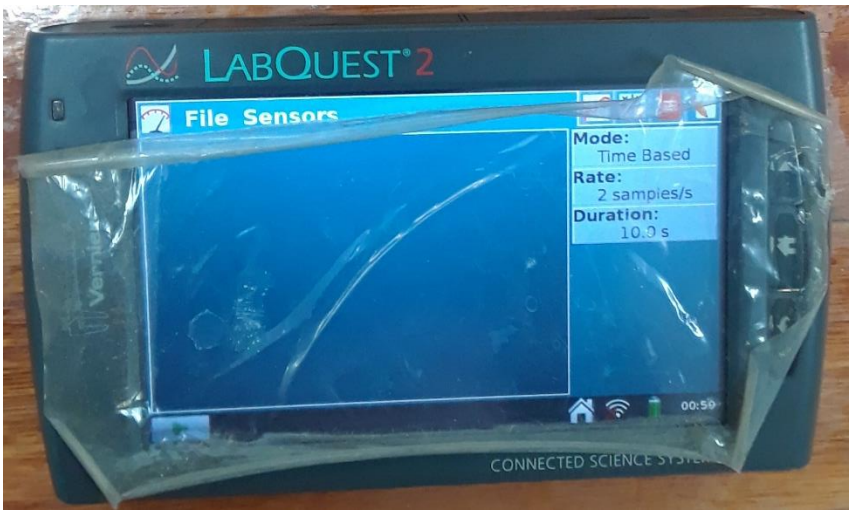

Figure A. 3. 5. Photographic image of Labquest 2 device.

Figure A. 3. 6. Photographic image of the automated water bath

Figure A. 3. 7. Photographic image of the pH controller.

Figure A. 3. 8. Photographic image of the food colouring used during the analysis of RTD.

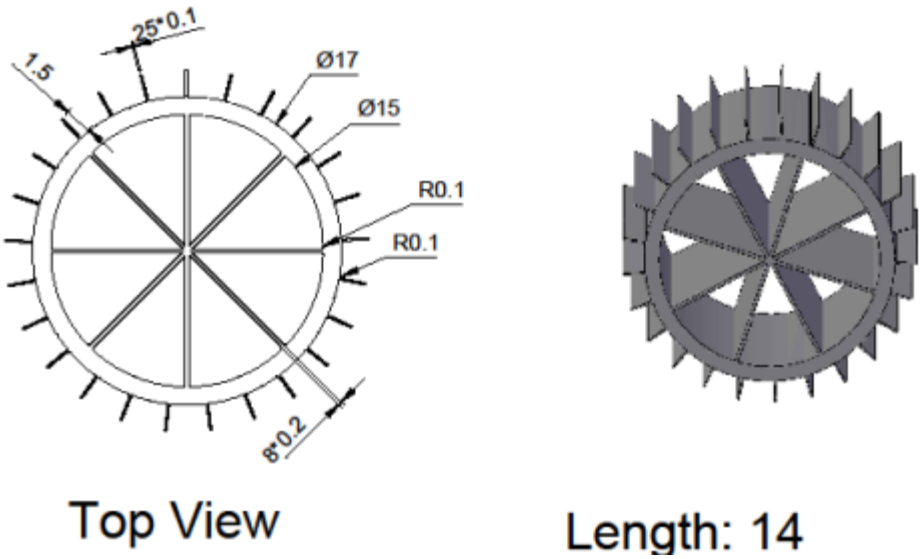

Figure A. 3. 9. Isometric drawing of K1-type carrier materials used in the reactors. Units: mm.

11 APPENDIX B

Table A. 4. 1. Affiliations of ANAMMOX bacteria in MBBR, H-UASB and GLR (%).

Sample	MBBR		H-UASB		GLR	
1	*Candidatus* Kuenenia Stuttgartiensis (43.15), *Candidatus* Kuenenia spp. enrichment culture clone hzsB K (0.00024), *Candidatus* Brocadia spp. 40 (0.00024)					
125	*Ca.* Kuenenia Stutt. (0.76)		*Ca.* Kuenenia Stutt. (5.13)		*Ca.* Kuenenia Stutt. (0.0044)	
192	*Ca.* Kuenenia Stutt. (0.32)		*Ca.* Kuenenia Stutt. (32.03), *uncultured Ca. Brocadia* spp. (0.0011)		*Ca.* Kuenenia Stutt. (0.90)	
260	*Ca.* Kuenenia Stutt. (14.41), *Ca.* Brocadia spp. 40 (0.00043), *Ca.* Bro. anammoxidans (0.093), *Ca.* Brocadia fulgida (0.017), *Ca.* Bro. sinica (0.021),*Ca. Bro.* spp. enrichment culture clone hzsB B.a (0.0069), *Ca.* Jettenia asiatica (0.0052), *Ca.* Jettenia caeni (0.033)		*Ca.* Kuenenia Stutt. (73.90), *Ca.* Bro. anammoxidans (0.036), Ca. Brocadia fulgida (0.0040), *Ca.* Bro. sinica (0.0088),*Ca.* Bro. spp. enrichment culture clone hzsB B.a (0.0015), *Ca. Jettenia* asiatica (0.0016), *Ca.* Jettenia caeni (0.011)		*Ca.* Kuenenia Stutt. (22.74), *Ca.* Bro. anammoxidans (0.0013), *Ca.* Bro. sinica (0.00044),*Ca.* Jettenia caeni (0.00044)	
309	*Ca.* Kuenenia Stutt. (7.46), *Ca.* Bro. anammoxidans (0.26), *Ca.* Brocadia fulgida (0.039), *Ca.* Bro. sinica (0.074),*Ca.* Bro. spp. enrichment culture clone hzsB B.a (0.013), *Ca.* Jettenia asiatica (0.0081), *Ca.* Jettenia caeni (0.080), *Ca.* Bro. spp. enrichment culture clone HZO4 (0.00081), uncultured Scalindua spp. *(0.00043)*		*Ca.* Kuenenia Stutt. (65.81), uncultured *Ca.* Brocadia spp. 40 (0.00016), *Ca.* Bro. anammoxidans (0.084), *Ca.* Brocadia fulgida (0.017), *Ca.* Bro. sinica (0.029),*Ca.* Bro. spp. enrichment culture clone hzsB B.a (0.0023), *Ca.* Jettenia asiatica (0.0033), *Ca.* Jettenia caeni (0.029), *Ca.* Bro. spp. enrichment culture clone HZO4 (0.00016)		*Ca.* Kuenenia Stutt. (22.12), *Ca.* Brocadia spp. 40 (0.00059), *Ca.* Bro. anammoxidans (0.14), *Ca.* Brocadia fulgida (0.024), *Ca.* Bro. sinica (0.042),*Ca.* Bro. spp. enrichment culture clone hzsB B.a (0.0059), *Ca.* Jettenia asiatica (0.0089), *Ca.* Jettenia caeni (0.034)	
	SUSPENDED	*BIOFILM*	*SUSPENDED*	*BIOFILM*	*SUSPENDED*	*BIOFILM*
535	*Ca.* Kuenenia Stutt. (11.18), *Ca.* Bro. anammoxidans (0.16), *Ca.* Brocadia fulgida (0.03), *Ca.* Bro. sinica (0.08),*Ca.* Bro. spp. enrichment culture clone hzsB B.a (0.005), *Ca.* Jettenia asiatica (0.008), *Ca.* Jettenia caeni (0.07), uncultured Brocadia spp. *(0.002),* uncultured Scalindua spp. *(0.002)*	*Ca.* Kuenenia Stutt. (4.19), *Ca.* Bro. anammoxidans (0.14), *Ca.* Brocadia fulgida (0.03), *Ca.* Bro. sinica (0.06),*Ca.* Bro. spp. enrichment culture clone hzsB B.a (0.005), *Ca.* Jettenia asiatica (0.007), *Ca.* Jettenia caeni (0.07), uncultured Brocadia spp. *(0.002),* uncultured Scalindua spp. *(0.0007)*	*Ca.* Kuenenia Stutt. (33.28), *Ca.* Bro. anammoxidans (0.05), *Ca.* Brocadia fulgida (0.017), *Ca.* Bro. sinica (0.11), *Ca.* Bro. spp. enrichment culture clone hzsB B.a (0.01), *Ca.* Jettenia asiatica (0.03), *Ca.* Jettenia caeni (0.13), *Ca. Bro.* spp. enrichment culture clone HZO4 (0.002), uncultured Ca. Brocadia spp. *(0.005),* uncultured Scalindua spp. *(0.002)*	*Ca.* Kuenenia Stutt. (5.48), *Ca.* Bro. anammoxidans (0.08), *Ca.* Brocadia fulgida (0.01), *Ca.* Bro. sinica (0.05), *Ca.* Bro. spp. enrichment culture clone hzsB B.a (0.006), *Ca.* Jettenia caeni (0.07)	*Ca.* Kuenenia Stutt. (3.81), *Ca.* Bro. anammoxidans (0.13), *Ca.* Brocadia fulgida (0.02), *Ca.* Bro. sinica (0.05), *Ca.* Bro. spp. 40 (0.0005), *Ca.* Bro. spp. enrichment culture clone hzsB B.a (0.005), *Ca.* Jettenia asiatica (0.005), *Ca.* Jettenia caeni (0.06), uncultured Brocadia spp. (0.001).	*Ca.* Kuenenia Stutt. (4.04), *Ca.* Bro. anammoxidans (0.16), *Ca.* Brocadia fulgida (0.03), *Ca.* Bro. sinica (0.07), *Ca.* Bro. spp. enrichment culture clone hzsB B.a (0.004), *Ca.* Jettenia asiatica (0.01), *Ca.* Jettenia caeni (0.07), uncultured Brocadia spp. (0.004).

*MBBR SUSPENDED, **H-UASB SUSPENDED, ***GLR SUSPENDED, *#MBBR BIOFILM, **#H-UASB BIOFILM, ***#GLR BIOFLM, SUS – SUSPENDED, BIOF – BIOFILM

Table A. 4. 2. The relative abundance and affiliations of the dominant AOB and NOB in MBBR, H-UASB and GLR (%).

	AOB						NOB					
Phase	MBBR		UASB		GLR		MBBR		UASB		GLR	
I (Inoculum)	*Nitrosomonas europaea* (4.38)						*Nitrospira moscoviensis* (3.32)					
IV (day 125)	*Nitrosomonas europaea* (29.13*, 35.83**, 0.32***)						*Nitrospira defluvii* (5.38)		*Nitrobacter hamburgensis* (0.92)		*Nitrospira defluvii* (0.13)	
VI (day 192)	*Nitrosomonas europaea* (26.03*, 8.63**, 18.13***)						*Nitrospira defluvii* (5.03*,4.38**,0.84***)					
VII (day 260)	*Nitrosospira multiformis* (3.57*,0.44**,3.44***)						*Nitrospira moscoviensis* (6.46)		*Nitrospira defluvii (0.4)*		*Nitrobacter hamburgensis (0.85)*	
VII (day 309)	*Nitrosospira multiformis (0.46*,0.78**)*				*Nitrosomonas europaea (15.7)*		*Nitrospira moscoviensis* (19.60)		*Nitrospira defluvii (0.66)*		*Nitrobacter hamburgensis* (0.78)	
	MBBR		*UASB*		*GLR*		*MBBR*		*UASB*		*GLR*	
	SUS	*BIOF*	*SUS*	*BIOF*	*SUS*	*BIOF*	*SUS*	*BIOF*	*SUS*	*BIOF*	*SUS*	*BIOF*
XII (day 535)	*Nitrosospira multiformis (1.03*, 0.1*#, 0.8**, 0.33**#, 1.86***, 0.04***#*						*Nitrospira moscoviensis (2.13)*	*Nitrospira defluvii (1.75)*	*Nitrospira defluvii (0.4**, 4.23**#)*		*Nitrospira moscoviensis (0.21***, 3.25***#)*	
	*MBBR SUSPENDED, **UASB SUSPENDED, ***GLR SUSPENDED, *#MBBR BIOFILM, **#UASB BIOFILM, ***#GLR BIOFLM, SUS – SUSPENDED, BIOF – BIOFILM											

Table A. 4. 3. The relative abundance of nitrifying bacteria, ANAMMOX bacteria and ANAMMOX-like bacteria at genus level (*continued in the next page*).

Samples	NOB			AOB					AMX				AMX-like	CMX
	Nitrospira	*Nitrobacter*	*Nitrolancea*	*Nitrosococcus*	*Nitrosomonas*	*Nitrosospira*	*Nitrosovibrio*	*Candidatus_Nitrosoglobus*	*Candidatus* Scalindua	*Candidatus* Brocadia	*Candidatus* Jettenia	*Candidatus* Kuenenia	anammox-like bacteria	*Candidatus* Nitrospira inopinata
INOCULUM	6.41	0.13	0.00047	0.021	4.54	0.092	0.00071	0.0035	0	0.00024	0	43.15	0.004	0.9
MBBR125	10.3	0.22	0.0013	0.0048	37.65	0.26	0	0.0035	0	0	0	0.76	0.0043	0.46
H-UASB125	3.49	1.43	0.00091	0.0036	30.24	0.3	0.0003	0.0029	0	0	0	5.13	0.011	0.15
GLR125	0.23	0.036	0	0.0082	0.37	0.017	0.00038	0.00022	0	0	0	0.00044	0.000075	0.018
MBBR192	9.93	0.65	0.0027	0.0075	26.97	2.45	0.0015	0.003	0	0	0	0.32	0.0005	0.46
H-UASB192	8.85	0.53	0.00047	0.0075	8.94	2.41	0.00016	0.0011	0	0.0011	0	32.03	0.098	0.35
GLR192	1.65	0.94	0.0012	0.00769	18.82	1.98	0	0.0036	0	0	0	0.9	0.0043	0.08
MBBR260	11.84	8.57	0.0022	0.011	0.48	3.66	0.00086	0.0022	0.00043	0.14	0.038	14.41	0.33	1.19
H-UASB260	0.8	0.11	0.00015	0.0047	0.3	0.46	0.00015	0.00015	0	0.052	0.012	73.9	0.42	0.042
GLR260	1.16	1.3	0.0018	0.0058	1.2	3.52	0.00044	0	0	0.0018	0.00044	22.74	0.1	0.088
MBBR309	30.66	0.31	0	0.0321	0.17	0.48	0	0	0	0.39	0.088	7.46	0.76	4.48
H-UASB309	1.24	0.23	0.00049	0.0052	0.72	0.79	0.00066	0.00016	0	0.13	0.032	65.81	0.5	0.079

GLR309	1.21	1.27	0.00059	0.0048	15.99	1.87	0	0.0083	0	0.21	0.034	22.12	0.5	0.11
MBBR SUSP535	4.51	0.15	0	0.01	0.09	1.06	0	0.002	0.002	0.28	0.08	11.19	0.43	0.64
MBBR BIOF535	3.99	0.08	0.001	0.01	0.05	0.11	0	0	0.0007	0.24	0.08	4.19	0.39	0.51
H-UASB SUSP535	0.75	0.33	0.007	0.01	0.14	0.83	0.002	0	0.002	0.41	0.16	33.28	0.65	0.07
H-UASB BIOF535	7.44	0.36	0.02	0.02	0.33	0.34	0	0.003	0	0.16	0.07	5.48	0.27	0.56
GLR SUSP535	0.42	0.34	0.002	0.01	0.08	1.91	0.0005	0	0	0.21	0.07	3.81	0.31	0.07
GLR BIOF535	7.18	0.1	0.0008	0.02	0.1	0.05	0.0008	0.0008	0	0.27	0.08	4.04	0.46	0.71
AMX - ANAMMOX bacteria, CMX - comammox bacteria, SUSP - suspension, BIOF - biofilm														

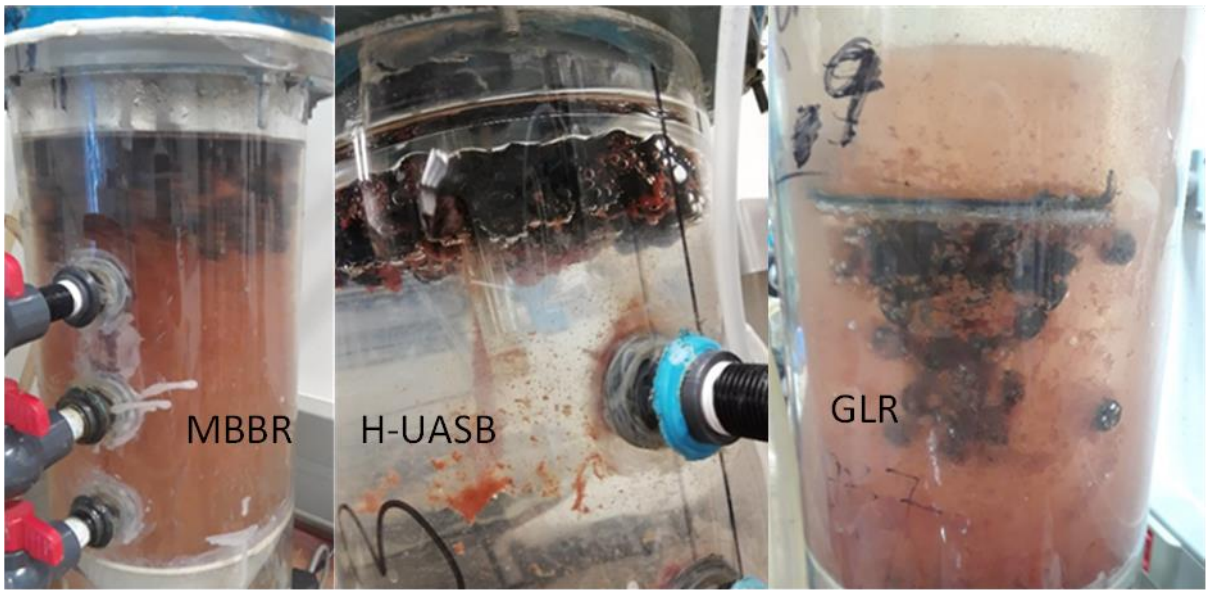

Figure A. 4. 1. Photographic images of the reactors during the study.

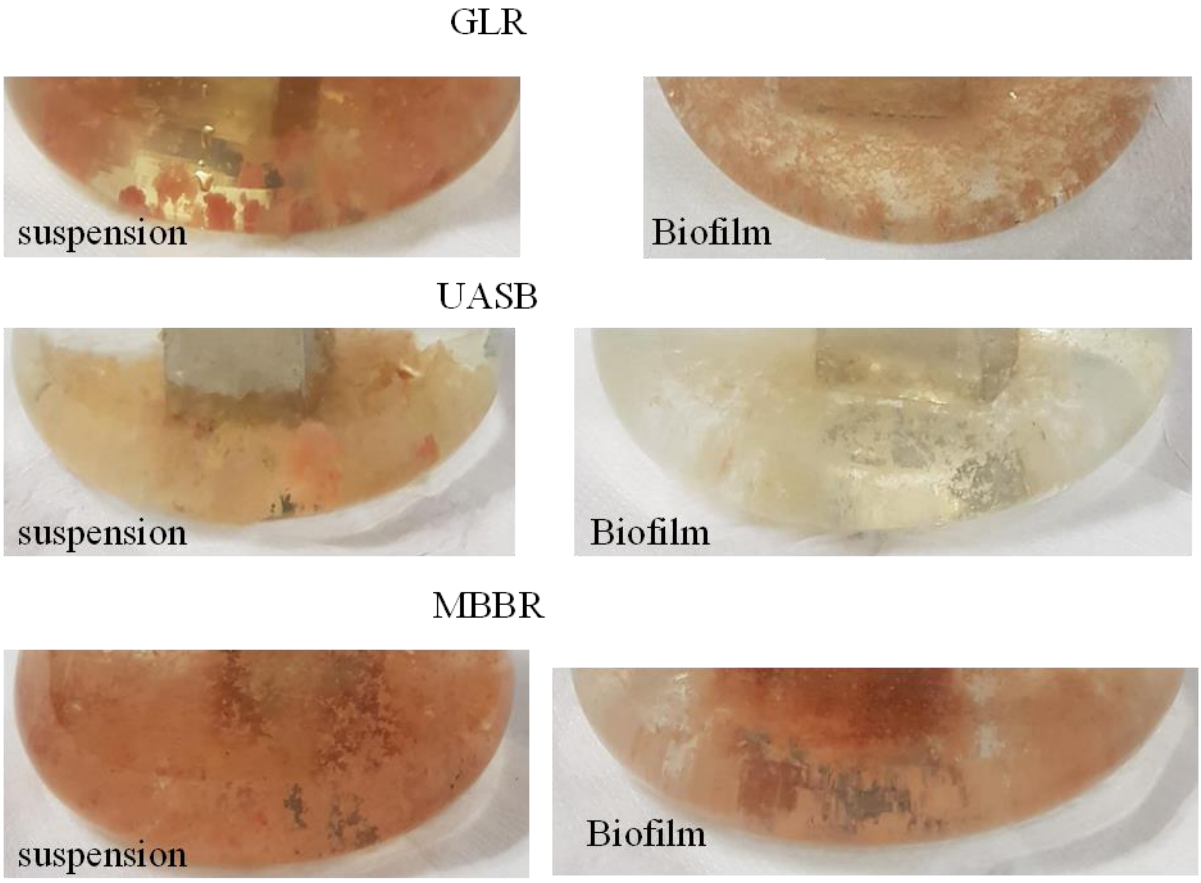

Figure A. 4. 2. Suspended and biofilm-extracted biomass from the reactors on day 519.

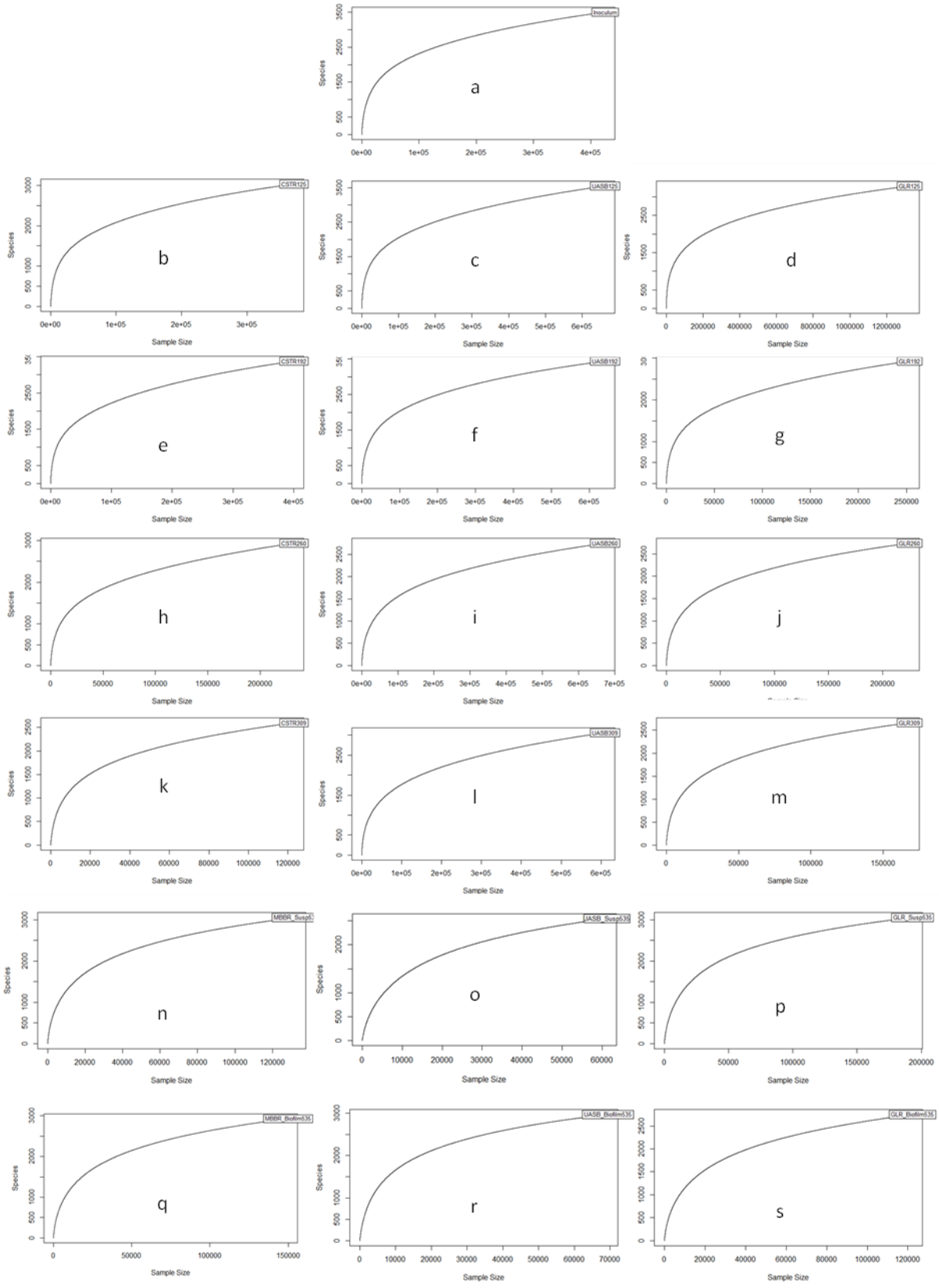

Figure A. 4. 3. Rarefaction curves: a - inoculum; b, e , h, k & n - MBBR suspended biomass; q - MBBR biofilms; c, f, i, l & o - H-UASB suspended biomass; r - H-UASB biofilms; d, g, j, m & p - GLR suspended biomass; s - GLR biofilms.

12 APPENDIX C

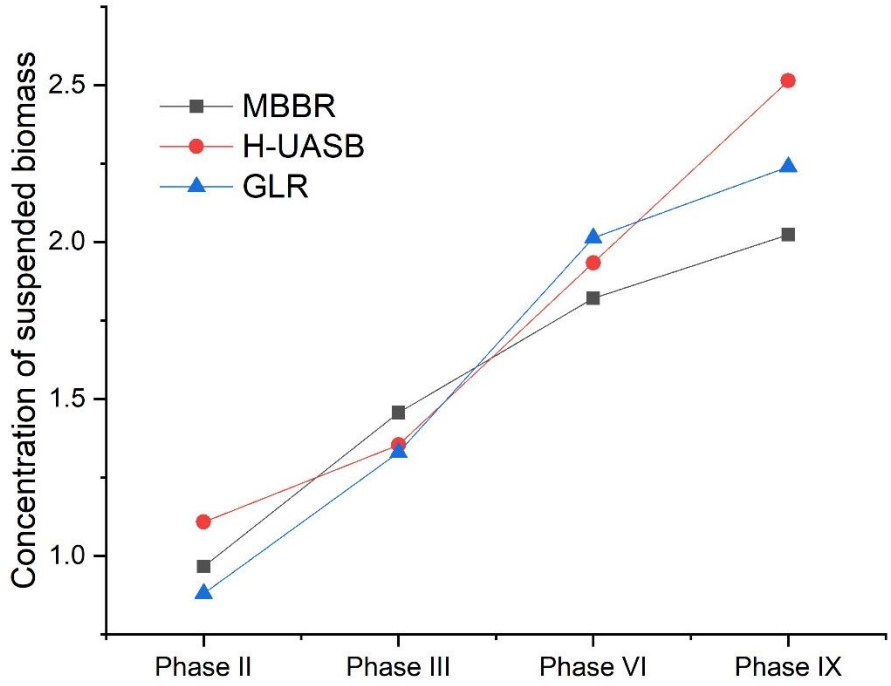

Figure A. 5. 1. Concentration of suspended biomass in the MBBR, H-UASB and GLR in phases II, III, VI and IX.

13 APPENDIX D

Table A. 6. 1. Model-predicted relative abundance of AOB, *Nitrospira* spp. *Nitrobacter* spp. ANAMMOX bacteria and COMAMMOX bacteria in the 5 CSTRs in H-UASB.

	AOB	*Nitrobacter* spp.	*Nitrospira* spp.	COMAMMOX bacteria	ANAMMOX bacteria
CSTR 1					
125	0.259714494	0.00355	0.094797	0.002937	99.01105
192	0.000113575	3.06E-08	3.21E-06	7.29E-07	99.69419
260	2.97157E-14	6.15E-14	2.81E-11	7.06E-12	99.79346
309	1.35239E-21	9.33E-18	1.22E-14	2.54E-15	99.79528
535	5.13864E-55	1.86E-35	3.85E-30	5.41E-31	99.79738
CSTR 2					
125	12.87467925	0.103683	0.056352	0.006223	84.34201
192	13.6861913	1.54E-08	3.44E-06	9.72E-06	81.69583
260	1.4789E-06	3.19E-08	3.79E-06	1.47E-07	83.8494
309	2.29728E-14	4.68E-05	0.000966	4.34E-08	62.0832
535	8.78593E-53	33.19173	4.918061	2.99E-15	0.172337
CSTR 3					
125	17.27985015	0.047369459	0.119815277	0.011285931	80.621504
192	15.97607768	7.0663E-08	7.2017E-06	1.61245E-05	81.53451943
260	1.16229E-06	4.14091E-07	1.90709E-05	3.51187E-07	93.67216312
309	1.7022E-14	0.002856497	0.017702569	2.07806E-07	84.62913658
535	2.06221E-52	75.35499674	6.184879456	4.94561E-15	0.21427276
CSTR 4					
125	17.89881319	0.177759	0.043542	0.006779	80.13878
192	16.02179234	2.69E-08	2.64E-06	9.62E-06	82.15489
260	9.47848E-07	1.86E-07	8.08E-06	2.17E-07	96.47195
309	1.34393E-14	0.00163	0.009202	1.43E-07	91.46678
535	1.72588E-52	85.20478	5.582841	4.59E-15	0.249652
CSTR 5					
125	17.57335971	0.853775	0.021245	0.00504596	80.52991
192	15.8546138	1.31E-08	1.3E-06	7.29263E-06	82.41771
260	8.40117E-07	9.51E-08	4.19E-06	1.66983E-07	97.63311
309	1.15424E-14	0.000899	0.005093	1.13633E-07	94.31263
535	1.51059E-52	88.72663	5.155944	4.73553E-15	0.272711

Table A. 6. 2. The model-predicted relative abundance of nitrifying and ANAMMOX bacteria in the reactors at baseline conditions.

	MBBR				
Samples	**AOB**	***Nitrobacter* spp.**	***Nitrospira* spp.**	**COMAMMOX bacteria**	**ANAMMOX bacteria**
1	4.54	0.13	6.41	0.9	43.15
125	0.259714	0.00355	0.094797	0.002937	99.01105
193	6.57E-05	1.82E-08	2.03E-06	4.92E-07	99.69963
260	2.97E-14	6.15E-14	2.81E-11	7.06E-12	99.79346
309	1.35E-21	9.33E-18	1.22E-14	2.54E-15	99.79528
535	4.89E-55	1.86E-35	3.85E-30	5.41E-31	99.79738
	H-UASB				
	AOB	***Nitrobacter* spp.**	***Nitrospira* spp.**	**COMAMMOX bacteria**	**ANAMMOX bacteria**
1	4.54	0.13	6.41	0.9	43.15
125	13.17728	0.237227	0.06715	0.006454	84.92865
192	12.30776	3.13E-08	3.56E-06	8.7E-06	85.49943
260	8.86E-07	1.45E-07	7.03E-06	1.77E-07	94.28402
309	1.3E-14	0.001086	0.006593	1.02E-07	86.45741
535	1.24E-52	56.49563	4.368345	3.45E-15	20.14127
	GLR				
	AOB	***Nitrobacter* spp.**	***Nitrospira* spp.**	**COMAMMOX bacteria**	**ANAMMOX bacteria**
1	4.54	0.13	6.41	0.9	43.15
125	0.257072	0.003788	0.101094	0.003117	99.30717
192	1.473416	4.56E-08	5.69E-06	7.92E-06	98.07233
260	1.03E-07	1.89E-07	1.19E-05	1.78E-07	98.72212
309	1.46E-15	0.001128	0.009811	9.46E-08	96.42208
535	2.14E-52	52.50424	7.400219	9.78E-15	21.31365

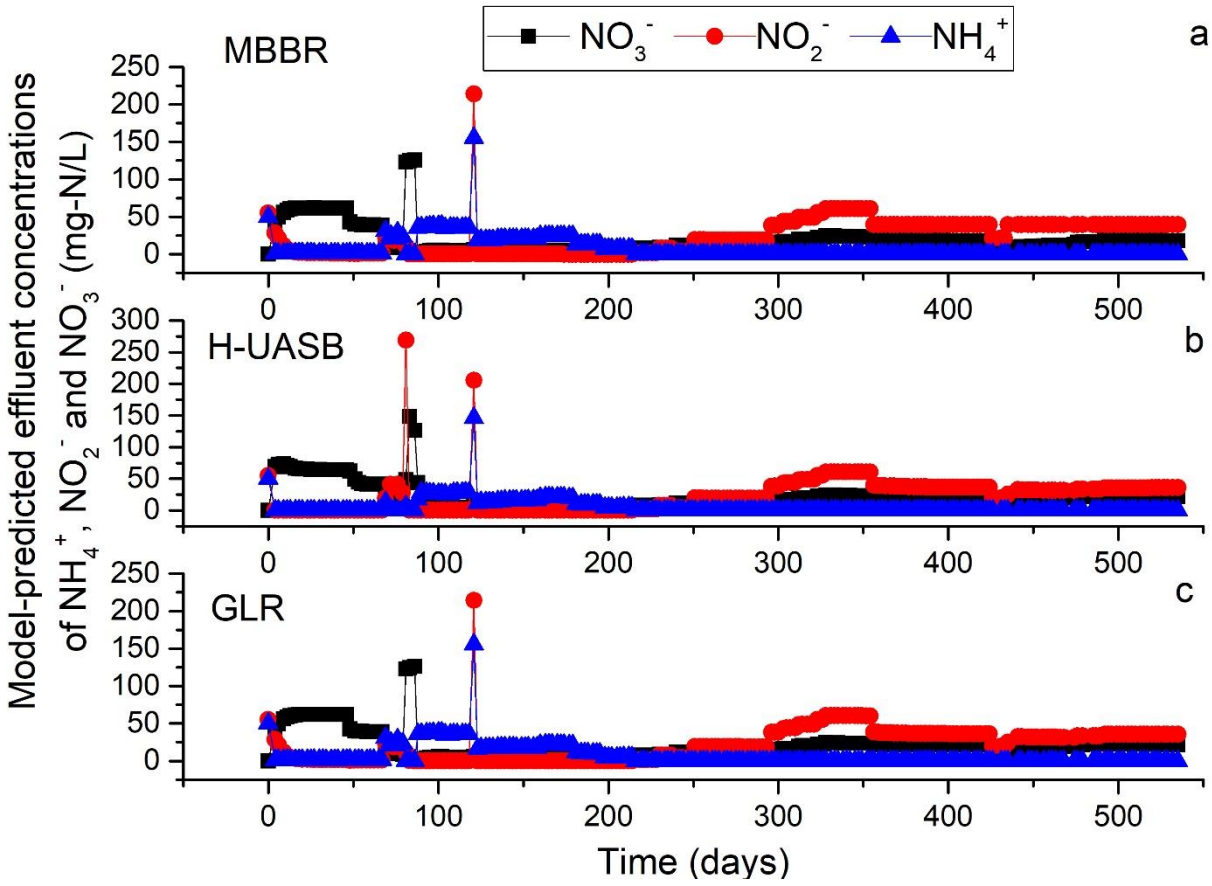

Figure A. 6. 1. Model-predicted effluent concentrations of NH_4^+, NO_2^- and NO_3^- in MBBR (a), H-UASB (b) and GLR (c) at baseline conditions (similar NLRs and Cs in all the reactors).

Table A. 6. 3. Model-predicted relative abundance of nitrifying and ANAMMOX bacteria in MBBR at oxygen concentration of 0.1 mg-O_2/L between days 1-79 and between days 87-535.

Sample	AOB	*Nitrobacter* spp.	*Nitrospira* spp.	COMAMMOX bacteria	ANAMMOX bacteria
1	4.54	0.13	6.41	0.9	43.15
125	2.24	4.75E-04	0.018	0.0029	96.77
193	0.90	4.25E-09	6.52E-07	2.07E-06	98.49
260	9.90E-04	1.2E-10	1.64E-08	2.13E-08	99.73
309	3.33E-10	3.09E-11	3.1E-09	2.69E-10	99.77
535	1.05E-43	2.42E-25	8.08E-22	1.57E-24	99.79

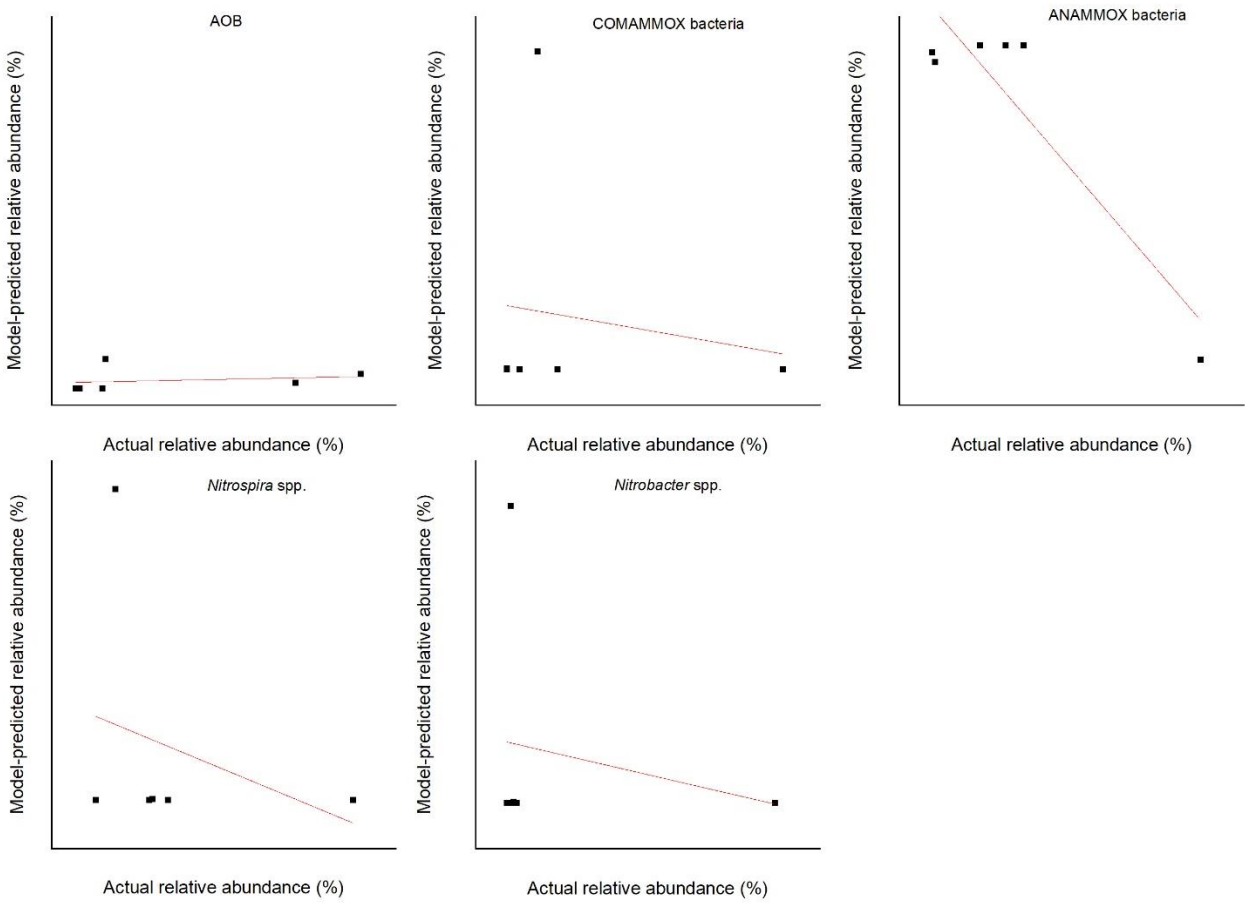

Figure A. 6. 2. The correlation of the model-predicted relative abundance of nitrifying and ANAMMOX bacteria in MBBR at 0.1 mg-O_2/L oxygen saturation concentration between days 1-79 and between days 87-535.

Table A. 6. 4. Model-predicted relative abundance of nitrifying and ANAMMOX bacteria in GLR at 0.1 mg-O_2/L oxygen saturation concentration between days 1-79 and between days 87-535.

Sample	AOB	*Nitrobacter* spp.	*Nitrospira* spp.	COMAMMOX bacteria	ANAMMOX bacteria
1	4.54	0.13	6.41	0.9	43.15
125	2.08	1.66E-04	0.01	0.002	97.36
192	2.33	3.07E-09	8.42E-07	5.42E-06	97.16
260	2.04E-04	1.55E-08	1.96E-06	3.07E-07	99.47
309	5.18E-11	1.40E-04	0.002301	2.09E-07	98.65
535	1.43E-44	63.47	9.53	7.21E-14	22.11

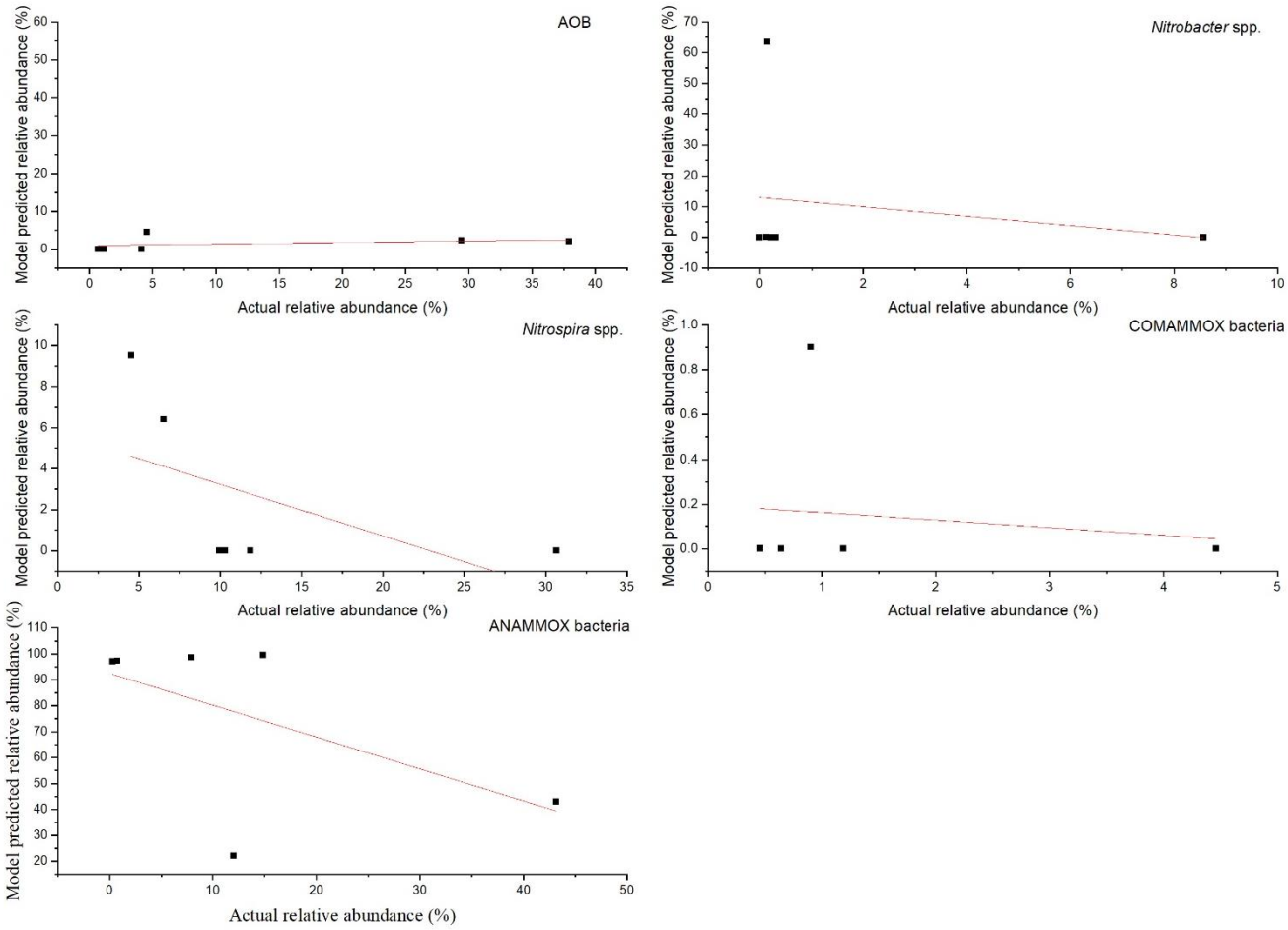

Figure A. 6. 3. Correlation of the model-predicted relative abundance of nitrifying and ANAMMOX bacteria in GLR on maintenance of 0.1 mg-O_2/L oxygen saturation concentration between days 1-79 and between days 87-535.

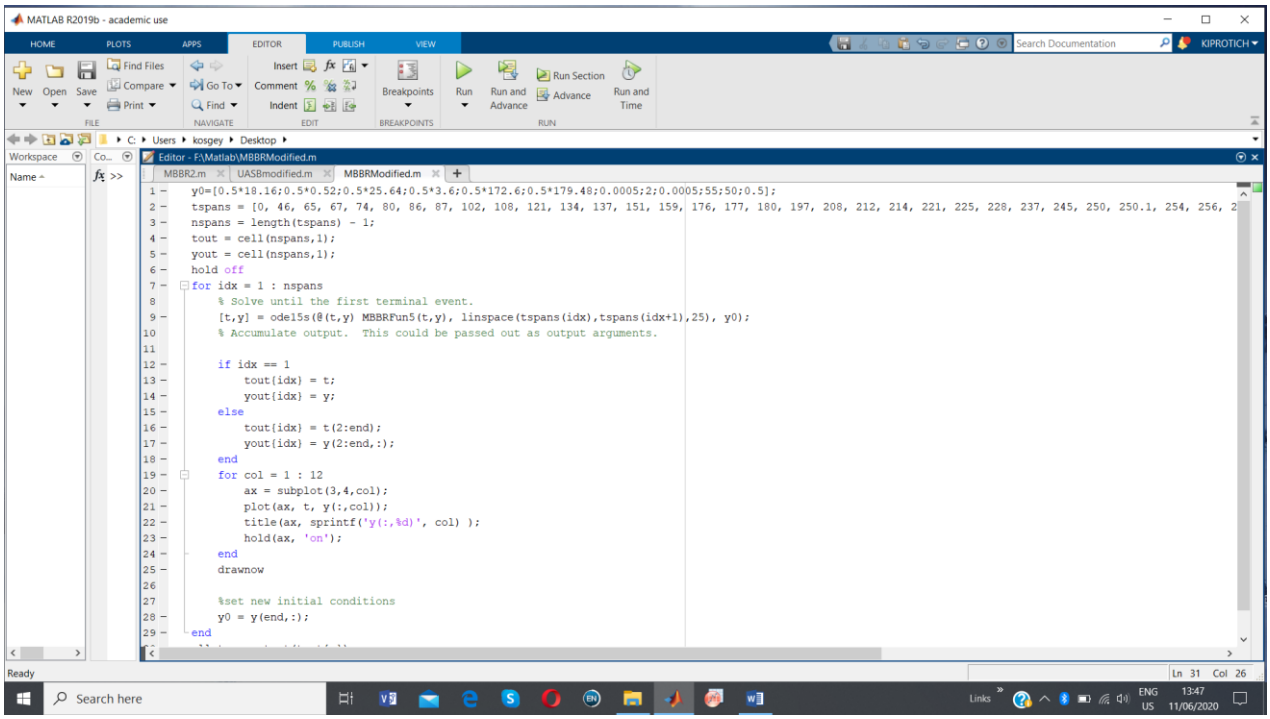

Figure A. 6. 4. Snapshot of the modelling script for MBBR.

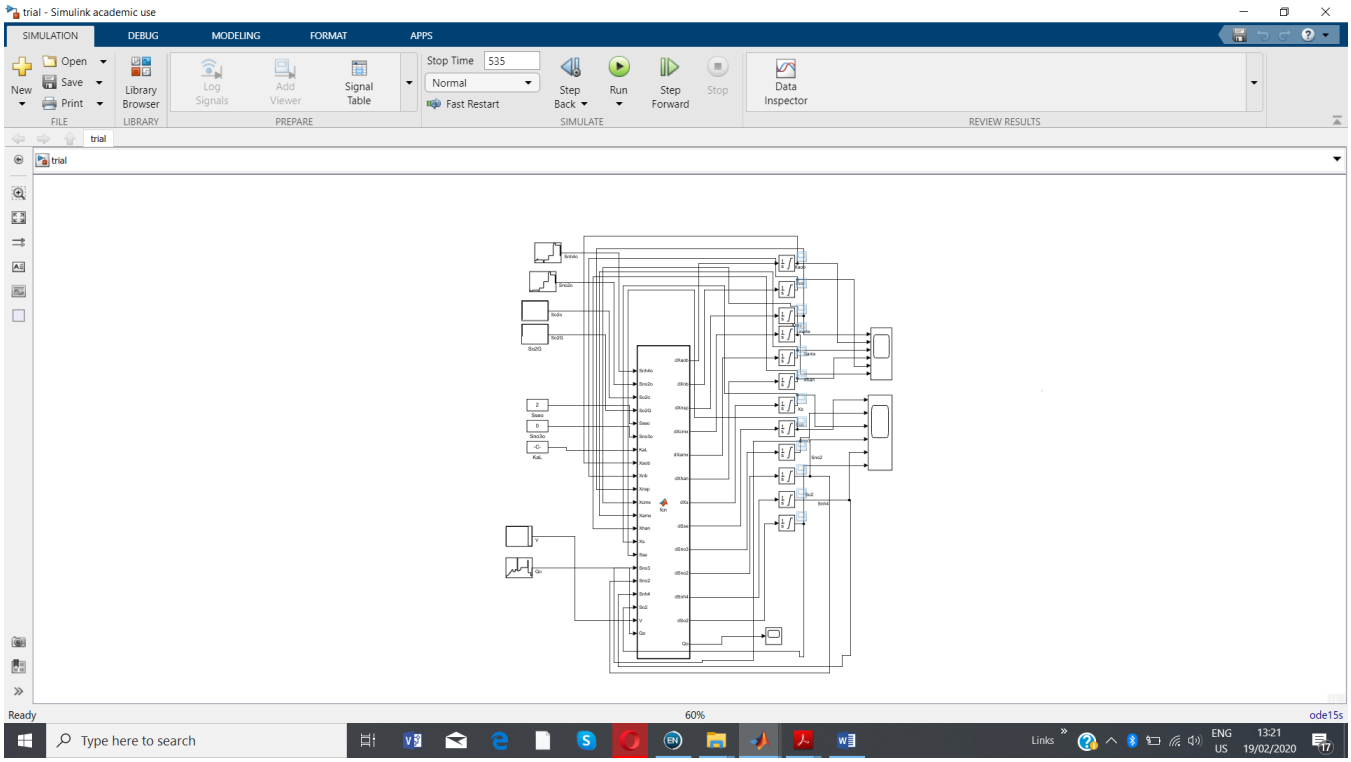

Figure A. 6. 5. Snapshot of Simulink encoder for MBBR.

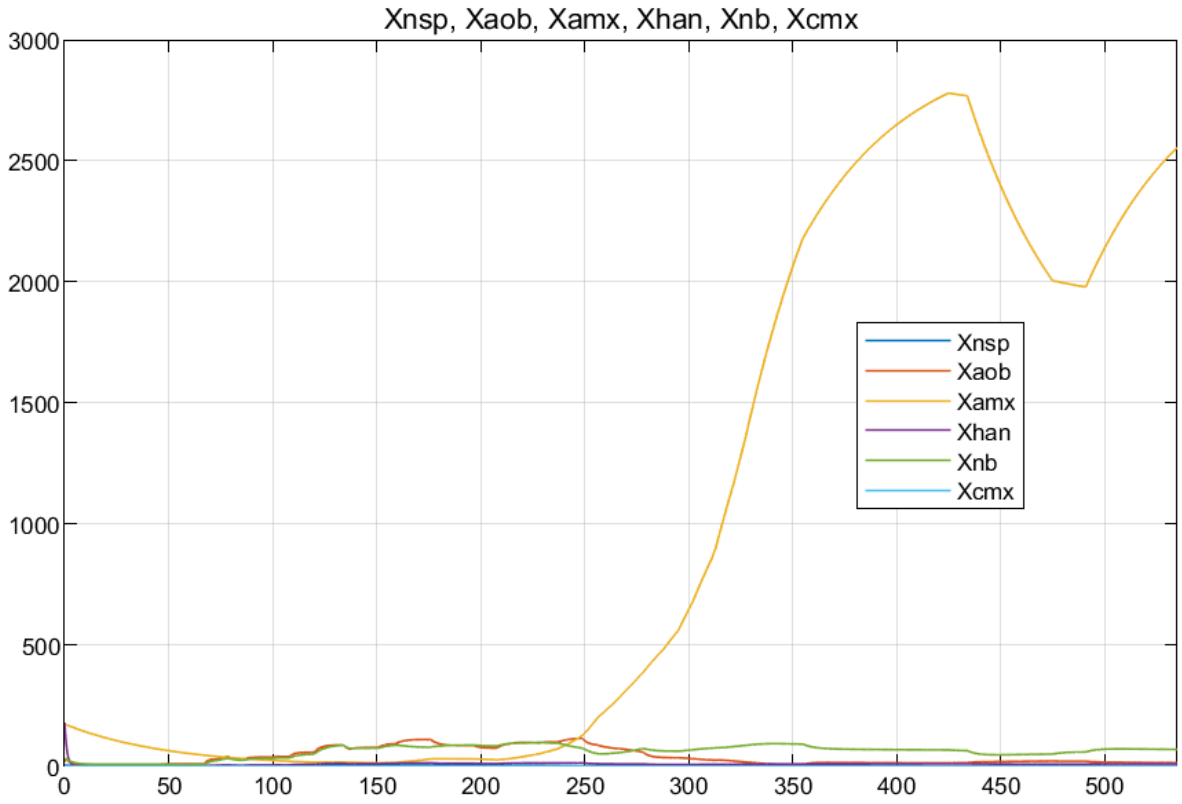

Figure A. 6. 6. Simulation of bacterial population dynamics in MBBR using Simulink.

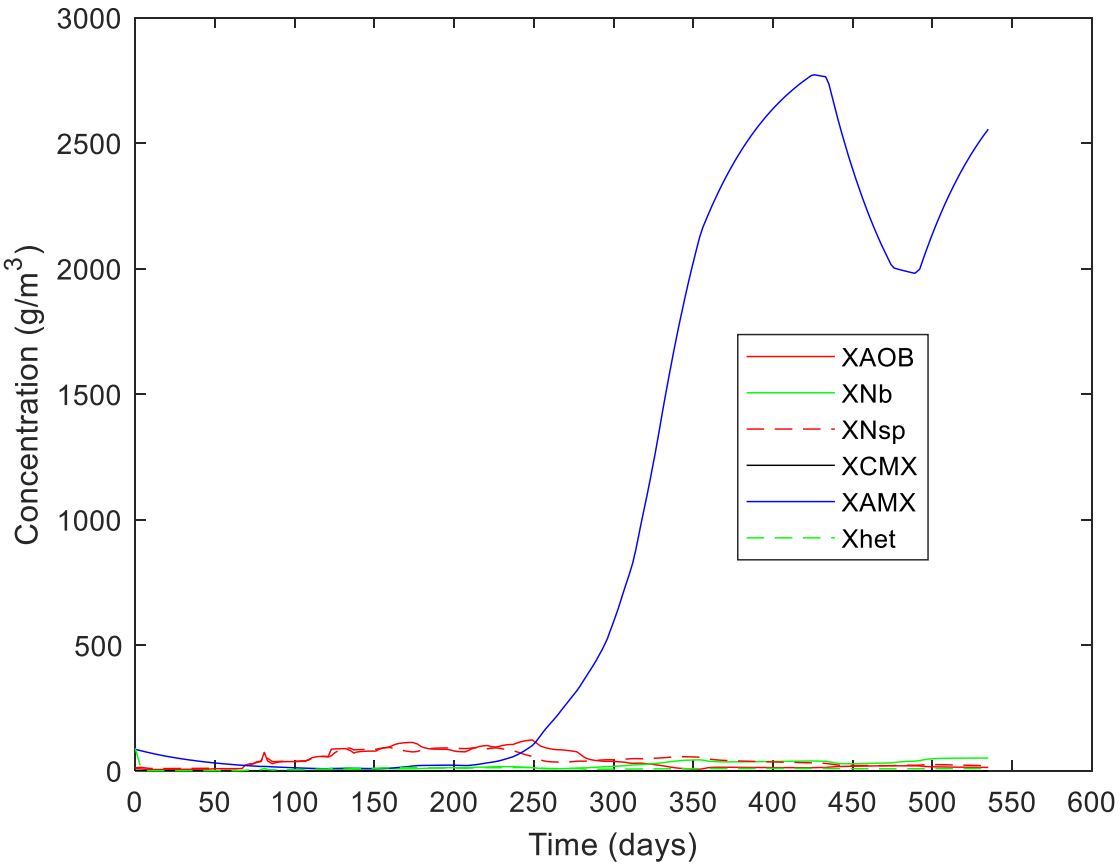

Figure A. 6. 7. Simulation of bacterial population dynamics in MBBR using Matlab 2019b.

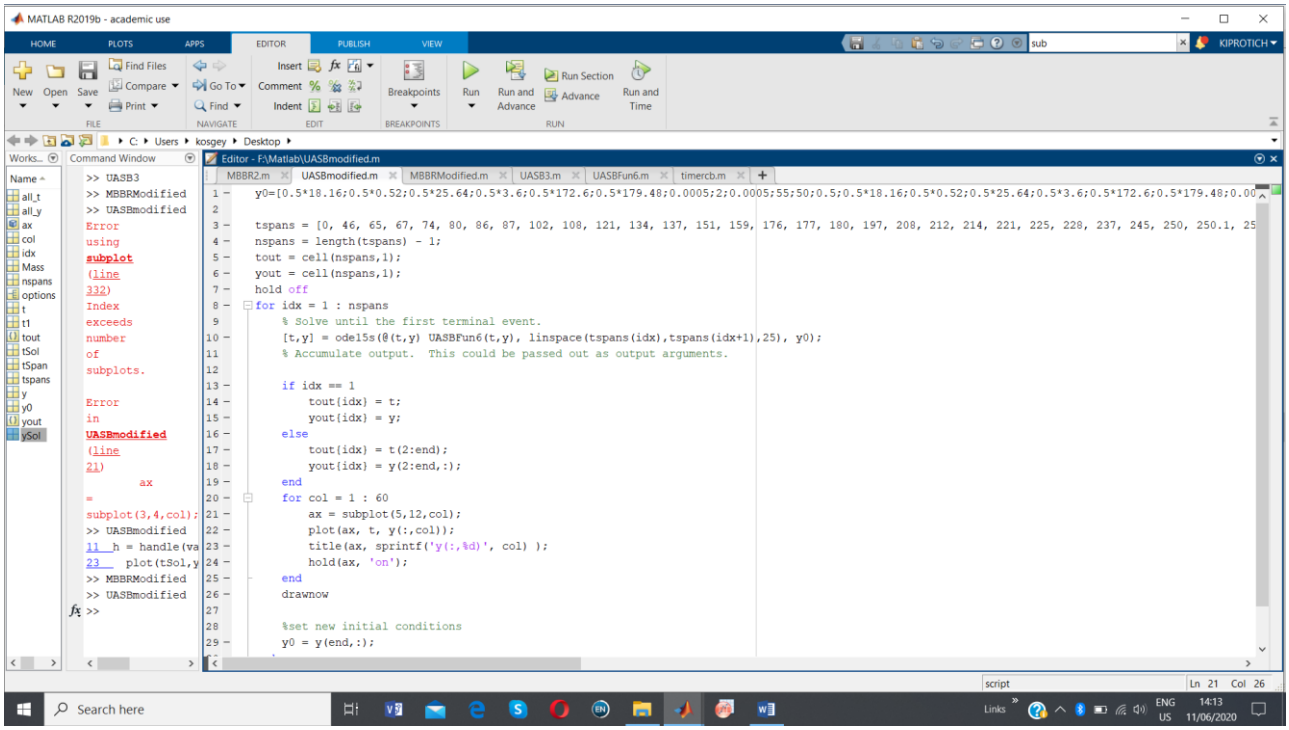

Figure A. 6. 8. Snapshot of the modelling script for H-UASB.

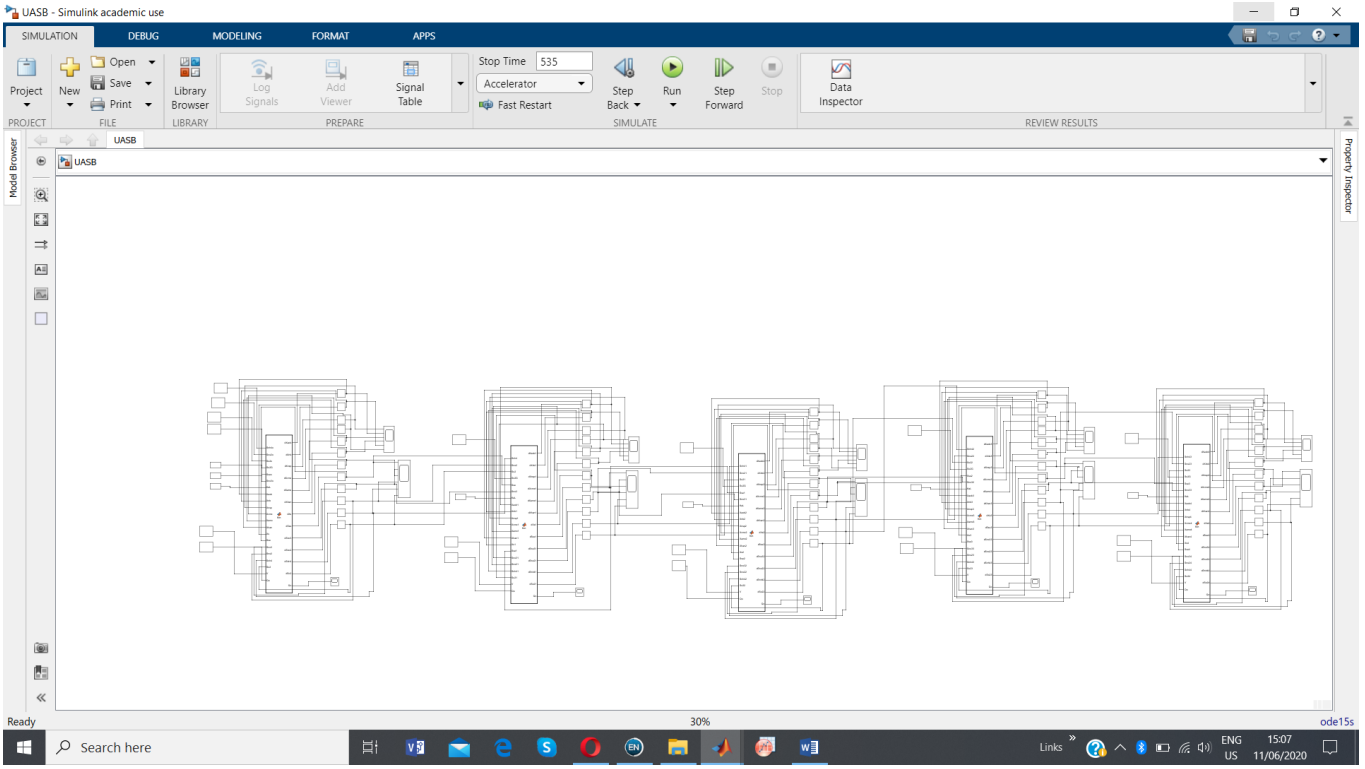

Figure A. 6. 9. Snapshot of Simulink encoder for H-UASB.

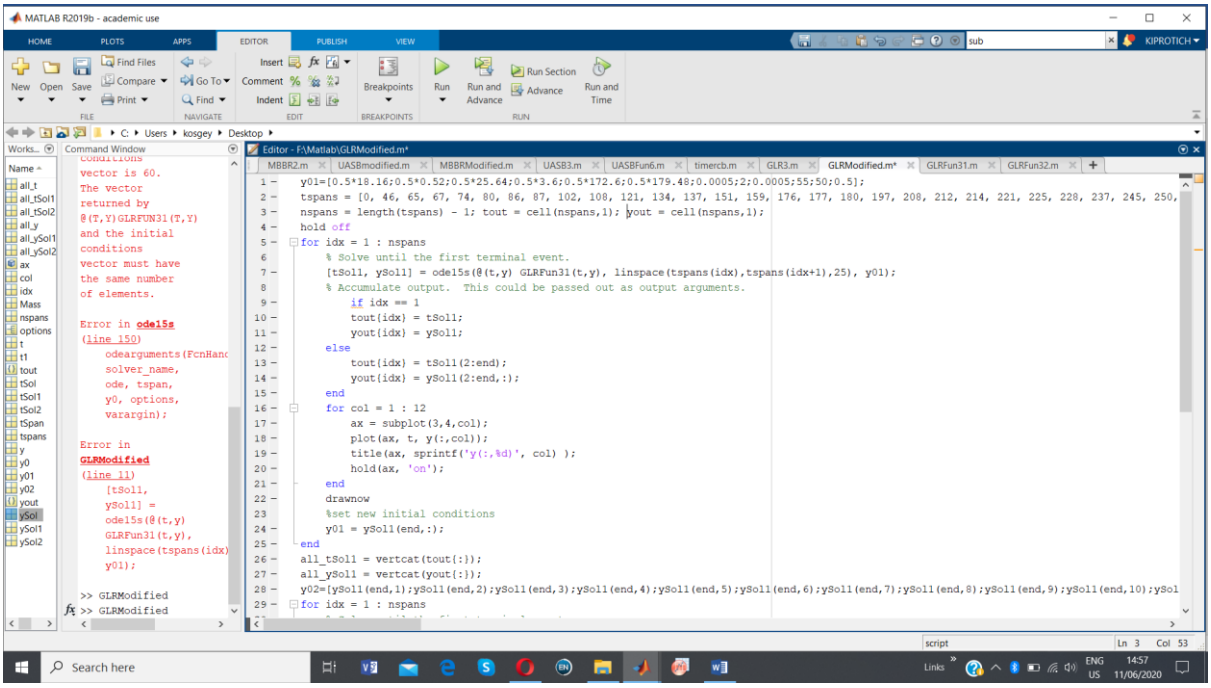

Figure A. 6. 10. Snapshot of the modelling script for GLR.